

厚生労働科学研究費補助金
労災疾病臨床研究事業

悪性胸膜中皮腫のヒト化 CD26 抗体療法確立のための
予後・治療効果予測バイオマーカーの開発

令和元年度 総括・分担研究報告書

研究代表者 森本 幾夫

令和 2(2020)年 3 月

目 次

I. 総括研究報告

悪性胸膜中皮腫のヒト化CD26抗体療法確立のための予後・治療効果予測バイオマーカーの開発	1
---	---

研究代表者 森本 幾夫
順天堂大学大学院医学研究科 免疫病・がん先端治療学講座 特任教授

II. 分担研究報告

1. ヒト化CD26抗体の予後・治療効果予測バイオマーカーの探索： 国内第I/II相臨床試験の血清および末梢血リンパ球の解析結果について	13
--	----

研究代表者 森本 幾夫
順天堂大学大学院医学研究科 免疫病・がん先端治療学講座 特任教授

研究分担者 岸本 卓巳
独立行政法人労働者健康安全機構
アスベスト疾患研究・研修センター 所長

研究分担者 山田 健人
埼玉医科大学 病理学 教授

研究協力者 波多野 良
順天堂大学大学院医学研究科 免疫病・がん先端治療学講座 特任助教

研究協力者 大沼 圭
順天堂大学大学院医学研究科 免疫病・がん先端治療学講座 准教授

研究協力者 藤本 伸一
岡山労災病院 腫瘍内科部長

研究協力者 青江 啓介
山口宇部医療センター 腫瘍内科 内科系診療部長

2. 悪性胸膜中皮腫におけるCD26発現評価とヒト化CD26抗体療法における 予後・治療効果予測バイオマーカーの開発.....	25
--	----

研究分担者 山田 健人
埼玉医科大学 病理学 教授

研究分担者 岸本 卓巳
独立行政法人労働者健康安全機構
アスベスト疾患研究・研修センター 所長

研究協力者 藤本 伸一
岡山労災病院 腫瘍内科部長

研究協力者 青江 啓介
山口宇部医療センター 腫瘍内科 内科系診療部長

研究協力者 波多野 良
順天堂大学大学院医学研究科 免疫病・がん先端治療学講座 特任助教

3. ヒト化抗 CD26 抗体投与後の血清中溶存 CD26/DPP4 値の変動と
予後・治療効果との相関関係の解析・・・・・・・・・・30

研究代表者 森本 幾夫
順天堂大学大学院医学研究科 免疫病・がん先端治療学講座 特任教授

研究分担者 岸本 卓巳
独立行政法人労働者健康安全機構
アスベスト疾患研究・研修センター 所長

研究分担者 山田 健人
埼玉医科大学 病理学 教授

研究協力者 金子 有太郎
ワイズ・エー・シー株式会社 CEO
近畿大学 客員教授(元)

研究協力者 波多野 良
順天堂大学大学院医学研究科 免疫病・がん先端治療学講座 特任助教

III. 研究成果の刊行に関する一覧表・・・・・・・・・・38

IV. 研究成果の刊行物・別刷

I. 総括研究報告

労災疾病臨床研究事業費補助金
総括研究報告書
悪性胸膜中皮腫のヒト化 CD26 抗体療法確立のための
予後・治療効果予測バイオマーカーの開発

研究代表者 森本 幾夫 順天堂大学大学院医学研究科
免疫病・がん先端治療学講座 特任教授

研究要旨

悪性胸膜中皮腫はアスベストばく露によって起こる難治性悪性腫瘍であり、現時点で満足できる治療法はなく、新たな治療法の確立が望まれる。研究代表者は抗腫瘍効果の強いヒト化 CD26 抗体 YS110 の開発に成功し、フランスにて悪性中皮腫を中心とした CD26 陽性腫瘍に対する First-in-Human 第 I 相臨床試験を施行した。2017 年 7 月から国内でも悪性中皮腫に対する第 I/II 相臨床試験を施行中である。

ヒト化 CD26 抗体が有効な患者を予測できる新たなバイオマーカーを同定するために、国内第 I/II 相臨床試験患者の血清中サイトカイン・ケモカインの多項目解析を行い、SDF-1, MIP-1d, MCP2, Gro-b, GCP-2 等が CD26 抗体の有効性を予測する新規バイオマーカー候補になる可能性を見出した。また、国内第 I/II 相臨床試験患者の末梢血リンパ球のフェノタイプ解析により、YS110 (ヒト化 CD26 抗体) 有効例では特に CD8 T 細胞で細胞傷害性エフェクター T 細胞 (CD26 陰性・CD28 陰性・KLRG1 陽性サブセット) の割合が高く、免疫チェックポイント分子の中で PD1 と TIGIT の発現陽性率が高い可能性を見出した。

国内第 I/II 相臨床試験において、悪性中皮腫の病理検体として、第 I 相は 9 例中 6 例、第 II 相では、31 例全例の計 37 症例 (組織型は、上皮型 29 例、二相型 5 例、肉腫型 3 例) が収集され、36 例は CD26 発現の評価が可能であった。そこで R&D 社ポリクローナル抗体による免疫染色 (フランスでの治験と同一、A 法) および新規開発されたコンパニオン診断キットによる免疫染色 (B 法) の二つの染色方法により CD26 発現について検討した。その結果、A 法での CD26 陽性率が 20%以上の症例は、37 例中 30 例、20%未満の症例が 6 例であったのに対して、B 法では 20%以上の症例は、37 例中 32 例、20%未満の症例が 4 例であった。また A 法よりも B 法で CD26 陽性率が上昇した症例は 36 例中 23 例であり、その中で陽性率が 20%以上上昇した症例が 11 例認められた。正常ヒト組織での CD26 染色性の向上が B 法で認められたことも考えると、この新規コンパニオン診断キットによる免疫染色法が中皮腫における CD26 発現をより正確に評価するのに適していると考えられた。

ヒト化抗 CD26 モノクローナル抗体 (YS110) による悪性胸膜中皮腫を主たる対象としたフランスにおける第 I 相臨床試験により得られた、YS110 投与に伴う血清中溶存 CD26/DPP4 (sCD26/DPP4) titer の変動が、YS110 投与の予後・治療効果を予測するバイオマーカーになり得るかの検討を行い、バイオマーカーとして有用である可能性が得られた。その中で、臨床試験で

観察された、YS110 投与によって血清中 sCD26/DPP4 titer が低下するメカニズムを明らかにするために、CD26 陽性/陰性の腫瘍及び正常細胞を用いて、in vitro での検証を行った。細胞膜上の CD26 の発現が高い細胞であれば腫瘍・正常細胞ともに培養上清中に sCD26 を産生し、YS110 の容量依存的、及び経時的に sCD26 の産生が阻害されることを明らかにした。

研究分担者

岸本 卓巳：独立行政法人労働者健康安全
機構 アスベスト疾患研究・
研修センター 所長
山田 健人：埼玉医科大学 病理学 教授

研究協力者

藤本 伸一：岡山労災病院 腫瘍内科部長
青江 啓介：山口宇部医療センター 腫瘍
内科 内科系診療部長
大沼 圭：順天堂大学大学院医学研究科
免疫病・がん先端治療学講座
准教授
波多野 良：順天堂大学大学院医学研究科
免疫病・がん先端治療学講座
特任助教
金子有太郎：ワイズ・エー・シー株式会社
CEO, 近畿大学 客員教授(元)

合することで腫瘍の増殖抑制に働くこと、さらに近年では腫瘍免疫の促進にも働きうることを明らかにしてきた(Clin Cancer Res. 2007, 2012, PLoS One. 2013, Br J Cancer. 2014, Nat Immunol. 2015)。さらに、抗体療法の確立に不可欠な病理組織の CD26 発現診断用抗体、可溶性 CD26/DPPIV 値測定系を開発し、フランスにて治療抵抗性悪性中皮腫を中心とした First-in-Human 第 I 相臨床試験を施行した。免疫チェックポイント阻害薬のような自己免疫疾患様の特記すべき有害事象もなく、有効性を示唆するデータも得られたが(Br J Cancer. 2017)、どの患者が CD26 抗体療法の適用となるかを予測できるバイオマーカーの開発が課題とされた。

そこでフランスでの臨床試験患者血清を解析し、CD26/DPPIV 値の変動解析が Stable Disease (SD)/Progressive Disease (PD) の予測バイオマーカーとなる可能性が示唆された ($p < 0.016$)。2017 年 7 月から開始した国内第 I 相臨床試験は、2018 年 3 月に最終患者への投与が終了し(第 1~3 コホート各 3 例、全 9 例)、自己免疫疾患様の重篤な副作用が出ることなく、抗腫瘍効果としてもフランスでの第 I 相臨床試験と同様に有効性を強く示唆する結果が得られた(Lung Cancer. 2019)。2018 年 6 月から第 II 相臨床試験がスタートした。2019 年 4 月初めに国内第 II 相臨床試験全 31 例への CD26 抗体投与が終了した。昨年度に引き続き、国内第 II 相臨床試験検体を用いて(1)腫瘍病理組織での

A. 研究目的

悪性胸膜中皮腫は現時点で効果的な治療法はなく、予後は極めて不良で労災疾病行政上でも大きな問題であり、有効な新規治療法の確立は急務である。

研究代表者は CD26 単クローン抗体の開発、CD26 cDNA の単離を世界に先駆けて行い(J Immunol. 1989, 1992)、抗腫瘍効果の強いヒト化 CD26 抗体の開発に成功した。悪性中皮腫における CD26 発現の解析、抗体の抗腫瘍作用機構の解明に取り組み、この抗体は抗体医薬特有の ADCC に加え、CD26 陽性腫瘍に結

CD26 発現解析と(3)末梢血リンパ球の解析を行った。また、国内第 I/II 相臨床試験患者の(2)血清中サイトカイン・ケモカインの多項目解析、ならびに血清中可溶性 CD26/DPPIV 酵素活性値の測定を行い、CD26 抗体の抗腫瘍効果と相関する新規バイオマーカー候補の絞り込みを行った。

令和 2 年度は、国内第 I/II 相臨床試験検体の合計 40 例の中で、Partial Response (PR) または SD が 4 サイクル(約 6 ヶ月)以上持続した検体に焦点を絞り、(1)腫瘍組織 DNA・RNA profile の解析を行う。また、これまでの解析で得られた(2)血清バイオマーカー、及び(3)末梢血リンパ球バイオマーカーに関して、腫瘍周囲の免疫細胞における発現を免疫組織染色によって解析する。これにより、血清中 CD26/DPPIV 値の変動解析や新規バイオマーカー候補によって、CD26 抗体療法が有効な患者を判別し得るかを明らかにし、**安全かつ革新的な CD26 抗体療法の確立と、抗体療法適用患者の適切な選択を可能にする。**

B. 研究方法

各分担研究報告書に著述

(倫理面への配慮)

成人健常者ならびに岡山労災病院、山口宇部医療センターの悪性胸膜中皮腫患者・良性石綿胸水患者の末梢血を用いた研究については、森本が講座責任者である順天堂大学大学院医学研究科、岸本・藤本が勤務する岡山労災病院、青江が勤務する山口宇部医療センターそれぞれの施設で、本研究を行うための研究計画書等を倫理審査委員会へ提出し、承認を得ている(順大医倫第 2018127 号、岡山労災病院 115 号、山口宇部医療センター 29-21

号)。また、ヒト化 CD26 抗体の国内第 I/II 相臨床試験の被験者検体を用いたバイオマーカー探索研究については、キッセイ薬品工業株式会社内の臨床試験審査委員会、各治験実施施設内の治験審査委員会にて、試験の実施と合わせてバイオマーカー探索用採血・腫瘍組織検体の提供について協議され、実施承認を取得済みである。検体の提供を受ける際には、研究対象者に対する人的擁護上の配慮及び研究により研究対象者が受ける不利益、利益等の説明を行い、書面でのインフォームド・コンセントを得ている。

フランスでの第 I 相臨床試験におけるヒトおよびヒト由来の試料を対象とした研究は、世界医師会によって作成された人体実験に関する一連の倫理的原則に従って実施された。血清検体の提供を受ける際には、研究対象者に対する人的擁護上の配慮及び研究により研究対象者が受ける不利益、利益等の説明を行い、書面でのインフォームド・コンセントを得ている。

C. 研究結果

1) 国内第 I / II 相臨床試験患者の血清中サイトカイン・ケモカインの多項目解析

今回の解析では長期間持続のラインを 4 サイクル(24 週間)以上に設定した。つまりは、CD26 抗体投与を開始して 24 週間以上 PR または SD が持続した症例を long SD・PR、SD の持続期間が 6 週間以上 24 週間未満の症例を short SD、抗体投与を開始して 6 週間後の抗腫瘍効果判定で PD だった症例は PD 症例として解析を行った。まだ第 II 相臨床試験の結果は公表されていないため、long SD・PR、short SD、PD それぞれの具体的な症例数に関してまだ記載はできない。まず、

血清に関しては、第 I 相全 9 例・第 II 相全 31 例の計 40 例のうち、バイオマーカー解析の同意を得られたのが 29 例で、そのうち 4 例は抗腫瘍効果の評価が不可であった。Bio-Plex システムによりサイトカイン・ケモカイン 49 種類の多項目測定を行い、抗腫瘍効果評価可能 25 症例を解析した結果、ケモカイン SDF-1 α , β / CXCL12 及び MIP-1d / CCL15 の血清中濃度が、悪性中皮腫患者の中で特に PD 症例で高値を示し、一方で long SD・PR 症例では低値を示す傾向が見られた。また、long SD・PR 症例と short SD 症例との間で大きな差は見られないが、ケモカイン MCP2/CCL8, Gro-b/CXCL2, GCP-2/CXCL6 の血清中濃度が、悪性中皮腫患者の中で特に PD 症例で高値を示したのに対し、short SD 症例と long SD・PR 症例では比較的に低値を示す傾向が見られた。このことから、これらの因子は CD26 抗体が有効ではない PD 症例と、CD26 抗体による抗腫瘍効果が少なくとも一定期間以上認められる症例 (short SD を含む SD 症例及び PR 症例) との判別には有用である可能性が示唆された。

2) 国内第 I / II 相臨床試験患者の末梢血リンパ球のフェノタイプ解析

次に、末梢血リンパ球に関して、成人健常者 8 例及び国内第 I/II 相臨床試験患者の末梢血を用いて、フローサイトメトリーによるフェノタイプの比較を行った。末梢血リンパ球に関しては、第 I 相全 9 例・第 II 相全 31 例の計 40 例のうち、バイオマーカー解析の同意を得られたのが 28 例で、そのうち 4 例は抗腫瘍効果の評価が不可であった。末梢血リンパ球の解析は CD26 抗体初回投与前 1 点のみ解析を行った。血清の解析と同様に、PD、short SD、long SD・PR に分類して解析を行

った結果、健常者と比較して悪性中皮腫患者の末梢血 CD8 T 細胞は、細胞傷害性エフェクター T 細胞のマーカーである CD26 陰性・CD28 陰性の割合が顕著に高いが、特に long SD・PR 症例ではその割合が高い傾向が見られた。また、抗原感作マーカーである KLRG1 の陽性率においても、特に long SD・PR 症例ではその割合が高い傾向が見られ、細胞傷害性エフェクター T 細胞マーカーである CD57 の陽性率においても同様の傾向が見られた。

近年、免疫系に抑制シグナルを伝達するチェックポイント分子をブロックすることで腫瘍免疫を活性化させる免疫チェックポイント阻害薬が新たながん治療法として非常に注目されている。代表的な免疫チェックポイント分子の発現を解析した結果、健常者、悪性中皮腫患者ともに末梢血 CD4 T 細胞・CD8 T 細胞に CTLA4, LAG3, CD160 はほとんど発現しておらず (陽性率 0-3%)、TIM3 と BTLA の発現陽性率も 5%未満と非常に低かった。一方、PD1, TIGIT, 2B4, CD39, CD73 は明確な発現が認められた。

今回の CD26 抗体の国内第 I/II 相臨床試験には、抗ヒト PD1 抗体ニボルマブを投与して無効だった患者も含まれている (まだ第 II 相臨床試験結果は公表されていないため、具体的な症例数は記載不可)。末梢血 CD4 T 細胞・CD8 T 細胞の PD1 陽性率を解析した結果、以前にニボルマブを投与した経験のあるニボルマブ無効例では CD4 T 細胞・CD8 T 細胞ともに PD1 の陽性率が極端に低かった。このことは、今回のフローサイトメトリーの解析に用いた PD1 抗体 (clone EH12. 2H7) のエピトープがニボルマブのエピトープと重複しているために、PD1 に結合できなかったか、もしくはニボルマブの投与によって PD1 陽

性細胞が減少していたかによるものと考えられる。そこで、PD1 の解析はニボルマブ無効例を除いたニボルマブ投与歴のない患者に絞って行った結果、long SD・PR 症例では末梢血 CD4 T 細胞・CD8 T 細胞ともに PD1 陽性率が高い傾向が見られた。TIGIT に関しては、CD4 T 細胞では健常者と悪性中皮腫患者との間で大きな違いは見られなかったが、CD8 T 細胞の TIGIT 陽性率は中皮腫患者の方が健常者よりも高く、特に long SD・PR 症例で高い傾向が見られた。

3) 国内第 I / II 相臨床試験での病理解析について

国内第 I/II 相臨床試験（第 I 相は 9 例中 6 例、第 II 相では 31 例全例）における悪性中皮腫 37 症例について、病理組織像および R&D 社ポリクローナル抗体による免疫染色（フランスでの治験と同一の方法、A 法）および新規コンパニオン診断キット（B 法）による CD26 発現について検討した。37 症例の組織型は、上皮型 29 例、二相型 5 例、肉腫型 3 例であった。なお 37 例中 1 例は腫瘍細胞が数個のみであったため評価対象外とし、36 例の検体で CD26 発現の評価を行なった。A 法での結果では、CD26 発現は、上皮型で 5%以下 1 例、5%～50% 3 例、50%～70% 11 例、70%～100% 13 例であり、二相型では、2%、12%、20%、70%がそれぞれ 1 例、肉腫型では 2%、5%、50%がそれぞれ 1 例であった。これらの症例の中で CD26 発現と YS110 治療効果の関係をみると、Stable disease (SD) 以上の効果が見られた上皮型の症例は陽性率が 30%であったが、二相型と肉腫型では陽性率が 1%、2%の症例にも SD が認められた。症例数が少ないため、組織型および CD26 発現と YS110 効果との統計学的な有意な相

関関係は明らかではないが、CD26 陽性率と治療効果には相関関係はなさそうであった。

4) フランスでの第 I 相臨床試験の臨床データを用いた統計解析

YS110 投与前後の血清中 sCD26/DPP4 titer の変動 (V) と抗腫瘍効果 (RECIST) 及び PFS との関連性の解析における変数として、(a) YS110 の投与頻度 (2 週または 1 週に 1 回投与 : Q2W または Q1W)、(b) 投与量 : 体重当たりの投与量 (mg/kg)、(c) 腫瘍の CD26 発現陽性率 (%)、(d) 癌腫 (MPM, 腎がん (RCC))、(e) 性差、等があり、その中で変数 (b) 投与量及び (c) 腫瘍の CD26 発現陽性率 (%) は RECIST 判定及び PFS との関連性がないことが判明している。一つの解析例として、変数 (a) において Q2W 症例数 18 例 (全解析対象 26 例) について、腫瘍計測が不能だった MPM 1 症例を除いた 17 例 (MPM : 11 症例、RCC : 6 症例) を RECIST 評価 SD、PD 症例それぞれ 8 (黒丸) 及び 9 (白丸) 症例で層別し、血清中 sCD26 titer の変動 (%) (Y 軸) と腫瘍量 RECIST 判定の Day43 における変動 (%) (X 軸) の座標に、YS110 投与前後別 Day1post, Day15Pre/Post, Day29Pre/Post に plotting し解析した。その結果、投与頻度 Q2W の場合、Day29Pre (3 回目投与前) において、明らかに Day43 における RECIST 評価を予測することが統計学的有意差 ($p=0.012$) を持って示された。この結果は、血清中 sCD26 titer の変動 V が YS110 の抗腫瘍効果を予測するバイオマーカーであることを示唆している。

5) In vitro での sCD26 産生細胞、及び YS110 が sCD26 産生に与える影響の解析

YS110 の臨床試験から、MPM 患者の血清中 sCD26 titer は YS110 の投与によって顕著に低下することが示された (Br J Cancer. 2017,

Lung Cancer, 2019)。そこで、YS110 が血清中 sCD26 titer を低下させるメカニズムを明らかにするために、YS110 が sCD26 産生に与える影響を *in vitro* で解析した。生体内には T 細胞や血管内皮細胞、上皮細胞、線維芽細胞、脂肪細胞など多様な CD26 陽性細胞が存在し、細胞膜上の CD26 分子を切断して sCD26 を放出させる酵素も明確にはわかっておらず、sCD26 の主な産生源についても明確ではない。そこで CD26 陽性・CD26 陰性 MPM 細胞株及び、CD26 陽性・CD26 陰性正常細胞（非腫瘍細胞）を用いて、*in vitro* で培養上清中に sCD26 が産生されるかを解析した。MPM 細胞株の中で細胞膜上に CD26 を発現していない MST0 parent と JMN CD26-shRNA の培養上清中では sCD26 は検出されなかったが、細胞膜上に CD26 を発現する MST0-CD26、JMN ctrl-shRNA、H226 の培養上清中では sCD26 が検出された。正常細胞においても細胞膜上に CD26 を発現していない乳腺上皮細胞株 MCF10A と臍帯静脈内皮細胞 HUVEC、並びに細胞膜上の CD26 発現が弱い胸膜中皮細胞株 MeT-5A の培養上清中では sCD26 は検出されなかったが、細胞膜上に CD26 を発現する肺線維芽細胞株 TIG-1、皮膚微小血管内皮細胞 HDMVEC の培養上清中では sCD26 が検出された。重要なことに、YS110 を添加して 72 時間培養した培養上清では、MPM 細胞株からも正常細胞からも sCD26 産生が同程度に低下することが示された。

そこで YS110 の容量依存的、経時的な作用を検証した。細胞膜上の CD26 発現が高い MPM 細胞株として MST0-CD26 を、正常細胞として TIG-1 を選択し、YS110 存在下で培養したところ、MST0-CD26、TIG-1 のどちらも YS110 の容量依存的に培養上清中の sCD26 量が減

少した。また、MST0-CD26 を YS110 存在下で 1, 3, 7 日間培養した結果、培養 1 日でも培養上清中に sCD26 が検出され、YS110 による産生量の減少も見られた。

これらの結果から、sCD26 は CD26 を発現する腫瘍からも正常細胞からも産生され、YS110 は腫瘍と正常細胞の両方に作用して、sCD26 産生を容量依存的、経時的に減少させることが示された。この YS110 の作用は、MPM 患者の血清中 sCD26 titer が YS110 投与によって顕著に低下するメカニズムの一つと考えられる。

D. 考察

ヒト化 CD26 抗体の予後・治療効果予測バイオマーカーを開発するために、今年度は国内第 I/II 相臨床試験患者の血清中サイトカイン・ケモカインの多項目解析と、末梢血リンパ球のフェノタイプ解析、免疫チェックポイント分子の発現解析を主に行った。

本年度の解析により、CD26 抗体の予後・治療効果を予測する新規バイオマーカー候補として、血清では SDF-1 α , β /CXCL12 及び MIP-1d/CCL15、また、PR・SD 症例と PD 症例とを判別するマーカー候補として MCP2/CCL8、Gro-b/CXCL2、GCP-2/CXCL6 を見出した。SDF-1 α , β /CXCL12 は CXCR4 と CXCR7 のリガンドであり、リンパ球遊走の他に、白血球活性化や癌増殖、転移促進、血管新生等の機能が報告されている。MIP-1d/CCL15 は CCR1 と CCR3 のリガンドであり、好中球・単球・リンパ球遊走機能が報告されている。今回の解析結果では、CD26 抗体が有効な症例では血清中のこれらのケモカイン濃度がいずれも低値を示しており、今後、これらのケモカインの機能の詳細を調べ、ヒト化 CD26

抗体の作用機序との関係性について考察する必要がある。我々は健常者の末梢血 CD4 T 細胞を用いて、強い CD26 共刺激シグナルが伝達すると転写因子 EGR2 の顕著な発現上昇と IL-10 の高産生が誘導されることを報告している (J Immunol. 2015)。悪性中皮腫細胞自身にも CD26 のリガンドである caveolin-1 が発現しているため、中皮腫周囲に浸潤した T 細胞に CD26 共刺激が伝達して IL-10 の高産生を誘導している可能性が考えられる。ヒト化 CD26 抗体は CD26 に結合して、CD26 と caveolin-1 との結合阻害にも働くことから、免疫抑制性サイトカインである IL-10 の産生抑制に働くことが期待される。

フランスでのヒト化 CD26 抗体の第 I 相臨床試験の結果から、CD26 抗体を投与すると容量依存的に血清中の可溶性 CD26 量および DPPiV 酵素活性が低下するデータを得ている (Br J Cancer. 2017)。このことから、CD26 抗体を投与した場合においても、DPPiV によって切断されるケモカインの量が減少し、ケモカインの活性維持、がん細胞周囲に集積する免疫細胞数の増加が起こる可能性が考えられ、その点に関しても今後の解析が必要とされる。がん微小環境に浸潤した T 細胞は、がん細胞自身が産生する免疫抑制性因子や PD1/PDL1・PDL2、CTLA4/CD80・CD86 に代表される免疫チェックポイント分子シグナルによって、エフェクター機能が抑制されていることが様々ながん種で報告されている。悪性中皮腫患者では末梢血 CD8 T 細胞中の細胞傷害性エフェクター T 細胞 (CD26 陰性 CD28 陰性 CD57 陽性 KLRG1 陽性) の割合が健常者と比較して明らかに高いことが示された。このような perforin などを発現する細胞傷害性

エフェクター T 細胞は本来、ウイルスに感染した細胞やがん細胞を体内から除去するために働く細胞だが、悪性中皮腫患者の末梢血中にどうして細胞傷害活性を有する T 細胞がこれほど多く存在するのか、何の抗原に対して活性化された T 細胞なのか、アスベストばく露による慢性的な炎症が関係しているのかは興味深い疑問である。免疫チェックポイント分子の中で、悪性中皮腫患者の末梢血 CD8 T 細胞は TIGIT の発現陽性率が健常者よりも明白に高く、long SD・PR 症例では特に PD1 と TIGIT の陽性率が高い傾向が見られた。免疫チェックポイント分子の発現は T 細胞の活性化状態や血清中の TGF- β 濃度などと関係していることが予想される。

国内第 I/II 相臨床試験の悪性中皮腫病理組織および正常ヒト組織での CD26 染色性の向上が認められたことから、新規コンパニオン診断キットによる免疫染色法が中皮腫における CD26 発現をより正確に評価するのに適していると考えられた。今後、これらの CD26 陽性率と YS110 療法の効果や既存の治療法や各種臨床パラメーターとの相関について解析する予定である。

フランスでの第 I 相臨床試験の臨床検体データの解析により、YS110 投与前後における血清中 sCD26 titer の変動 (V) が治療効果 (RECIST 判定による直接抗腫瘍効果、及び無増悪生存期間 PFS に対する効果) を予測できるバイオマーカーであることが統計学的に示された。フランスでの第 I 相臨床試験において観察された YS110 投与と V との関係 (YS110 による血清中 sCD26 titer の低下) について、そのメカニズムを解明するために in vitro での検証を行った。CD26 陽性の MPM 細胞株及び CD26 陽性の正常細胞 (非腫瘍細

胞)のどちらもから sCD26 が産生されること、また、YS110 添加により腫瘍、正常細胞のどちらに対しても YS110 の容量依存的に sCD26 産生が阻害されることが示された。この結果は、YS110 の臨床試験で観察される YS110 投与後の血清中 sCD26/DPP4 titer の顕著な低下の理由の一つと考えられる。フランスでの第 I 相臨床試験の血清中 sCD26/DPP4 titer の結果では、YS110 を投与した当日に大幅に減少し、次に YS110 を投与するまでの間に sCD26/ DPP4 titer は徐々に回復し、YS110 を投与すると再び減少する変動パターンを示している (Br J Cancer. 2017)。YS110 投与直後の Day1Post, Day15Post, Day29Post ではいずれも SD 症例と PD 症例の間で血清中 sCD26/DPP4 titer に有意な差は見られなかった。一方で、2 週に一度の頻度で YS110 を投与して 3 回目の抗体を投与する前 (Day29Pre) の血清中 sCD26/DPP4 titer は、PD 症例と比較して SD 症例で有意に低いことが示された。これらの結果から、SD/PD に関わらず YS110 投与直後は血清中 sCD26/DPP4 titer は同等に低下するが、YS110 投与後の血清中 sCD26/DPP4 titer の回復が SD 症例と比較して PD 症例では早い、もしくは強いことが考えられる。YS110 を投与して一度低下した血清中 sCD26/ DPP4 titer のその後の回復の違いが、何を反映した結果なのかについて今後解析していく必要がある。

E. 結論

1) 国内第 I/II 相臨床試験患者の血清中サイトカイン・ケモカインの多項目解析を行い、ヒト化 CD26 抗体の予後・治療効果予測バイオマーカー候補として、SDF-1, MIP-1d, MCP2, Gro-b, GCP-2 を見出した。また、国内第 I/II

相臨床試験患者の末梢血リンパ球のフェノタイプ解析により、CD26 抗体有効例では特に CD8 T 細胞で細胞傷害性エフェクター T 細胞 (CD26 陰性・CD28 陰性・KLRG1 陽性サブセット) の割合が高く、免疫チェックポイント分子の中で PD1 と TIGIT の発現陽性率が高い可能性を見出した。

2) 臨床試験における悪性中皮腫検体における CD26 発現評価を行い、半定量的解析法を確立した。また CD26 抗体療法におけるコンパニオン診断キットの開発に成功した。

3) ヒト化抗 CD26 モノクローナル抗体 (YS110) による悪性胸膜中皮腫を主たる対象としたフランスにおける第 I 相臨床試験により得られた、YS110 投与に伴う血清中溶存 CD26/DPP4 (sCD26/DPP4) titer の変動を詳細に解析した結果、CD26 抗体の予後・治療効果を予測するバイオマーカーとして有用である可能性が得られた。細胞膜上の CD26 の発現が高い細胞であれば腫瘍・正常細胞ともに培養上清中に sCD26 を産生し、YS110 の容量依存的、及び経時的に sCD26 の産生が阻害されることを明らかにした。

F. 健康危険情報

現時点では特記すべき健康危険情報は無い。

G. 今後の展望

1) 今年度の解析で得られた血清中の新規バイオマーカー候補について sandwich ELISA で個別に測定を行い、今回の Bio-Plex システムでの結果の再現性を確認する。また、中皮腫病理組織を用いて腫瘍浸潤リンパ球のフェノタイプ解析を行い、末梢血 T 細胞のフェノタイプとの関係性や、ヒト化 CD26 抗体の治療有効性との相関関係を解析し、予後・

治療効果バイオマーカーを確立する。

2) 悪性中皮腫における CD26 発現について免疫染色にて評価し、組織型とともに発現パターン（細胞局在、陽性率、陽性強度などの各種パラメーター）を詳細に定量評価することにより、抗体療法の効果や予後などとの関連性あるいは臨床パラメーターを検証する基礎を構築していく。腫瘍組織の DNA・RNA profile 解析を行い、YS110 の効果との関係を解析する。

3) YS110 の抗腫瘍作用メカニズムの更なる解明を目指し、腫瘍細胞膜上の CD26 に YS110 が結合してから核内まで移行するメカニズムの詳細を検討する。また、YS110 投与後に一度低下した血清中 sCD26/DPP4 titer のその後の回復の違いが何を反映した結果であるのかを明らかにし、血清中 sCD26/DPP4 titer の変動解析が YS110 の予後・治療効果を予測するバイオマーカーとして有用であることをより確かなものにする。

H. 研究発表

1. 論文発表

- 1) Itoh T, Hatano R, Komiya E, Otsuka H, Narita Y, Aune TM, Dang NH, Matsuoka S, Naito H, Tominaga M, Takamori K, Morimoto C, Ohnuma K. Biological effects of IL-26 on T cell-mediated skin inflammation including psoriasis. *J Invest Dermatol.* 2019; 139(4): 878-889
- 2) Santos MF, Rappa G, Karbanova J, Vanier C, Morimoto C, Corbeil D, Lorico A. Anti-human CD9 antibody Fab fragment impairs the internalization of extracellular vesicles and the nuclear transfer of their cargo proteins. *J Cell Mol Med.* 2019; 23(6): 4408-4421
- 3) Mezawa Y, Daigo Y, Takano A, Miyagi Y, Yokose T, Yamashita T, Morimoto C, Hino O, Orimo A. CD26 expression is attenuated by TGF- β and SDF-1 autocrine signaling on stromal myofibroblasts in human breast cancers. *Cancer Med.* 2019; 8(8): 3936-3948
- 4) Hatano R, Yamada T, Madokoro H, Otsuka H, Komiya E, Itoh T, Narita Y, Iwata S, Yamazaki H, Matsuoka S, Dang NH, Ohnuma K, Morimoto C. Development of novel monoclonal antibodies with specific binding affinity for denatured human CD26 in formalin-fixed paraffin-embedded and decalcified specimens. *PLoS One.* 2019; 14(6): e0218330
- 5) Hatano R, Itoh T, Otsuka H, Okamoto S, Komiya E, Iwata S, Aune TM, Dang NH, Kuwahara-Arai K, Ohnuma K, Morimoto C. Characterization of novel anti-IL-26 neutralizing monoclonal antibodies for the treatment of inflammatory diseases including psoriasis. *MAbs.* 2019; 11(8): 1428-1442
- 6) Hayashi M, Madokoro H, Yamada K, Nishida H, Morimoto C, Sakamoto M, Yanagawa H, Yamada T. Novel Antibody-Drug Conjugate with Anti-CD26 Humanized Monoclonal Antibody and Transcription Factor I1H(TFI1H) Inhibitor, Triptolide, Inhibits Tumor Growth via Impairing mRNA Synthesis. *Cancers (Basel).* 2019; 11(8): E1138
- 7) Takeda T, Ohe Y, Horinouchi H, Hida T,

- Shimizu J, Seto T, Nosaki K, Kishimoto T, Miyashita I, Yamada M, Kaneko Y, Morimoto C, Nakagawa K. Phase I study of YS110, a recombinant humanized monoclonal antibody to CD26, in Japanese patients with advanced malignant pleural mesothelioma. *Lung Cancer* 2019; 137: 64-70
- 8) Sato T, Tatekoshi A, Takada K, Iyama S, Kamihara Y, Jawaid P, Rehman MU, Noguchi K, Kondo T, Kajikawa S, Arita K, Wada A, Murakami J, Arai M, Yasuda I, Dang NH, Hatano R, Iwao N, Ohnuma K, Morimoto C. DPP8 is a novel therapeutic target for multiple myeloma. *Sci Rep.* 2019; 9(1): 18094
- 9) Ohnuma K, Hatano R, Dang NH, Morimoto C. Rheumatic diseases associated with immune checkpoint inhibitors in cancer immunotherapy. *Mod Rheumatol.* 2019; 29(5): 721-732
- 10) Nishida H, Yamada T. Monoclonal Antibody Therapies in Multiple Myeloma: A Challenge to Develop Novel Targets. *J Oncol.* 2019; 2019: 6084012
- 11) Amatya VJ, Kushitani K, Mawas AS, Miyata Y, Okada M, Kishimoto T, Inai K, Takeshima Y. Reply to 'MUC4 staining in sarcomatoid carcinomas' by Berg et al. *Mod Pathol.* 2019; 32(1): 158
- 12) Sato H, Soh J, Aoe K, Fujimoto N, Tanaka S, Nanba K, Torigoe H, Shien K, Yamamoto H, Tomida S, Tao H, Okabe K, Kishimoto T, Toyooka S. Droplet digital PCR as a novel system for the detection of microRNA-34b/c methylation in circulating DNA in malignant pleural mesothelioma. *Int J Oncol.* 2019; 54(6): 2139-2148
- 13) Nagamatsu Y, Oze I, Aoe K, Hotta K, Kato K, Nakagawa J, Hara K, Kishimoto T, Fujimoto N. Physician requests by patients with malignant pleural mesothelioma in Japan. *BMC Cancer* 2019; 19(1): 383
- 14) Takada K, Fujimoto N, Ozeki T, Nishimura J, Miyamoto Y, Asano M, Fuchimoto Y, Wada S, Ozaki S, Igawa T, Sonobe H, Kishimoto T. Small intestinal intussusception in an adult. *J Clin Pathol.* 2019; 72(7): 510
- 15) Okada M, Kijima T, Aoe K, Kato T, Fujimoto N, Nakagawa K, Takeda Y, Hida T, Kanai K, Imamura F, Oizumi S, Takahashi T, Takenoyama M, Tanaka H, Hirano J, Namba Y, Ohe Y. Clinical Efficacy and Safety of Nivolumab: Results of a Multicenter, Open-label, Single-arm, Japanese Phase II study in Malignant Pleural Mesothelioma (MERIT). *Clin Cancer Res.* 2019; 25(18):5 485-5492
- 16) Kishimoto T, Fujimoto N, Ebara T, Omori T, Oguri T, Niimi A, Yokoyama T, Kato M, Usami I, Nishio M, Yoshikawa K, Tokuyama T, Tamura M, Yokoyama Y, Takahashi S, Abdelsied M, Alexander W T, Alexander D B, Tsuda H. Serum levels of the chemokine CCL2 are elevated in malignant pleural mesothelioma patients. *BMC Cancer.* 2019; 19(1): 1204
- 17) Fujimoto N. Immunocheckpoint Blockade in Malignant Pleural Mesothelioma. *IntechOpen.* DOI: 10.5772/intechopen.

89116. (September 5th, 2019)

- 18) 岩尾憲明, 大沼圭, 波多野良, 大塚春奈, 古宮栄利子, 伊藤匠, 森本幾夫. GVHD の発症と慢性炎症. 別冊 Bio Clinica: 慢性炎症と疾患, 2019; 8(1): 120-125
- 19) 岸本卓巳. 石綿 (アスベスト) が人体に与える影響. 産業保健 21. 2019; 25(1): 5-7
- 20) 岸本卓巳, 藤本伸一, 加藤勝也, 井内康輝. 石綿関連疾患の診断と治療 Diagnosis and treatment of asbestos related diseases. 産業医学レビュー. 2019; 32(2): 99-130
- 21) 藤本伸一. 石綿 (アスベスト) 関連肺・胸膜疾患の的確な診断と新規治療法の導入. 産業保健 21. 2019; 25(1): 17
- 22) 藤本伸一. 胸膜・腹膜の病理 胸膜・腹膜疾患への臨床的アプローチ -治療を中心として-. 病理と臨床 2019; 37(11): 1055-1061

2. 著書

- 1) Okamoto T, Hatano R, Nakano K, Yamada T, Yamazaki H, Kaneko Y, Dang NH, Morimoto C, Ohnuma K. Regulation of proliferation of malignant mesothelioma cells by CD26-cyclophilin A molecular complex. In: Advanced in Medicine and Biology. Nova Science Publishers, Inc., Hauppauge, NY, Editor: Leon V. Berhardt, 2019; Volume 156: Chapter 8: 165-185

3. 学会発表

- 1) Komiya E, Hatano R, Itoh T, Otsuka H, Ohnuma K, Tominaga M, Morimoto C,

Takamori K. CD26/DPPIV regulates mechanical itch by enzymatic degradation of mu-opioid receptor ligands. 24th World Congress of Dermatology (WCD), Milan, 2019.6.15

- 2) Komiya E, Hatano R, Itoh T, Otsuka H, Kamata Y, Honda K, Toyama S, Moniaga CS, Ohnuma K, Tominaga M, Morimoto C, Takamori K. Possible role for CD26/DPPIV in regulating mechanical itch (Alloknesis). 28th European Academy of Dermatology and Venereology (EADV) Congress, Madrid, 2019.10.9
- 3) Komiya E, Hatano R, Itoh T, Otsuka H, Kamata Y, Honda K, Toyama S, Moniaga CS, Ohnuma K, Tominaga M, Morimoto C, Takamori K. Possible regulation of mechanical itch by CD26/DPPIV. 10th World Congress on Itch (WCI), Sydney, 2019.11.17
- 4) 古宮栄利子, 富永光俊, 波多野良, 伊藤匠, 大塚春奈, 本田耕太郎, 外山扇雅, 鎌田弥生, 大沼圭, 森本幾夫, 高森建二. 加齢皮膚で誘発される機械的かゆみ調節機構の解明. 第15回加齢皮膚医学研究会, 熊本, 2019年3月9日
- 5) Hiroko Nishida, Mutsumi Hayashi, Chikao Morimoto, Michiie Sakamoto, Taketo Yamada. CD26 is a potential therapeutic target by humanized monoclonal antibody in multiple myeloma. 第108回日本病理学会総会, 東京, 2019年5月10日
- 6) 古宮栄利子, 波多野良, 富永光俊, 伊藤匠, 鎌田弥生, 本田耕太郎, 外山扇雅, カタリナサギタモニアガ, 大沼圭,

森本幾夫, 高森建二. CD26/
dipeptidyl- peptidase IV は機械的か
ゆみの抑制因子である. 第 24 回 日本
病態プロテアーゼ学会, 岐阜, 2019 年
8 月 2 日

- 7) 山田健人, 坂元亨宇, 森本幾夫, 林睦.
Anti-CD26 humanized antibody-triptolide
conjugate transports into nucleus and
inhibits RNA polymerase II activity. 第 78
回 日本癌学会学術総会, 京都, 2019 年
9 月 27 日
- 8) Hiroko Nishida, Mustumi Hayashi, Chikao
Morimoto, Michiie Sakamoto, Taketo
Yamada. Humanized anti-CD26
monoclonal antibody clonogenic side
population cells in multiple myeloma. 第
81 回 日本血液学会学術集会, 東京,
2019 年 10 月 12 日
- 9) Hayashi M, Madokoro H, Yamada T.
Anti-CD26 Humanized Monoclonal
Antibody Conjugated to Triptolide
Inhibits Tumor Cell Growth via
Transportation into Nucleus and Impaired
RNA Polymerase II. 第 42 回日本分子生
物学会年会, 福岡, 2019 年 12 月 3 日

H. 知的財産権の出願・登録状況（予定を含む）

1. 特許取得
大沼圭, 森本幾夫, 波多野良: 免疫チ
ェックポイント阻害剤. 特願
2019-004480
2. 実用新案登録
なし
3. その他
なし

II. 分担研究報告

労災疾病臨床研究事業費補助金

分担研究報告書

ヒト化 CD26 抗体の予後・治療効果予測バイオマーカーの探索：
国内第 I/II 相臨床試験の血清および末梢血リンパ球の解析結果について

研究代表者	森本 幾夫	順天堂大学大学院医学研究科 免疫病・がん先端治療学講座 特任教授
研究分担者	岸本 卓巳	独立行政法人労働者健康安全機構 アスベスト疾患研究・研修センター 所長
研究分担者	山田 健人	埼玉医科大学医学部 病理学 教授
研究協力者	波多野 良	順天堂大学大学院医学研究科 免疫病・がん先端治療学講座 特任助教
研究協力者	大沼 圭	順天堂大学大学院医学研究科 免疫病・がん先端治療学講座 准教授
研究協力者	藤本 伸一	岡山労災病院 腫瘍内科部長
研究協力者	青江 啓介	山口宇部医療センター 腫瘍内科 内科系診療部長

研究要旨

悪性胸膜中皮腫はアスベストばく露によって起こる難治性悪性腫瘍であり、現時点で満足できる治療法はなく、新たな治療法の確立が望まれる。われわれは、新規治療標的分子として悪性胸膜中皮腫に発現する CD26 に着目し、ヒト化 CD26 抗体を開発しフランスにて第 I 相臨床試験を行った。安全性が確認され治療薬としての有効性を示唆する結果も得られ、2017 年 7 月から国内で第 I/II 相臨床試験を開始した。2018 年 3 月に第 I 相臨床試験最終患者への投与が終了し、同年 6 月からスタートした第 II 相臨床試験も患者のリクルートが順調に進み、2019 年中に最終患者への投与が終了し、現在結果を集計中である。今年度は国内第 I/II 相臨床試験患者の血清中サイトカイン・ケモカインの多項目解析を行い、SDF-1, MIP-1d, MCP2, Gro-b, GCP-2 等が CD26 抗体の有効性を予測する新規バイオマーカー候補になる可能性を見出した。また、国内第 I/II 相臨床試験患者の末梢血リンパ球のフェノタイプ解析により、CD26 抗体有効例では特に CD8 T 細胞で細胞傷害性エフェクター T 細胞(CD26 陰性・CD28 陰性・KLRG1 陽性サブセット)の割合が高く、免疫チェックポイント分子の中で PD1 と TIGIT の発現陽性率が高い可能性を見出した。これらバイオマーカー候補について次年度に更なる検証を行うとともに、中皮腫病理組織を用いた解析を追加し、ヒト化 CD26 抗体の予後・治療効果バイオマーカーを同定する。

A. 研究目的

悪性胸膜中皮腫はアスベストばく露によ

って起こる胸膜中皮由来の難治性悪性腫瘍
である。アスベストばく露から発症までの潜

伏期間は 30-50 年とされ、日本を含めアジアやヨーロッパなど世界規模で患者数は今後ますます増加すると考えられている。予後は極めて悪く、手術療法、化学療法、放射線療法などが行われるが、いずれも満足できる治療成績ではなく、新たな治療法の確立が望まれる。われわれは、新規治療標的分子として悪性中皮腫細胞に発現する CD26 に着目し、ヒト化 CD26 抗体を開発してフランスにて悪性中皮腫を中心に First-in-Human 第 I 相臨床試験を行った。Infusion reaction (急性輸注反応)を除いて特記すべき副作用もなく、安全性が確認されるとともに、抗がん剤抵抗性の悪性中皮腫患者 19 例中 10 例が modified RESIST 評価で Stable Disease (SD)となり、そのうち 5 例は 6 ヶ月以上、最長で投与を開始してから 399 日 SD が持続し、治療薬としての有効性を示唆する結果も得られた(Br J Cancer. 2017)。

このフランスでの第 I 相臨床試験の結果を受け、いかなる患者が CD26 抗体療法の適用となるのか、CD26 抗体療法の治療効果や予後を予測できるバイオマーカーの探索が課題として挙げられた。このことは、本抗体療法がより安全かつ効果的に行われるうえで極めて重要であり、かつ、抗体療法適用患者を適切に選択できれば期待していた治療効果が得られない患者にまで高額な抗体医薬の医療費負担を強いることがなくなる。

我々はこれまでにヒト化 CD26 抗体の抗腫瘍作用メカニズムとして、抗体医薬特有の抗体依存性細胞傷害(ADCC)活性・補体依存性細胞傷害(CDC)活性に加え、CD26 陽性腫瘍に抗体が結合することによる直接的な作用があることを明らかにしてきた。がん細胞の細胞膜上の CD26 にヒト化 CD26 抗体が

結合すると、cyclin dependent kinase inhibitor である p21 や p27 の発現が上昇し cell cycle arrest を起こさせること(Clin Cancer Res. 2001, Immunology. 2002, Clin Cancer Res. 2007, Cancer Cell Int. 2016)、CD26 抗体と CD26 の複合体が細胞膜から細胞質、さらに核内へと移行し、RNA polymerase II のサブユニットである POLR2A 遺伝子の転写領域下流に結合することで POLA2A の転写を抑制し増殖抑制に働くことを明らかにした(PLoS One. 2013)。

また、CD26 はヒト T 細胞に活性化シグナルを伝達する T 細胞共刺激分子でもあり、ヒト化 CD26 抗体は CD26 のリガンドである caveolin-1 と CD26 との結合、つまりは T 細胞への CD26 共刺激シグナルの伝達をブロックする。また、CD26 の機能の一つに dipeptidyl peptidase IV (DPPIV)酵素活性があり、N 末から 2 番目にプロリンまたはアラニンを含むペプチドの 2 アミノ酸を切断する。生体内で様々な生理活性物質がその基質となることが知られているが、いくつかのケモカインも DPPIV による切断を受けその細胞遊走活性が不活性化される。ヒト化 CD26 抗体は DPPIV 酵素活性自体に直接は影響しないが、フランスでの第 I 相臨床試験の結果から CD26 抗体の投与により血中の可溶性 CD26 の量が顕著に低下し、DPPIV 酵素活性も同様に低下することが示されている(Br J Cancer. 2017)。DPPIV 酵素活性の低下により IP-10(CXCL10)や Eotaxin (CCL11)などのケモカインの切断と不活性化が抑えられ、免疫細胞が腫瘍組織に遊走しやすくなる可能性が考えられる(Nat Immunol. 2015, Nat Immunol. 2019)。これらの知見から、CD26 抗体は免疫系にも影響

する可能性が強く示唆される。

そこで、これまでに我々が解明してきた CD26 抗体の抗腫瘍作用メカニズムに基づき、本抗体の予後・治療効果予測バイオマーカーを同定するために、2017年7月から本邦で開始した治療抵抗性(標準治療で Progressive Disease (PD))の悪性胸膜中皮腫に対するヒト化 CD26 抗体の第 I/II 相臨床試験患者の(1)中皮腫病理組織、(2)血清、(3)末梢血リンパ球の解析を行う。(1)中皮腫病理組織に関しては、中皮腫の CD26 発現、病理学的パラメーター(組織型、細胞増殖期率、核内 p53 発現、脈管侵襲など)と CD26 抗体の有効性との相関関係を解析する。(2)血清に関しては、フランスでの第 I 相臨床試験患者の血清を解析した結果、CD26 抗体投与による血清中可溶性 CD26 値および DPPIV 酵素活性の変動解析は、CD26 抗体の治療効果予測バイオマーカーとなる可能性が示唆され($p < 0.016$)、国内臨床試験患者の検体を用いて検証を行う。また、前に述べたように CD26 抗体は T 細胞への CD26 共刺激シグナルの伝達阻害ならびに DPPIV 酵素活性の低下にも作用するため、免疫系にも何かしらの影響があることが予想される。そのため、CD26/DPPIV と関連するサイトカイン・ケモカインの多項目解析を行い、悪性中皮腫に特徴的なサイトカイン・ケモカインの解明、さらに CD26 抗体投与による血清中濃度の変動を解析し、CD26 抗体の有効性との相関関係を解析する。(3)末梢血リンパ球に関しては、末梢血中の CD4 T 細胞・CD8 T 細胞・CD25 強陽性の制御性 CD4 T 細胞の細胞数・割合、CD26 および CXCR3(ケモカイン CXCL10 の受容体)の発現、Perforin や Granzyme といったがん細胞や感染細胞

を除去するための細胞傷害活性を有するエフェクター T 細胞の細胞数・割合、近年着目されている代表的な免疫チェックポイント分子の発現を解析し、CD26 抗体の有効性との相関関係を解析する。

2017年7月から開始した第 I 相臨床試験は、2018年3月に最終患者への投与が終了し(第 1~3 コホート各 3 例、全 9 例)、免疫チェックポイント阻害薬で報告されているような自己免疫疾患様の重篤な副作用が出ることなく、安全性が確認された。また、抗腫瘍効果としても全 9 例中抗腫瘍効果評価可能例は 6 例で、内訳は Partial Response (PR) 1 例、SD 4 例、PD 1 例と、フランスでの第 I 相臨床試験と同様に有効性を強く示唆する結果が得られた(Lung Cancer, 2019)。2018年6月から第 II 相臨床試験がスタートし、患者のリクルートも順調に進み 2019 年中に全 31 例への投与が終了、現在結果を集計中である。まだ第 II 相臨床試験の結果は公表されていないため、本報告書においても PR・SD・PD 症例の具体的な n 数に関しては記載ができないが、今年度の本パートでは、健常者と国内第 I/II 相臨床試験患者の(2)血清と(3)末梢血リンパ球を用いて、血清中サイトカイン・ケモカインの多項目解析と、末梢血リンパ球のフェノタイプ及びサブセット解析を行った。

B. 研究方法

1) 国内第 I/II 相臨床試験プロトコル

第 I 相臨床試験はヒト化 CD26 抗体を 2mg/kg, 4mg/kg, 6mg/kg でそれぞれ 3 例ずつ、初回投与日を day1 として day1, day8, day15, day22, day29 まで週 1 回の間隔で 5 回静脈内投与を行い、投与を開始してから 6

週間後(day42)の時点で医師による抗腫瘍効果の判定が行われ、PR または SD と判定された患者は、上記の抗体 5 回投与、6 週間後に抗腫瘍効果判定を 1 サイクルとして PD になるまでサイクルを継続した。

第 II 相臨床試験は全 31 例に CD26 抗体を 6mg/kg で週 1 回の間隔で 5 回静脈内投与を行い、上記と同様に抗体 5 回投与、6 週間後に抗腫瘍効果判定を 1 サイクルとして PD になるまでサイクルを継続した。

2) Bio-Plex マルチプレックスアッセイ

成人健常者および国内第 I/II 相臨床試験患者の CD26 抗体初回投与前(day1pre)・投与後(day1post)・3 回目投与前(day15pre)・投与後(day15post)・5 回目投与前(day29pre)・投与後(day29post)の 6 time point で血清の提供を受け、血清中サイトカイン・ケモカイン濃度を Bio-Plex マルチプレックスシステムにより測定した。Bio-Plex Pro Human Chemokine 40-Plex panel および Bio-Plex Pro Human Th17 Cytokine 15-Plex panel (Bio-Rad)を用いて、付属のプロトコルに従い Bio-Plex system (Bio-Rad)で測定を行い、得られたデータを Bio-Plex Manager (Bio-Rad)で解析した。

3) 抗体と試薬

Flow cytometry には下記のヒト抗原特異抗体を用いた。PE-labeled anti-CD26 mAb (clone M-A261)は BD Biosciences から購入した。PE/Cy7-labeled anti-KLRG1 mAb (clone 13F12F2), PE/Cy7-labeled anti-TIGIT mAb (clone MBSA43), APC-labeled anti-KLRG1 mAb (clone 13F12F2), APC-labeled anti-TIGIT mAb (clone MBSA43)

及び APC-labeled anti-LAG3 mAb (clone 3DS223H)は eBioscience から購入した。FITC-labeled anti-CD4 mAb (clone RPA-T4), FITC-labeled anti-CD8 mAb (clone HIT8a), PE/Cy7-labeled anti-CD25 mAb (clone clone M-A251), PE/Cy7-labeled anti-CD28 mAb (clone clone CD28.2), PE/Cy7-labeled anti-CD56 mAb (clone 5.1H11), PE/Cy7-labeled anti-PD1 mAb (clone EH12.2H7), APC-labeled anti-CD28 mAb (clone clone CD28.2), APC-labeled anti-CD57 mAb (clone clone HCD57), APC-labeled anti-CXCR3 mAb (clone G025H7), APC-labeled anti-TRAIL mAb (clone RIK-2), APC-labeled anti-BTLA mAb (clone MIH26), APC-labeled anti-PD1 mAb (clone EH12.2H7), APC-labeled anti-Tim3 mAb (clone F38-2E2)及び抗体の非特異的な結合をブロックするための Human TruStain FcX は BioLegend から購入した。

4) フローサイトメトリー

成人健常者および国内第 I/II 相臨床試験患者から提供を受けた末梢血を、BD Pharm Lyse Lysing Buffer (BD Biosciences)にて溶血処理を行い、洗浄した後、Human TruStain FcX を添加し、続いて蛍光色素で標識した各種抗体を添加して細胞膜上の目的タンパク質の染色を行った。FACS Calibur (BD Biosciences)で測定を行い、得られたデータを FlowJo (BD Biosciences)で解析した。

(倫理面への配慮)

成人健常者ならびに岡山労災病院、山口宇

部医療センターの悪性胸膜中皮腫患者・良性石綿胸水患者の末梢血を用いた研究については、森本が講座責任者である順天堂大学大学院医学研究科、岸本・藤本が勤務する岡山労災病院、青江が勤務する山口宇部医療センターそれぞれの施設で、本研究を行うための研究計画書等を倫理審査委員会へ提出し、承認を得ている(順大医倫第 2018127 号、岡山労災病院 115 号、山口宇部医療センター 29-21 号)。また、ヒト化 CD26 抗体の国内第 I/II 相臨床試験の患者検体を用いたバイオマーカー探索研究については、臨床試験審査委員会、各治験実施施設内の治験審査委員会にて、試験の実施と合わせてバイオマーカー探索用採血・腫瘍組織検体の提供について協議され、実施承認を取得済みである。末梢血の提供を受ける際には、研究対象者に対する人的擁護上の配慮及び研究により研究対象者が受ける不利益、利益等の説明を行い、書面でのインフォームド・コンセントを得ている。

C. 研究結果

1) 国内第 I/II 相臨床試験患者の血清中サイトカイン・ケモカインの多項目解析

本研究課題の目的は、ヒト化 CD26 抗体の予後・治療効果を予測可能なバイオマーカーを探索することである。そのために、CD26 抗体の投与によって PR もしくは SD が長期間持続した症例を区別して解析を行う必要があり、今回の解析では長期間持続のラインを 4 サイクル(24 週間)以上に設定した。つまりは、CD26 抗体投与を開始して 24 週間以上 PR または SD が持続した症例を long SD・PR、SD の持続期間が 6 週間以上 24 週間未満の症例を short SD、抗体投与

を開始して 6 週間後の抗腫瘍効果判定で PD だった症例は PD 症例として解析を行った。まだ第 II 相臨床試験の結果は公表されていないため、long SD・PR、short SD、PD それぞれの具体的な症例数に関してまだ記載はできない。まず、血清に関しては、第 I 相全 9 例・第 II 相全 31 例の計 40 例のうち、バイオマーカー解析の同意を得られたのが 29 例で、そのうち 4 例は抗腫瘍効果の評価が不可であった。Bio-Plex システムによりサイトカイン・ケモカイン 49 種類の多項目測定を行い、抗腫瘍効果評価可能 25 症例を解析した結果、ケモカイン SDF-1 α , β /CXCL12 及び MIP-1d/CCL15 の血清中濃度が、悪性中皮腫患者の中で特に PD 症例で高値を示し、一方で long SD・PR 症例では低値を示す傾向が見られた(図 1)。図中には各群の CD26 抗体初回投与前(day1pre)・3 回目投与前(day15pre)・5 回目投与前(day29pre)の 3 time point の平均値を示した。

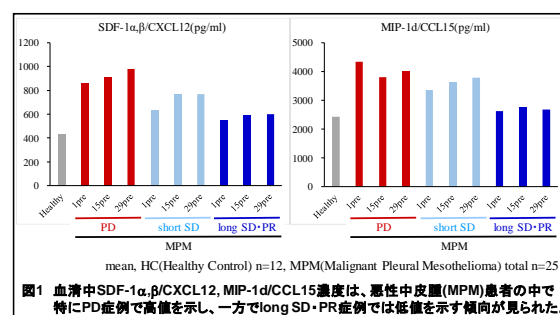
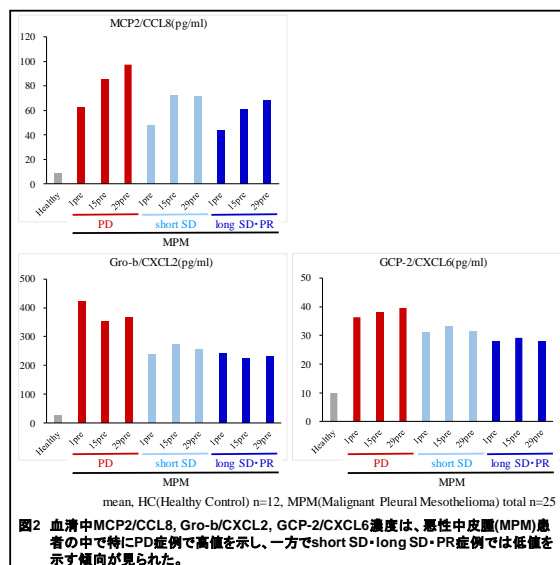


図1 血清中SDF-1 α , β /CXCL12, MIP-1d/CCL15濃度は、悪性中皮腫(MPM)患者の中で特にPD症例で高値を示し、一方でlong SD・PR症例では低値を示す傾向が見られた。

また、long SD・PR 症例と short SD 症例との間で大きな差は見られないが、ケモカイン MCP2/CCL8、Gro-b/CXCL2、GCP-2/CXCL6 の血清中濃度が、悪性中皮腫患者の中で特に PD 症例で高値を示したのに対し、short SD 症例と long SD・PR 症例では比較的に低値を示す傾向が見られた(図 2)。この

ことから、これらの因子は CD26 抗体が有効ではない PD 症例と、CD26 抗体による抗腫瘍効果が少なくとも一定期間以上認められる症例(short SD を含む SD 症例及び PR 症例)との判別には有用である可能性が期待される。



興味深いことに、図 2 中の MCP2/CCL8 のように CD26 抗体初回投与前(day1pre)と比較して 3 回目投与前(day15pre)・5 回目投与前(day29pre)の方が血清中の濃度が明らかに増加しているサイトカイン・ケモカインがあり、反対に CD26 抗体の投与によって血清中の濃度が明らかに減少するサイトカイン・ケモカインも見られた(データ未掲載)。それらの因子は CD26 抗体の抗腫瘍効果を予測できるバイオマーカーとしては有用ではなかったが、CD26 抗体を投与した患者の 7-8 割に共通した変化であり、CD26 抗体が免疫系に与える影響として今後も着目する必要があると思われる。Bio-Plex システムによる多項目解析は、少ない検体量で多項目を同時に高感度で測定できる利点があるが、今回選んだ因子に関して sandwich ELISA

での測定も加え、結果の信頼性をより強固にする必要がある。

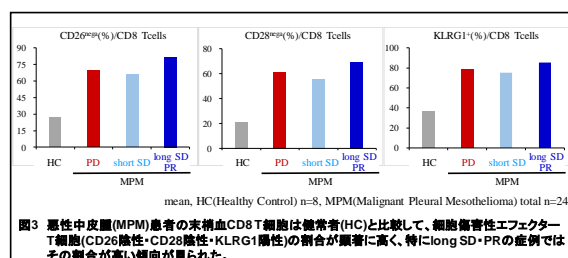
2) 国内第 I/II 相臨床試験患者の末梢血リンパ球のフェノタイプ解析

次に、末梢血リンパ球に関して、成人健常者 8 例及び国内第 I/II 相臨床試験患者の末梢血を用いて、フローサイトメトリーによるフェノタイプの比較を行った。末梢血リンパ球に関しては、第 I 相全 9 例・第 II 相全 31 例の計 40 例のうち、バイオマーカー解析の同意を得られたのが 28 例で、そのうち 4 例は抗腫瘍効果の評価が不可であった。血清は day1・day15・day29 の time point で解析を行うことができたが、末梢血リンパ球の解析は CD26 抗体初回投与前 1 点のみ解析を行った。

まず、末梢血単核球中の CD4 T 細胞・CD4⁺CD25^{high} 制御性 T 細胞・CD8 T 細胞・NK 細胞・単球の細胞数及び割合と、long SD・PR 症例との間に共通した傾向が見られるか解析を行ったが、いずれも特徴的な相関は認められなかった(データ未掲載)。

次に、細胞傷害性エフェクター T 細胞の割合に着目した。CD26 は健常者の末梢血 CD4 T 細胞、CD8 T 細胞ともに、CD26 高発現(CD26^{high})・CD26 低発現(CD26^{low/int})・CD26 陰性(CD26^{nega})の三相性の特徴的な発現パターンを示し、それぞれが Naive・Central Memory・Effector Memory・Terminal Effector といった T 細胞の分化段階と密接に関係している(Immunology. 2013)。代表的な T 細胞共刺激分子である CD28 と組み合わせ CD26/CD28 の発現分布を解析した結果、悪性中皮腫患者の CD4 T 細胞は、約半数の患者は健常者と同等の発現パターンを示したが、約半数は健常者と比較して

CD26^{neg}CD28^{neg} の割合が多かった(昨年度報告書に記載)。CD8 T 細胞の CD26/CD28 の発現分布を解析した結果、意外なことに、ほとんどの悪性中皮腫患者の末梢血 CD8 T 細胞は、Terminal Effector を意味する CD26^{neg}CD28^{neg} の割合が非常に高く、健常者と比較して末梢血中の CD8 T 細胞が異常に活性化した状態にあることが示唆された(昨年度報告書に記載)。極少数例(28 例中 3 例)は、健常者と同等の発現パターンを示した。これらの結果から、悪性中皮腫患者の末梢血 T 細胞、特に CD8 T 細胞は健常者と比較して CD26 陰性の割合が高いことが示された。そこで、血清の解析と同様に、PD、short SD、long SD・PR に分類して解析を行った結果、健常者と比較して悪性中皮腫患者の末梢血 CD8 T 細胞は、細胞傷害性エフェクター T 細胞のマーカーである CD26 陰性・CD28 陰性の割合が顕著に高いが、特に long SD・PR 症例ではその割合が高い傾向が見られた(図 3)。また、抗原感作マーカーである KLRG1 の陽性率においても、特に long SD・PR 症例ではその割合が高い傾向が見られ(図 3)、細胞傷害性エフェクター T 細胞マーカーである CD57 の陽性率においても同様の傾向が見られた(データ未掲載)。



近年、免疫系に抑制シグナルを伝達するチェックポイント分子をブロックすることで

腫瘍免疫を活性化させる免疫チェックポイント阻害薬が新たながん治療法として非常に注目されている。多くの総説で取りあげられ注目されている免疫チェックポイント分子として、既に治療薬として承認されている CTLA4, PD1 に加え、現在臨床試験が行われている LAG3、その他 TIM3, TIGIT, BTLA, CD160, 2B4(CD244)、また、ATP を分解してアデノシンを産生する酵素活性を有する CD39, CD73 などがある。健常者、悪性中皮腫患者ともに末梢血 CD4 T 細胞・CD8 T 細胞に CTLA4, LAG3, CD160 はほとんど発現しておらず(陽性率 0-3%)、TIM3 と BTLA の発現陽性率も 5%未満と非常に低かった(データ未掲載)。一方、PD1, TIGIT, 2B4, CD39, CD73 は明確な発現が認められた(データ未掲載)。

今回の CD26 抗体の国内第 I/II 相臨床試験には、抗ヒト PD1 抗体ニボルマブを投与して無効だったニボルマブ無効例の患者も含まれている(まだ第 II 相臨床試験の結果は公表されていないため、具体的な症例数は記載不可)。末梢血 CD4 T 細胞・CD8 T 細胞の PD1 陽性率を解析した結果、以前にニボルマブを投与した経験のあるニボルマブ無効例では CD4 T 細胞・CD8 T 細胞ともに PD1 の陽性率が極端に低かった(図 4)。このことは、今回のフローサイトメトリーの解析に用いた PD1 抗体(clone EH12.2H7)のエピトープがニボルマブのエピトープと重複しているために、PD1 に結合できなかったか、もしくはニボルマブの投与によって PD1 陽性細胞が減少していたかによるものと考えられる。そこで、今回の PD1 の解析はニボルマブ無効例を除いたニボルマブ投与歴のない患者に絞って行った結果、long SD・PR

症例では末梢血 CD4 T 細胞・CD8 T 細胞ともに PD1 陽性率が高い傾向が見られた(図 4)。TIGIT に関しては、CD4 T 細胞では健常者と悪性中皮腫患者との間で大きな違いは見られなかったが、CD8 T 細胞の TIGIT 陽性率は中皮腫患者の方が健常者よりも高く、特に long SD・PR 症例で高い傾向が見られた(図 4)。今後、末梢血 CD8 T 細胞の細胞傷害性エフェクターT 細胞の割合、CD4 T 細胞の PD1 陽性率、CD8 T 細胞の PD1 と TIGIT の陽性率に着目し、CD26 抗体の治療有効性との関係性を明らかにする。

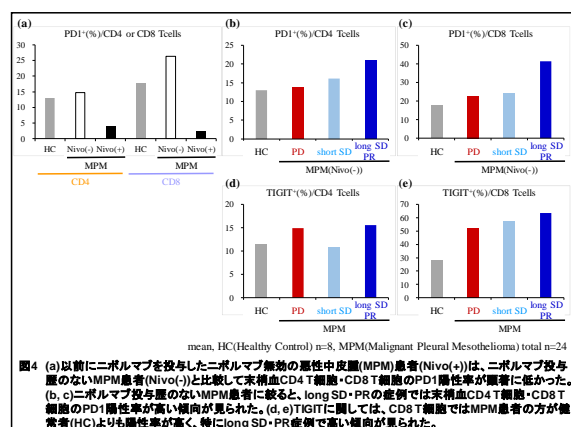


図4 (a)以前にニボルマブを投与したニボルマブ無効の悪性中皮腫(MPM)患者(Nivo(+))は、ニボルマブ投与歴のないMPM患者(Nivo(-))と比較して末梢血CD4 T細胞・CD8 T細胞のPD1陽性率が顕著に低かった。(b, c)ニボルマブ投与歴のないMPM患者に絞ると、long SD・PRの症例では末梢血CD4 T細胞・CD8 T細胞のPD1陽性率が高い傾向が見られた。(d, e)TIGITに関しては、CD8 T細胞ではMPM患者の方が健常者(HC)よりも陽性率が高く、特にlong SD・PR症例で高い傾向が見られた。

D. 考察

ヒト化 CD26 抗体の予後・治療効果予測バイオマーカーを開発するために、今年度の本パートでは、国内第 I/II 相臨床試験患者の血清中サイトカイン・ケモカインの多項目解析と、末梢血リンパ球のフェノタイプ解析、免疫チェックポイント分子の発現解析を主に行った。

ヒト化 CD26 抗体の予後・治療効果を予測可能なバイオマーカーを探索するために、CD26 抗体の投与によって PR もしくは SD が長期間持続した症例を区別して解析を行う必要があり、今回の解析では長期間持続のラインを 4 サイクル(24 週間)以上に設定し

た。このラインに絶対的な正当性はなく、無増悪生存期間(Progression-Free Survival: PFS)等の全ての臨床試験結果が公開された後には、PFS と各項目の値をプロットした相関解析の方がより望ましいと考えられる。

本年度の解析により、CD26 抗体の予後・治療効果を予測する新規バイオマーカー候補として、血清では SDF-1 α,β /CXCL12 及び MIP-1d/CCL15、また、PR・SD 症例と PD 症例とを判別するマーカー候補として MCP2/CCL8、Gro-b/CXCL2、GCP-2/CXCL6 を見出した。ケモカインはケモカインレセプターとの関係性が 1 対 1 対応しておらず、1 種類のケモカインが複数のケモカインレセプターに結合することや、複数種類のケモカインが 1 つのケモカインレセプターに結合する関係にあり、細胞遊走活性だけでも非常に複雑で多様な作用が考えられる。また、細胞遊走以外の機能が報告されているものも存在する。SDF-1 α,β /CXCL12 は CXCR4 と CXCR7 のリガンドであり、リンパ球遊走の他に、白血球活性化や癌増殖、転移促進、血管新生等の機能が報告されている。MIP-1d/CCL15 は CCR1 と CCR3 のリガンドであり、好中球・単球・リンパ球遊走機能が報告されている。今回の解析の結果、CD26 抗体が有効な症例では血清中のこれらのケモカイン濃度がいずれも低値を示しており、今後、これらのケモカインの機能の詳細を調べ、ヒト化 CD26 抗体の作用機序との関係性について考察する必要がある。

我々は健常者の末梢血 CD4 T 細胞を用いて、強い CD26 共刺激シグナルが伝達すると転写因子 EGR2 の顕著な発現上昇と IL-10 の高産生が誘導されることを報告している(J Immunol. 2015)。悪性中皮腫細胞

自身にも CD26 のリガンドである caveolin-1 が発現しているため、中皮腫周囲に浸潤した T 細胞に CD26 共刺激が伝達して IL-10 の高産生を誘導している可能性が考えられる。ヒト化 CD26 抗体は CD26 に結合して、CD26 と caveolin-1 との結合阻害にも働くことから、免疫抑制性サイトカインである IL-10 の産生抑制に働くことが期待される。今回報告したケモカイン以外にも、IL-10 や IL-31、IL-33 など個人差(バラつき)が大きく取り上げなかった因子もあり、それらの因子に関しては次年度に sandwich ELISA で個別に測定を行い、CD26 抗体の治療有効性との関係性を明らかにする。

近年、マウス担癌モデルにおいて、DPPIV inhibitor (Sitagliptin)をエサと一緒にマウスに食べさせることで、腫瘍免疫が増強し、腫瘍サイズが縮小することが報告された(Nat Immunol. 2015, Nat Immunol. 2019)。そのメカニズムとして、がん微小環境から産生されるケモカインの中で DPPIV 酵素の基質の一つである IP-10/CXCL10 と Eotaxin/CCL11 に着目し、本来は産生されたそれらのケモカインが DPPIV 酵素による切断を受けると活性が低下するのに対し、DPPIV inhibitor を摂取することで活性が維持され、そのレセプターである CXCR3 陽性の CD4 T 細胞、CD8 T 細胞、NK 細胞や CCR3 陽性の好酸球ががん細胞周囲により集積するようになり、免疫細胞が腫瘍をより攻撃しやすくなることを示している。癌種によって多く産生するケモカインは異なり、DPPIV inhibitor の作用点も変わることを上記の論文は示唆している。フランスでのヒト化 CD26 抗体の第 I 相臨床試験の結果から、CD26 抗体を投与すると容量依存的に血清

中の可溶性 CD26 量および DPPIV 酵素活性が低下するデータを得ている(Br J Cancer. 2017)。このことから、CD26 抗体を投与した場合においても、DPPIV によって切断されるケモカインの量が減少し、ケモカインの活性維持、がん細胞周囲に集積する免疫細胞数の増加が起こる可能性が考えられ、その点に関しても今後の解析が必要とされる。

がん微小環境に浸潤した T 細胞は、がん細胞自身が産生する免疫抑制性因子や PD1/PDL1・PDL2、CTLA4/CD80・CD86 に代表される免疫チェックポイント分子シグナルによって、エフェクター機能が抑制されていることが様々ながん種で報告されている。悪性中皮腫患者では末梢血 CD8 T 細胞中の細胞傷害性エフェクター T 細胞(CD26 陰性 CD28 陰性 CD57 陽性 KLRG1 陽性)の割合が健常者と比較して明らかに高いことが示された(図 3)。このような perforin と granzyme を発現する細胞傷害性エフェクター T 細胞は本来、ウイルスに感染した細胞やがん細胞を体内から除去するために働く細胞だが、悪性中皮腫患者の末梢血中にどうして細胞傷害活性を有する T 細胞がこれほど多く存在するのか、何の抗原に対して活性化された T 細胞なのか、アスベストばく露による慢性的な炎症が関係しているのかは興味深い疑問である。免疫チェックポイント分子の中で、悪性中皮腫患者の末梢血 CD8 T 細胞は TIGIT の発現陽性率が健常者よりも明白に高く、long SD・PR 症例では特に PD1 と TIGIT の陽性率が高い傾向が見られた(図 4)。免疫チェックポイント分子の発現は T 細胞の活性化状態や血清中の TGF- β 濃度などと関係していることが予想される。末梢血中の細胞傷害性エフェクター T 細胞の

割合や CD8 T 細胞の PD1 及び TIGIT の陽性率が高いことと、悪性中皮腫周囲に浸潤した腫瘍浸潤リンパ球のフェノタイプとの関係性を明らかにするために、次年度に中皮腫病理組織を用いて腫瘍浸潤リンパ球の解析を行う。

E. 結論

今年度は国内第 I/II 相臨床試験患者の血清中サイトカイン・ケモカインの多項目解析を行い、ヒト化 CD26 抗体の予後・治療効果予測バイオマーカー候補として、SDF-1, MIP-1d, MCP2, Gro-b, GCP-2 を見出した。また、国内第 I/II 相臨床試験患者の末梢血リンパ球のフェノタイプ解析により、CD26 抗体有効例では特に CD8 T 細胞で細胞傷害性エフェクターT 細胞(CD26 陰性・CD28 陰性・KLRG1 陽性サブセット)の割合が高く、免疫チェックポイント分子の中で PD1 と TIGIT の発現陽性率が高い可能性を見出した。

F. 今後の展望

次年度は、今年度の解析で得られた血清中の新規バイオマーカー候補について sandwich ELISA で個別に測定を行い、今回の Bio-Plex システムでの結果の再現性を確認する。また、中皮腫病理組織を用いて腫瘍浸潤リンパ球のフェノタイプ解析を行い、末梢血 T 細胞のフェノタイプとの関係性や、ヒト化 CD26 抗体の治療有効性との相関関係を解析し、予後・治療効果バイオマーカーを確立する。

G. 研究発表

1. 論文発表

- 1) Itoh T, Hatano R, Komiya E, Otsuka H, Narita Y, Aune TM, Dang NH, Matsuoka S, Naito H, Tominaga M, Takamori K, Morimoto C, Ohnuma K. Biological effects of IL-26 on T cell-mediated skin inflammation including psoriasis. *J Invest Dermatol.* 2019; 139(4): 878-889
- 2) Santos MF, Rappa G, Karbanova J, Vanier C, Morimoto C, Corbeil D, Lorico A. Anti-human CD9 antibody Fab fragment impairs the internalization of extracellular vesicles and the nuclear transfer of their cargo proteins. *J Cell Mol Med.* 2019; 23(6): 4408-4421
- 3) Mezawa Y, Daigo Y, Takano A, Miyagi Y, Yokose T, Yamashita T, Morimoto C, Hino O, Orimo A. CD26 expression is attenuated by TGF- β and SDF-1 autocrine signaling on stromal myofibroblasts in human breast cancers. *Cancer Med.* 2019; 8(8): 3936-3948
- 4) Hatano R, Yamada T, Madokoro H, Otsuka H, Komiya E, Itoh T, Narita Y, Iwata S, Yamazaki H, Matsuoka S, Dang NH, Ohnuma K, Morimoto C. Development of novel monoclonal antibodies with specific binding affinity for denatured human CD26 in formalin-fixed paraffin-embedded and decalcified specimens. *PLoS One.* 2019; 14(6): e0218330
- 5) Hatano R, Itoh T, Otsuka H, Okamoto S, Komiya E, Iwata S, Aune TM, Dang NH, Kuwahara-Arai K, Ohnuma K, Morimoto C. Characterization of novel anti-IL-26 neutralizing monoclonal antibodies for the treatment of inflammatory diseases

- including psoriasis. *MAbs*. 2019; 11(8): 1428-1442
- 6) Hayashi M, Madokoro H, Yamada K, Nishida H, Morimoto C, Sakamoto M, Yanagawa H, Yamada T. Novel Antibody-Drug Conjugate with Anti-CD26 Humanized Monoclonal Antibody and Transcription Factor IIIH(TFIIIH) Inhibitor, Triptolide, Inhibits Tumor Growth via Impairing mRNA Synthesis. *Cancers* (Basel). 2019; 11(8): E1138
 - 7) Takeda T, Ohe Y, Horinouchi H, Hida T, Shimizu J, Seto T, Nosaki K, Kishimoto T, Miyashita I, Yamada M, Kaneko Y, Morimoto C, Nakagawa K. Phase I study of YS110, a recombinant humanized monoclonal antibody to CD26, in Japanese patients with advanced malignant pleural mesothelioma. *Lung Cancer* 2019; 137: 64-70
 - 8) Sato T, Tatekoshi A, Takada K, Iyama S, Kamihara Y, Jawaid P, Rehman MU, Noguchi K, Kondo T, Kajikawa S, Arita K, Wada A, Murakami J, Arai M, Yasuda I, Dang NH, Hatano R, Iwao N, Ohnuma K, Morimoto C. DPP8 is a novel therapeutic target for multiple myeloma. *Sci Rep*. 2019; 9(1): 18094
 - 9) Ohnuma K, Hatano R, Dang NH, Morimoto C. Rheumatic diseases associated with immune checkpoint inhibitors in cancer immunotherapy. *Mod Rheumatol*. 2019; 29(5): 721-732
 - 10) 岩尾憲明, 大沼圭, 波多野良, 大塚春奈, 古宮栄利子, 伊藤匠, 森本幾夫. GVHDの発症と慢性炎症. 別冊 *Bio Clinica*: 慢性炎症と疾患, 2019; 8(1): 120-125
- ## 2. 著書
- 1) Okamoto T, Hatano R, Nakano K, Yamada T, Yamazaki H, Kaneko Y, Dang NH, Morimoto C, Ohnuma K. Regulation of proliferation of malignant mesothelioma cells by CD26-cyclophilin A molecular complex. In: *Advanced in Medicine and Biology*. Nova Science Publishers, Inc., Hauppauge, NY, Editor: Leon V. Berhardt, 2019; Volume 156: Chapter 8: 165-185
- ## 3. 学会発表
- 1) Komiya E, Hatano R, Itoh T, Otsuka H, Ohnuma K, Tominaga M, Morimoto C, Takamori K. CD26/DPPIV regulates mechanical itch by enzymatic degradation of mu-opioid receptor ligands. 24th World Congress of Dermatology (WCD), Milan, 2019.6.15
 - 2) Komiya E, Hatano R, Itoh T, Otsuka H, Kamata Y, Honda K, Toyama S, Moniaga CS, Ohnuma K, Tominaga M, Morimoto C, Takamori K. Possible role for CD26/DPPIV in regulating mechanical itch (Alloknesis). 28th European Academy of Dermatology and Venereology (EADV) Congress, Madrid, 2019.10.9
 - 3) Komiya E, Hatano R, Itoh T, Otsuka H, Kamata Y, Honda K, Toyama S, Moniaga CS, Ohnuma K, Tominaga M, Morimoto C, Takamori K. Possible regulation of mechanical itch by CD26/DPPIV. 10th World Congress on Itch (WCI), Sydney, 2019.11.17

- | | |
|---|--|
| <p>4) 古宮栄利子, 富永光俊, 波多野良, 伊藤匠, 大塚春奈, 本田耕太郎, 外山扇雅, 鎌田弥生, 大沼圭, 森本幾夫, 高森建二. 加齢皮膚で誘発される機械的かゆみ調節機構の解明. 第 15 回 加齢皮膚医学研究会, 熊本, 2019 年 3 月 9 日</p> <p>5) Hiroko Nishida, Mutsumi Hayashi, Chikao Morimoto, Michiie Sakamoto, Taketo Yamada. CD26 is a potential therapeutic target by humanized monoclonal antibody in multiple myeloma. 第 108 回 日本病理学会総会, 東京, 2019 年 5 月 10 日</p> <p>6) 古宮栄利子, 波多野良, 富永光俊, 伊藤匠, 鎌田弥生, 本田耕太郎, 外山扇雅, カタリナサギタモニアガ, 大沼圭, 森本幾夫, 高森建二. CD26/ dipeptidyl-peptidase IV は機械的かゆみの抑制因子である. 第 24 回 日本病態プロテアーゼ学会, 岐阜, 2019 年 8 月 2 日</p> <p>7) 山田健人, 坂元亨宇, 森本幾夫, 林睦. Anti-CD26 humanized antibody-triptolide conjugate transports into nucleus and inhibits RNA polymerase II activity. 第 78 回 日本癌学会学術総会, 京都, 2019 年 9 月 27 日</p> <p>8) Hiroko Nishida, Mustumi Hayashi, Chikao Morimoto, Michiie Sakamoto, Taketo Yamada. Humanized anti-CD26 monoclonal antibody clonogenic side population cells in multiple myeloma. 第 81 回 日本血液学会学術集会, 東京, 2019 年 10 月 12 日</p> | <p>大沼圭, 森本幾夫, 波多野良: 免疫チェックポイント阻害剤. 特願 2019-004480</p> <p>2. 実用新案登録
なし</p> <p>3. その他
なし</p> |
|---|--|

H. 知的財産権の出願・登録状況（予定を含む）

1. 特許取得

労災疾病臨床研究事業費補助金
分担研究報告書

悪性胸膜中皮腫におけるCD26発現評価とヒト化CD26抗体療法における
予後・治療効果予測バイオマーカーの開発

研究分担者 山田 健人 埼玉医科大学 病理学 教授
研究分担者 岸本 卓巳 独立行政法人労働者健康安全機構
アスベスト疾患研究・研修センター 所長
研究協力者 藤本 伸一 岡山労災病院 腫瘍内科部長
研究協力者 青江 啓介 国立病院機構山口宇部医療センター 内科系診療部長
研究協力者 波多野 良 順天堂大学医学研究科 免疫病・がん先端治療学講座 特任助教

研究要旨

悪性胸膜中皮腫は現時点で効果的な治療法はなく、予後は極めて不良で労災疾病行政上も大きな問題であり、有効な新規治療法の確立は急務である。国内第I/II相臨床試験において、悪性中皮腫の病理検体として、第I相は9例中6例、第II相では、31例全例の計37症例（組織型は、上皮型29例、二相型5例、肉腫型3例）が収集された。その37例中36例の検体は、CD26発現の評価が可能であった。そこでR&D社ポリクローナル抗体による免疫染色（フランスでの治験と同一、A法）および新規開発されたコンパニオン診断キットによる免疫染色（B法）の二つの染色方法によりCD26発現について検討した。その結果、A法でのCD26陽性率が20%以上の症例は、37例中30例、20%未満の症例が6例であったのに対して、B法では20%以上の症例は、37例中32例、20%未満の症例が4例であった。それぞれ組織型におけるCD26陽性率20%以上の症例は、上皮型29例中A法B法ともに27例、二相型5例中A法2例、B法3例、肉腫型3例中A法1例、B法2例であった。またA法よりもB法でCD26陽性率が上昇した症例は36例中23例であり、その中で陽性率が20%以上上昇した症例が11例認められた。正常ヒト組織でのCD26染色性の向上がB法で認められたことも考えると、この新規コンパニオン診断キットによる免疫染色法が中皮腫におけるCD26発現をより正確に評価するのに適していると考えられた。

A. 研究目的

フランスで施行されたヒト化 CD26 抗体療法第 I 相臨床試験では、特記すべき有害事象なく、26 症例中 13 症例で「安定」(Stable Disease;SD)への導入が可能であり、安全性のみならず、その腫瘍効果も期待される成果が得られた (Br J Cancer 116:1126-1134, 2017)。本邦でも 2017 年

7月から第I相臨床試験がスタートし(第1～3コホート各3例)、2018年3月に終了、9例中8例が評価可能で Partial Response(PR) 1例、SD 5例と有効性も示唆された。6月からスタートした第II相臨床試験は、2019年10月時点で31例が終了している。そこで本研究においては、まず悪性中皮腫症例における CD26 発現を

詳細に明らかにし、標的分子としてどのような発現パターンを示すのかを明らかにし、CD26 抗体療法の治療効果との相関を明らかにするための基礎的検討を行った。また CD26 発現は現在用いられているアリムタ、シスプラチンなど化学療法剤の治療効果予測バイオマーカーとしても有望な結果を得て報告(Clin Cancer Res 18:1447, 2012)してきたが、さらに今回、CD26 発現を細胞局在、陽性率、陽性強度など様々な要素で解析し、各種の臨床パラメーターとの相関を明らかにすることで、バイオマーカーとなりうるかどうかを検討することを目的とした。

さらに CD26 発現評価のためにホルマリン固定パラフィン包埋 (FFPE) された臨床検体で CD26 を評価する新規コンパニオン診断キットの開発を行い、この新規の方法とこれまでの染色方法について同一検体を用いて比較検討した。

B. 研究方法

CD26 の発現解析には、ヒト組織としてホルマリン固定したパラフィン切片 (CD26 陽性である正常ヒト腎、肝、前立腺及び悪性中皮腫の組織および肺) および生検や手術材料を用いた。抗原賦活化として、オートクレーブ処置 (120℃、20 分、0.01M Citrate Buffer pH8.0) を行い、二次抗体は、Peroxidase 付加抗ラビット IgG 抗体 (ImmPRESS 社製) を用い、発色は、DAB 液 (Simple Stain DAB, Histofine) を用いた。国内第 I/II 相臨床試験 (YS1101、キッセイ薬品工業株式会社) における悪性中皮腫 37 症例症例の腫瘍の病理組織 (生検及び手術材料、10%ホルマリン固定、パラフィン切片) について、CD26 の免疫染色を行った。抗原賦活化は、オートクレーブ処置 (120℃、20 分、0.01M Citrate Buffer pH8.0) を行った。抗 CD26 抗体は、仏の臨床試験で使用した R&D 社製抗 CD26 ヤギ・

ポリクロナール抗体 (Lot. No. JOQ107061) を用いた。二次抗体は、Peroxidase 付加抗ヤギ IgG 抗体 (ImmPRESS 社製) あるいは Peroxidase 付加抗マウス IgG 抗体 (ImmPRESS 社製) を用い、発色は、DAB 液 (Simple Stain DAB, Histofine) を用いた。いずれの染色においても、陽性対照には、正常ヒト腎、肝、前立腺及び悪性中皮腫を用い、陰性対照には、これらの正常組織切片内の各種組織 (平滑筋、脂肪組織、結合組織など) と CD26 陰性肺癌組織を用いた。

新規コンパニオン診断キットは、一次抗体は仏の臨床試験で使用した R&D 社製抗 CD26 ヤギ・ポリクロナール抗体で同一であるが、抗原賦活化試薬や条件をキット用に開発・至適化しており、二次抗体や発色試薬も改良を加えた (ニチレイバイオサイエンス株式会社との共同研究)。スクリーニングは FFPE 切片 (CD26 陽性である正常ヒト腎、肝、前立腺及び悪性中皮腫の組織および肺) の免疫染色により行い、至適化されたプロトコルを用いて中皮腫検体の染色を行なった。

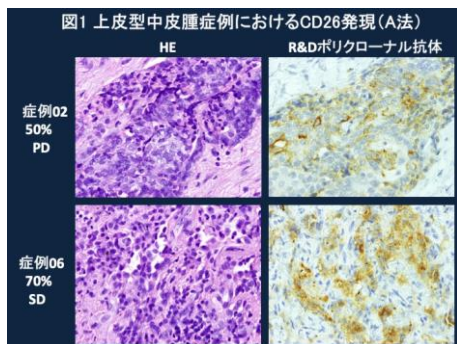
(倫理面への配慮)

患者検体などについては研究対象者に対する人権擁護上の配慮及び研究により研究対象者が受ける不利益、利益等の説明を患者及び遺族に対して行い、書面でのインフォームド・コンセントを得ている。また病理組織について免疫染色して CD26 発現を解析する研究については、埼玉医科大学の倫理審査委員会にて承認されている (承認番号 794, 861)。

C. 研究結果

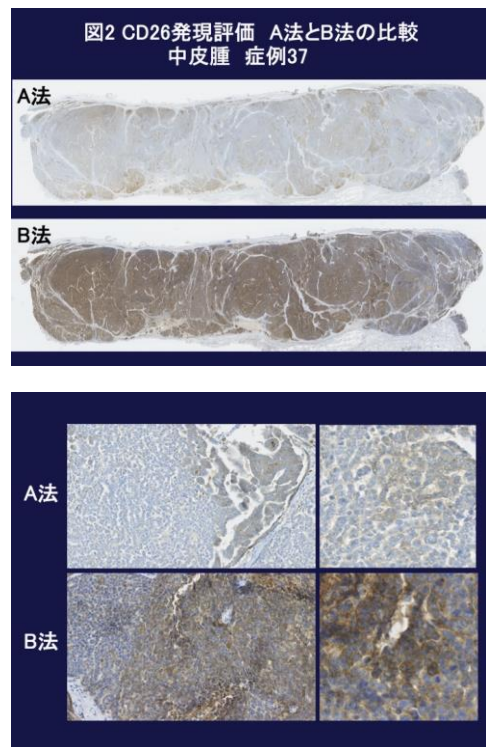
国内第 I/II 相臨床試験 (第 I 相は 9 例中 6 例、第 II 相では 31 例全例) における悪性中皮腫 37 症例について、病理組織像および R&D 社ポリクロナール抗体による

免疫染色（フランスでの治験と同一の方法、A法）および新規コンパニオン診断キット（B法）によるCD26発現について検討した。37症例の組織型は、上皮型29例、二相型5例、肉腫型3例であった。なお37例中1例は腫瘍細胞が数個のみであったため評価対象外とし、36例の検体でCD26発現の評価を行なった。A法での結果では、CD26発現は、上皮型で5%以下1例、5%～50%3例、50%～70%11例、70%～100%13例であり、二相型では、2%、12%、20%、70%がそれぞれ1例、肉腫型では2%、5%、50%がそれぞれ1例であった。これらの症例の中でCD26発現とYS110治療効果の関係をみると、Stable disease (SD)以上の効果が見られた上皮型の症例は陽性率が30%であったが、二相型と肉腫型では陽性率が1%、2%の症例にもSDが認められた（図1）。



症例数が少ないため、組織型およびCD26発現とYS110効果との統計学的な有意な相関関係は明らかではないが、CD26陽性率と治療効果には一定の傾向は明らかではなかった。これらの染色標本をデジタル画像とし、imageProPlusプログラムにて詳細に半定量的に発現解析を行った。その結果、CD26は細胞膜および細胞質に95%が、核内に1-2%の発現が認められた。現在、これらのデータベースを元に臨床パラメーターとの相関について検討している。

またFFPE臨床検体におけるCD26発現評価のために新規開発したB法と上記A法との比較を行った。その結果、A法でのCD26陽性率が20%以上の症例は、37例中30例、20%未満の症例が6例であったのに対して、B法では20%以上の症例は、37例中32例、20%未満の症例が4例であった。それぞれの組織型におけるCD26陽性率20%以上の症例は、上皮型29例中A法B法ともに27例、二相型5例中A法2例、B法3例、肉腫型3例中A法1例、B法2例であった。またA法よりもB法でCD26陽性率が上昇した症例は36例中23例であり、その中で陽性率が20%以上上昇した症例が11例認められた（図2）。また正常ヒト組織、特に肝臓や腎臓において、B法にお



いてA法よりも鮮明な染色結果が得られる組織が確認された。

D. 考察

これらの結果および正常ヒト組織でのCD26染色性の向上が認められたことから、

この新規コンパニオン診断キットによる免疫染色法が中皮腫における CD26 発現をより正確に評価するのに適していると考えられた。今後、これらの CD26 陽性率と YS110 療法の効果や既存の治療法や各種臨床パラメーターとの相関について解析する予定である。悪性中皮腫における CD26 発現について免疫染色にて評価し、組織型とともに発現パターン(細胞局在、陽性率、陽性強度などの各種パラメーター)を詳細に定量評価することにより、抗体療法の効果や予後などとの関連性あるいは臨床パラメーターを検証する基礎を構築していくことが重要と考える。

E. 結論

臨床試験における悪性中皮腫検体における CD26 発現評価を行い、半定量的解析法を確立した。また CD26 抗体療法におけるコンパニオン診断キットの開発に成功した。

G. 研究発表

1. 論文発表

- 1) Hatano R, Yamada T, Madokoro H, Otsuka H, Komiya E, Itoh T, Narita Y, Iwata S, Yamazaki H, Matsuoka S, Dang NH, Ohnuma K, Morimoto C. Development of novel monoclonal antibodies with specific binding affinity for denatured human CD26 in formalin-fixed paraffin-embedded and decalcified specimens. *PLoS One*. 2019; 14(6): e0218330
- 2) Nishida H, Yamada T. Monoclonal Antibody Therapies in Multiple Myeloma: A Challenge to Develop Novel Targets. *J Oncol*. 2019; 2019: 6084012
- 3) Hayashi M, Madokoro H, Yamada K, Nishida H, Morimoto C, Sakamoto M,

Yanagawa H, Yamada T. Novel Antibody-Drug Conjugate with Anti-CD26 Humanized Monoclonal Antibody and Transcription Factor IIIH(TFIIH) Inhibitor, Triptolide, Inhibits Tumor Growth via Impairing mRNA Synthesis. *Cancers (Basel)*. 2019; 11(8): E1138

2. 学会発表

- 1) Hayashi M, Madokoro H, Yamada T. Anti-CD26 Humanized Monoclonal Antibody Conjugated to Triptolide Inhibits Tumor Cell Growth via Transportation into Nucleus and Impaired RNA Polymerase II. 第 42 回日本分子生物学会年会 2019 年 12 月 3 日 (火) -6 日 (金) 福岡国際会議場
- 2) 山田 健人、坂元 亨宇、森本 幾夫、林 睦 Anti-CD26 humanized antibody-triptolide conjugate transports into nucleus and inhibits RNA polymerase II activity 第 78 回日本癌学会総会 2019 年 9 月 26-28 日 京都国際会議場
- 3) 西田浩子、林 睦、森本幾夫、坂元亨宇、山田健人 多発性骨髄腫において SP 細胞はヒト化モノクローナル抗体の治療標的となる 第 81 回日本血液学会学術集会 2019 年 10 月 11 日 (金曜日) -13 日 (日曜日) 東京国際フォーラム
- 4) 西田浩子、林 睦、森本幾夫、坂元亨宇、山田健人 CD26 is a potential therapeutic target by humanized monoclonal antibody in multiple myeloma 第 108 回日本病理学会総会、2019 年 5 月 9-11 日、東京国際フォーラム

H. 知的財産権の出願・登録状況（予定を含む）

1. 特許

なし

2. 実用新案登録

なし

3. その他

なし

労災疾病臨床研究事業費補助金
分担研究報告書

ヒト化抗 CD26 抗体投与後の血清中溶存 CD26/DPP4 値の変動と
予後・治療効果との相関関係の解析

研究代表者	森本 幾夫	順天堂大学大学院医学研究科 免疫病・がん先端治療学講座 特任教授
研究分担者	岸本 卓巳	独立行政法人労働者健康安全機構 アスベスト疾患研究・研修センター 所長
研究分担者	山田 健人	埼玉医科大学医学部 病理学 教授
研究協力者	金子 有太郎	ワイズ・エー・シー株式会社 CEO 近畿大学 客員教授(元)
研究協力者	波多野 良	順天堂大学大学院医学研究科 免疫病・がん先端治療学講座 特任助教

研究要旨

ヒト化抗 CD26 モノクローナル抗体(YS110)による悪性胸膜中皮腫を主たる対象としたフランスにおける第 I 相臨床試験により得られた、YS110 投与に伴う血清中溶存 CD26/DPP4(sCD26/DPP4) titer の変動が、CD26 抗体の予後・治療効果を予測するバイオマーカーになり得るかについて検討を続け、バイオマーカーとして有用である可能性が得られた。その中で、臨床試験で観察された、YS110 投与によって血清中 sCD26/DPP4 titer が低下するメカニズムを明らかにするために、CD26 陽性/陰性の腫瘍及び正常細胞を用いて、in vitro での検証を行った。細胞膜上の CD26 の発現が高い細胞であれば腫瘍・正常細胞ともに培養上清中に sCD26 を産生し、YS110 の容量依存的、及び経時的に sCD26 の産生が阻害されることを明らかにした。今後、CD26 陽性腫瘍細胞において CD26 分子が腫瘍増殖にいかに関与しているかを明らかにし、血清中 sCD26/DPP4 titer の変動が何故 CD26 抗体の予後・治療効果を予測するバイオマーカーになり得るかを解明する。

A. 研究目的

ヒト化抗 CD26 モノクローナル抗体(YS110)による悪性胸膜中皮腫(MPM)治療において、予後・治療効果を予測することができるバイオマーカーを確立することを目的として、フランスにて MPM を中心に行った First-in-Human 第 I 相臨床試験(Br J

Cancer. 2017)の臨床データの統計学的解析と、その現象のメカニズムの一端を明らかにするために in vitro での検証を行った。

B. 研究方法

1) フランスでの第 I 相臨床試験の臨床データを用いた統計解析

YS110 投与前後 (Day1Pre/Post, Day15 Pre/Post, Day29Pre/Post) における血清中 溶存 CD26(sCD26) titer の変動 (%) と RECIST 評価による腫瘍量の変動 (%) (Day43) 及び無増悪生存期間 (Progression-Free Survival: PFS) との関連性について解析を行った。

2) 細胞株と培養

ヒト MPM 細胞株には MSTO, JMN, H226 を用いた。CD26 陰性の MSTO (MSTO parent) にヒト CD26 の全長を安定的に発現させた MSTO-CD26、ならびに CD26 陽性の JMN に control-shRNA または CD26-shRNA を安定的に発現させた JMN ctrl-shRNA, JMN CD26-shRNA は当研究室で作製した (Br J Cancer. 2014, BBRC. 2012)。正常細胞 (非腫瘍細胞) には、不死化ヒト胸膜中皮細胞株 MeT-5A、ヒト乳腺上皮細胞株 MCF10A、ヒト胎児肺線維芽細胞株 TIG-1、ヒト臍帯静脈内皮細胞 HUVEC、ヒト皮膚微小血管内皮細胞 HDMVEC を用いた。全ての MPM 細胞株と MeT-5A は 10% FBS を添加した RPMI 1640 培地で培養した。TIG-1 は 10% FBS を添加した DMEM 培地で培養した。MCF10A, HUVEC, HDMVEC はそれぞれ LONZA で購入した MEGM, EGM-2, EGM-2MV 培地で培養した。全ての細胞は 37°C, 5% CO₂ インキュベーター内で培養した。

3) 抗体

血清中または培養上清中の sCD26 の ELISA には、当研究室で開発された mouse anti-human CD26 mAb である 5F8 と 9C11 を用いた。ヒト化抗 CD26 抗体 YS110 はワ

イズ・エー・シー株式会社から供与された。ヒト IgG ポリクローナル抗体 (venilon-I) は Alfresa Corporation より購入した。Flow cytometry には PE-labeled mouse anti-human CD26 mAb (clone M-A261) (BD Biosciences) を用いた。

4) 培養上清の調製

MSTO parent (4×10^4), MSTO-CD26 (3.5×10^4), JMN ctrl-shRNA (3.5×10^4), JMN CD26-shRNA (3.5×10^4), H226 (3.5×10^4), MCF10A (1.0×10^5), HUVEC (9.0×10^4), MeT-5A (6.0×10^4), TIG-1 (5.0×10^4) or HDMVEC (9.0×10^4) を 24-well プレートに 500 μ l/well となるよう培地に懸濁して播種した。実験によってはコントロールヒト IgG または YS110 を添加して 37°C で 3 日間培養した。YS110 の経時的な影響を解析する実験では、MSTO-CD26 (1.5×10^5 , 4×10^4 , or 4×10^3) を 24-well プレートに 500 μ l/well となるよう RPMI 1640 培地に懸濁して播種した。YS110 を 1, 3, 10 μ g/ml で添加し、37°C で 1, 3, 7 日間培養した。培養後、コンフルエントの細胞から培養上清を回収し、sCD26 濃度を ELISA にて測定した。

5) sCD26 の測定 < sandwich ELISA >

1. 捕捉抗体プレートの作成

96 穴平底プレートに、5 μ g/ml の捕捉抗体 (CD26 mAb: 5F8) を各穴 100 μ l ずつ分注し、4°C で一晩静置する。

2. 捕捉抗体プレートのブロッキング

上記 1 のプレートを各穴 300 μ l の PBS-Tween で 3 回洗浄後、200 μ l のブロッキングバッファーを分注し、室温で 2 時間静置し、各穴 300 μ l の PBS-Tween で 3 回洗浄

して3の検体分注に供する。

3. 測定検体(血清または培養上清)及び標準曲線用組換え sCD26 の添加

PBS-Tween20 で 20 倍に希釈した対象血清、または 2 倍希釈した培養上清を 100 μ l ずつ 2 穴に分注する。標準曲線を作成するため、段階希釈(500, 250, 125, 62.5, 31.3, 15.6, 7.8, 3.9, 1.95, 0.98, 0.49, 0 ng/ml)した組換え sCD26 標準試薬(R&D Systems)を 100 μ l ずつ 2 穴に分注する。プレートを密封し、4°C で一晩静置する。

4. sCD26 の測定

上記3のプレートを各穴 300 μ l の PBS-Tween で 3 回洗浄後、0.5 μ g/ml の検出抗体(ビオチン化 CD26 mAb: 9C11)を各穴 100 μ l ずつ分注し、室温で 2 時間静置する。300 μ l の PBS-Tween で 3 回洗浄後、1 万倍希釈した ExtrAvidin-Alkaline Phosphatase 液を 100 μ l ずつ分注する。プレートを遮光して、室温で 1 時間静置する。300 μ l の PBS-Tween で 3 回洗浄後、PNPP を 100 μ l ずつ分注し、遮光して室温で 10 分間静置した後、2N-NaOH 溶液を 100 μ l ずつ分注して、発色反応を停止させる。プレートリーダーで吸光度を測定する(吸光度 405 nm、レファレンス 655 nm)。

6) フローサイトメトリー

トリプシン処理をして各種細胞を培養用ディッシュから回収し、洗浄した後、PE 標識した抗ヒト CD26 mAb を添加した。遮光して 4°C で 25 分間静置した後、洗浄し、FACS Calibur (BD Biosciences)で測定を行った。得られたデータを FlowJo (BD Biosciences)で解析した。

(倫理面への配慮)

フランスでの第 I 相臨床試験におけるヒトおよびヒト由来の試料を対象とした研究は、世界医師会によって作成された人体実験に関する一連の倫理的原則に従って実施された。血清検体の提供を受ける際には、研究対象者に対する人的擁護上の配慮及び研究により研究対象者が受ける不利益、利益等の説明を行い、書面でのインフォームド・コンセントを得ている。

C. 研究結果

1) フランスでの第 I 相臨床試験の臨床データをを用いた統計解析

YS110 投与前後の血清中 sCD26/DPP4 titer の変動(V)と抗腫瘍効果(RECIST)及び PFS との関連性の解析における変数として、(a)YS110 の投与頻度(2 週または 1 週に 1 回投与 : Q2W または Q1W)、(b)投与量 : 体重当たりの投与量(mg/kg)、(c)腫瘍の CD26 発現陽性率(%)、(d)癌腫(MPM, 腎がん(RCC))、(e)性差、等があり、その中で変数(b)投与量及び (c)腫瘍の CD26 発現陽性率(%)は RECIST 判定及び PFS との関連性がないことが判明している。一つの解析例として、変数(a)において Q2W 症例数 18 例(全解析対象 26 例)について、腫瘍計測が不能だった MPM 1 症例を除いた 17 例(MPM: 11 症例、RCC : 6 症例)を RECIST 評価 SD、PD 症例それぞれ 8(黒丸)及び 9(白丸)症例で層別し、血清中 sCD26 titer の変動(%) (Y 軸)と腫瘍量 RECIST 判定の Day43 における変動(%) (X 軸)の座標に、YS110 投与前後別 Day1post, Day15Pre/Post, Day29Pre/Post に plotting し解析した(データ未掲載)。その結果、投与頻度 Q2W の場合、Day29Pre(3

回目投与の前)において、明らかに Day43 における RECIST 評価を予測することが統計学的有意差($p=0.012$)を持って示された。この結果は、血清中 sCD26 titer の変動 V が YS110 の抗腫瘍効果を予測するバイオマーカーであることを示していると考えられる。なお、YS110 投与直後(Post)は血清中 sCD26 titer が一律に低下し、SD/PD の差を見にくくしていると思われる。さらに、YS110 投与頻度 Q2W における投与前後の各 plot の統計学的解析により、Day29Pre の値によってその後の SD 判定(Day43)、及び 180 日以上の PFS 判定を予測可能な V 値がそれぞれ統計学的有意差、 $p<0.01$ (AUC:0.89), $p<0.01$ (AUC:0.84)を持って示された(データ未掲載)。以上の結果から、V 値が YS110 によるがん治療における有効性のバイオマーカーとして有用である可能性を示していると考えられる。

なお、血清中 sCD26 titer の測定に用いている抗ヒト CD26 モノクローナル抗体(5F8 及び 9C11)は、YS110 とはエピトープが重複しない抗体を選択しており、YS110 投与による血清中 sCD26 titer の低下は、YS110 が血清中 sCD26 に結合しているために ELISA で検出できなくなっているわけではないことが既に確認されている(J Clin Lab Anal. 2015)。また、YS110 の CD26 分子における結合領域は N 末側に近い主に 248-358 aa であることが示されており(Mol Immunol. 1998)、一方で DPP4 酵素活性は C 末端(630, 730, 740 aa)であり、YS110 は CD26 に結合しても DPP4 酵素活性は阻害しない(USA-IND 100657, section 8.2.1.5 P289, 2008, by Y'sAC Co., Ltd.)。従って、YS110 は血清中の sCD26 量自体を低下させ

るが、CD26 分子あたりの DPP4 酵素活性に対しては直接的な影響はないと考えられる。

2) in vitro での sCD26 産生細胞、及び YS110 が sCD26 産生に与える影響の解析

YS110 の臨床試験から、MPM 患者の血清中 sCD26 titer は YS110 の投与によって顕著に低下することが示された(Br J Cancer. 2017, Lung Cancer. 2019)。そこで、YS110 が血清中 sCD26 titer を低下させるメカニズムを明らかにするために、YS110 が sCD26 産生に与える影響を in vitro で解析した。生体内には T 細胞や血管内皮細胞、上皮細胞、線維芽細胞、脂肪細胞など多様な CD26 陽性細胞が存在し、細胞膜上の CD26 分子を切断して sCD26 を放出させる酵素も明確にはわかっておらず、sCD26 の主な産生源についても明確には示されていない。そこでまず、CD26 陽性・CD26 陰性 MPM 細胞株及び、CD26 陽性・CD26 陰性正常細胞(非腫瘍細胞)を用いて、in vitro で培養上清中に sCD26 が産生されるかを解析した。MPM 細胞株の中で細胞膜上に CD26 を発現していない MSTO parent と JMN CD26-shRNA の培養上清中では sCD26 は検出されなかったが、細胞膜上に CD26 を発現する MSTO-CD26, JMN ctrl-shRNA, H226 の培養上清中では sCD26 が検出された(データ未掲載)。正常細胞においても同様に、細胞膜上に CD26 を発現していない乳腺上皮細胞株 MCF10A と臍帯静脈内皮細胞 HUVEC、並びに細胞膜上の CD26 発現が弱い胸膜中皮細胞株 MeT-5A の培養上清中では sCD26 は検出されなかったが、細胞膜上に CD26 を発現する肺線維芽細胞株 TIG-1,

皮膚微小血管内皮細胞 HDMVEC の培養上清中では sCD26 が検出された(データ未掲載)。重要なことに、YS110 を添加して 72 時間培養した培養上清では、MPM 細胞株からも正常細胞からも sCD26 産生が同程度に低下することが示された(データ未掲載)。

そこで次に、YS110 の容量依存的、経時的な作用を検証した。細胞膜上の CD26 発現が高い MPM 細胞株として MSTO-CD26 を、正常細胞として TIG-1 を選択し、YS110 存在下で培養したところ、MSTO-CD26、TIG-1 のどちらも YS110 の容量依存的に培養上清中の sCD26 量が減少した(データ未掲載)。また、MSTO-CD26 を YS110 存在下で 1, 3, 7 日間培養した結果、培養 1 日でも培養上清中に sCD26 が検出され、YS110 による産生量の減少も見られた(データ未掲載)。培養期間が長いほど培養上清中に溜まる sCD26 の量も増加したが、いずれの日数でも YS110 の作用は同程度に認められた(データ未掲載)。

これらの結果から、sCD26 は細胞膜上に CD26 を発現する腫瘍からも正常細胞からも産生され、YS110 は腫瘍と正常細胞の両方に作用して、sCD26 産生を容量依存的、経時的に減少させることが示された。この YS110 の作用は、MPM 患者の血清中 sCD26 titer が YS110 投与によって顕著に低下するメカニズムの一つと考えられる。

D. 考察

フランスでの第 I 相臨床試験の臨床データの解析により、YS110 投与前後における血清中 sCD26 titer の変動(V)が治療効果 (RECIST 判定による直接抗腫瘍効果、及び無増悪生存期間 PFS に対する効果)を予測

できるバイオマーカーであることが統計学的に示された。ただし、V 値変動を用いて予後の予測を決定する場合、治療プロトコルの中で YS110 の投与頻度により V 値の決定時期に変化があると考えられる。

フランスでの第 I 相臨床試験において観察された YS110 投与と V との関係(YS110 による血清中 sCD26 titer の低下)について、そのメカニズムを解明するために *in vitro* での検証を行った。本研究により、CD26 陽性の MPM 細胞株及び CD26 陽性の正常細胞(非腫瘍細胞)のどちらもから sCD26 が産生されること、また、YS110 添加により腫瘍、正常細胞のどちらに対しても YS110 の容量依存的に sCD26 産生が阻害されることが示された。この結果は、YS110 の臨床試験で観察される YS110 投与後の血清中 sCD26/DPP4 titer の顕著な低下の理由の一つと考えられる。フランスでの第 I 相臨床試験の血清中 sCD26/DPP4 titer の結果では、YS110 を投与したその日に大幅に減少し、次に YS110 を投与するまでの間に sCD26/DPP4 titer は徐々に回復し、YS110 を投与すると再び減少する変動パターンを示している(Br J Cancer. 2017)。YS110 投与直後の Day1Post, Day15Post, Day29Post ではいずれも SD 症例と PD 症例の間で血清中 sCD26/DPP4 titer に有意な差は見られなかった。一方で、2 週に一度の頻度で YS110 を投与して 3 回目の抗体を投与する前 (Day29Pre)の血清中 sCD26/DPP4 titer は、PD 症例と比較して SD 症例で有意に低いことが示された(データ未掲載)。これらの結果から、SD/PD に関わらず YS110 投与直後は血清中 sCD26/DPP4 titer は同等に低下するが、YS110 投与後の血清中 sCD26/DPP4

titer の回復が SD 症例と比較して PD 症例では早い、もしくは強いことが考えられる。YS110 を投与して一度低下した血清中 sCD26/ DPP4 titer のその後の回復の違いが、何を反映した結果なのかについて今後解析していく必要がある。

YS110 は腫瘍細胞膜上の CD26 に結合すると複合体(CD26-YS110 Complex: CYC)を形成したまま直ちに細胞質に取り込まれ、さらに細胞核内にまで移行して RNA polymerase 2 のサブユニットの一つである POLR2A の転写を阻害することを報告している(PLoS One. 2013)。即ち、YS110 の抗腫瘍作用メカニズムの一つに、CYC の核移行とそれによる腫瘍細胞の直接的な遺伝子発現制御が考えられる。なお、CD26 陽性の正常細胞においては、CYC は細胞核内までは到達しないことも示している(PLoS One. 2013)。CYC が何故、腫瘍細胞では核内まで移行するのか、その詳細なメカニズムの解明は、新しい抗腫瘍薬を創造する糸口となることと期待される。

E. 結論

ヒト化抗 CD26 モノクローナル抗体(YS110)による悪性胸膜中皮腫を主たる対象としたフランスにおける第 I 相臨床試験により得られた、YS110 投与に伴う血清中溶存 CD26/ DPP4(sCD26/DPP4) titer の変動を詳細に解析した結果、CD26 抗体の予後・治療効果を予測するバイオマーカーとして有用である可能性が得られた。細胞膜上の CD26 の発現が高い細胞であれば腫瘍・正常細胞ともに培養上清中に sCD26 を産生し、YS110 の容量依存的、及び経時的に sCD26 の産生が阻害されることを明らかにした。

F. 今後の展望

次年度は YS110 の抗腫瘍作用メカニズムの更なる解明を目指し、腫瘍細胞膜上の CD26 に YS110 が結合してから核内まで移行するメカニズムの詳細を検討する。また、YS110 投与後に一度低下した血清中 sCD26/DPP4 titer のその後の回復の違いが何を反映した結果であるのかを明らかにし、血清中 sCD26/DPP4 titer の変動解析が YS110 の予後・治療効果を予測するバイオマーカーとして有用であることをより確かなものにする。

G. 研究発表

1. 論文発表

- 1) Itoh T, Hatano R, Komiya E, Otsuka H, Narita Y, Aune TM, Dang NH, Matsuoka S, Naito H, Tominaga M, Takamori K, Morimoto C, Ohnuma K. Biological effects of IL-26 on T cell-mediated skin inflammation including psoriasis. *J Invest Dermatol.* 2019; 139(4): 878-889
- 2) Santos MF, Rappa G, Karbanova J, Vanier C, Morimoto C, Corbeil D, Lorico A. Anti-human CD9 antibody Fab fragment impairs the internalization of extracellular vesicles and the nuclear transfer of their cargo proteins. *J Cell Mol Med.* 2019; 23(6): 4408-4421
- 3) Mezawa Y, Daigo Y, Takano A, Miyagi Y, Yokose T, Yamashita T, Morimoto C, Hino O, Orimo A. CD26 expression is attenuated by TGF- β and SDF-1 autocrine signaling on stromal myofibroblasts in

- human breast cancers. *Cancer Med.* 2019; 8(8): 3936-3948
- 4) Hatano R, Yamada T, Madokoro H, Otsuka H, Komiya E, Itoh T, Narita Y, Iwata S, Yamazaki H, Matsuoka S, Dang NH, Ohnuma K, Morimoto C. Development of novel monoclonal antibodies with specific binding affinity for denatured human CD26 in formalin-fixed paraffin-embedded and decalcified specimens. *PLoS One.* 2019; 14(6): e0218330
 - 5) Hatano R, Itoh T, Otsuka H, Okamoto S, Komiya E, Iwata S, Aune TM, Dang NH, Kuwahara-Arai K, Ohnuma K, Morimoto C. Characterization of novel anti-IL-26 neutralizing monoclonal antibodies for the treatment of inflammatory diseases including psoriasis. *MAbs.* 2019; 11(8): 1428-1442
 - 6) Hayashi M, Madokoro H, Yamada K, Nishida H, Morimoto C, Sakamoto M, Yanagawa H, Yamada T. Novel Antibody-Drug Conjugate with Anti-CD26 Humanized Monoclonal Antibody and Transcription Factor IIIH(TFIIIH) Inhibitor, Triptolide, Inhibits Tumor Growth via Impairing mRNA Synthesis. *Cancers (Basel).* 2019; 11(8): E1138
 - 7) Takeda T, Ohe Y, Horinouchi H, Hida T, Shimizu J, Seto T, Nosaki K, Kishimoto T, Miyashita I, Yamada M, Kaneko Y, Morimoto C, Nakagawa K. Phase I study of YS110, a recombinant humanized monoclonal antibody to CD26, in Japanese patients with advanced malignant pleural mesothelioma. *Lung Cancer* 2019; 137: 64-70
 - 8) Sato T, Tatekoshi A, Takada K, Iyama S, Kamihara Y, Jawaid P, Rehman MU, Noguchi K, Kondo T, Kajikawa S, Arita K, Wada A, Murakami J, Arai M, Yasuda I, Dang NH, Hatano R, Iwao N, Ohnuma K, Morimoto C. DPP8 is a novel therapeutic target for multiple myeloma. *Sci Rep.* 2019; 9(1): 18094
 - 9) Ohnuma K, Hatano R, Dang NH, Morimoto C. Rheumatic diseases associated with immune checkpoint inhibitors in cancer immunotherapy. *Mod Rheumatol.* 2019; 29(5): 721-732
 - 10) 岩尾憲明, 大沼圭, 波多野良, 大塚春奈, 古宮栄利子, 伊藤匠, 森本幾夫. GVHDの発症と慢性炎症. 別冊 *Bio Clinica: 慢性炎症と疾患*, 2019; 8(1): 120-125
- ## 2. 著書
- 1) Okamoto T, Hatano R, Nakano K, Yamada T, Yamazaki H, Kaneko Y, Dang NH, Morimoto C, Ohnuma K. Regulation of proliferation of malignant mesothelioma cells by CD26-cyclophilin A molecular complex. In: *Advanced in Medicine and Biology.* Nova Science Publishers, Inc., Hauppauge, NY, Editor: Leon V. Berhardt, 2019; Volume 156: Chapter 8: 165-185
- ## 3. 学会発表
- 1) Komiya E, Hatano R, Itoh T, Otsuka H, Ohnuma K, Tominaga M, Morimoto C, Takamori K. CD26/DPPIV regulates mechanical itch by enzymatic degradation of mu-opioid receptor ligands. 24th World

- Congress of Dermatology (WCD), Milan, 2019.6.15
- 2) Komiya E, Hatano R, Itoh T, Otsuka H, Kamata Y, Honda K, Toyama S, Moniaga CS, Ohnuma K, Tominaga M, Morimoto C, Takamori K. Possible role for CD26/DPPIV in regulating mechanical itch (Alloknesis). 28th European Academy of Dermatology and Venereology (EADV) Congress, Madrid, 2019.10.9
- 3) Komiya E, Hatano R, Itoh T, Otsuka H, Kamata Y, Honda K, Toyama S, Moniaga CS, Ohnuma K, Tominaga M, Morimoto C, Takamori K. Possible regulation of mechanical itch by CD26/DPPIV. 10th World Congress on Itch (WCI), Sydney, 2019.11.17
- 4) 古宮栄利子, 富永光俊, 波多野良, 伊藤匠, 大塚春奈, 本田耕太郎, 外山扇雅, 鎌田弥生, 大沼圭, 森本幾夫, 高森建二. 加齢皮膚で誘発される機械的かゆみ調節機構の解明. 第15回 加齢皮膚医学研究会, 熊本, 2019年3月9日
- 5) Hiroko Nishida, Mutsumi Hayashi, Chikao Morimoto, Michiie Sakamoto, Taketo Yamada. CD26 is a potential therapeutic target by humanized monoclonal antibody in multiple myeloma. 第108回 日本病理学会総会, 東京, 2019年5月10日
- 6) 古宮栄利子, 波多野良, 富永光俊, 伊藤匠, 鎌田弥生, 本田耕太郎, 外山扇雅, カタリナサギタモニアガ, 大沼圭, 森本幾夫, 高森建二. CD26/ dipeptidyl-peptidase IV は機械的かゆみの抑制因子である. 第24回 日本病態プロテアーゼ学会, 岐阜, 2019年8月2日
- 7) 山田健人, 坂元亨宇, 森本幾夫, 林睦. Anti-CD26 humanized antibody-triptolide conjugate transports into nucleus and inhibits RNA polymerase II activity. 第78回 日本癌学会学術総会, 京都, 2019年9月27日
- 8) Hiroko Nishida, Mustumi Hayashi, Chikao Morimoto, Michiie Sakamoto, Taketo Yamada. Humanized anti-CD26 monoclonal antibody clonogenic side population cells in multiple myeloma. 第81回 日本血液学会学術集会, 東京, 2019年10月12日
- H.** 知的財産権の出願・登録状況（予定を含む）
1. 特許取得
大沼圭, 森本幾夫, 波多野良: 免疫チェックポイント阻害剤. 特願 2019-004480
 2. 実用新案登録
なし
 3. その他
なし

Ⅲ. 研究成果の刊行に関する一覧表

<研究成果の刊行に関する一覧表>

【書 籍】

著者氏名	論文タイトル名	書籍全体の編集者名	書 籍 名	出版社名	出版地	出版年	ページ
Okamoto T, Hatano R, Nakano K, Yamada T, Yamazaki H, Kaneko Y, Dang NH, Morimoto C, Ohnuma K.	Regulation of proliferation of malignant mesothelioma cells by CD26-cyclophilin A molecular complex.	Leon V. Berhardt	Advances in Medicine and Biology	Nova Science Publishers, Inc	USA	2019	165-185

【雑 誌】

発表者氏名	論文タイトル名	発表誌名	巻号	ページ	出版年
Itoh T, Hatano R, Komiya E, Otsuka H, Narita Y, Aune TM, Dang NH, Matsuoka S, Naito H, Tominaga M, Takamori K, Morimoto C, Ohnuma K	Biological effects of IL-26 on T cell-mediated skin inflammation including psoriasis	J Invest Dermatol.	139(4)	878-889	2019
Santos MF, Rappa G, Karbanova J, Vanier C, Morimoto C, Corbeil D, Lorico A	Anti-human CD9 antibody Fab fragment impairs the internalization of extracellular vesicles and the nuclear transfer of their cargo proteins.	J Cell Mol Med.	23(6)	4408-4421	2019
Mezawa Y, Daigo Y, Takano A, Miyagi Y, Yokose T, Yamashita T, Morimoto C, Hino O, Orimo A	CD26 expression is attenuated by TGF- β and SDF-1 autocrine signaling on stromal myofibroblasts in human breast cancers.	Cancer Med.	8(8)	3936-3948	2019

発表者氏名	論文タイトル名	発表誌名	巻号	ページ	出版年
Hatano R, Yamada T, Madokoro H, Otsuka H, Komiya E, Itoh T, Narita Y, Iwata S, Yamazaki H, Matsuoka S, Dang NH, Ohnuma K, Morimoto C	Development of novel monoclonal antibodies with specific binding affinity for denatured human CD26 in formalin-fixed paraffin-embedded and decalcified specimens.	PLoS One.	14(6)	e0218330	2019
Hatano R, Itoh T, Otsuka H, Okamoto S, Komiya E, Iwata S, Aune TM, Dang NH, Kuwahara-Arai K, Ohnuma K, Morimoto C	Characterization of novel anti-IL-26 neutralizing monoclonal antibodies for the treatment of inflammatory diseases including psoriasis.	MAbs.	11(8)	1428-1442	2019
Hayashi M, Madokoro H, Yamada K, Nishida H, Morimoto C, Sakamoto M, Yanagawa H, Yamada T	Novel Antibody-Drug Conjugate with Anti-CD26 Humanized Monoclonal Antibody and Transcription Factor IIH(TFIIH) Inhibitor, Triptolide, Inhibits Tumor Growth via Impairing mRNA Synthesis.	Cancers (Basel).	11(8)	E1138	2019
Takeda T, Ohe Y, Horinouchi H, Hida T, Shimizu J, Seto T, Nosaki K, Kishimoto T, Miyashita I, Yamada M, Kaneko Y, Morimoto C, Nakagawa K	Phase I study of YS110, a recombinant humanized monoclonal antibody to CD26, in Japanese patients with advanced malignant pleural mesothelioma	Lung Cancer	137	64-70	2019

発表者氏名	論文タイトル名	発表誌名	巻号	ページ	出版年
Sato T, Tatekoshi A, Takada K, Iyama S, Kamihara Y, Jawaid P, Rehman MU, Noguchi K, Kondo T, Kajikawa S, Arita K, Wada A, Murakami J, Arai M, Yasuda I, Dang NH, Hatano R, Iwao N, Ohnuma K, Morimoto C	DPP8 is a novel therapeutic target for multiple myeloma.	Sci Rep.	9(1)	18094	2019
Ohnuma K, Hatano R, Dang NH, Morimoto C	Rheumatic diseases associated with immune checkpoint inhibitors in cancer immunotherapy	Mod Rheumatol	29(5)	721-732	2019
Nishida H, Yamada T	Monoclonal Antibody Therapies in Multiple Myeloma: A Challenge to Develop Novel Targets	J Oncol.	2019	6084012	2019
Amatya VJ, Kushitani K, Mawas AS, Miyata Y, Okada M, Kishimoto T, Inai K, Takeshima Y	Reply to 'MUC4 staining in sarcomatoid carcinomas' by Berg et al.	Mod Pathol.	32(1)	158	2019
Sato H, Soh J, Aoe K, Fujimoto N, Tanaka S, Nanba K, Torigoe H, Shien K, Yamamoto H, Tomida S, Tao H, Okabe K, Kishimoto T, Toyooka S.	Droplet digital PCR as a novel system for the detection of microRNA-34b/c methylation in circulating DNA in malignant pleural mesothelioma	Int J Oncol.	54(6)	2139-2148	2019
Nagamatsu Y, Oze I, Aoe K, Hotta K, Kato K, Nakagawa J, Hara K, Kishimoto T, Fujimoto N	Physician requests by patients with malignant pleural mesothelioma in Japan	BMC Cancer	19(1)	383	2019

発表者氏名	論文タイトル名	発表誌名	巻号	ページ	出版年
Takada K, Fujimoto N, Ozeki T, Nishimura J, Miyamoto Y, Asano M, Fuchimoto Y, Wada S, Ozaki S, Igawa T, Sonobe H, Kishimoto T.	Small intestinal intussusception in an adult	J Clin Pathol.	72(7)	510	2019
Okada M, Kijima T, Aoe K, Kato T, Fujimoto N, Nakagawa K, Takeda Y, Hida T, Kanai K, Imamura F, Oizumi S, Takahashi T, Takenoyama M, Tanaka H, Hirano J, Namba Y, Ohe Y	Clinical Efficacy and Safety of Nivolumab: Results of a Multicenter, Open-label, Single-arm, Japanese Phase II study in Malignant Pleural Mesothelioma (MERIT)	Clin Cancer Res.	25(18)	5485-5492	2019
Kishimoto T, Fujimoto N, Ebara T, Omori T, Oguri T, Niimi A, Yokoyama T, Kato M, Usami I, Nishio M, Yoshikawa K, Tokuyama T, Tamura M, Yokoyama Y, Takahashi S, Abdelsied M, Alexander W T, Alexander D B, Tsuda H	Serum levels of the chemokine CCL2 are elevated in malignant pleural mesothelioma patients	BMC Cancer	19(1)	1204	2019
Fujimoto N	Immunecheckpoint Blockade in Malignant Pleural Mesothelioma	IntechOpen	89116		2019
岩尾憲明, 大沼圭, 波多野良, 大塚春奈, 古宮栄利子, 伊藤匠, 森本幾夫	GVHDの発症と慢性炎症	別冊Bio Clinica: 慢性炎症と疾患	8(1)	120-125	2019

発表者氏名	論文タイトル名	発表誌名	巻号	ページ	出版年
岸本卓巳	石綿（アスベスト）が 人体に与える影響	産業保健21	25(1)	5-7	2019
岸本卓巳、藤本伸一、 加藤勝也、井内康輝	石綿関連疾患の診断と 治療 Diagnosis and treatment of asbestos related diseases	産業医学レビュ ー	32(2)	99-130	2019
藤本伸一	石綿（アスベスト）関 連肺・胸膜疾患の的確 な診断と新規治療法の 導入	産業保健21	25(1)	17	2019
藤本伸一	胸膜・腹膜の病理 胸 膜・腹膜疾患への臨床 的アプローチ -治療を 中心として-	病理と臨床	37(11)	1055- 1061	2019

IV. 研究成果の別刷

Chapter 8

**REGULATION OF PROLIFERATION
OF MALIGNANT MESOTHELIOMA CELLS
BY CD26-CYCLOPHILIN A
MOLECULAR COMPLEX**

***Toshihiro Okamoto¹, PhD, Ryo Hatano¹, PhD,
Kenji Nakano², MD, PhD, Taketo Yamada^{3,4}, MD, PhD,
Hiroto Yamazaki¹, MD, PhD, Yutaro Kaneko⁵,
Nam H. Dang⁶, MD, PhD, Chikao Morimoto¹, MD, PhD
and Kei Ohnuma, MD, PhD^{1,*}***

¹Department of Therapy Development and Innovation
for Immune Disorders and Cancers, Graduate School of Medicine,
Juntendo University, Tokyo, Japan

²Graduate School of Pharmaceutical Sciences, Osaka University,
Suita, Japan

³Department of Pathology, Keio University School of Medicine,
Tokyo, Japan

⁴Department of Pathology, Saitama Medical University, Saitama, Japan

* Corresponding Author's Email: kohnuma@juntendo.ac.jp.

⁵Y's AC Co., Ltd., Tokyo, Japan

⁶Division of Hematology/Oncology, University of Florida,
Gainesville, FL, US

ABSTRACT

Malignant pleural mesothelioma (MPM) is a rare and aggressive neoplasm deriving from the pleural mesothelial lining. More than 80% of cases are related to previous occupational asbestos exposure, with its worldwide incidence being expected to increase in the future. Despite the modest clinical benefit of a multimodality treatment approach including surgery, combination chemotherapy and radiation, prognosis remains grim with poor overall survival. For the vast majority of MPM patients ineligible for potentially curative surgery at diagnosis, systemic chemotherapy is the best option to improve survival. We have had a long-standing interest in the role of CD26 in cancer biology and its suitability as a novel therapeutic target in selected neoplasms. Recently, we presented robust *in vivo* data on the anti-tumor activity of anti-CD26 monoclonal antibody in mouse xenograft models. Moreover, we have published the results of the first-in-human (FIH) phase 1 clinical trial of a humanized anti-CD26 monoclonal antibody (HuCD26mAb, YS110) for CD26-expressing solid tumors, particularly refractory MPM. Our FIH study demonstrated that YS110 therapy exhibited a favorable safety profile and resulted in encouraging disease stabilization in selected patients with advanced/refractory CD26-expressing cancers. On the other hand, microarray analysis of CD26-knockdown and CD26-transfected cells revealed that CD26-expression was closely linked to the expression of several genes contributing to cell proliferation and cell cycle regulation. It is conceivable that CD26-mediated cell cycle regulating events, which remain to be clarified, have a pivotal role in MPM cell biology. We herein present our latest findings that cell cycle regulation via CD26 is mediated by its association with cyclophilin A (CyPA), which regulates protein folding and trafficking with peptidyl prolyl *cis-trans* isomerase activity. Our data strongly suggest that targeting the CD26-CyPA complex in combination with HuCD26mAb therapy could improve the clinical outcome of MPM patients.

1. INTRODUCTION

Malignant pleural mesothelioma (MPM) is a rare and aggressive neoplasm arising from the pleural mesothelial lining [1], with more than 80% of cases being related to previous occupational asbestos exposure [2]. Despite the modest clinical benefit of a multimodality treatment approach including surgery, combination chemotherapy and radiation, prognosis remains grim with poor overall survival [3]. Due to the lack of efficacy of conventional treatments, novel therapeutic strategies are urgently needed to improve the clinical outcomes for MPM [1].

CD26 is a 110-kDa, type II transmembrane glycoprotein with known dipeptidyl peptidase IV (DPPIV, EC 3.4.14.5) activity in its extracellular domain and is capable of cleaving N-terminal dipeptides with either L-proline or L-alanine at the penultimate position [4]. Our previous work demonstrated that CD26 is preferentially expressed in MPM cells but not in normal mesothelial cells, and suggested that CD26 expression level correlates with clinical outcomes, while being a potential therapeutic target in MPM [5, 6]. The first-in-human (FIH) phase 1 clinical trial of a humanized anti-CD26 monoclonal antibody (HuCD26mAb, YS110) for CD26-expressing solid tumors, particularly refractory MPM, was conducted with results being recently published [7]. Our FIH study demonstrated that YS110 therapy exhibited a favorable safety profile and resulted in encouraging disease stabilization in a number of patients with advanced/refractory CD26-expressing cancers. However, new treatment combinations consisting of other novel agents and HuCD26mAb are needed to potentially achieve greater efficacy for the treatment of MPM. Molecular analysis of cellular events associated with HuCD26mAb therapy revealed that CD26-expression was closely linked to the expression of several genes contributing to cell proliferation and cell cycle regulation [6, 8, 9]. It is conceivable that CD26-mediated cell cycle regulating events, which remain to be clarified, have a pivotal role in MPM cell biology.

As CD26 exerts its biological activities through interacting with other molecules [8-10], it is a reasonable assumption that CD26 promotes tumor progression by interacting with other oncogenic proteins. Since it is a

prognostic marker for several types of cancers [11-15], we speculated that CD26 associates with other prognostic molecules, including cyclophilin A (CyPA). It is a ubiquitously distributed protein belonging to the immunophilin family, and has peptidyl prolyl *cis-trans* isomerase (PPIase) activity, which regulates protein folding and trafficking. CyPA is also a novel prognostic factor for endometrial carcinoma and clear-cell renal carcinoma [16, 17]. In addition, CyPA is overexpressed in various human cancers and may be a promising target for cancer therapy [18-21]. Of interest, CyPA forms a complex with other molecules to exhibit biological effects [22-24]. We therefore examined whether CD26 exerts its tumorigenic activity via CyPA and found that CD26 formed a complex with CyPA in the cytosol by immunoprecipitation assay and super-resolution stimulated emission depletion (STED) microscopy analysis [25].

In the current study, focusing on the association between CyPA and CD26, we examined the physical and functional interaction between CD26 and CyPA in MPM cells. Our results hence suggest that a combined therapeutic approach targeting CyPA and CD26 can potentially improve the clinical outcome of MPM patients.

2. METHODS

2.1. Antibodies

Mouse monoclonal anti-human CD26 Ab (1F7) was produced in our laboratory [26]. Control IgG was purchased from Sigma-Aldrich (Cat#12511). For immunofluorescence (IF) and western blotting (WB), mouse monoclonal anti-CyPA Ab (abcam: ab58144, 1:200 for IF, 1:1000 for WB), rabbit monoclonal anti-CyPA Ab (Cat#ab126738, 1:200 for immunohistochemistry (IHC)), rabbit polyclonal anti-actin Ab (abcam: ab1801, 1:1000 for WB), goat polyclonal anti-human CD26 Ab (R&D Systems: AF1180, 1:100 for IF, 1:1000 for WB, 1:100 for IHC) were purchased. For flow cytometry, PE conjugated mouse anti-human CD26 Ab (BD Pharmingen: Cat#555437) was used. Secondary Abs used for IF

were Alexa Fluor® 647 donkey anti-goat IgG (Invitrogen: Cat#A21447, 1:500), Alexa Fluor® 488 donkey anti-rabbit IgG (Invitrogen: Cat#A21206, 1:500), and Alexa Fluor™ 555 donkey anti-mouse IgG (Invitrogen: Cat#A31570, 1:500).

2.2. Cell Lines

Each cell line was maintained in RPMI-1640 medium supplemented with 10% heat-inactivated fetal calf serum (FCS), penicillin (100 U/ml) and streptomycin (100 µg/ml) at 37°C and 5% CO₂. NCI-H226 (H226) (CRL-5826), MSTO-211H (MSTO) (CRL-2081), and NCI-H28 (H28) (CRL-5820) were mesothelioma cell lines obtained from the American Type Culture Collection (ATCC). JMN was a mesothelioma cell line provided by Dr. Brenda Gerwin (Laboratory of Human Carcinogenesis, NIH, Bethesda, MD). HCC4006 (CTL-2871), HCC827 (CRL-2868), HCC2935 (CRL-2869), and A549 (CCL-185) were lung carcinoma cell lines obtained from ATCC. PC14 (RCB0446) and Lu99 (RCB1900) were lung carcinoma cell lines obtained from Riken BRC. AsPC-1 (CRL-1682) and PANC-1 (CRL-1469) were pancreatic cancer cell lines obtained from ATCC.

2.3. Transfection of CD26 cDNA

Full-length CD26 cDNA was subcloned into a retroviral plasmid pLNCX2 vector (Clontech) and transfected into MSTO cells using Lipofectamine reagent (Invitrogen). As a control, cells were transfected with the empty pLNCX2 vector. Expression of transfected cDNA was confirmed by western blot and flow cytometry. The method for generating the transfectants was described in detail in our previous report [8].

2.4. Transfection of siRNAs

CD26-siRNA was obtained from QIAGEN, and siRNAs for CyPA were obtained from Sigma-Aldrich. As control siRNA, AllStars Negative control siRNA (QIAGEN) and Mission siRNA universal negative control (Sigma-Aldrich) were used. Target sequences were as follows:

CD26si: (NM_001935) ACACTCTAACTGATTACTTAA

CyPA_{si-1}: (NM_021130) GGTGTTTGGCAAAGTGAAA

CyPA_{si-2}: (NM_021130) CGTTTGAGTTAAGAGTGTT

2.5. Flow Cytometry

Cells were harvested with 0.05% trypsin (Gibco), resuspended with phosphate buffered saline (PBS) containing 2% FCS, and stained with PE labeled anti-CD26 Ab or isotype-matched IgG for 30 min on ice. After being washed twice with PBS containing 2% FCS, cells were analyzed by BD FACS Calibur (BD Biosciences). Data were analyzed by FlowJo software (BD Biosciences).

2.6 Western Blotting

Cells were treated with lysis buffer (50 mM HEPES pH 7.4, 150 mM NaCl, 1.0% Triton X-100, and 1/100 vol of Proteinase Inhibitor Cocktail). The cell lysates were centrifuged at 15,000 rpm for 15 min at 4°C, then SDS-buffer was added to the supernatants, followed by boiling at 100°C for 5 min. Proteins from 2×10^3 cells were electrophoresed on 4-20% Mini-PROTEAN precast acrylamide gel (BIO-RAD), and transferred to Immobilon-P membrane (Millipore). The blots were probed with the indicated Abs and incubated with horseradish peroxidase-conjugated Ab. Subsequently, protein was detected with Western Lightning (PerkinElmer) by using ImageQuant LAS4000 (GE Healthcare). Quantification of protein

expression was conducted using C-Digit Blot Scanner (M&S Instruments Inc). To separate cytoplasm and nucleus, NE-PER nuclear and cytoplasmic extraction reagents (Thermo Scientific) was used according to the manufacturer's instruction.

2.7. Immunoprecipitation

Cells (2×10^6) were lysed in 1 ml of lysis buffer and incubated on ice for 30 min. The cell lysates were centrifuged at 15,000 rpm for 15 min at 4°C and supernatants were incubated for 2 hrs with the first antibody at 4°C. The immunocomplexes were precipitated by adding 30 μ l of protein G agarose beads (GE Healthcare) to the lysate and incubated for 1 hr at 4°C, then washed 5 times with ice-cold lysis buffer. Next, the samples were suspended and denatured in SDS sample buffer (50 mM Tris pH 6.8, 2% SDS, 100 mM dithiothreitol, 10% glycerol, 0.01% bromophenol blue). Finally, the samples were boiled at 100°C for 5 min, and cooled on ice. For western blotting analysis, immunoprecipitants were collected by centrifuge at 15,000 rpm for 1 min.

2.8. Immunohistochemistry

Histological sections of eighty-four MPM tissue samples were previously examined [2]. For immunohistochemistry, sections were washed with PBS and subjected to antigen retrieval by heating at 100°C in 0.01M sodium citrate (pH 6.0) for 10 min. Then, the samples were treated with 3% H₂O₂ before incubation with the primary Ab against CyPA. Immune complexes were detected by using an ImmPRESS REAGENT KIT (Vector Laboratories). Histological studies were conducted in the Department of Pathology of Keio University School of Medicine (Tokyo, Japan), after official approval of the Keio University School of Medicine Review Board was obtained (ID number 2012-100-1).

2.9. Immunofluorescence Analysis

MPM cells were cultured on Lab-Tek chamber slide (Thermo Fisher) and fixed in 4% paraformaldehyde for 30 min at 4°C. After washing three times with PBS, cells were permeabilized with 0.1% Triton X-100. Cells were washed three times with PBS and treated with normal antiserum for 30 min at room temperature. Then, cells were treated with primary antibody at 37°C for 1 hr. After washing three times with PBS, cells were treated with secondary antibody at room temperature for 45 min. After washing three times with PBS, cells were applied with antifade mounting medium with DAPI (Vector laboratories). Cells were viewed by confocal fluorescence microscopy (TCS-SP5, Leica) and STED microscopy (Leica TCS GateA STED CW). Data were imaged using Leica Microscope Software. For STED microscopy, CD26 was detected by anti-CD26 mAb (1F7) labeled with Oregon Green 488. CyPA was detected by anti-CyPA Ab labeled with Alexa Fluor 532.

2.10. qRT-PCR

Total RNA was isolated using RNeasy Mini kit (Qiagen). RNAs were reverse transcribed by Prime Script RT (TAKARA BIO Inc.) and cDNAs were subjected to RT-PCR analysis with 7500 FAST REAL-TIME PCR System using the SYBER-Green Master PCR Mix (Applied Biosystem) in triplicates. HPRT1 was used as internal control. The primer sequences were as follows;

CD26: Forward:CAAATTGAAGCAGCCAGACA

Reverse: GTTGGGAGACCCATGTAACG

CyPA: Forward: TTCATCTGCACTGCCAAGAC

Reverse: TCGAGTTGTCCACAGTCAGC

HPRT1: Forward: TGCTCGAGATGTGATGAAGG

Reverse:TCCCCTGTTGACTGGTCATT

2.11. MTT Cell Proliferation Assay

Cell proliferation was measured by MTT assay using Tetra Color ONE system (Seikagaku Biosciences). Cells (2×10^3) were seeded into a 96 well culture plate in the RPMI-1640 medium supplemented with 10% FCS, and MTT assay was performed at day 2.

2.12. Microarray Analysis

H226 and JMN cells were treated with anti-CD26 Ab for 16 hrs, and total RNA was isolated, subjected to DNA microarray analysis with DNA Chip 3D Gene (TORAY). A heat map of tetraspanin genes differentially expressed between anti-CD26 Ab and control Ab treated mesothelioma cells was constructed by hierarchical cluster analysis using cluster 3.0 software and the results were displayed with the TreeView program. The data discussed in this publication have been deposited in NCBI's Gene Expression Omnibus and are accessible through GEO Series accession number GSE100848.

2.13. Statistical Analysis

Data in figure legends are represented as Mean and SE. For mice xenograft study, data are represented by Mean and SD. The exact value of sample size (n) is given in the figure legends. Statistical analyses were performed with two-tailed Student *t*-test. *P* value <0.01 was considered as statistically significant.

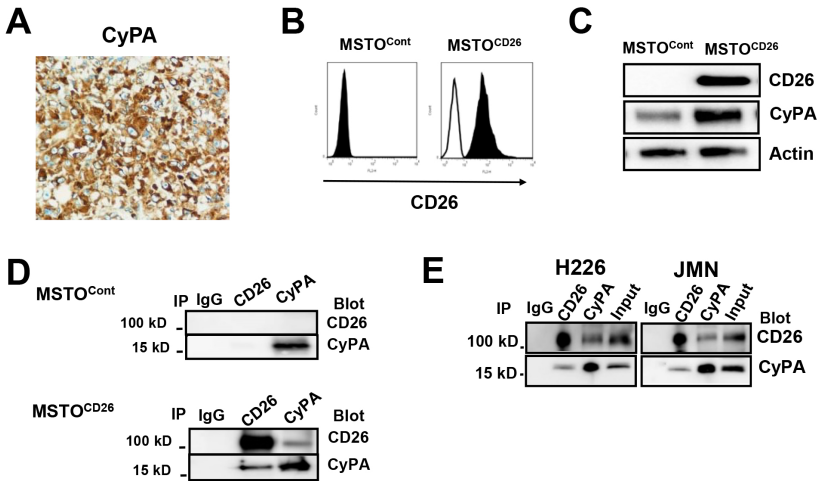
3. RESULTS

3.1. Cyclophilin A Associates with CD26 Biochemically

CD26 exerts its biological activities by interacting with other molecules [8-10]. CD26 is also known to be a potential prognostic factor in many types of cancers, and it displays its tumorigenic activity via its association with other prognostic molecules [11-15]. Therefore, we conducted a search for new proteins interacting with the CD26 molecule by utilizing microarray analysis, culminating in our findings of a strong association between CD26 with CyPA (Accession No GSE100848) (<https://www.ncbi.nlm.nih.gov/geo/query/acc.cgi?acc=GSE100848>). CyPA has been shown previously to be a novel prognostic factor for endometrial carcinoma and clear-cell renal carcinoma [16, 17]. In addition, CyPA is overexpressed in various human cancers and has been suggested to be a promising target for cancer therapy [19-21]. Moreover, CyPA is known to be a binding partner of various proteins and functions as part of protein complexes [22-24]. Therefore, we hypothesized that CyPA is associated with CD26 functionally and physiologically.

We first examined localization of CyPA by immunohistochemical analysis and found that CyPA was strongly expressed in the cytosol of MPM specimens (Figure 1A). We next investigated whether CD26 associates with CyPA in MPM cells. For this purpose, we used the CD26-negative MPM cell line MSTO, and established CD26-positive MSTO by transfecting CD26-gene (MSTOCD26) (Figure 1B). MSTO with control vector (MSTOcont) cells expressed less CyPA than MSTOCD26, suggesting that transfection of CD26 augments the expression of CyPA (Figure 1C). In the MSTOCD26 cells, CyPA was co-immunoprecipitated by anti-CD26 antibody. Reciprocal immunoprecipitation with anti-CyPA antibody also pulled down CD26 (Figure 1D), indicating that exogenously introduced CD26 can form a complex with CyPA. To confirm an association between CD26 and CyPA, we examined whether CD26 associates with CyPA in the MPM cell lines H226 and JMN, with CD26 being natively expressed. In immunoprecipitation assay, CyPA was co-

precipitated with the CD26 molecule in both H226 and JMN cells (Figure 1E). These results strongly suggest that CD26 interacts with CyPA in CD26-positive MPM cells.



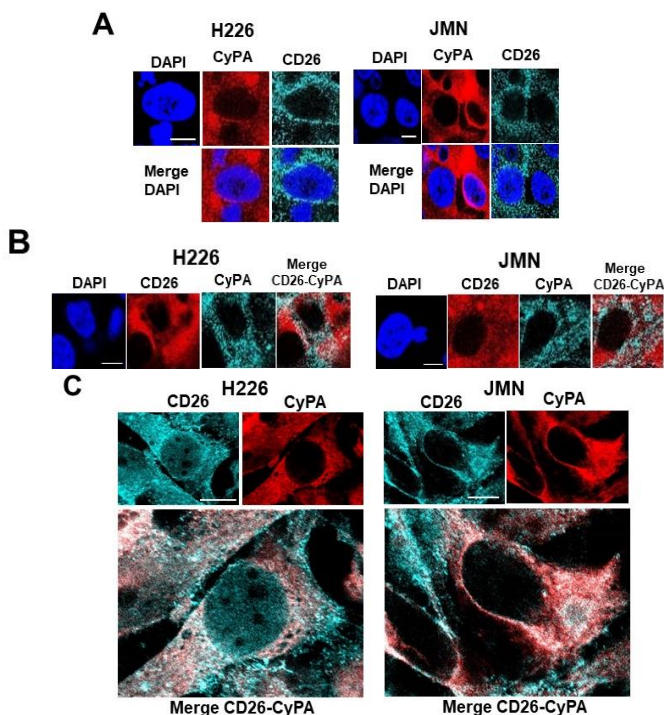
(A) Immunohistochemical analysis of CyPA. CyPA was expressed abundantly in the cytosol of MPM specimen. Original magnification, x400.
 (B) Flow cytometry analysis of CD26-expressions in MSTO^{cont} and MSTO^{CD26} cells.
 (C) Comparison between the MSTO^{CD26} and MSTO^{cont} cells for the expression of YB-1, CD26, and CyPA. The expression of CyPA was engineered to be elevated in the MSTO^{CD26} cells.
 (D) Immunoprecipitation by anti-CD26 (1F7) and anti-CyPA Abs in the MSTO^{CD26} and MSTO^{cont} cells. CD26 and CyPA co-precipitated with each other only in the MSTO^{CD26} cells.
 (E) Immunoprecipitation assay of the MPM cells using anti-CD26 (1F7) and anti-CyPA Abs. Co-precipitation of CD26 and CyPA was observed with their respective antibody, indicating their physical association in the cytosol.

Figure 1. Biochemical association of CyPA and CD26.

3.2. Subcellular Co-Localization of Cyclophilin A and CD26

To further characterize the CD26-CyPA molecular complex, we examined its subcellular co-localization utilizing confocal microscopy. In MPM cell lines, both CD26 and CyPA were expressed mostly in the cytosol (Figure 2A), with co-localization (white) of CD26 (red) and CyPA

(blue) being clearly observed (Figure 2B). We next conducted more detailed analysis utilizing super-resolution STED microscopy. This microscopic examination has extremely high resolution, allowing for detection of direct binding of different proteins. As shown in Figure 2C, co-localization (pink or white) of CD26 (blue) and CyPA (red) was clearly detected in the cytosol. These results strongly suggest that CD26 interacts with CyPA in the cytosol.

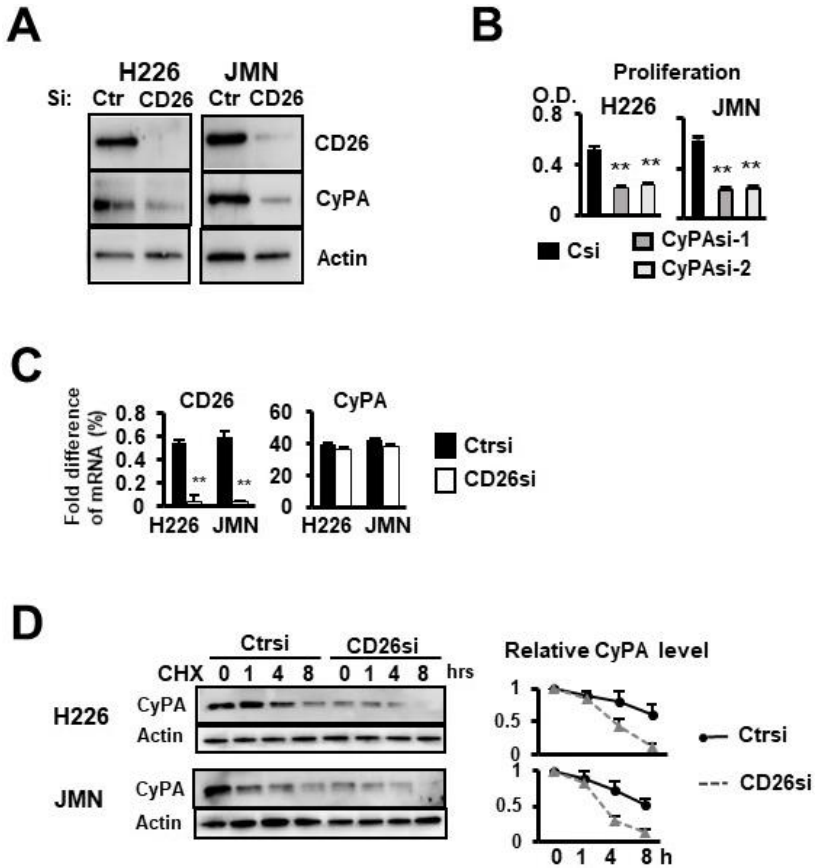


(A) Confocal microscopy analysis of CyPA and CD26. Strong expressions of CyPA (red, Alexa Fluor 555) and CD26 (blue, Alexa Fluor 647) were observed in the cytosol of MPM cells. Nuclei were stained with DAPI (purple). Scale bars, 10 μm.

(B) Colocalization of CD26 (red, Alexa Fluor 647) and CyPA (blue, Alexa Fluor 555) in the cytosol of MPM cells. Nuclei were stained with DAPI (purple). Colocalization was observed in confocal microscopy analysis (white). Scale bars, 10 μm.

(C) STED microscopy analysis of the MPM cells. Colocalization (white or pink) of CD26 (blue, Oregon Green 488 labeled 1F7 mAb) and CyPA (red, Alexa Fluor 532 labeled anti-CyPA Ab) was also confirmed by STED microscopy, indicating direct binding of CD26 and CyPA to each other to form a complex. Scale bars, 10 μm.

Figure 2. Subcellular co-localization of CyPA and CD26.



(A) Effect of CD26-siRNA on CyPA protein expression. The MPM cells were transfected with control (Ctr) or CD26-siRNA for 24 hrs, then subjected to western blot analysis. Expression of CyPA was decreased by the CD26-siRNA.
 (B) Knockdown of CyPA by siRNA. CyPA siRNA-1 and -2 were transfected into the MPM cells for 24 hrs, which were then subjected to MTT assay. Both CyPA-siRNA inhibited cell proliferation. (n = 6, **p < 0.001).
 (C) Effect on CyPA mRNA expression by CD26-knockdown. The MPM cells were transfected with CD26-siRNA for 24 hrs, then subjected to qRT-PCR. CyPA mRNA level was not affected by the CD26-siRNA. (n = 3, **p < 0.001).
 (D) Cycloheximide (CHX) chase assay and effect of CD26-knockdown on CyPA protein expression. MPM cells were transfected with the CD26-siRNA for 24 hrs, CHX (inhibitor of protein translation, 50 µg/ml) was then added. The cell lysates were extracted at the indicated time points for western blot analysis (left panels). Right panels are line graphs of the relative CyPA-expression. CD26-siRNA decreased the stability of CyPA protein.

Figure 3. Physical and functional interaction of CyPA and CD26 in MPM cells.

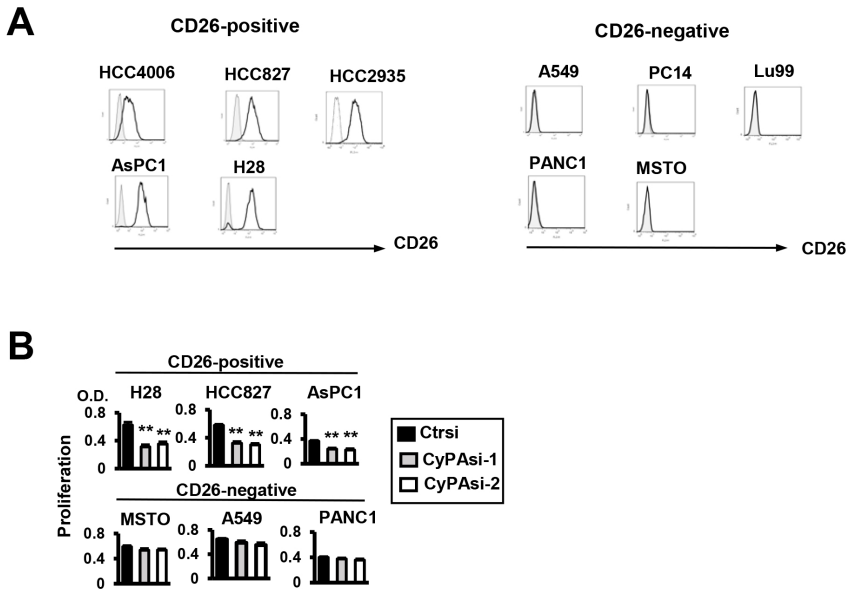
3.3. Regulation of CyPA by CD26 Expression in MPM Cells

To examine the functional interaction between CD26 and CyPA in MPM cells, we next investigated the effect of CD26-knockdown by siRNA on CyPA expression. Interestingly, knockdown of CD26 significantly suppressed the expression of CyPA (Figure 3A). We then conducted CyPA knockdown experiment utilizing siRNA. We prepared 2 different CyPA-siRNAs (CyPA_{si-1} and si-2) and showed that both of them inhibited the proliferation of MPM cells (Figure 3B). These findings suggest that CD26-mediated proliferation of MPM cells is exerted through the CyPA molecule. To further analyze CD26-mediated regulation of CyPA expression, we investigated the effect of CD26-knockdown on the stability of CyPA protein, finding that suppression of CD26 did not affect mRNA-expression of CyPA (Figure 3C). In contrast, cycloheximide (CHX) chase assay revealed that CD26-knockdown decreased stability of CyPA protein (Figure 3D). These results indicate that CD26 has a role in stabilizing the CyPA protein and promotes tumor progression by forming a complex with CyPA.

3.4. Suppression of CyPA in CD26-Positive Cancer Cells Inhibits Cell Proliferation

To further investigate the role of CD26 in promoting tumor progression by forming a complex with CyPA, we analyzed additional cell lines besides MPM cells. For this purpose, we used the CD26-positive cell lines HCC4006, HCC837, HCC2935 (lung cancer), AsPC1 (pancreatic cancer), and H28 (MPM); and the CD26-negative cell lines A549, PC14, Lu99 (lung cancer), PANC1 (pancreatic cancer), and MSTO (MPM) (Figure 4A) to further examine the effect of CyPA-knockdown by siRNA. Figure 4B showed that proliferation of the CD26-positive cells was strongly suppressed by CyPA-knockdown (upper panels). In contrast, proliferation of the CD26-negative cells was not affected by CyPA-knockdown (lower panels of Figure 4B). These results suggest that CyPA

promotes tumor progression by forming a complex with CD26 in various cancer cells.



(A) Flow cytometry analysis of CD26-positive and -negative cell lines originating from various tumors.

(B) Effect of CyPA-siRNA on the proliferation of CD26-positive (upper panels) and -negative cells (lower panels). The cells were transfected with CyPA siRNA-1 and -2 for 24 hrs, then subjected to MTT assay. Both CyPA-siRNAs inhibited the proliferation of CD26-positive cells, but not the CD26-negative cells. (n = 6, **p < 0.001).

Figure 4. Inhibition of cell proliferation by CyPA suppression in various CD26-positive cancer cells.

4. DISCUSSION

Despite the modest clinical benefit of a multimodality treatment approach including surgery, combination chemotherapy and radiation, prognosis of MPM patients remains grim with poor overall survival [3]. For the vast majority of MPM patients ineligible for potentially curative surgery at diagnosis, systemic chemotherapy is the best option to improve survival [27]. We have had a long-standing interest in the role of CD26 in

cancer biology and its suitability as a novel therapeutic target in selected neoplasms [28]. Recently, we reported robust *in vivo* data on the anti-tumor activity of anti-CD26 monoclonal antibody in mouse xenograft models [8, 9, 29, 30]. Moreover, we have published the results of the FIH phase 1 clinical trial of HuCD26mAb, YS110 for CD26-expressing solid tumors, particularly refractory MPM [7]. Our FIH study demonstrated that YS110 therapy had a favorable safety profile and resulted in encouraging disease stabilization in a number of patients with advanced/refractory CD26-expressing cancers [7]. Meanwhile, microarray analysis of CD26-knockdown and CD26-transfected cells also revealed that CD26-expression was closely linked to the expression of several genes contributing to cell proliferation and cell cycle regulation [6]. It is conceivable that CD26-mediated cell cycle regulating events, which remain to be clarified, have a pivotal role in MPM cell biology [31, 32].

As CD26 exerts its biological functions by interacting with other molecules [8-10], CD26 has been speculated to interact with several oncogenic molecules to promote tumorigenesis. One such candidate is CyPA, which has been shown to be a potential prognostic factor for many cancers while playing an oncogenic role [16-20] through its binding to other molecules [16, 17]. In view of this context, we focused on CyPA as a possible binding partner of CD26. In confocal microscopy analysis, CD26 and CyPA were colocalized in the cytosol. Moreover, immunoprecipitation assay confirmed that CD26 was physically associated with CyPA. In addition, STED microscopy [25] detected the direct binding of cytosolic CD26 to CyPA to form a protein complex. Importantly, CyPA knockdown resulted in significant inhibition of cell proliferation, hence suggesting a tumorigenic role for CyPA in MPM cells. However, knockdown of CD26 did not suppress the expression of CyPA-mRNA, but did decrease the stability of CyPA protein. Since complex formation can play a major role in protein stabilization [33, 34], it is a possibility that the CD26-CyPA protein complex enhances CyPA protein stability.

In summary, we showed that regulation of proliferation of MPM cells via CD26 is mediated by its association with CyPA, a molecule which regulates protein folding and trafficking with peptidyl prolyl *cis-trans*

isomerase activity. Our data strongly suggest that targeting the CD26-CyPA complex as part of a therapeutic combination involving HuCD26mAb could improve the clinical outcome of MPM patients.

ACKNOWLEDGMENTS

We thank Drs. H. Kato (Leica Microsystems K. K.), Y. Kojima, K. Miyahara, S. Nakamura (Laboratory of Morphology and Image Analysis, Research Support Center, Juntendo University) and H. Nakayama (Institute for Environmental and Gender Specific Medicine, Laboratory of Biochemistry/Faculty of Health Care and Nursing, Juntendo University) for helping immunofluorescent and STED microscopy analysis, and K. Kajino (Department of Pathology and Oncology, Juntendo University) for helpful discussion.

FUNDING

This study was supported in part by a grant of the Ministry of Health, Labour, and Welfare, Japan (Grant Number 150401-01 (C.M.) and 180101-01 (C.M.)), JSPS KAKENHI Grant Numbers JP16H05345 (C.M.), JP18H02782 (K.O.), JP17K10008 (R.H.), and JP19H03517 (K.N.).

This study was also supported in part by a Project for Development of Innovative Research on Cancer Therapeutics from Japan Agency for Medical Research and Development (Grant Number: 16ck0106082h0003) (K.N.).

REFERENCES

- [1] Kondola, S., Manners, D., Nowak, A. K. Malignant pleural mesothelioma: an update on diagnosis and treatment options. *Ther*

- Adv Respir Dis* 2016; 10: 275-288. DOI: 10.1177/1753465816628800.
- [2] Takeshima, Y., Inai, K., Amatya, V. J., et al. Accuracy of pathological diagnosis of mesothelioma cases in Japan: clinicopathological analysis of 382 cases. *Lung Cancer* 2009; 66: 191-197. DOI: 10.1016/j.lungcan.2009.01.011.
- [3] Maggioni, C., Barletta, G., Rijavec, E. et al. Advances in treatment of mesothelioma. *Expert Opin Pharmacother* 2016; 17: 1197-1205. DOI: 10.1080/14656566.2016.1176145.
- [4] Ohnuma, K., Dang, N. H., Morimoto, C. Revisiting an old acquaintance: CD26 and its molecular mechanisms in T cell function. *Trends Immunol* 2008; 29: 295-301. DOI: 10.1016/j.it.2008.02.010.
- [5] Amatya, V. J., Takeshima, Y., Kushitani, K. et al. Overexpression of CD26/DPPIV in mesothelioma tissue and mesothelioma cell lines. *Oncol Rep* 2011; 26: 1369-1375. DOI: 10.3892/or.2011.1449.
- [6] Aoe, K., Amatya, V. J., Fujimoto, N et al. CD26 overexpression is associated with prolonged survival and enhanced chemosensitivity in malignant pleural mesothelioma. *Clin Cancer Res* 2012; 18: 1447-1456. DOI: 10.1158/1078-0432.CCR-11-1990.
- [7] Angevin, E., Isambert, N., Trillet-Lenoir, V. et al. First-in-human phase 1 of YS110, a monoclonal antibody directed against CD26 in advanced CD26-expressing cancers. *Br J Cancer* 2017; 116: 1126-1134. DOI: 10.1038/bjc.2017.62.
- [8] Yamamoto, J, Ohnuma, K., Hatano, R. et al. Regulation of somatostatin receptor 4-mediated cytostatic effects by CD26 in malignant pleural mesothelioma. *Br J Cancer* 2014; 110: 2232-2245. DOI: 10.1038/bjc.2014.151.
- [9] Okamoto, T., Iwata, S., Yamazaki, H. et al. CD9 negatively regulates CD26 expression and inhibits CD26-mediated enhancement of invasive potential of malignant mesothelioma cells. *PLoS One* 2014; 9: e86671. DOI: 10.1371/journal.pone.0086671.
- [10] Kameoka J, Tanaka T, Nojima Y et al. Direct association of adenosine deaminase with a T cell activation antigen, CD26. *Science*

- 1993; 261: 466-469. <https://www.ncbi.nlm.nih.gov/pubmed/8101391>.
- [11] Cro L, Morabito F, Zucal N et al. CD26 expression in mature B-cell neoplasia: its possible role as a new prognostic marker in B-CLL. *Hematol Oncol* 2009; 27: 140-147. DOI: 10.1002/hon.888.
- [12] Saigusa S, Toiyama Y, Tanaka K et al. Prognostic relevance of stromal CD26 expression in rectal cancer after chemoradiotherapy. *Int J Clin Oncol* 2016; 21: 350-358. DOI: 10.1007/s10147-015-0902-8.
- [13] Liang P. I., Yeh B. W., Li W. M. et al. DPP4/CD26 overexpression in urothelial carcinoma confers an independent prognostic impact and correlates with intrinsic biological aggressiveness. *Oncotarget* 2017; 8: 2995-3008. DOI: 10.18632/oncotarget.13820.
- [14] Kapoor S. CD26: A prognostic marker of other systemic malignancies besides colo-rectal carcinomas. *World J Clin Oncol* 2012; 3: 126-127. DOI: 10.5306/wjco.v3.i8.126.
- [15] Lam C. S., Cheung A. H., Wong S. K. et al. Prognostic significance of CD26 in patients with colorectal cancer. *PLoS One* 2014; 9: e98582. DOI: 10.1371/journal.pone.0098582.
- [16] Li Z, Zhao X, Bai S et al. Proteomics identification of cyclophilin A as a potential prognostic factor and therapeutic target in endometrial carcinoma. *Mol Cell Proteomics* 2008; 7: 1810-1823. DOI: 10.1074/mcp.M700544-MCP200.
- [17] Yang, J., Li, A., Yang, Y., Li, X. Identification of cyclophilin A as a potential prognostic factor for clear-cell renal cell carcinoma by comparative proteomic analysis. *Cancer Biol Ther* 2011; 11: 535-546. DOI: 10.4161/cbt.11.5.14678.
- [18] Li, M., Zhai, Q., Bharadwaj, U. et al. Cyclophilin A is overexpressed in human pancreatic cancer cells and stimulates cell proliferation through CD147. *Cancer* 2006; 106: 2284-2294. DOI: 10.1002/cncr.21862.
- [19] Huang, C. F., Sun, Z. J., Zhao, Y. F. et al. Increased expression of peroxiredoxin 6 and cyclophilin A in squamous cell carcinoma of the

- tongue. *Oral Dis* 2011; 17: 328-334. DOI: 10.1111/j.1601-0825.2010.01730.x.
- [20] Gong, Z., Chi, C., Huang, X. et al. Cyclophilin A is overexpressed in hepatocellular carcinoma and is associated with the cell cycle. *Anticancer Res* 2017; 37: 4443-4447. DOI: 10.21873/anticancer.11839.
- [21] Lee, J, Kim, S. S. An overview of cyclophilins in human cancers. *J Int Med Res* 2010; 38: 1561-1574. DOI: 10.1177/147323001003800501.
- [22] Fischer, G., Tradler, T., Zarnt, T. The mode of action of peptidyl prolyl cis/trans isomerases in vivo: binding vs. catalysis. *FEBS Lett* 1998; 426: 17-20. <https://www.ncbi.nlm.nih.gov/pubmed/9598969>.
- [23] Zhu, D., Wang, Z., Zhao, J. J. et al. The Cyclophilin A-CD147 complex promotes the proliferation and homing of multiple myeloma cells. *Nat Med* 2015; 21: 572-580. DOI: 10.1038/nm.3867.
- [24] Saleh, T., Jankowski, W., Sriram G et al. Cyclophilin A promotes cell migration via the Abl-Crk signaling pathway. *Nat Chem Biol* 2016; 12: 117-123. DOI: 10.1038/nchembio.1981.
- [25] Vicidomini G, Bianchini P, Diaspro A. STED super-resolved microscopy. *Nat Methods* 2018; 15: 173-182. DOI: 10.1038/nmeth.4593.
- [26] Morimoto C, Torimoto Y, Levinson G et al. 1F7, a novel cell surface molecule, involved in helper function of CD4 cells. *J Immunol*, 1989; 143, 3430-9. <https://www.ncbi.nlm.nih.gov/pubmed/2479677>.
- [27] de Gooijer CJ, Baas P, Burgers JA. Current chemotherapy strategies in malignant pleural mesothelioma. *Transl Lung Cancer Res* 2018; 7: 574-583. DOI: 10.21037/tlcr.2018.04.10.
- [28] Havre PA, Abe M, Urasaki Y et al. The role of CD26/dipeptidyl peptidase IV in cancer. *Front Biosci* 2008; 13: 1634-1645. DOI: 10.2741/2787.
- [29] Inamoto T, Yamada T, Ohnuma K et al. Humanized anti-CD26 monoclonal antibody as a treatment for malignant mesothelioma tumors. *Clin Cancer Res* 2007; 13: 4191-4200. DOI: 10.1158/1078-0432.CCR-07-0110.

- [30] Inamoto T, Yamochi T, Ohnuma K et al. Anti-CD26 monoclonal antibody-mediated G1-S arrest of human renal clear cell carcinoma Caki-2 is associated with retinoblastoma substrate dephosphorylation, cyclin-dependent kinase 2 reduction, p27^{kip1} enhancement, and disruption of binding to the extracellular matrix. *Clin Cancer Res* 2006; 12: 3470-3477. DOI: 10.1158/1078-0432.CCR-06-0361.
- [31] P. Doonan B, Ohnuma K, H. Dang L et al. Current and emerging therapy for malignant pleural mesothelioma: Focus on CD26/dipeptidyl peptidase IV as a therapeutic target. *Current Cancer Therapy Reviews* 2017; 13: 76-88. DOI: 10.2174/1573394713666170907160734.
- [32] Ohnuma K, Hatano R, Komiya E et al. A novel role for CD26/dipeptidyl peptidase IV as a therapeutic target. *Front Biosci (Landmark Ed)* 2018; 23: 1754-1779. DOI: 10.2741/4671.
- [33] Basso AD, Solit DB, Chiosis G et al. Akt forms an intracellular complex with heat shock protein 90 (Hsp90) and Cdc37 and is destabilized by inhibitors of Hsp90 function. *J Biol Chem* 2002; 277: 39858-39866. DOI: 10.1074/jbc.M206322200.
- [34] Chew, J. L., Loh, Y. H., Zhang W et al. Reciprocal transcriptional regulation of Pou5f1 and Sox2 via the Oct4/Sox2 complex in embryonic stem cells. *Mol Cell Biol* 2005; 25: 6031-6046. DOI: 10.1128/MCB.25.14.6031-6046.2005.

Biological Effects of IL-26 on T Cell–Mediated Skin Inflammation, Including Psoriasis



Takumi Itoh¹, Ryo Hatano², Eriko Komiya^{2,3}, Haruna Otsuka², Yuka Narita², Thomas M. Aune⁴, Nam H. Dang⁵, Shuji Matsuoka⁶, Hisashi Naito¹, Mitsutoshi Tominaga³, Kenji Takamori³, Chikao Morimoto² and Kei Ohnuma²

Psoriasis is a chronic inflammatory skin disease characterized mainly by epidermal hyperplasia, scaling, and erythema; T helper 17 cells have a role in its pathogenesis. Although IL-26, known as a T helper 17 cytokine, is upregulated in psoriatic skin lesions, its precise role is unclear. We investigated the role of IL-26 in the imiquimod-induced psoriasis-like murine model using human *IL-26* transgenic mice. Erythema symptoms induced by daily applications of imiquimod increased dramatically in human *IL-26* transgenic mice compared with controls. Vascularization and immune cell infiltration were prominent in skin lesions of human *IL-26* transgenic mice. Levels of fibroblast growth factor (FGF) 1, FGF2, and FGF7 were significantly upregulated in the skin lesions of imiquimod-treated human *IL-26* transgenic mice and psoriasis patients. In vitro analysis demonstrated that FGF1, FGF2, and FGF7 levels were elevated in human keratinocytes and vascular endothelial cells following IL-26 stimulation. Furthermore, IL-26 acted directly on vascular endothelial cells, promoting proliferation and tube formation, possibly through protein kinase B, extracellular signal–regulated kinase, and NF- κ B pathways. Moreover, similar effects of IL-26 were observed in the murine contact hypersensitivity model, indicating that these effects are not restricted to psoriasis. Altogether, our data indicate that IL-26 may be a promising therapeutic target in T cell–mediated skin inflammation, including psoriasis.

Journal of Investigative Dermatology (2019) **139**, 878–889; doi:10.1016/j.jid.2018.09.037

INTRODUCTION

Psoriasis is a chronic inflammatory skin disease with characteristic histopathologic changes (Boehncke and Schon, 2015). Initiating events cause release of cytokines by keratinocytes, recruiting neutrophils and macrophages to inflammatory sites and activating dendritic cells. Release of cytokines such as IFN- α by dendritic cells induces Th helper (Th) 1 and Th17 T cell differentiation to contribute to the psoriatic events. The proinflammatory cascade continues with additional recruitment of inflammatory cells and cause hyperproliferation of the epidermal layer (Batycka-Baran et al., 2014; Tortola et al., 2012).

Th17 cells play an important role in the pathogenesis of psoriasis and other inflammatory disorders by producing cytokines promoting keratinocyte proliferation and other psoriatic changes (Lowe et al., 2008; Wilson et al., 2007). Human IL-26 is a 171-amino acid protein belonging to the IL-10 cytokine family (Donnelly et al., 2010; Kotenko, 2002), and is conserved in several vertebrate species, but is not found in mice and rats (Schoenborn et al., 2007). IL-26 is produced mainly by Th1, Th17, or natural killer cells (Corvaisier et al., 2012; Pene et al., 2008; Wolk et al., 2002), and it binds to a distinct cell surface receptor consisting of IL-20RA and IL-10RB to activate cells via STAT3 phosphorylation (Hor et al., 2004). We recently showed that IL-26 receptor is expressed on both human and murine fibroblasts, and IL-26 activates fibroblasts, leading to increased collagen production (Ohnuma et al., 2015). IL-26 induces monocyte and natural killer cell production of selected cytokines, including TNF- α , upregulates cell surface tumor necrosis factor–related apoptosis-inducing ligand expression and promotes generation of Th17 cells (Corvaisier et al., 2012). Although it has been suggested that IL-26 is involved in the pathophysiology of various chronic inflammatory disorders (Corvaisier et al., 2012; Dambacher et al., 2009; Ohnuma et al., 2015), its precise functions and target cells in inflammatory disorders remain to be elucidated.

A number of mouse models mimicking aspects of human psoriasis have been established (Gudjonsson et al., 2007; Schon, 2008). Imiquimod (IMQ) is a potent TLR7 and TLR8 agonist, and is used to treat selected skin disorders (Beutner and Ferenczy, 1997; Drobits et al., 2012; Szeimies et al., 2004). The development of psoriasis-like skin inflammation was reported as a side effect of IMQ application (Wu et al.,

¹Graduate School of Health and Sports Science, Juntendo University, Chiba, Japan; ²Department of Therapy Development and Innovation for Immune Disorders and Cancers, Graduate School of Medicine, Juntendo University, Tokyo, Japan; ³Institute for Environmental and Gender Specific Medicine, Juntendo University Graduate School of Medicine, Chiba, Japan; ⁴Department of Medicine, Vanderbilt University School of Medicine, Vanderbilt University Medical Center, Nashville, Tennessee, USA; ⁵Division of Hematology/Oncology, University of Florida, Gainesville, Florida, USA; and ⁶Department of Immunological Diagnosis, Juntendo University Graduate School of Medicine, Tokyo, Japan

Correspondence: Kei Ohnuma, Department of Therapy Development and Innovation for Immune Disorders and Cancers, Graduate School of Medicine, Juntendo University, 2-1-1, Hongo, Bunkyo-ku, Tokyo 113-8421, Japan. E-mail: kohnuma@juntendo.ac.jp

Abbreviations: CNS, conserved noncoding sequence; FGF, fibroblast growth factor; hIL-26Tg, human IL-26 transgenic; HUVEC, human umbilical vein endothelial cell; IMQ, imiquimod; NHDF, normal human dermal fibroblasts; NHEK, normal human epidermal keratinocytes; PASI, Psoriasis Area and Severity Index; siRNA, small interfering RNA; Tg, transgenic; Th, T helper; VEGF, vascular endothelial growth factor

Received 19 June 2018; revised 25 September 2018; accepted 26 September 2018; accepted manuscript published online 10 November 2018; corrected proof published online 17 January 2019

2004), and IMQ-induced psoriasis-like murine model has been established to study human psoriasis (van der Fits et al., 2009). The topical application of IMQ-containing cream to the skin of mice is now widely accepted as a convenient and cost-effective murine model for studying early events of psoriasis (Alrefai et al., 2016; van der Fits et al., 2009; Zanvit et al., 2015).

In the present study, because the gene encoding IL-26 is absent in mice, we investigate the role of IL-26 in the IMQ-induced psoriasis-like murine model using human *IL-26* bacterial artificial chromosome transgenic (hIL-26Tg) mice (Collins et al., 2010, 2012). We found that vascularization and immune cell infiltration induced by daily applications of IMQ were enhanced dramatically in hIL-26Tg mice, and associated with increased expression of fibroblast growth factor (FGF) 1, FGF2, and FGF7 in the skin lesions. Moreover, the effect of IL-26 on angiogenesis and inflammation was commonly observed in the murine contact hypersensitivity model. These results strongly suggest that IL-26 may represent a promising therapeutic target for T cell-mediated skin inflammation, including psoriasis and contact hypersensitivity reactions.

RESULTS

IL-26 exacerbates skin inflammation by inducing vascular invasion and immune cell infiltration in the IMQ-induced psoriasis model

Although the IL-26 gene is absent in rodents, IL-20RA and IL-10RB, which are part of the IL-10 family of cytokine receptors, are also expressed in mice, and human IL-26 functions in both human and murine cells (Hor et al., 2004; Ohnuma et al., 2015; Schoenborn et al., 2007). To explore the role of IL-26 in the pathology of psoriasis, hIL-26Tg mice were compared with Δ conserved noncoding sequence (CNS)-77 transgenic (Tg) mice (control Tg mice with deleting human IL-26 transcription) utilizing the IMQ-induced psoriasis model. We applied daily 40 mg of IMQ cream on the back skin of each mouse and assessed disease severity every day utilizing the clinical Psoriasis Area and Severity Index (PASI) score. We first confirmed that there was no significant difference in the appearance and the PASI scores between Δ CNS-77 Tg mice and C57BL/6 wild-type mice (Supplementary Figure S1 online), validating the use of Δ CNS-77 Tg mice as a control group compared with hIL-26Tg mice in this study. The back skin of hIL-26Tg mice appeared markedly affected and especially exhibited increased erythema symptoms compared with Δ CNS-77 Tg mice, and all of the PASI scores of hIL-26Tg mice were higher than those of control mice (Figure 1a, 1b). Excessive blood vessel formation and vascular invasion were observed in subcutaneous tissues of hIL-26Tg mice (Figure 1c, 1d). Moreover, CD31-positive blood vessels were markedly increased in the back skin of hIL-26Tg mice (Figure 1e). We next conducted histologic studies of IMQ-induced psoriatic skin. There was increased infiltration of blood cells and blood vessels in the skin of hIL-26Tg mice compared with control mice from day 2 (Figure 1f).

The infiltrating cell types in the IMQ-induced psoriatic skin of hIL-26Tg mice were then characterized by flow cytometry. The cell type with the most prominent difference between hIL-26Tg mice and Δ CNS-77 Tg mice was neutrophils

(Figure 2a). In addition, the number of TCR β^+ CD4 $^+$ T cells infiltrating the skin lesions of hIL-26Tg mice was significantly increased compared with Δ CNS-77 Tg mice on day 3 and day 4 (Figure 2b). There was no significant difference in the number of TCR β^+ CD8 $^+$ T cells and $\gamma\delta$ T cells between hIL-26Tg mice and control mice (Figure 2c, 2d), and similar results were also seen with macrophages and mast cells (data not shown). To better evaluate the level of neutrophil invasion, we performed immunofluorescence staining for Ly6g. Ly6g-positive cells were markedly increased in the back skin of hIL-26Tg mice (Figure 2e). mRNA expression levels of the neutrophil recruitment chemokines CXCL1 and CXCL2 in the skin were also markedly increased in hIL-26Tg mice compared with Δ CNS-77 Tg mice (Supplementary Figure S2 online). Taken together, these results indicate that IL-26 exaggerates the severity of psoriatic skin inflammation by inducing angiogenesis and immune cell infiltration.

IL-26 upregulates expression of FGF1, FGF2, and FGF7 in IMQ-induced psoriasis model

To elucidate the molecular mechanism associated with IL-26-dependent angiogenesis, we examined the kinetics of mRNA expression of neoangiogenesis factors. mRNA expression of human IL-26 was markedly increased in the skin of hIL-26Tg mice following daily application of IMQ cream, whereas no expression of human IL-26 was detected in the skin of Δ CNS-77 Tg mice (Figure 3a). Expression of vascular endothelial growth factor (VEGF)-A was gradually increased from day 1, but the difference was hardly observed between hIL-26Tg mice and control mice (Figure 3a). On the other hand, in the skin lesions from hIL-26Tg mice, the mRNA expression levels of VEGF-C, epidermal growth factor, hypoxia-inducible factor1- α , FGF1, FGF2, FGF7, angiopoietin-1, and angiopoietin-2 were significantly increased compared with control mice (Figure 3a). There was no marked difference in expression levels of VEGF-D, TNF- α , and TYMP between hIL-26Tg mice and control mice (Supplementary Figure S2).

Although VEGF-A is a particularly important angiogenic factor, FGF2 also functions as a main growth factor associated with angiogenesis, and the serum level of FGF2 is increased and significantly correlated with PASI value in psoriasis patients (Andrys et al., 2007). In addition, FGF7 is implicated in psoriatic angiogenesis (Finch et al., 1997; Seghezzi et al., 1998). We therefore focused on FGF1, FGF2, and FGF7 and examined their protein expression levels by immunofluorescence staining of the IMQ-induced skin lesions. IL-26-producing cells (shown in green, Supplementary Figure S3 online) were hardly observed in hIL-26Tg and control mice at day 0, whereas these cells were clearly detected in the dermis, particularly under the basement membrane of hIL-26Tg mice (Figure 3b). In addition, the infiltration of CD4-positive cells (shown in red) was prominent in the skin of hIL-26Tg mice as compared with control mice (Figure 3b). Likewise, prior to IMQ application (day 0), protein expression of FGF1, FGF2, and FGF7 was hardly observed both in hIL-26Tg and control mice (Supplementary Figure S3), while expression of FGF1, FGF2, and FGF7 was remarkably increased in hIL-26Tg mice (Figure 3b). In IMQ-treated hIL-26Tg mice, FGF1 was seen in

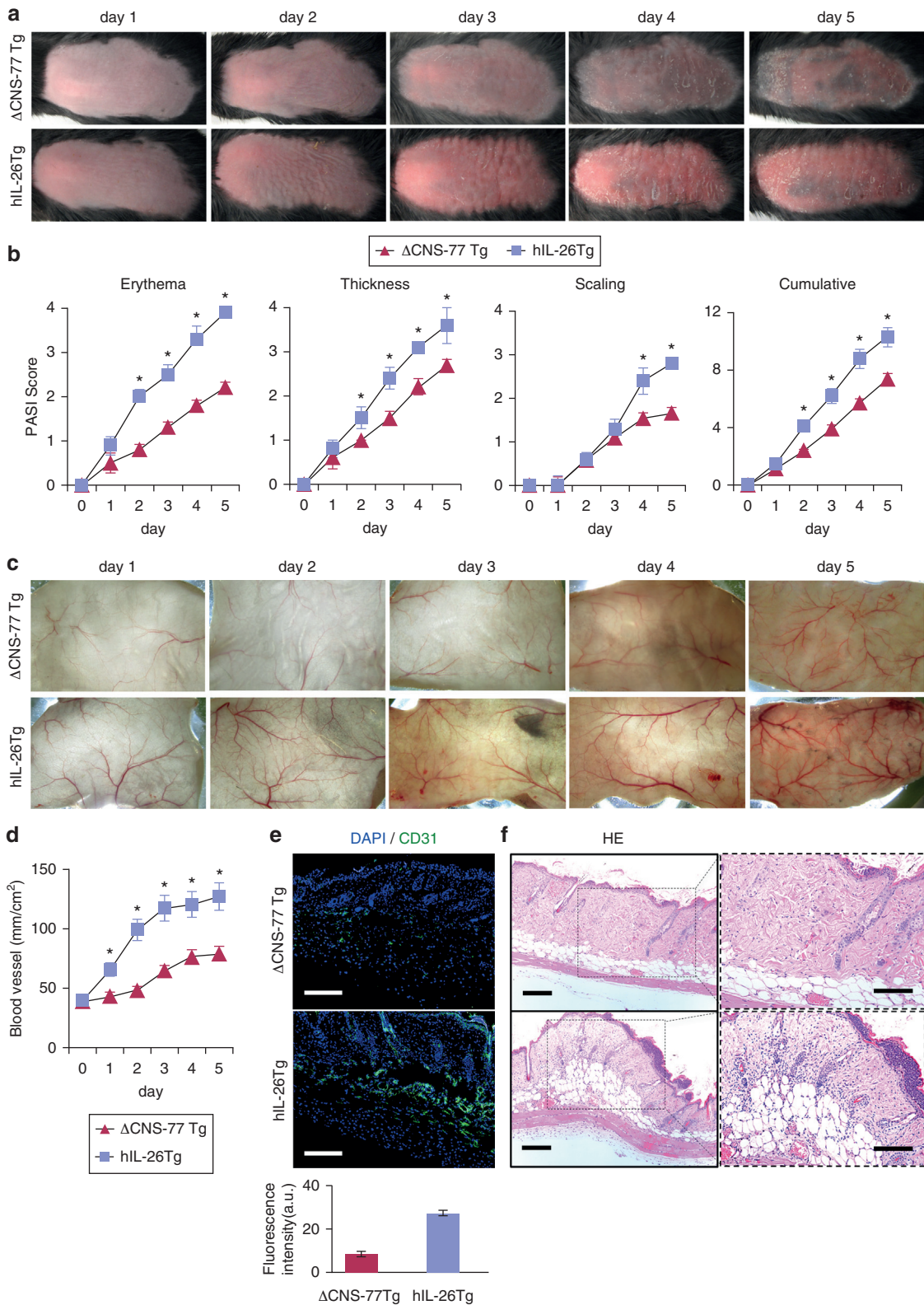


Figure 1. Markedly enhanced angiogenesis is observed in psoriatic skin lesions of IMQ-applied hIL-26Tg mice. (a) Phenotypical representation of IMQ-induced skin inflammation in each mice. (b) Time course of Psoriasis Area and Severity Index scores (erythema, thickness, and scaling were scored daily on a scale from 0 to 4, respectively) in each mice. (c, d) Subcutaneous vascular formation of IMQ-treated back skin in each mice (c) was measured by ImageJ software (d). (e, f) Immunofluorescence staining (CD31, green) (e) or HE staining (f) of IMQ-treated back skin from each mice on day 3. Scale bar = 200 μ m, 100 μ m (right panels in f). n = 8 mice for each group at each time point. (b, d) Mean \pm standard error of the mean of each group. **P* < 0.01. HE, hematoxylin and eosin; hIL-26Tg, human IL-26 transgenic; IMQ, imiquimod.

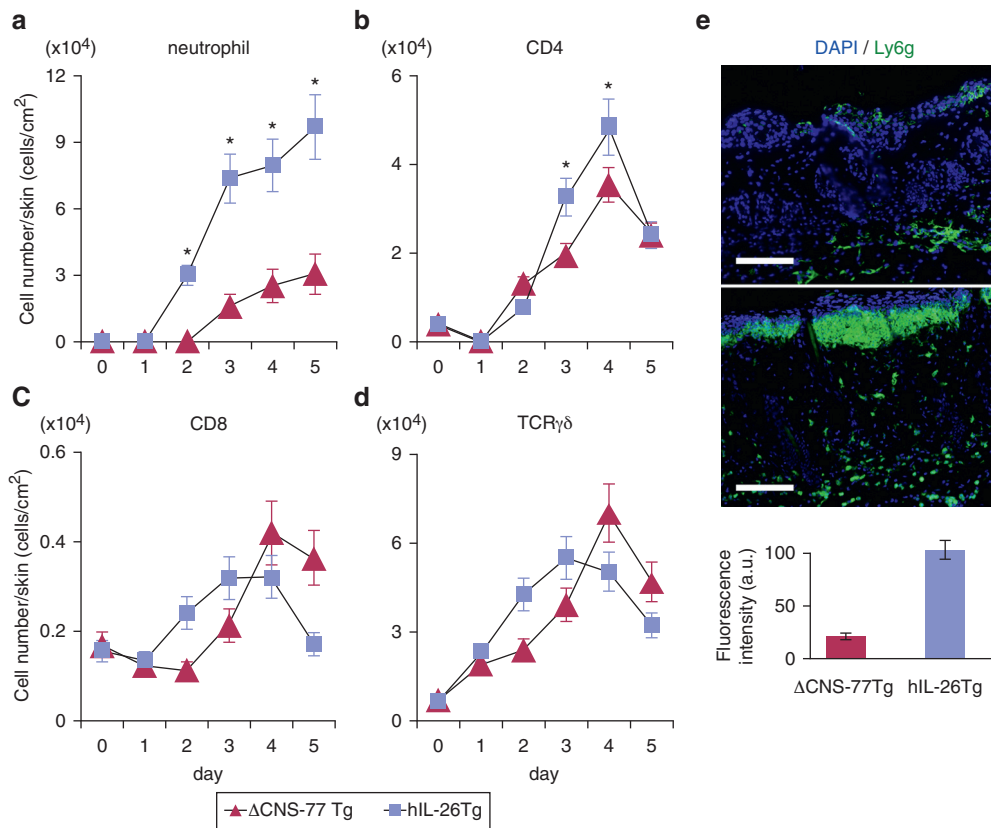


Figure 2. IL-26 enhances infiltration of neutrophils and CD4⁺ T cells in IMQ-induced psoriatic skin lesions.

Absolute cell numbers of neutrophils (a), CD4⁺ T cells (b), CD8⁺ T cells (c), and γδ T cells (d) in IMQ-treated skin lesions from each mice (n = 5 mice for each group at each time point) were quantified by flow cytometry. Single-suspension cells isolated from the skin lesions were analyzed, and the percentages of CD11b⁺CD11c^{low/nega}Ly6G⁺F4/80^{nega} (a), TCRβ⁺TCRγδ^{nega}CD4⁺CD8^{nega} (b), TCRβ⁺TCRγδ^{nega}CD4^{nega}CD8⁺ (c), or TCRβ^{nega}TCRγδ⁺ (d) were calculated. Mean ± standard error of the mean of each group. *P < 0.01. (e) Immunofluorescence staining (Ly6g, green) of IMQ-treated back skin from each mice on day 3. n = 4 mice for each. Scale bar = 200 μm. IMQ, imiquimod.

the epidermal tissue, particularly in the upper layer around the corneum, and the expression of FGF2 and FGF7 was observed in the dermis and adipose tissue, under the basement membrane and around blood vessels. These results indicate that IL-26 enhances the expression of FGF1, FGF2, and FGF7 in the IMQ-induced skin. To confirm the expression and localization of IL-26 and FGFs in humans, we conducted immunofluorescence staining of human skin specimens obtained from patients with psoriasis and healthy volunteers. Histologic findings of the skin specimens of psoriasis patients revealed characteristics of psoriatic skin, such as acanthosis, parakeratosis, papillomatosis, and infiltration of inflammatory cells (Figure 3c). Similar to these findings, protein expression of FGF1, FGF2, FGF7, and IL-26 was markedly increased in the skin lesions of psoriasis patients compared with healthy controls (Figure 3d). These findings suggest that IL-26 and FGFs play an important role in the pathophysiology of psoriasis in humans, as well as the IMQ-induced psoriasis model.

IL-26 enhances the production of FGF1, FGF2, and FGF7 from keratinocytes and vascular endothelial cells

We hypothesized that IL-26 induces angiogenesis in psoriatic skin through production of FGFs from the cells constituting the skin tissue. To validate this assumption, we examined FGF production from normal human epidermal keratinocytes (NHEKs) and normal human dermal fibroblasts (NHDFs) by ELISA following IL-26 stimulation. FGF1 and FGF2 production from NHEKs was enhanced by IL-26 stimulation in a dose-dependent manner (Figure 4a, 4b). Meanwhile,

constitutive production of FGF2 and FGF7 from NHDFs was not influenced by IL-26 treatment (Figure 4b, 4c). We next investigated whether IL-26 directly affected FGF expression in vascular endothelial cells. IL-26 enhanced FGF2 production from human umbilical vein endothelial cells (HUVECs) (Figure 4b). Although the amount of FGF7 produced from HUVECs was relatively small compared with NHDFs, IL-26 also enhanced FGF7 production from HUVECs (Figure 4c).

Stimulation of inflammatory cytokines and antimicrobial peptides, such as IL-17 and LL-37, enhances angiogenesis in psoriasis through the induction of angiogenic factors from keratinocytes (Morizane and Gallo, 2012). We therefore examined the effect of IL-26 in combination with various psoriasis-associated inflammatory cytokines on expression of FGFs. We examined mRNA expression levels of FGF1 and FGF2 in NHEKs, and FGF2 and FGF7 in NHDFs and HUVECs by quantitative real-time reverse transcriptase PCR. Consistent with our findings regarding protein production, stimulation with IL-26 alone enhanced expression levels of FGF1 and FGF2 in NHEKs (Figure 4d), and FGF2 and FGF7 in HUVECs (Figure 4f), while having no effect on FGF2 and FGF7 levels in NHDFs (Figure 4e). Intriguingly, stimulation with IL-26 in combination with psoriasis-associated cytokines resulted in much greater enhancement in mRNA expression levels of FGF1 and FGF2 in NHEKs and FGF2 and FGF7 in HUVECs (Figure 4d, 4f). Among psoriasis-associated cytokines used in this study, we found that IL-1β in NHEKs and IFN-α in HUVECs were key cytokines for enhancing FGF2 expression in synergy with IL-26 (Figure 4d, 4f). Moreover, addition of IFN-α plus IFN-γ resulted in increased

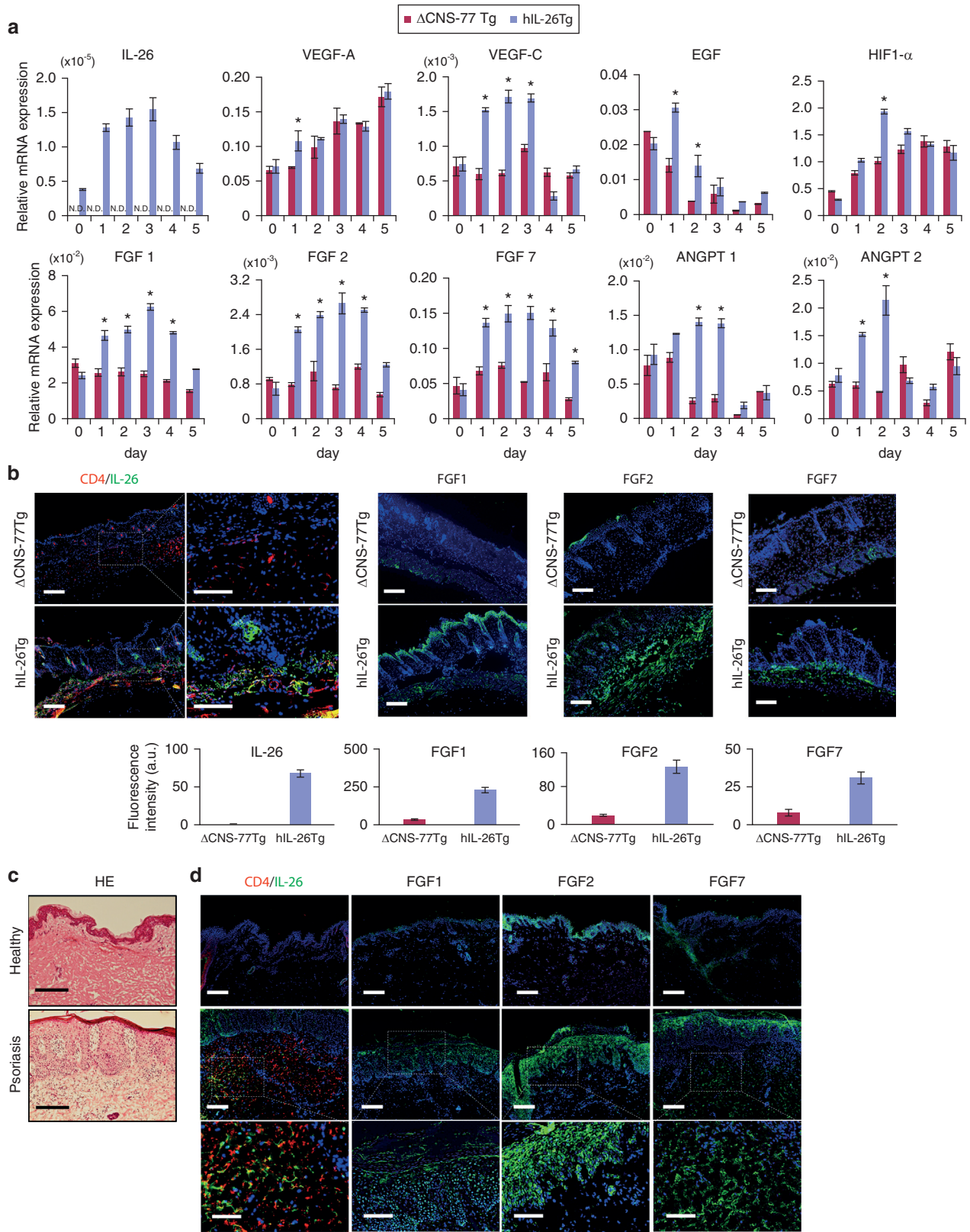


Figure 3. IL-26 increases levels of FGF1, FGF2, FGF7, and other biomarkers associated with angiogenesis in IMQ-induced psoriasis-like skin inflammation. (a) Kinetics of mRNA expression levels of IL-26 or angiogenesis factors in IMQ-treated skin lesions from each mice (n = 6 mice for each group at each time point). Mean ± standard error of the mean of each group. *P < 0.01. (b, d) Immunofluorescence staining of IMQ-treated back skin from each mice on day 3 (b) or human skin samples (d) using anti-CD4 (red) plus IL-26, FGF1, FGF2, or FGF7 (IL-26 and FGFs, green). Scale bar = 200 μm, 100 μm (right panels of CD4/IL-26 in b, lower panels in d). (c) HE staining of human skin samples. Scale bar = 100 μm. For each, n = 4 mice (b), n = 3 (c, d). ANGPT, angiopoietin; EGF, epidermal growth factor; FGF, fibroblast growth factor; HE, hematoxylin and eosin; HIF, hypoxia inducible factor; IMQ, imiquimod; ND, not detectable.

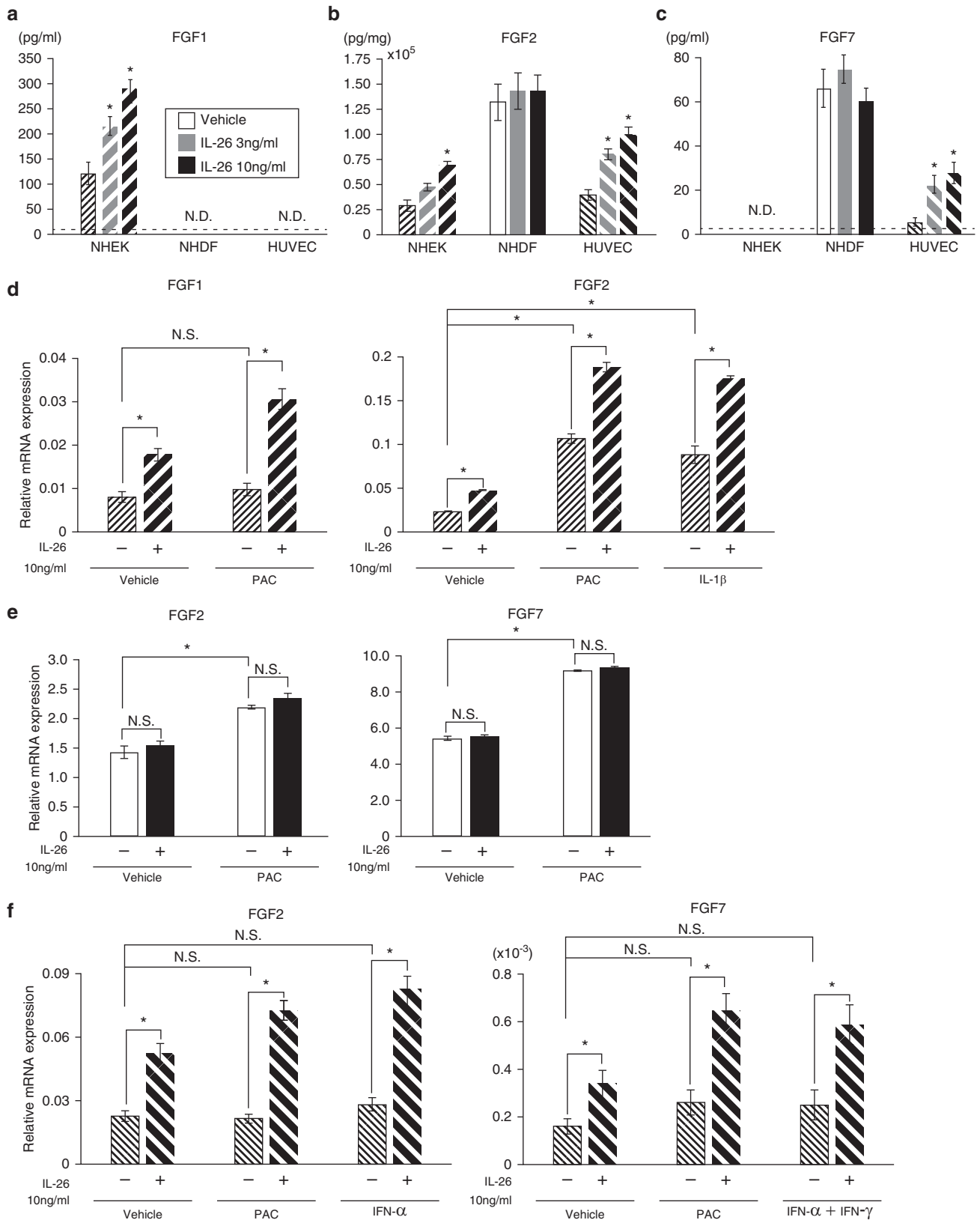


Figure 4. Stimulation with IL-26 and psoriasis-associated cytokines induces enhanced expression of FGF1, FGF2, and FGF7 in keratinocytes and vascular endothelial cells. (a, b, c) NHEKs, NHDFs, and HUVECs were stimulated with IL-26 for 24 hours. Production of FGF1 (a), FGF2 (b), or FGF7 (c) was evaluated using specific ELISA. The dashed lines indicate the detection limit. NHEKs (d), NHDFs (e), and HUVECs (f) were stimulated with IL-26 alone (10 ng/ml) or in combination with PAC (10 ng/ml each) for 6 hours. mRNA expression levels of FGF1, FGF2, or FGF7 were quantified by quantitative real-time reverse transcriptase PCR. (a–f) Mean \pm standard deviation of triplicate samples. * $P < 0.01$. FGF, fibroblast growth factor; HUVEC, human umbilical vein endothelial cells; IMQ, imiquimod; ND, not detectable; NHDF, normal human dermal fibroblast; NHEK, normal human epidermal keratinocyte; PAC, psoriasis-associated cytokines.

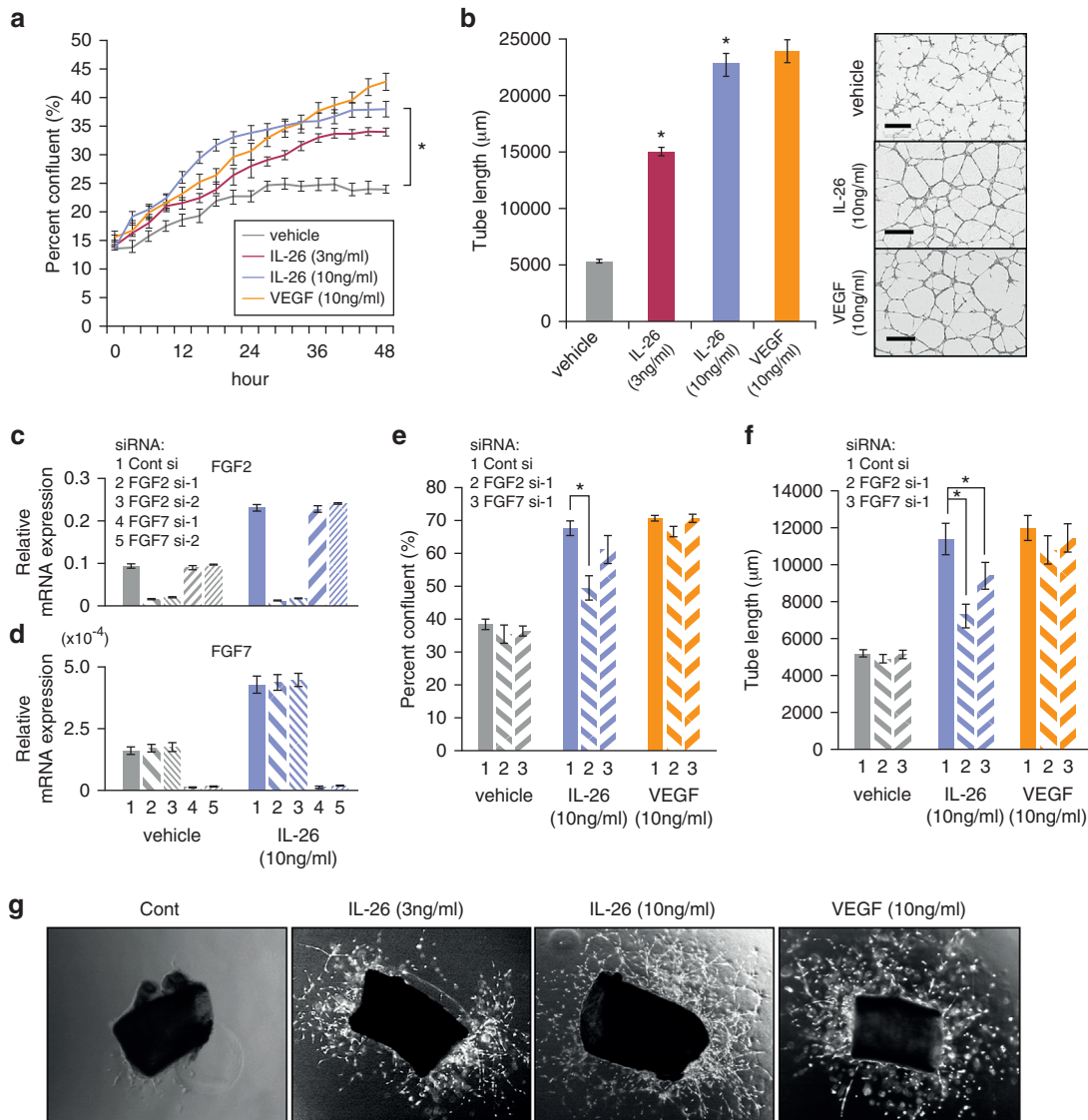


Figure 5. IL-26 enhances proliferation and tube formation of HUVECs by inducing FGF2 and FGF7 production. HUVECs were stimulated with IL-26 or VEGF for 48 hours (a) or 9 hours (b). (a) Proliferation was assessed by cell confluence. (b) Tube formation was assessed by cell sprouts formation. Mean ± standard deviation of triplicate samples. **P* < 0.01. Scale bar = 300 µm. HUVECs were transfected with siRNA and stimulated with IL-26 for 6 hours. mRNA expression levels were quantified by quantitative real-time reverse transcriptase PCR (c, d). Transfected HUVECs were stimulated with IL-26 or VEGF for 48 hours (e) or 9 hours (f), and assessed as described here. Mean ± standard deviation of triplicate samples. **P* < 0.01. (g) Mouse aorta ring explants were stimulated with IL-26 or VEGF for 10 days. FGF, fibroblast growth factor; HUVEC, human umbilical vein endothelial cell; siRNA, small interfering RNA; VEGF, vascular endothelial growth factor.

enhancement of FGF7 expression in HUVECs in synergy with IL-26 (Figure 4f). There were no specific factors identified for enhancing FGF1 expression in NHEKs. On the other hand, stimulation with psoriasis-associated cytokines without IL-26 led to elevated expression of FGF2 and FGF7 in NHDFs, but no additional enhancement was observed when cells were stimulated with these cytokines in the presence of IL-26 (Figure 4e). These results indicate that IL-26 acts directly on not only keratinocytes, but also vascular endothelial cells to enhance production of FGFs.

IL-26 acts directly on vascular endothelial cells, resulting in enhanced proliferation and tube formation

We next examined IL-26 effect on vascular endothelial cell function. For this purpose, we assayed for HUVECs

proliferation and tube formation following IL-26 stimulation. Surprisingly, IL-26 promoted proliferation and tube formation of HUVECs in a dose-dependent manner, similar to VEGF effect (Figure 5a, 5b). We confirmed that both FGF2 and FGF7 enhanced HUVECs proliferation and tube formation (Supplementary Figure S4 online). From these results, we next conducted knockdown experiments using small interfering RNA (siRNA) against FGF2 and FGF7 in HUVECs to determine whether FGF2 or FGF7 production was involved in HUVECs activation following IL-26 stimulation. Expression level of FGF2 and FGF7 in HUVECs stimulated with IL-26 or vehicle was determined by quantitative real-time reverse transcriptase PCR in the presence of control siRNA or two different sequences of FGF2-siRNA or FGF7-siRNA. FGF2-siRNA treatment clearly reduced FGF2 expression as

compared with control siRNA or FGF7-siRNA, which was associated with a significant decrease in IL-26-stimulated proliferation and tube formation of HUVECs (Figure 5c, 5e, 5f). Treatment with FGF7-siRNA markedly reduced FGF7 expression compared with control siRNA or FGF2-siRNA (Figure 5d), which was associated with a partial reduction in IL-26-stimulated HUVECs tube formation, and only a slight effect on HUVECs proliferation (Figure 5e, 5f). Similar results were also obtained with a different siRNA sense 2, as described in Materials and Methods (data not shown). On the other hand, stimulation with VEGF led to enhancement of HUVECs proliferation and tube formation regardless of FGF2 or FGF7-siRNA treatment (Figure 5e, 5f), strongly suggesting that the observed reduction in proliferation or tube formation of FGF2 or FGF7-siRNA-treated HUVECs following IL-26 stimulation was not due to non-specific toxicity of the transfection procedure or off-target effects. Similar results were observed in the experiment utilizing FGF2 or FGF7-neutralizing antibodies (Supplementary Figure S5 online). Given our findings on angiogenesis in the IMQ-induced psoriatic skin of hIL-26Tg mice, we conducted studies to investigate the direct effect of IL-26 on murine blood vessels by evaluating whether IL-26 stimulation induced vessel formation in mouse aortic rings. Aortic rings stimulated with IL-26 strongly produced sprouts in a dose-dependent manner (Figure 5g). Taken together, our data strongly suggest that IL-26 acts directly on vascular endothelial cells, resulting in enhanced FGF2 and FGF7 production and prominent blood vessel formation.

PI3K-Akt, Raf-MEK-ERK, and I κ B-NF- κ B signalings are indispensable for IL-26-mediated activation of vascular endothelial cells

We next examined the signaling events in HUVECs following IL-26 stimulation. Downstream signaling of IL-26 involves the JAK-STAT3 pathway substantially, but other pathways mediated by Akt or ERK1/2 have been also reported (Dambacher et al., 2009). In addition, FGF2 activates HUVECs via Akt, p38, and I κ B phosphorylation (Stavri et al., 1995). We therefore examined phosphorylation of Akt, ERK1/2, p38, c-Jun N-terminal kinase, I κ B, and STAT3 in HUVECs following IL-26 stimulation by Western blotting. Stimulation with IL-26 resulted in the prominent phosphorylation of Akt, ERK1/2, p38, and I κ B, whereas c-Jun N-terminal kinase and STAT3 phosphorylation was not significantly enhanced in HUVECs following IL-26 stimulation (Figure 6a). Of note, the intensity of Akt, ERK1/2, p38, and I κ B phosphorylation following IL-26 stimulation was as strong as FGF2 stimulation (Figure 6a). To identify the signals involved in the activation of HUVECs following IL-26 stimulation, we examined the effect of signal inhibitors. The inhibitor against Akt, mitogen-activated protein kinase/ERK kinase 1/2, and NF- κ B markedly inhibited HUVECs proliferation and tube formation following IL-26 stimulation in a dose-dependent manner (Figure 6b, 6c). In addition, to characterize the signals involved in FGF2 or FGF7 production from HUVECs, we performed quantitative real-time reverse transcriptase PCR analysis. The Akt inhibitor and NF- κ B inhibitor suppressed expression of both FGF2 and FGF7 in HUVECs following IL-26 stimulation (Figure 6d, 6e). Taken together, these data strongly suggest

that stimulation with IL-26 activates various signal pathways in HUVECs, and among them, PI3K-Akt, Raf-MEK-ERK, and I κ B-NF- κ B signaling events are particularly important for IL-26-mediated angiogenesis.

Finally, to determine whether the effect of IL-26 on angiogenesis and inflammation is specific for the IMQ-induced psoriasis model or can be commonly observed in other types of inflammatory models, we evaluated the role of IL-26 in the DNFB-induced contact hypersensitivity model (Takamori et al., 2018). Similar to the IMQ-induced psoriasis model, excessive blood vessel formation and vascular invasion were observed in the ear skin of hIL-26Tg mice with DNFB-induced contact hypersensitivity (Supplementary Figure S6a online). Thickening of the ear skin was also enhanced in hIL-26Tg mice compared with Δ CNS-77 Tg mice (Supplementary Figure S6b). Moreover, IL-26-producing cells and CD31-positive blood vessels were clearly detected in the dermis of hIL-26Tg mice (Supplementary Figure S6c, S6d). Histologic findings showed that infiltration of inflammatory cells was increased in the ear skin of hIL-26Tg mice compared with control mice (Supplementary Figure S6e). These results indicate that IL-26 plays an important and potentially universal role in angiogenesis and inflammation in skin inflammatory lesions, including psoriasis and T cell-mediated contact hypersensitivity reactions.

DISCUSSION

Our present work showed that vascularization and immune cell infiltration induced by daily applications of IMQ were dramatically enhanced in hIL-26Tg mice. We demonstrate that IL-26 acts directly on vascular endothelial cells and enhances proliferation and tube formation, at a level similar to VEGF. Moreover, the effect of IL-26 on angiogenesis and inflammation was commonly observed in the DNFB-induced contact hypersensitivity model, indicating that this angiogenic effect of IL-26 is not restricted to psoriasis but is also seen in T cell-mediated contact hypersensitivity reactions.

Our in vitro assay showed the direct effect of IL-26 on vascular endothelial cells to promote proliferation and tube formation, involving both FGF2 and FGF7. Besides FGF2 and FGF7, recombinant FGF1 enhanced both proliferation and tube formation of HUVECs (Supplementary Figure S4), suggesting that the markedly increased expression of FGF1 in the keratinocytes of IMQ-induced hIL-26Tg mice shown in Figure 3b may also be associated with in vivo blood vessel formation. In addition, because expression levels of various angiogenic factors other than FGFs, such as VEGF-C, angiopoietin-1, and angiopoietin-2, were increased in the IMQ-induced skin lesions of hIL-26Tg mice (Figure 3a), further work will be needed to better characterize the cellular mechanisms involved in in vivo IL-26-induced excessive blood vessel formation in inflammatory lesions. Thickening and scaling of the back skin were also enhanced in hIL-26Tg mice compared with Δ CNS-77 Tg mice (Figure 1b). Enhanced expression of FGF1, FGF2, and FGF7 in the IMQ-induced skin of hIL-26Tg mice was likely associated with the excessive and abnormal proliferation of keratinocytes. Furthermore, increased levels of neutrophils and CD4⁺ T cells infiltrating the skin lesions may exacerbate inflammatory responses, in turn affecting the thickness and scaling of the skin of hIL-26Tg mice.

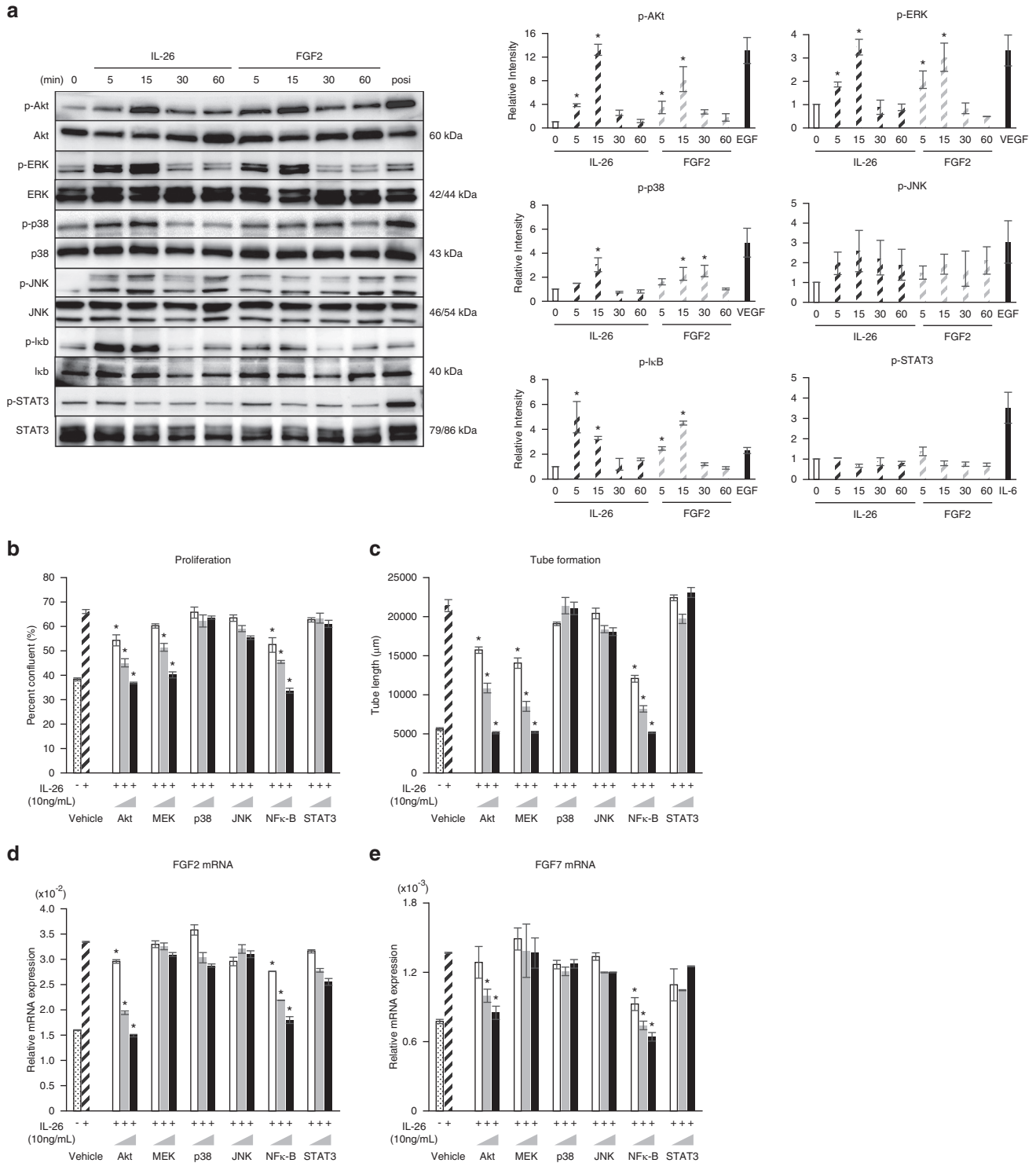


Figure 6. PI3K-Akt, Raf-MEK-ERK, and IκB-NFκB-mediated signaling are indispensable for HUVECs activation following IL-26 stimulation. (a) HUVECs were stimulated with IL-26 or FGF2. Phosphorylation of each protein was detected by immunoblotting. The same blots were stripped and reprobbed with anti-pan protein antibodies. Band intensity of phospho-proteins was normalized to pan proteins, respectively. Mean ± standard error of the mean from three independent experiments. **P* < 0.01. HUVECs were stimulated with IL-26 for 48 hours (b), 9 hours (c) or 6 hours (d, e) in the presence of vehicle or signal inhibitors. (b) Proliferation was assessed by cell confluence. (c) Tube formation was assessed by cell sprouts formation. (d, e) mRNA expression levels were quantified by quantitative real-time reverse transcriptase PCR. Mean ± standard deviation of triplicate samples. **P* < 0.01. HUVEC, human umbilical vein endothelial cell; JNK, c-Jun N-terminal kinase; MEK, mitogen activated protein kinase/ERK kinase.

Binding of IL-26 to a distinct cell surface receptor consisting of IL-20RA and IL-10RB results in functional activation via STAT3 phosphorylation (Hor et al., 2004). Our data indicated that IL-26 activated Akt, ERK1/2, p38, and IκB in

HUVECs, whereas STAT3 phosphorylation was not clearly enhanced following IL-26 stimulation (Figure 6a). These results strongly suggest that the signals transduced in HUVECs following IL-26 stimulation were not mediated by

the well-known receptor IL-20RA/IL-10RB. In fact, quantitative real-time reverse transcriptase PCR analysis did not detect mRNA expression of IL-20RA in HUVECs, while IL-10RB was easily detected (data not shown). IL-26 is an unusual cationic and amphipathic cytokine, closely resembling the structure of antimicrobial peptides (Meller et al., 2015). Because polycationic proteins bind to various molecules, it is possible that activation of vascular endothelial cells by IL-26 is mediated by a heretofore unknown receptor other than IL-20RA and IL-10RB.

The hIL-26Tg mice carry a 190-kb bacterial artificial chromosome transgene with the human *IFNG* gene and 90 kb of both upstream and downstream sequences, and distal regulatory elements in addition to human *IFNG* and *IL26* genes are contained in this region (Collins et al., 2012). CD4⁺ T cells of hIL-26Tg mice produce IL-26 under Th1- or Th17-polarizing conditions (Collins et al., 2012). While immunofluorescence staining of skin sections of hIL-26Tg mice indicated that IL-26 was produced by CD4-positive cells as well as other cell types, the cells involved may differ in the IMQ-induced psoriasis model from psoriasis patients (Figure 3b, 3d). In addition to Th17 cells, other IL-26-producing cells have been identified recently (Che et al., 2014, 2017; Corvaisier et al., 2012; Poli et al., 2017). In the skin lesions of psoriatic patients, IL-17 is produced not only from CD4⁺ T cells, but also from CD8⁺ T cells and $\gamma\delta$ T cells (Golden et al., 2013; Matos et al., 2017). Further studies are needed to identify the signaling events regulating IL-26 expression in psoriatic patients and psoriasis murine model.

Localization of FGFs differed in human patients compared with the IMQ-induced murine model. In the mouse model, FGF2 was observed in the epidermis, dermis, and adipose tissue, while FGF7 was seen mainly in the dermis and adipose tissue (Figure 3b). Meanwhile, FGF2 and FGF7 expression was found mainly in the epidermal tissue, as well as in the dermis of psoriasis patients (Figure 3d). While the IMQ-induced psoriasis model is a widely accepted murine model for studying early events of psoriasis, it does not adequately replicate the chronic and complex human psoriatic inflammatory condition. Because we examined FGF expression in skin samples obtained from only three untreated psoriasis patients, additional in-depth work with more patient samples is needed to address important issues relating to FGF biology in psoriatic patients.

Invasion of blood vessels in the dermis is a histologic hallmark of psoriatic skin lesions (Heidenreich et al., 2009). Our current work indicates that IL-26 plays a significant role in angiogenesis and leukocyte recruitment, and control of the excessive angiogenesis in the inflammatory skin lesions, including psoriasis and T cell-mediated contact hypersensitivity reactions by modulating IL-26 is potentially important in the clinical setting.

MATERIALS AND METHODS

Cell culture and reagents

NHEKs were cultured in Humedia-KGM2 medium (Kurabo, Osaka, Japan). NHDFs were cultured in FGM-2 medium (Lonza, Walkersville, MD). HUVECs were cultured in EGM-2 medium (Lonza). Cells were cultured at 37°C in a humidified 5% CO₂ incubator. For cell

stimulation, recombinant human IL-1 β , IL-6, IL-17A, IL-21, IL-22, IL-23, TNF- α , IFN- α , IFN- γ , and LL-37 (all the mixture was used as psoriasis-associated cytokines) were purchased from BioLegend (San Diego, CA). Recombinant human IL-26 dimer was purchased from R&D Systems (Minneapolis, MN). Commercial inhibitors used in this study are shown in [Supplementary Table S1 online](#). siRNAs against FGF2 and FGF7 were purchased from ThermoFisher Scientific (Waltham, MA) (sequences are shown in [Supplementary Table S2 online](#)), and negative control siRNA (oligonucleotide sequences are not disclosed) was purchased from Qiagen (Hilden, Germany).

Antibodies

Commercial antibodies used in this study are shown in [Supplementary Table S3 online](#). Mouse anti-human IL-26 monoclonal antibody (clone 69-10) was developed in our laboratory by subcutaneously immunizing BALB/c mice with recombinant human IL-26 protein (R&D Systems). Biotinylated anti-IL-26 monoclonal antibody was used for immunofluorescence staining.

Mice

hIL-26Tg mice and Δ CNS-77 Tg mice were kindly provided by Thomas Aune's laboratory (Collins et al., 2010, 2012). The characteristics and the details of these mice are described in [Supplementary Materials and Methods online](#). All mice used in this study were kept under specific pathogen-free facility in microisolator cages. Female mice at 8–12 weeks of age were used.

IMQ-induced psoriasis model

Mice received a daily topical dose of 40 mg 5% IMQ cream (Beselna Cream; Mochida Pharmaceutical, Tokyo, Japan) on the shaved back for 5 consecutive days. The severity of inflammation of the back skin was measured by an objective scoring system based on the clinical PASI (Alrefai et al., 2016). Subcutaneous vessels were measured by ImageJ software (National Institutes of Health, Bethesda, MD).

Clinical samples

Skin punch biopsies were obtained from three untreated psoriasis patients (two males, one female; aged 72, 55, and 77 years, PASI score, 7.8, 18, and 23.1) and three healthy controls (two males, one female; aged 69, 49, and 38 years) at Juntendo University Urayasu Hospital.

Proliferation assay for HUVECs

HUVECs or siRNA-transfected HUVECs (5×10^3) were incubated in the EGM-2 containing 2% fetal calf serum on 96-well plates (Corning, Tewksbury, MA) for 12 hours at 37°C, and then stimulated with IL-26 or each angiogenic factor in the presence or absence of signal inhibitors and neutralizing antibody. Cell growth was measured as cell confluence using IncuCyte ZOOM (Essen Bioscience, Ann Arbor, MI).

Tube formation assay

HUVECs or siRNA-transfected HUVECs (1×10^6) were incubated in EGM-2 containing 2% fetal calf serum for 12 hours at 37°C. After incubation, cells (1.5×10^3) were seeded on 50 μ l of Cultex Basement Membrane Extract (R&D Systems) in a 96-well plate. Seeded cells were stimulated with IL-26 or each angiogenic factor. Tube form length was measured using the MetaMorph image analysis system (Molecular Device, Sunnyvale, CA).

Aortic ring assay

Mouse thoracic aortas and renal arteries were dissected from C57BL/6 mice at 6 weeks of age, and cleared of fat and connective tissues. Mouse aortas were cut into 0.5–1.0-mm-thick rings and embedded in 100 μ l of Cultex Basement Membrane Extract containing IL-26 or VEGF. The aorta rings were cultured in 500 μ l of EGM-2 containing

2% fetal calf serum for 10 days. Thereafter, images of endothelial sprouts and interconnected capillary tubes were observed using a microscope (Carl Zeiss, Oberkochen, Germany).

Methods for immunofluorescence staining and immunohistochemical staining of skin sections, quantitative real-time reverse transcriptase PCR, ELISA, Western blotting and flow cytometry

Additional materials and methods are detailed in the [Supplementary Materials and Methods](#).

Statistics

Data were analyzed by two-tailed Student *t* test for two-group comparison or by one-way analysis of variance test with Tukey's for multiple comparison testing. The assay was performed in triplicate, and data are presented as mean \pm standard deviation of triplicate samples of the representative experiment, or mean \pm standard error of triplicate samples of independent experiments. Significance was analyzed using MS Excel (Microsoft, Redmond, WA) and values of $P < 0.01$ were considered significant and are indicated in the corresponding figures and figure legends.

Study approval

Human study protocols were approved by the Ethics Committees at Juntendo University and performed according to the principles set out in the Declaration of Helsinki. Written informed patient consent was obtained from all participants (three psoriasis patients and three healthy volunteers) prior to inclusion in this study. Animal experiments were conducted following protocols approved by the Animal Care and Use Committees at Juntendo University.

CONFLICTS OF INTERESTS

The authors state no conflict of interest.

ACKNOWLEDGMENTS

The authors thank Yasushi Suga and Utako Kimura (Department of Dermatology, Juntendo University Urayasu Hospital) for excellent technical assistance in obtaining human skin samples.

This study was supported in part by a grant of the Ministry of Health, Labour and Welfare, Japan (grant numbers 150401-01 and 180101-01 to CM), Japanese Society for the Promotion of Science KAKENHI grant numbers JP16H05345 to CM, JP15H04879 and JP18H02782 to KO, JP17K10008 and 26860760 to RH, Japanese Society for the Promotion of Science Research Fellowships for Young Scientists to RH, and a Grant-in-Aid (S1311011) from the Foundation of Strategic Research Projects in Private Universities from the Ministry of Education, Culture, Sports, Science, and Technology, Japan (to KO and CM). This work was also supported by a research grant from the Japan Research Institute of Industrial Science (to RH and TI), a research grant from the joint research program of Juntendo University of Faculty of Health and Sports Science (TI), and a research grant from the Japanese Society of Hematology (RH).

SUPPLEMENTARY MATERIAL

Supplementary material is linked to the online version of the paper at www.jidonline.org, and at <https://doi.org/10.1016/j.jid.2018.09.037>.

REFERENCES

- Alrefai H, Muhammad K, Rudolf R, Pham DA, Klein-Hessling S, Patra AK, et al. NFATc1 supports imiquimod-induced skin inflammation by suppressing IL-10 synthesis in B cells. *Nat Commun* 2016;7:11724.
- Andrys C, Borska L, Pohl D, Fiala Z, Hamakova K, Krejsk J. Angiogenic activity in patients with psoriasis is significantly decreased by Goeckerman's therapy. *Arch Dermatol Res* 2007;298:479–83.
- Batycka-Baran A, Maj J, Wolf R, Szepietowski JC. The new insight into the role of antimicrobial proteins-alarmins in the immunopathogenesis of psoriasis. *J Immunol Res* 2014;2014:628289.
- Beutner KR, Ferenczy A. Therapeutic approaches to genital warts. *Am J Med* 1997;102(5A):28–37.
- Boehncke WH, Schon MP. Psoriasis. *Lancet* 2015;386(9997):983–94.
- Che KF, Kaarteenaho R, Lappi-Blanco E, Levanen B, Sun J, Wheelock A, et al. Interleukin-26 production in human primary bronchial epithelial cells in response to viral stimulation: modulation by Th17 cytokines. *Mol Med* 2017;23.
- Che KF, Tengvall S, Levanen B, Silverpil E, Smith ME, Awad M, et al. Interleukin-26 in antibacterial host defense of human lungs. Effects on neutrophil mobilization. *Am J Respir Crit Care Med* 2014;190:1022–31.
- Collins PL, Chang S, Henderson M, Soutto M, Davis GM, McLoed AG, et al. Distal regions of the human IFNG locus direct cell type-specific expression. *J Immunol* 2010;185:1492–501.
- Collins PL, Henderson MA, Aune TM. Lineage-specific adjacent IFNG and IL26 genes share a common distal enhancer element. *Genes Immun* 2012;13:481–8.
- Corvaisier M, Delneste Y, Jeanvoine H, Preisser L, Blanchard S, Garo E, et al. IL-26 is overexpressed in rheumatoid arthritis and induces proinflammatory cytokine production and Th17 cell generation. *PLoS Biol* 2012;10:e1001395.
- Dambacher J, Beigel F, Zitzmann K, De Toni EN, Goke B, Diepolder HM, et al. The role of the novel Th17 cytokine IL-26 in intestinal inflammation. *Gut* 2009;58:1207–17.
- Donnelly RP, Sheikh F, Dickensheets H, Savan R, Young HA, Walter MR. Interleukin-26: an IL-10-related cytokine produced by Th17 cells. *Cytokine Growth Factor Rev* 2010;21:393–401.
- Drobits B, Holcman M, Amberg N, Swiecki M, Grundtner R, Hammer M, et al. Imiquimod clears tumors in mice independent of adaptive immunity by converting pDCs into tumor-killing effector cells. *J Clin Invest* 2012;122:575–85.
- Finch PW, Murphy F, Cardinale I, Krueger JG. Altered expression of keratinocyte growth factor and its receptor in psoriasis. *Am J Pathol* 1997;151:1619–28.
- Golden JB, McCormick TS, Ward NL. IL-17 in psoriasis: implications for therapy and cardiovascular co-morbidities. *Cytokine* 2013;62:195–201.
- Gudjonsson JE, Johnston A, Dyson M, Valdimarsson H, Elder JT. Mouse models of psoriasis. *J Invest Dermatol* 2007;127:1292–308.
- Heidenreich R, Rocken M, Ghoreschi K. Angiogenesis drives psoriasis pathogenesis. *Int J Exp Pathol* 2009;90:232–48.
- Hor S, Pirzer H, Dumoutier L, Bauer F, Wittmann S, Sticht H, et al. The T-cell lymphokine interleukin-26 targets epithelial cells through the interleukin-20 receptor 1 and interleukin-10 receptor 2 chains. *J Biol Chem* 2004;279:33343–51.
- Kotenko SV. The family of IL-10-related cytokines and their receptors: related, but to what extent? *Cytokine Growth Factor Rev* 2002;13:223–40.
- Lowes MA, Kikuchi T, Fuentes-Duculan J, Cardinale I, Zaba LC, Haider AS, et al. Psoriasis vulgaris lesions contain discrete populations of Th1 and Th17 T cells. *J Invest Dermatol* 2008;128:1207–11.
- Matos TR, O'Malley JT, Lowry EL, Hamm D, Kirsch IR, Robins HS, et al. Clinically resolved psoriatic lesions contain psoriasis-specific IL-17-producing alphabeta T cell clones. *J Clin Invest* 2017;127:4031–41.
- Meller S, Di Domizio J, Voo KS, Friedrich HC, Chamilos G, Ganguly D, et al. T(H)17 cells promote microbial killing and innate immune sensing of DNA via interleukin 26. *Nat Immunol* 2015;16:970–9.
- Morizane S, Gallo RL. Antimicrobial peptides in the pathogenesis of psoriasis. *J Dermatol* 2012;39:225–30.
- Ohnuma K, Hatano R, Aune TM, Otsuka H, Iwata S, Dang NH, et al. Regulation of pulmonary graft-versus-host disease by IL-26+CD26+CD4 T lymphocytes. *J Immunol* 2015;194:3697–712.
- Pene J, Chevalier S, Preisser L, Venereau E, Guilleux MH, Ghannam S, et al. Chronically inflamed human tissues are infiltrated by highly differentiated Th17 lymphocytes. *J Immunol* 2008;180:7423–30.
- Poli C, Augusto JF, Dauve J, Adam C, Preisser L, Larochette V, et al. IL-26 confers proinflammatory properties to extracellular DNA. *J Immunol* 2017;198:3650–61.
- Schoenborn JR, Dorschner MO, Sekimata M, Santer DM, Shnyreva M, Fitzpatrick DR, et al. Comprehensive epigenetic profiling identifies multiple distal regulatory elements directing transcription of the gene encoding interferon-gamma. *Nat Immunol* 2007;8:732–42.
- Schon MP. Animal models of psoriasis: a critical appraisal. *Exp Dermatol* 2008;17:703–12.

- Seghezzi G, Patel S, Ren CJ, Gualandris A, Pintucci G, Robbins ES, et al. Fibroblast growth factor-2 (FGF-2) induces vascular endothelial growth factor (VEGF) expression in the endothelial cells of forming capillaries: an autocrine mechanism contributing to angiogenesis. *J Cell Biol* 1998;141:1659–73.
- Stavri GT, Zachary IC, Baskerville PA, Martin JF, Erusalimsky JD. Basic fibroblast growth factor upregulates the expression of vascular endothelial growth factor in vascular smooth muscle cells. Synergistic interaction with hypoxia. *Circulation* 1995;92:11–4.
- Szeimies RM, Gerritsen MJ, Gupta G, Ortonne JP, Serresi S, Bichel J, et al. Imiquimod 5% cream for the treatment of actinic keratosis: results from a phase III, randomized, double-blind, vehicle-controlled, clinical trial with histology. *J Am Acad Dermatol* 2004;51:547–55.
- Takamori A, Nambu A, Sato K, Yamaguchi S, Matsuda K, Numata T, et al. IL-31 is crucial for induction of pruritus, but not inflammation, in contact hypersensitivity. *Sci Rep* 2018;8:6639.
- Tortola L, Rosenwald E, Abel B, Blumberg H, Schafer M, Coyle AJ, et al. Psoriasisiform dermatitis is driven by IL-36-mediated DC-keratinocyte crosstalk. *J Clin Invest* 2012;122:3965–76.
- van der Fits L, Mourits S, Voerman JS, Kant M, Boon L, Laman JD, et al. Imiquimod-induced psoriasis-like skin inflammation in mice is mediated via the IL-23/IL-17 axis. *J Immunol* 2009;182:5836–45.
- Wilson NJ, Boniface K, Chan JR, McKenzie BS, Blumenschein WM, Mattson JD, et al. Development, cytokine profile and function of human interleukin 17-producing helper T cells. *Nat Immunol* 2007;8:950–7.
- Wolk K, Kunz S, Asadullah K, Sabat R. Cutting edge: immune cells as sources and targets of the IL-10 family members? *J Immunol* 2002;168:5397–402.
- Wu JK, Siller G, Strutton G. Psoriasis induced by topical imiquimod. *Australas J Dermatol* 2004;45:47–50.
- Zanvit P, Konkel JE, Jiao X, Kasagi S, Zhang D, Wu R, et al. Antibiotics in neonatal life increase murine susceptibility to experimental psoriasis. *Nat Commun* 2015;6:8424.

ORIGINAL ARTICLE

Anti-human CD9 antibody Fab fragment impairs the internalization of extracellular vesicles and the nuclear transfer of their cargo proteins

Mark F. Santos¹ | Germana Rappa¹ | Jana Karbanová² | Cheryl Vanier¹ |
Chikao Morimoto³ | Denis Corbeil²  | Aurelio Lorico^{1,4} 

¹College of Medicine, Touro University Nevada, Henderson, Nevada

²Biotechnology Center and Center for Molecular and Cellular Bioengineering, Technische Universität Dresden, Dresden, Germany

³Department of Therapy Development and Innovation for Immune Disorders and Cancers, Graduate School of Medicine, Juntendo University, Bunkyo-ku, Tokyo, Japan

⁴Mediterranean Institute of Oncology, Viagrande, Italy

Correspondence

Aurelio Lorico, College of Medicine, Touro University Nevada, 874 American Pacific Drive, Henderson, NV 89014.

Email: aurelio.lorico@tun.touro.edu and

Denis Corbeil, Tissue Engineering Laboratories, Biotechnology Center (BIOTEC), Technische Universität Dresden, Tatzberg 47-49, 01307 Dresden, Germany. Email: denis.corbeil@tu-dresden.de

Abstract

The intercellular communication mediated by extracellular vesicles (EVs) has gained international interest during the last decade. Interfering with the mechanisms regulating this cellular process might find application particularly in oncology where cancer cell-derived EVs play a role in tumour microenvironment transformation. Although several mechanisms were ascribed to explain the internalization of EVs, little is our knowledge about the fate of their cargos, which are crucial to mediate their function. We recently demonstrated a new intracellular pathway in which a fraction of endocytosed EV-associated proteins is transported into the nucleoplasm of the host cell via a subpopulation of late endosomes penetrating into the nucleoplasmic reticulum. Silencing tetraspanin CD9 both in EVs and recipient cells strongly decreased the endocytosis of EVs and abolished the nuclear transfer of their cargos. Here, we investigated whether monovalent Fab fragments derived from 5H9 anti-CD9 monoclonal antibody (referred hereafter as CD9 Fab) interfered with these cellular processes. To monitor the intracellular transport of proteins, we used fluorescent EVs containing CD9-green fluorescent protein fusion protein and various melanoma cell lines and bone marrow-derived mesenchymal stromal cells as recipient cells. Interestingly, CD9 Fab considerably reduced EV uptake and the nuclear transfer of their proteins in all examined cells. In contrast, the divalent CD9 antibody stimulated both events. By impeding intercellular communication in the tumour microenvironment, CD9 Fab-mediated inhibition of EV uptake, combined with direct targeting of cancerous cells could lead to the development of novel anti-melanoma therapeutic strategies.

KEYWORDS

cancer, CD9, endocytosis, extracellular vesicle, Fab fragment, nucleoplasm

1 | INTRODUCTION

Growing evidence indicate that intercellular communication in multicellular organisms is mediated not only by direct cell-cell

contact or soluble molecules, but also by extracellular vesicles (EVs), ie lipid bilayer-enclosed nanobiological units actively released from all cell types.^{1,2} In contrast to soluble signalling molecules, bioactive compounds associated with EVs (eg, proteins,

This is an open access article under the terms of the Creative Commons Attribution License, which permits use, distribution and reproduction in any medium, provided the original work is properly cited.

© 2019 The Authors. Journal of Cellular and Molecular Medicine published by John Wiley & Sons Ltd and Foundation for Cellular and Molecular Medicine.

nucleic acids such as non-coding RNA [including microRNA], mRNA and genomic DNA) are protected from degradation.^{3,4} EVs are found in internal and external bodily fluids and act as mediators of long-distance transfer of biological information. Physiological and pathological conditions determine the nature of EVs released by the producing cells as well as the abundance of their bioactive cargo molecules.⁵ Under physiological states, EVs can play important roles during embryonic development and afterward in the homeostasis of various organ systems (reviewed in Ref.⁶). In cancer, they could promote pro-angiogenic events and alter the surrounding cellular components as well as extracellular matrix to develop the pre-metastatic niche.^{7,8} With regard to clinical purposes, EVs attract additional interest because their production is deregulated in human diseases, notably in cancer; hence, their cargo molecules can be monitored as biofluid-associated markers.^{9,10} Furthermore, EVs can be engineered for the selective therapeutic delivery of biomacromolecules.^{6,11}

Two major general pathways were ascribed to explain the biogenesis and release of EVs by donor cells as exosomes or ectosomes.¹² The first class of EVs is derived from the internal intraluminal vesicles of multivesicular bodies (MVBs) that are formed by the inward budding of the endosomal membrane during the maturation of MVBs. Upon fusion with the plasma membrane, MVBs release them outside the cell. The diameter of exosomes varies from 30 to 120 nm. Outward budding and fission of plasma membrane generate the second class of EV. Thus, ectosomes are typically larger than exosomes and their diameter varies from 100 nm to 1 μ m. We have previously shown that ectosomes can bud from microvilli and/or cilia.^{13,14} Once released into the extracellular milieu, the uptake of EVs by recipient cells can be accomplished by several molecular mechanisms of internalization, which are not mutually exclusive,¹⁵⁻¹⁸ such as clathrin-mediated endocytosis¹⁷ or lipid raft-dependent endocytosis.¹⁹ In spite of this knowledge, fundamental questions remain about the fate of endocytosed EVs particularly their biological cargo, which is crucial for their function.²⁰

Our groups are studying EVs released by stem cells and cancerous cells, notably melanoma cells. We have extensively characterized those secreted by metastatic FEMX-I cells. Electron microscopy examination has revealed the presence of a mixture of small and large EVs, suggesting that exosomes and ectosomes are simultaneously produced.²¹ The proteomic analysis of EVs, particularly those harbouring the stem (cancer stem) cell marker CD133,²² has defined their contents. They are particularly rich in tetraspanin proteins (CD9, CD63 and CD81) and in pro-metastatic proteins, notably CD44, MAPK4K, ADAM10 and Annexin A2. Importin β 1, a protein mediating nuclear transportation of cytoplasmic proteins through the nuclear pore complex, was also found therein. By monitoring the internalization of melanoma-derived EVs and the intracellular routes of their content, particularly CD9 (see below), we discovered that EV-associated proteins are transported into the nucleus of the host cell through late endosomes entering the nucleoplasmic reticulum (Figure 1A).²³ Therein, EV-associated cargo molecules can modify

the gene expression of the host cells. These surprising findings are in line with numerous studies showing the atypical nuclear localization of the EV-associated proteins CD9 and CD133 as well as the shuttling of proteins and nucleic acids to nucleoplasm of recipient cells.^{3,24-28} Recently, we described that two proteins, ie vesicle-associated membrane protein-associated protein A (VAP-A) and the cytoplasmic oxysterol-binding protein-related protein 3 (ORP3), are essential for the entry and the tethering of late endosomes to nuclear envelope invaginations of type II (Figure 1B). They form a tripartite complex with late endosome-associated Rab7 proteins.²⁹ Silencing VAP-A or ORP3 abrogated the association of Rab7-positive late endosomes with nuclear envelope invaginations, hence the transport of internalized EV-derived cargo molecules to the nucleoplasm of recipient cells.²⁹ The nuclear pores play a role in these processes given the treatment with importazole, a small molecule inhibitor of importin- β -mediated nuclear import, impaired the nuclear transfer of EV-derived proteins.²³ Finally, the initial internalization of CD9⁺ EVs occurs by endocytosis, which is an essential step for the nuclear localization of EV-associated materials, given dynasore and methyl- β -cyclodextrin, two compounds known to inhibit the endocytosis mediated by clathrin/dynamin and lipid raft respectively, abrogated it.²³

CD9 (alias Tetraspanin-29, motility-related protein-1) is an integral membrane protein that is physiologically involved in cell fusion, adhesion and motility.³⁰⁻³² For instance, CD9 has an important role in muscle cell fusion and in canine distemper virus and HIV-1-induced cell-cell fusion.³³⁻³⁵ Depending on the context, CD9 functions have a metastasis suppressor or promoter activity (reviewed in Ref.³⁶). CD9 has been extensively studied as a potential therapeutic target. Anti-CD9 monoclonal antibodies (Ab) were found to specifically inhibit the trans-endothelial migration of melanoma cells.³⁷ We have shown that anti-CD9, but not anti-CD133, Ab enhances the nuclear uptake of EVs in recipient cells (Figure 1C).²³ This effect is greater in melanoma cells than in mesenchymal stromal cells (MSCs), presumably because of the higher expression level of CD9 in cancer cells in comparison to stromal cells. Moreover, silencing CD9 in EVs and/or recipient cells strongly decreased the endocytosis of EVs and abolished the nuclear transfer of their contents, even in the presence of the anti-CD9 Ab (Figure 1C).²³

Here, we designed a strategy to block the uptake of EVs and the nuclear translocation of their cargos by recipient cells. To that aim, we generated an antigen-binding fragment (Fab fragment; hereafter CD9 Fab) from 5H9 anti-CD9 Ab (CD9 Ab), which could potentially saturate CD9 molecules present at the cell surface of host cells and EV-associated ones and hence impair their function.³⁸ The Ab and Fab fragment derived therefrom have been successfully employed for the treatment of different types of cancer, mainly through the inhibition of cell surface receptors.³⁹ We report that monovalent CD9 Fab at doses achievable *in vivo*⁴⁰ impedes the uptake of EVs in different melanoma cell lines and primary MSCs and consequently inhibits the nuclear transfer of their cargo proteins. Combined with other approaches, notably the direct targeting of cancer cells, such setting could lead to a

new modality in cancer treatment by inhibiting the intercellular communication within the cancer cell niche.

2 | METHODS

2.1 | Cell culture

The FEMX-I cell line was originally derived from the lymph node metastasis of a patient with malignant melanoma.⁴¹ FEMX-I cells were highly metastatic in immunodeficient mice.^{41,42} They were found to be wild-type for BRAF, PTEN and NRAS.^{23,29} The human A375 melanoma cell line was obtained from the American Type Culture Collection (catalog number #CRL-1619TM), whereas the human C8161 melanoma cell line was obtained from G. Pizzorno (University of Tennessee College of Medicine, Chattanooga, TN).^{43,44} All cell lines were cultured in RPMI-1640 (#10-041-CV; Corning Inc., Corning, NY) containing 10% foetal bovine serum (FBS; Atlanta Biologicals Inc., Flowery Branch, GA), 2 mmol/L L-glutamine, 100 U/mL penicillin and 100 µg/mL streptomycin (Corning Inc.). Cells were used between passages 3 and 15. Cell lines were authenticated by morphology, proteomics and gene expression analysis as described.⁴⁵ They were regularly tested for mycoplasma contamination using VenorTM GeM mycoplasma detection kit (Sigma-Aldrich, St. Louis, MO).

Human bone marrow-derived MSCs, isolated from bone marrow aspirates from normal adult donors after obtaining informed consent as described,⁴⁶ were obtained from Dr. D. J. Prockop (Texas A&M) and prepared under a protocol approved by the Texas A&M Institutional Review Board. MSCs were used between passages 2 and 5. Their multipotency was regularly monitored by their differentiation into adipocytes and osteoblasts.⁴⁷ MSCs and FEMX-I cells expressing ectopically CD9-green fluorescent protein (GFP) fusion protein were established as described.²³ Under these conditions, almost all cells are positive. They were used to produce fluorescent EVs (see below). FEMX-I cells depleted of CD9 by means of CD9 shRNA lentiviral particles were previously described.²³ Approximately 85% of infected cells showed no CD9 expression (data not shown).

2.2 | Production of CD9 antibody Fab fragment

Culture of 5H9 hybridoma cells³⁸ and the production of CD9 Ab were performed at Mayo Clinic (Antibody Hybridoma Core, Rochester, MN). Conditioned media from hybridoma cultures growing in roller bottles in IMDM media (#12440-053, Thermo Fisher Scientific, Gibco, Waltham, MA) containing 10% premium FBS (#S11150, Atlanta Biologicals Inc., Flowery Branch, GA) was pelleted in 250 mL centrifuge tubes at 1600 g. The supernatant was clarified through 0.45-µm Nalgene filters to remove remaining cell debris. The clarified supernatant was then passed through and bound to Protein G Sepharose FF HiLoadTM 26/40 columns (GE Healthcare, Pittsburgh, PA). Bound antibody was eluted with 100 mmol/L glycine buffer, pH 2.7. Eluted Ab was then immediately neutralized with 1 mol/L Tris-HCl, pH 9 and desalted with HiPrep 26/10 columns (GE Healthcare). The buffer was exchanged with 1X PBS and the protein concentration was determined by measuring

absorbance at 280 nm. Aliquots of the antibody (1 mg/mL) were stored at -80°C without addition of sodium azide.

The Fab fragment was generated using the Pierce Fab Purification kit (#44985; Thermo Fisher Scientific). Briefly, the CD9 Ab (500 µg) was incubated with papain immobilized on agarose resin for 3 hours at 37°C. The digested antibody was collected by centrifugation (5000 g, 1 minute) using a spin column and the flow through containing the antibody was placed in a new tube. The column was then washed once with PBS to recover any remaining antibody, which was pooled with the flow through. The fragment crystalline (Fc) fragment was then removed from digested antibody samples using NAb Protein A Plus Spin Column. After 10 minutes of centrifugation (1000 g), the Fab fragment found in the flow through was collected. The column was then washed twice with PBS. Each washing fraction was pooled with the Fab fraction. Antibody was concentrated using MicrosepTM Advance Centrifugal Devices (10K molecular weight cut-off; Pall Corporation). The final concentration of CD9 Fab was 0.75-0.85 mg/mL. The Fab preparation was assessed using sodium dodecyl sulphate-polyacrylamide gel electrophoresis (SDS-PAGE) and Coomassie blue staining (see below).

2.3 | SDS-PAGE and immunoblotting

Preparation of Fab fragments was assessed using SDS-PAGE under non-reduced or reduced (ie in the presence of β-mercaptoethanol) conditions. Samples were run on a 4%-12% Bis-Tris precast gel (Thermo Fisher Scientific, Life Technologies) and stained with Coomassie blue (Teknova, Hollister, CA) for 10 minutes. The gel was destained with 40% methanol/10% acetic acid solution.

Cells were solubilized in lysis buffer (1% Triton X-100, 100 mmol/L NaCl, 50 mmol/L Tris-HCl, pH 7.5) supplemented with the Set III protease inhibitor cocktail (Calbiochem, Burlington, MA) for 30 minutes on ice. Cell lysates were centrifuged at 12 000 g for 10 minutes in 4°C. The supernatant was collected and Laemmli sample buffer without reducing agent was added. Proteins were separated using either 12% SDS-PAGE gel (Figure 2 and Figure S1) or a precast gel (see above; Figure S3) along with the Trident prestained protein molecular weight ladder (GeneTex, Irvine, CA) and transferred overnight at 4°C to a nitrocellulose membrane (Thermo Fisher Scientific) or poly(vinylidene difluoride) membrane (Millipore, Bedford, MA; pore size 0.45 µm). After transfer, membranes were incubated in a blocking buffer (PBS containing 1% bovine serum albumin [BSA] or 5% low fat milk powder and 0.3% Tween 20) for 60 minutes at room temperature (RT). Afterward, the membranes were probed using either primary CD9 Fab (1 µg/mL) generated from mouse 5H9 Ab (see above) or commercial mouse anti-CD9 (clone P1/33/2, #sc-20048; Santa Cruz Biotechnology, Santa Cruz, CA) or anti-β-actin (clone C4, #sc-47778; Santa Cruz Biotechnology) Ab for 60 minutes at RT. After three washing steps of 10 minutes each with PBS containing 0.1% Tween 20, the antigen-antibody complexes were detected using two protocols. In the case of CD9 Fab, we used goat anti-mouse Fab specific horseradish peroxidase (HRP)-conjugated secondary antibody (#A2304; Sigma-Aldrich), which was

visualized with enhanced chemiluminescence reagents (ECL system; Amersham Corp., Arlington Heights, IL). The membranes were exposed to films (Hyperfilm ECL; Amersham-Pharmacia). With other Abs, the IRDye 680RD anti-mouse IgG (#926-68070; LI-COR Biosciences, Lincoln, NE) was applied. Membranes were washed thrice (10 minutes each) in PBS containing 0.1% Tween 20, rinsed in ddH₂O and antigen-antibody complexes were visualized using an Odyssey CLx system (LI-COR).

2.4 | Production of CD9-GFP⁺ EVs

Extracellular vesicles were enriched by differential centrifugation from 72 hour-conditioned media (serum-free Dulbecco's modified eagle medium [DMEM]/Ham's F-12 1:1, supplemented with 2% B-27 [Thermo Fisher Scientific]) of engineered FEMX-I cells and MSCs expressing CD9-GFP as described previously.^{21,22} Conditioned medium was centrifuged at 10 000 g for 30 minutes at 4°C and the resulting supernatant was centrifuged at 200 000 g for 60 minutes at 4°C. The pellet was re-suspended in 200 µL of PBS. To determine the EV concentration, we used the light-scattering characteristics of 488-nm laser light on EV preparations undergoing Brownian motion injected by continuous flow into the sample chamber of a Nanosight LM10 unit (Malvern Panalytical Inc., Westborough, MA). The calculated EV concentration was an average of six 30-second video recordings. As described previously, the average size of EVs produced by FEMX-I cells and MSCs was 123 and 114 nm respectively.²³ Those produced by FEMX-I cells were formerly characterized by electron microscopy.²¹

2.5 | Incubation of cells with EVs

Cells (1×10^5) were plated into 35-mm microscopy dishes containing 0.17-mm thick glass coverslips on the bottom and incubated overnight at 37°C to allow complete cell adherence (MatTek Corporation, Ashland, MA). Afterward, they were incubated with various concentrations of CD9-GFP⁺ EVs (eg, 5×10^7 particles per mL [0.075 µg protein per mL]; 2.5×10^8 particles per mL [0.375 µg protein per mL] or 1×10^9 particles per mL [1.5 µg protein per mL]) for 5 hours at 37°C

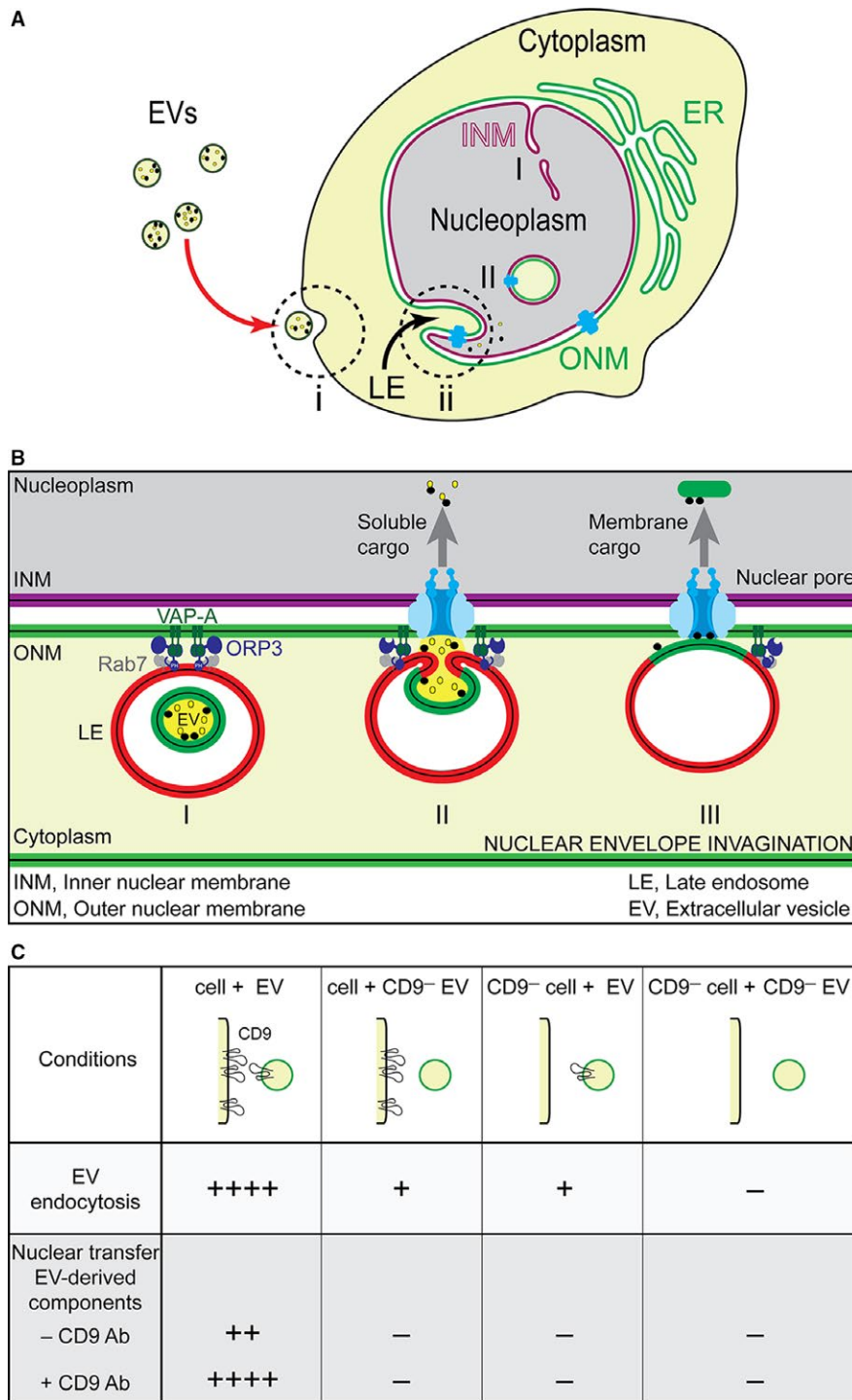
prior to fixation. EVs were derived from the same cell type as used for the recipients except for A375 and C8161 cells in which EVs were produced from CD9-GFP transfected FEMX-I cells. In some experiments, EVs and/or cells were pre-incubated with CD9 Fab or CD9 Ab at various concentrations as indicated for 30 minutes at 4 and 37°C respectively. The EVs and cells were then incubated together in the presence of antibodies (or without as control) for 5 hours at 37°C prior to analysis.

2.6 | Confocal laser scanning microscopy and fluorescence quantification

Cell surface immunolabelling of native or CD9-depleted FEMX-I cells was performed as described.⁴⁸ Briefly, cells growing on fibronectin-coated coverslips were washed with ice-cold PBS containing 1 mmol/L CaCl₂ and 0.5 mmol/L MgCl₂ (Ca/Mg-PBS) and incubated in blocking buffer I (Ca/Mg-PBS containing 0.2% gelatin) for 10 minutes. Cells were then incubated for 30 minutes with CD9 Fab or CD9 Ab at different concentrations (eg, 5, 10, 25 and 50 µg/mL) diluted in blocking buffer. The whole procedure was performed at 4°C. Afterward, they were fixed in 4% paraformaldehyde (PFA) for 30 minutes at RT, quenched with 50 mmol/L NH₄Cl for 10 minutes, washed in PBS and incubated in blocking buffer II (PBS containing 0.2% gelatin) for 20 minutes. Samples were incubated with fluorescein isothiocyanate (FITC)-conjugated secondary antibody specific either for the mouse Fab or Fc fragment (#F4018, #F5387 respectively, 1:200; Sigma-Aldrich) diluted in blocking buffer II. Nuclei were labelled with 4'-6-diamidino-2-phenylindole (1 µg/mL; Sigma-Aldrich). Cells were washed with PBS and distilled water then mounted in Mowiol 4.88 (Merck, Darmstadt, Germany). Images were captured with Leica SP5 upright confocal microscope under the same settings for both Fab- and Fc-specific secondary antibody labelling. Composites of 27-30 optical sections are shown (Figure 2A,B). The images were prepared using Fiji⁴⁹ and Adobe Illustrator software.

Alternatively, cells incubated with CD9-GFP⁺ EVs (see above) were fixed in 4% PFA and afterward permeabilized with 0.2% Tween 20 diluted in PBS (permeabilization buffer). Both steps

FIGURE 1 Entry and delivery of extracellular vesicles (EV)-derived cargo molecules into the nucleoplasm of recipient cells. A, Two major steps were proposed to explain the delivery of EV-associated molecules to the nuclear compartment of recipient cells. First, the EVs are internalized by endocytosis at the plasma membrane (i). Second, once inside the endocytic pathway, a fraction of late endosomes (LE) penetrates the type II nuclear envelope invaginations where their content, notably the endocytosed EV-associated molecules, are transferred into the nucleoplasm (ii). Two types of nuclear envelope invaginations are described. Type I invaginations (I) are those in which solely the inner nuclear membrane (INM) penetrates into the nucleoplasm, whereas type II invaginations (II) involve both the outer nuclear membrane (ONM) and INM. The endoplasmic reticulum (ER) is a continuation of ONM. B, Key players involved in the translocation of Rab7⁺ late endosomes to nuclear envelope invagination. Two proteins, vesicle-associated membrane protein-associated protein A (VAP-A) and the cytoplasmic oxysterol-binding protein-related protein 3 (ORP3) forming a tripartite complex with late endosome-associated Rab7 protein, are indispensable for the entry of late endosomes to the nuclear envelope invagination and/or their tether to ONM (I). Nuclear pores are somehow involved in the translocation of EV-associated soluble (II) and membranous (III) cargo molecules into the nucleus. It remains to be explained how membranous components of EVs are extracted from the late endosomal membrane upon fusion of the former with the latter and the transport mechanism through nuclear pores, which are size restricted. C, Silencing CD9 in recipient cells and/or EVs or both interferes with the endocytosis of EVs and the nuclear transfer of their cargo molecules. Although the presence of divalent CD9 Ab stimulated these events with native cells and EVs, the lack of CD9 abrogated them.²³ Panels A and B were modified from Ref.²⁹



were performed for 15 minutes at RT. They were then incubated in blocking buffer III (PBS containing 1% BSA) and labelled with mouse anti-SUN2 Ab (clone A-10, #sc-515330; Santa Cruz Biotechnology) for 60 minutes each step at RT. Cells were washed twice with PBS, incubated with tetramethylrhodamine (TRITC)-conjugated anti-mouse IgG (#715-025-150; Jackson ImmunoResearch, West Grove, PA) or Cy5-conjugated anti-mouse IgG (#715-175-150; Jackson ImmunoResearch) secondary antibodies for 30 minutes and again washed twice prior to observation. All antibodies were

diluted in permeabilization buffer containing 1% BSA. Cells were imaged in PBS using confocal laser scanning microscopy (CLSM) using a Nikon A1R+ inverted confocal microscope with a 60X Apo-TIRF oil-immersion objective and a numerical aperture of 1.49 at either 512 × 512 or 1024 × 1024 pixel resolution. Solid-state lasers of 488, 561 and 638 nm solid-state lasers were used to excite GFP, TRITC and Cy5 respectively and corresponding fluorescence emissions were collected using 500-550, 570-620 and 662-737 nm long pass filters.

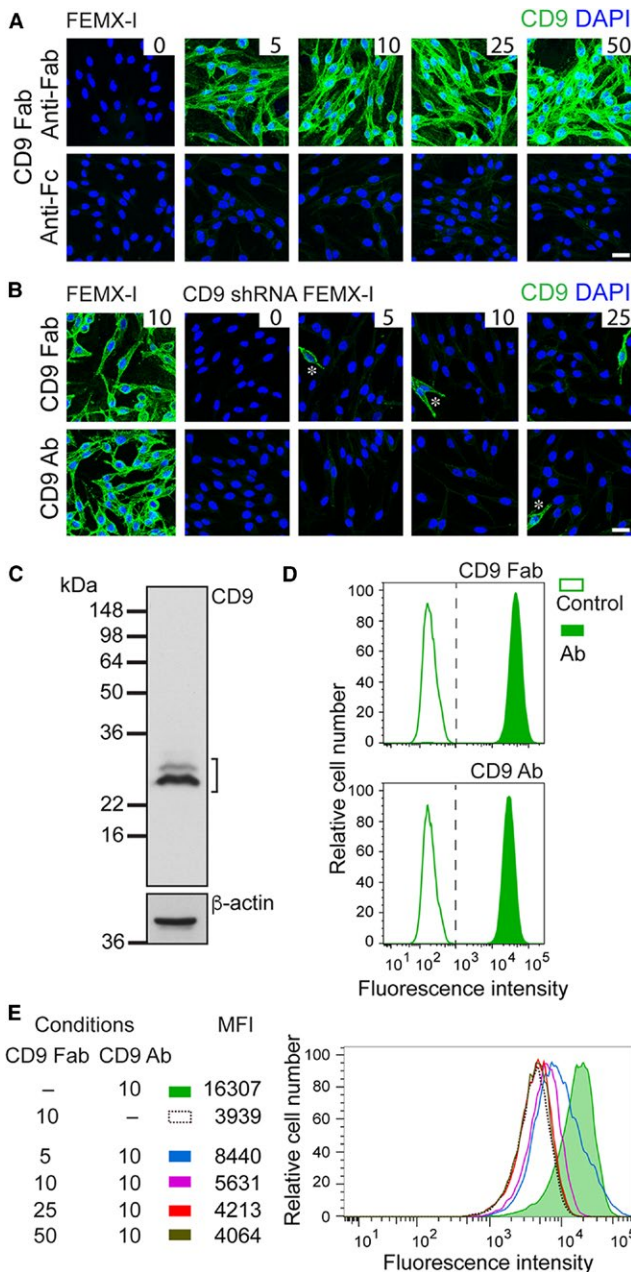


FIGURE 2 Characterization of CD9 Fab. A, Cell surface immunofluorescence on native FEMX-I cells. FEMX-I cells were surface labelled in the cold with CD9 Fab at different concentrations as indicated ($\mu\text{g}/\text{mL}$), PFA-fixed and incubated with either anti-Fab (top panels) or anti-Fc (bottom panels) specific secondary conjugated to a fluorochrome (green). Nuclei were counterstained with 4'-6-diamidino-2-phenylindole (DAPI). B, Cell surface immunofluorescence on CD9-depleted FEMX-I cells. Native FEMX-I cells and CD9 shRNA-transduced cells were surface-labelled in the cold with CD9 Fab (top panels) or CD9 Ab (bottom panels) at different concentrations ($\mu\text{g}/\text{mL}$), as indicated, PFA-fixed and incubated with anti-Fab or anti-Fc specific secondary conjugated to a fluorochrome (green) respectively, prior to DAPI staining. Note that under these conditions, about 15% of infected cells still express CD9 in a proportion similar to native cells (asterisks). Scale bar, 25 μm . C, Immunoblotting. Detergent cell lysate (100- μg protein) prepared from melanoma FEMX-I cells was probed using Fab CD9 and horseradish peroxidase-coupled anti-Fab specific secondary antibody. β -actin was used as control. Position of prestained molecular weight markers (kDa) are indicated. Bracket, CD9 immunoreactivity. D, Flow cytometry. FEMX-I cells were surface labelled with either CD9 Fab (10 $\mu\text{g}/\text{mL}$, top) or CD9 Ab (10 $\mu\text{g}/\text{mL}$, bottom) followed by fluorochrome-conjugated anti-Fab or anti-Fc specific secondary antibody respectively. E, CD9 Fab inhibits the cell binding of native CD9 Ab. FEMX-I cells were sequentially labelled with CD9 Fab at different concentrations as indicated ($\mu\text{g}/\text{mL}$) followed by CD9 Ab (10 $\mu\text{g}/\text{mL}$) and fluorochrome-conjugated anti-Fc specific secondary antibody. Samples were analysed using flow cytometry. The median fluorescence intensity (MFI) is indicated. As negative and background controls, primary Ab (D) or CD9 Ab (E) was omitted

2.7 | Flow cytometry

FEMX-I cells were trypsinized using 0.05% trypsin with 0.53 mmol/L EDTA (Corning Inc.), washed twice in PBS and re-suspended in PBS containing 1% BSA. Cell suspension aliquots of 100 μL (1×10^6 cells) were incubated with either CD9 Fab or CD9 Ab (clone 5H9) (both at 10 $\mu\text{g}/\text{mL}$ in PBS containing 1% BSA) for 30 minutes at 4°C. After two washing steps with PBS, samples were incubated with FITC-conjugated secondary antibody specific either for the mouse Fab or Fc fragment (see above, 1:600) for another 30 minutes at 4°C. As negative controls, primary Ab was omitted. For competitive inhibition experiment, cells were incubated first with CD9 Fab at different concentrations (0, 5, 10, 25 and 50 $\mu\text{g}/\text{mL}$) and then with CD9 Ab (10 $\mu\text{g}/\text{mL}$) followed by Fc-specific FITC-conjugated secondary antibodies. All incubations were performed for 30 minutes at 4°C. To set up the background staining reminiscent of a residual undigested CD9 Ab in CD9 Fab preparation, we omitted CD9 Ab. After washing with PBS, 20 000 events were acquired on a LSRII flow cytometer (BD Biosciences). Instrument settings and gating strategies were established using cells incubated solely with individual secondary antibody as negative controls. Data were analysed using FlowJo software (TreeStar, Ashland, USA). Median fluorescence intensity (MFI) was calculated as a difference of MFI values of stained and negative control populations.

All images were acquired under the same microscope settings for subsequent calculations of mean fluorescence intensity and recorded using NIS Elements software (Nikon). Raw images were processed using Fiji. Each optical section through the cell (21 sections of 0.4 μm for cancer cells and 0.2 μm for MSCs) was assessed individually. Any observed GFP fluorescent signal was counted as EV-derived biomaterials and data collectively calculated. To count nuclear fluorescent materials, a region of interest (ROI) was drawn along the nucleus on each optical section and an auto threshold generated by Fiji was applied. Positive signals were counted using the "analyze particle" function. To determine the value of cytoplasmic GFP fluorescence for each cell, an ROI was also drawn around the cytoplasm, using the cell border as a guide, but excluding the nucleus.

To determine the amount of cell surface CD9 molecules in a given cell, Quantum™ Simply Cellular® anti-mouse IgG kit (#815; Bangs Laboratories Inc., Fishers, IN) was utilized. Cells (1×10^5) and 4 microsphere populations, containing increasing levels of Fc-specific capture antibody, were incubated with phycoerythrin-conjugated anti-CD9 Ab (clone M-L13, #555372; BD Biosciences, San Jose, CA) in PBS containing 0.5% BSA for 30 minutes on ice. Both cells and microspheres were then analysed using flow cytometry using the same settings as above according to manufacturer's instructions. A standard curve was generated using the median channel values of the microspheres and the amount of CD9 molecules per cell was determined from this curve. All calculations were performed with the QuickCal analysis program provided in the kit.

2.8 | Statistical analysis

All experiments were performed at least in triplicate. A minimum of 30 cells was analysed in each experiment. Error bars in graphical data represent means \pm standard deviation. Statistical analysis was determined by one-way analysis of variance followed by pairwise comparison of means with Dunnett's multiple comparison adjustment using the statistical program Stata 12 (StataCorp LLC, College Station, TX). *P*-values inferior to 0.05 were considered significant.

3 | RESULTS

3.1 | Generation of CD9 antibody Fab fragment

Given the positive impact of divalent Ab directed against CD9 on the uptake of CD9⁺ EVs by melanoma cells and the negative impact upon silencing CD9 on either EVs or recipient cells,²³ we sought whether CD9 Fab could influence the internalization and consequently the intercellular transfer of EV-associated cargo molecules. To investigate this issue, we generated CD9 Fab from 5H9 Ab, which recognizes an unidentified epitope in the extracellular part of CD9 (Figure S1A).³⁸ The Ab (IgG₁ kappa) produced from hybridoma clone 5H9 was digested with papain to generate the Fab and Fc fragments. The latter were removed selectively using immobilized protein A (Figure S1B). As observed using SDS-PAGE under non-reducing and reducing conditions, the 5H9 Ab was successfully digested and the 50-kDa CD9 Fab was isolated (Figure S1C).

3.2 | Characterization of CD9 Fab

To determine the functionality of CD9 Fab, we evaluated its binding to melanoma FEMX-I cells by various methods. First, cells growing on fibronectin-coated support were surface labelled in the cold with CD9 Fab at different concentrations followed by a fluorochrome-conjugated secondary antibody specific either for the mouse Fab or Fc fragment. The CLSM analysis revealed that the antigen-CD9 Fab complex is recognized by anti-Fab secondary antibody already at low concentration of primary Ab (Figure 2A,

top panels). In contrast, solely a very weak labelling was detected with a secondary antibody directed against mouse Fc, indicating the effective papain digestion of CD9 Ab (Figure 2A, bottom panels). When a similar experiment was performed with CD9-depleted FEMX-I cells,²³ almost no immunolabelling was detected either with CD9 Fab or full-length antibody (Figure 2B, top and bottom panels respectively). Second, we analysed whether CD9 Fab can recognize CD9 by immunoblotting. To that end, detergent lysate prepared from FEMX-I cells was resolved on SDS-PAGE under non-denaturing condition and probed with CD9 Fab. As shown in Figure 2C, CD9 Fab recognized the CD9 molecules. Third, we evaluated the capacity of CD9 Fab to detect its antigen using flow cytometry. A suspension of FEMX-I cells was subjected to immunolabelling in the cold using either CD9 Fab or full CD9 Ab followed by fluorochrome-conjugated secondary antibody specific either for mouse Fab or Fc fragment respectively. As negative control, primary antibody was omitted. Flow cytometry analyses indicated that CD9 Fab could detect CD9⁺ cells similar to the native anti-CD9 Ab (Figure 2D). Altogether, these experiments demonstrated that CD9 Fab recognizes its antigen under various conditions, notably its native conformation.

3.3 | CD9 Fab interferes with the cell binding of native CD9 antibody

Can CD9 Fab interfere with the binding of corresponding native CD9 Ab? To address this issue, we pre-incubated FEMX-I cells in suspension with various concentrations of CD9 Fab prior to the addition of CD9 Ab and fluorochrome-conjugated secondary antibody specific for the Fc fragment. Samples were analysed by flow cytometry. As a positive control, CD9 Fab was omitted whereas CD9 Ab was absent for the background control. As shown in Figure 2E, CD9 Fab blocked the binding of the native Ab in a dose-dependent fashion, indicating that it could specifically label the cell surface CD9 molecules. We concluded that the monovalent CD9 Fab could be useful in achieving our objective, ie interfering with the uptake of CD9⁺ EVs.

3.4 | Differential effect of CD9 Fab versus native antibody on the internalization of EVs

To determine the impact of CD9 Fab on the internalization of EVs by melanoma cells, we used engineered FEMX-I cells to express the CD9-GFP fusion protein.²³ These cells release in vivo-labelled fluorescent EVs that could be used to monitor EV uptake upon incubation with recipient cells. CD9-GFP⁺ EVs released in the conditioned culture media were enriched by differential centrifugation (for details see Methods,²³). Prior to the exposure of native FEMX-I cells to CD9-GFP⁺ EVs, cells were pre-incubated for 30 minutes at 37°C with either CD9 Fab or CD9 Ab (25 µg/mL). As control, no antibody was added. Afterward, cells were incubated with CD9-GFP⁺ EVs (2.5×10^8 particle per mL) without removing the antibodies for 5 hours and then fixed, immunolabelled for protein SUN domain-containing protein 2 (SUN2), an inner nuclear membrane protein and analysed using CLSM. At first

glance, we noticed that the uptake of CD9-GFP⁺ EVs by recipient cells seemed variable under the native conditions, ie without the addition of CD9 Ab. Therein, GFP fluorescence appears as strong, medium or weak among cells (Figure S2A). In contrast, GFP fluorescence becomes more homogeneous within the cell population upon the addition of antibodies. A three-dimensional reconstruction of labelled recipient cell revealed that CD9-GFP signal associated with their cytoplasm

was considerably reduced in the presence of CD9 Fab by comparison to control (Figure 3A, uncut)—for an overview see Figure S2A. Quantification of each optical section confirmed it (Figure 3B). In contrast, the presence of CD9 Ab yielded the opposite effect, ie, an increase of cytoplasmic CD9-GFP was detected (Figure 3A, uncut; 3B). Interestingly, similar outcome were observed with two other melanoma cell lines, A375 and C8161, exposed to FEMX-I cell-derived

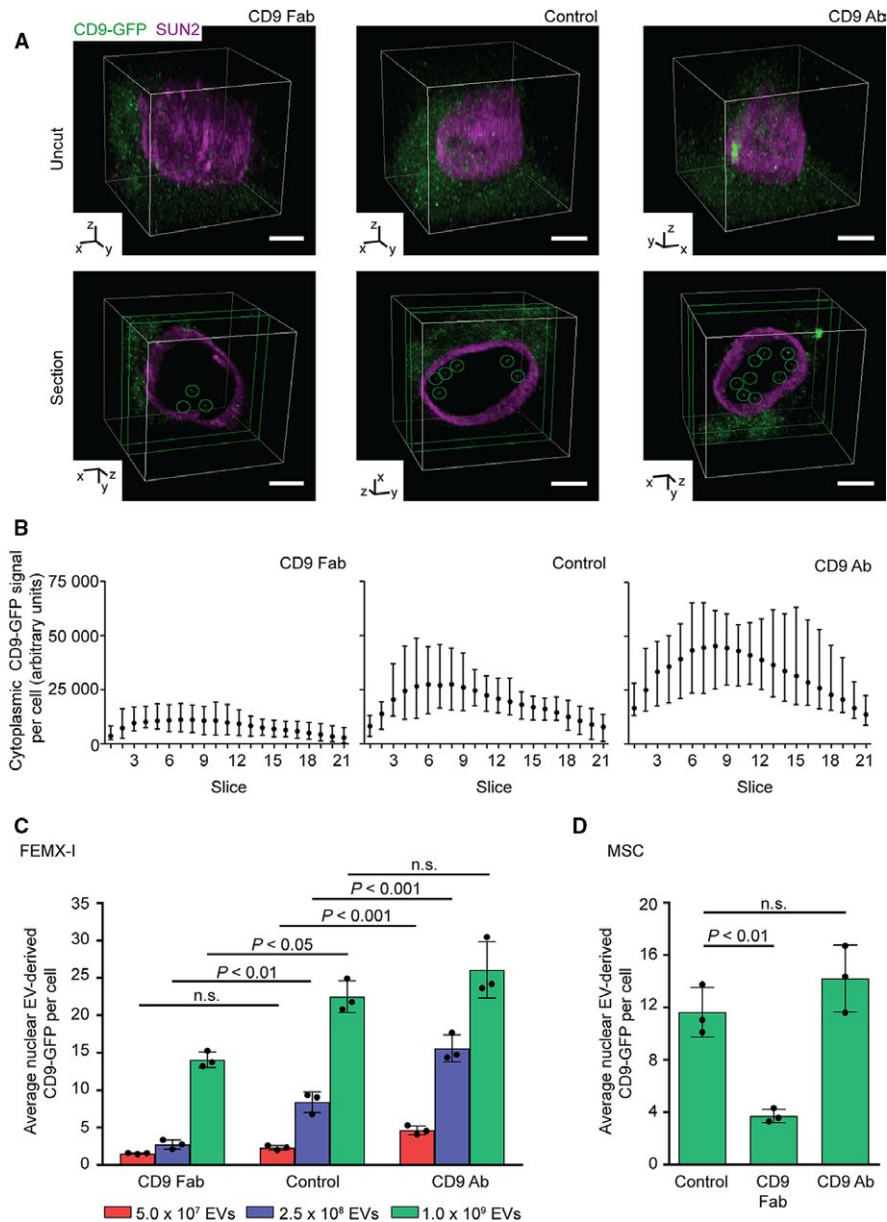
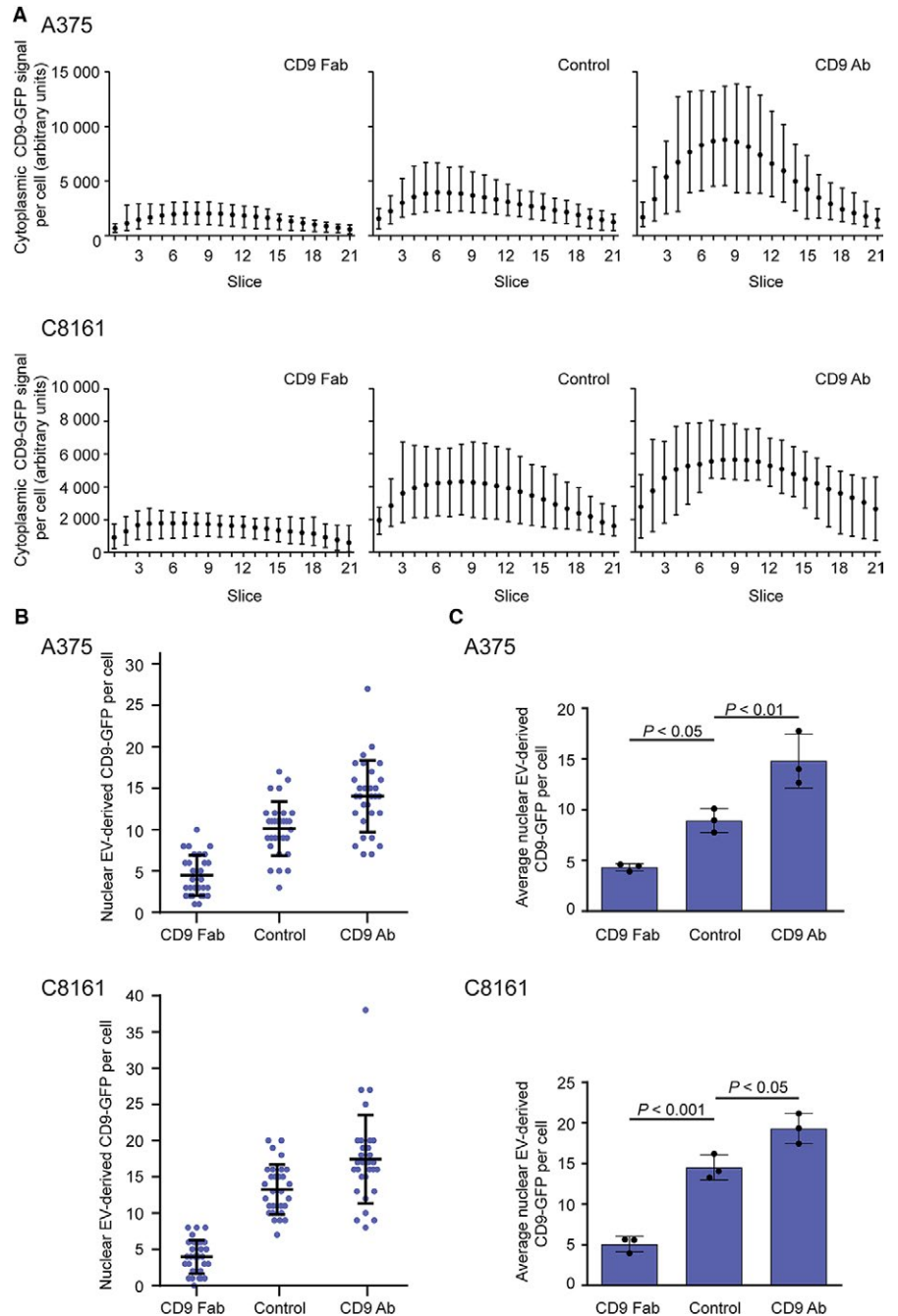


FIGURE 3 CD9 Fab impedes the uptake of extracellular vesicles (EVs) and nuclear transfer of their cargo proteins in melanoma and stromal cells. A–C, FEMX-I cells were pre-incubated (30 min) without (control) or with CD9 Fab or CD9 Ab (25 $\mu\text{g}/\text{mL}$) prior to the exposure to fluorescent EVs derived from CD9-GFP⁺ FEMX-I cells for 5 h. Different concentrations of EVs were used (A–C, 2.5×10^8 particle per mL [blue]; C, 5.0×10^7 [red] or 1.0×10^9 particle per mL [green]). Samples were then fixed and immunolabelled for SUN2 prior to confocal laser scanning microscopy. A three-dimensional reconstruction of the entire cell (uncut) or three sections (0.4- μm slices each, section) is shown (A). CD9-GFP appears as discrete punctate signals either in the cytoplasm or nucleoplasm (circles) of recipient cells. The amount of CD9-GFP signal was quantified using serial optical sections through a cell using the cytoplasmic (B) and nuclear (C) compartments as a region of interest (see Figure S2B). Mean with the range of fluorescence per slice from 10 individual cells are shown (B). D, Native MSCs were exposed to EVs (1.0×10^9 particle per mL) derived from CD9-GFP⁺ MSCs upon their pre-incubation without or with CD9 Fab or CD9 Ab as described above. Punctate nuclear CD9-GFP signal per cell was quantified. Means \pm SD are shown (C, D). 50 (C) or 20 (D) cells were evaluated per experiment ($n = 3$). P -values are indicated. N.S., not significant. Scale bars, 5 μm

FIGURE 4 CD9 Fab impedes the uptake of extracellular vesicles (EVs) and nuclear transfer of their cargo proteins in various malignant melanoma cells. (A-C) Melanoma A375 or C8161 cells were incubated (30 min) without (control) or with CD9 Fab or CD9 Ab (25 $\mu\text{g}/\text{mL}$) prior to the exposure to fluorescent EVs (2.5×10^8 particle per mL) derived from FEMX-I cells expressing CD9-GFP for 5 h. Samples were then fixed and immunolabelled for SUN2 prior to confocal laser scanning microscopy. Cytoplasmic (A) and nuclear (B, C) CD9-GFP signals per cell were quantified using Fiji. Means with the range of fluorescence per slice from 10 individual and representative cells are shown (A). 30 cells were evaluated per condition and experiment (B) and the means \pm SD of three independent experiments are shown (C). *P*-values are indicated



CD9-GFP⁺ EVs (Figure 4A), indicating that CD9 Fab inhibits the uptake of EVs.

3.5 | CD9 Fab inhibits the nuclear transfer of EV-derived cargo proteins

We previously reported that cargo proteins derived from EVs are not only internalized by host cells, but also a fraction of them is transferred to their nucleoplasm by the intermediate of late endosomes entering into nucleoplasmic reticulum.^{23,29} Does CD9 Fab interfere with this mechanism? The analysis of the nuclear compartment of melanoma cells pre-treated with monovalent or

divalent Abs prior to incubation with CD9-GFP⁺ EVs (2.5×10^8 particle per mL) showed a decrease or an increase in the CD9-GFP⁺ signals in the nucleoplasm respectively, compared to the control (Figure 3A, section, green circle; 3C; see also Table 1). As previously demonstrated,^{23,29} CD9-GFP⁺ signal in the nuclear compartment appeared with a punctate pattern (Figure 3A; Figure S2B, green circle).

The addition of different amounts of CD9-GFP⁺ EVs (eg, 5.0×10^7 or 1.0×10^9 particle per mL) was also evaluated in FEMX-I cells. In most cases, the numbers of nuclear CD9-GFP were significantly lower or higher in cells exposed to CD9 Fab or CD9 Ab respectively (Figure 3C). Only with a high amount of EVs (ie 1.0×10^9 particle per mL) no

Antibody	Experimental procedure ^a	Average nuclear EV-derived CD9-GFP per cell ^c	P-values (relative to control)	P-values (relative to procedure A)
Control ^b	A	8.42 ± 0.74	—	
	B	8.41 ± 0.61	—	
	C	8.02 ± 0.44	—	
CD9 Fab	A	2.89 ± 0.13	0.05	
	B	2.99 ± 0.45	0.001	
	C	1.53 ± 0.09	0.0001	0.05
CD9 Ab	A	15.67 ± 1.20	0.005	
	B	14.17 ± 0.76	0.001	
	C	14.20 ± 0.32	0.0001	0.5

^aA, Cells were pre-incubated with antibody (25 µg/mL, 30 min, 37°C) before the addition of CD9-GFP⁺EVs (5 h). B, CD9-GFP⁺EVs were pre-incubated with antibody (25 µg/mL, 30 min, 4°C) before their incubation with cells (5 h). C, Cells and CD9-GFP⁺EVs were pre-incubated with antibody (12.5 µg/mL each, 30 min, 37 or 4°C respectively) before their co-culture (5 h).

^bControl refers to the three experimental procedures (A-C) without the addition of antibody.

^cAt least 30 cells were evaluated per condition (n = 3).

significant difference was observed between CD9 Ab and control. Similar observations were made with A375 and C8161 cells (Figure 4B,C).

When the same experiments were performed with primary MSCs as recipient cells as well as donor cells for fluorescent EVs (1×10^9 particle per mL), we observed also a significant decrease in nuclear and cytoplasmic CD9-GFP in cells pre-treated with CD9 Fab (25 µg/mL) (Figure 3D; data not shown). The CD9 Ab did not significantly increase the EV uptake which can be explained by a limited quantity of CD9 molecules in MSCs in comparison to melanoma cells, as observed by immunoblotting and quantitative fluorescence analyses using flow cytometry (Figure S3A-C).

3.6 | A minimal concentration of CD9 Fab is necessary to interfere with EV uptake

We assessed whether the uptake of EVs is dependent on the concentration of CD9 Fab. FEMX-I cells were subjected to increasing concentrations of CD9 Fab or CD9 Ab prior to incubation with CD9-GFP⁺ EVs (2.5×10^8 particle per mL). As shown in Figure 5A, the uptake of EVs was progressively inhibited as the concentration of CD9 Fab increased, whereas the opposite effect was again observed in cells treated with CD9 Ab, ie more EVs were internalized with increasing CD9 Ab concentration. A similar trend was observed in the number of CD9-GFP signals in the nuclear compartment (Figure 5B). These results are in line with the interference of CD9 Fab to cell surface CD9 Ab binding observed using flow cytometry (Figure 2E). Thus, a minimal amount of antibody (ie 25 µg/mL) seems to be indispensable to inhibit (or promote) the EV uptake.

Lastly, we determined whether the pre-incubation of EVs with Ab (25 µg/mL) or of both EVs and cells individually, instead of cells

TABLE 1 Differential impact of CD9 antibody on the nuclear localization of extracellular vesicles (EV)-derived cargo protein

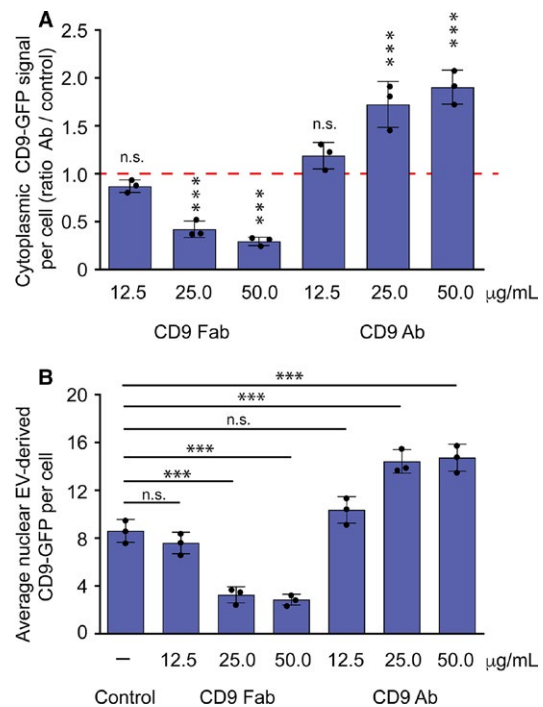


FIGURE 5 Dose-dependent inhibition of CD9 Fab on the extracellular vesicles (EV) uptake and nuclear transfer of their cargo proteins. (A, B) FEMX-I cells were pre-incubated (30 min) with different concentration of CD9 Fab or CD9 Ab as indicated prior to the exposure to CD9-GFP⁺ EVs (2.5×10^8 particles per mL) for 5 h. As control, no antibody was added (-). Cytoplasmic (A) and nuclear (B) CD9-GFP signals per cell were quantified using Fiji. Means ± SD are shown. 10 (A) or 30 (B) cells were evaluated per experiment (n = 3). They were evaluated in comparison to the control (A, red line; B, -). ***, $P \leq 0.001$. N.S., not significant

only as performed until now, influenced internalization and the nuclear localization of EV-derived cargo proteins. We wanted to rule out a potential negative impact of the addition of the Abs (CD9 Fab or CD9 Ab) to recipient cells, which could stimulate the internalization of cell surface CD9, hence limit the EV uptake. If it turned out to be the case, all acquired numbers would be underestimated. Similarly, we wished to exclude that the addition of Abs, particularly CD9 Ab, to EVs would reduce their internalization by favouring, for instance, their clustering. As presented in Table 1, we found that the pre-incubation of cells with Abs did not influence the final outcome when compared to the pre-incubation of EVs (procedure A vs. B). However, the nuclear localization of EV-derived cargo proteins was significantly reduced when both entities (EVs and cells) were pre-incubated individually with the monovalent, but not the divalent, Ab (see procedure C by comparison to A).

4 | DISCUSSION

In this study, we demonstrated that a monovalent Ab directed against tetraspanin CD9 interferes with the uptake of EVs by cancer cells and primary MSCs as well as with the nuclear transfer of their cargo proteins. The latter event is probably a direct consequence of the endocytosis inhibition of EVs.²³ Under these conditions, CD9 Fab could saturate the CD9 molecules located at the surface of cells and EVs and consequently interfere negatively with its function (Figure 6A; see below). The synergic impact of the pre-incubation of cells and EVs

individually with CD9 Fab is consistent with this scenario. Our data are in line with an elegant study showing the CD9 Fab can inhibit the transfer of materials between CD9-containing membranous vesicles, called epididymosomes and maturing epididymal spermatozoa.⁵⁰ In contrast, divalent CD9 Ab promotes these events, which can be correlated to antibody-induced cross-linking of CD9 associated with EVs and host cells (Figure 6B). Does CD9 play a role in the initial adhesion of EVs to the recipient cell? The earlier observation made with sperm-egg fusion suggests it. Jégou and colleagues demonstrated that the fertilization process is controlled by sperm-egg adhesion properties driven by CD9.⁵¹ In such process, CD9 might organize the components (proteins and lipids) of plasma membrane and/or EV membrane into a specific tetraspanin web (Figure 6B, green), whose constituents (eg, adhesion proteins) would somehow regulate the interaction with EVs and promote their endocytosis.⁵²⁻⁵⁵ Similarly, CD9 has been proposed to act as a scaffold in the regulation of adhesion molecules at the immune synapse and T lymphocyte activation.⁵⁶ It remains to be determined whether the cis-dimerization of CD9 in the membrane of recipient cells as well as in EVs is involved.⁵⁷ We could not exclude that a trans-dimerization of CD9, ie molecules expressed in opposite membranes, occurs. Indeed, our present data with divalent Ab as mentioned above and the complete lack of EV endocytosis previously observed in melanoma cells in which CD9 was silenced in both entities (cells and/or EVs), suggest it (Figure 1C).²³ It will be of interest to investigate the CD9 cis/trans-dimerization by co-immunoprecipitation using engineered CD9 proteins associated with cells and EVs with distinct epitope tags.

Besides the exact molecular mechanism regulating the adhesion of EVs to recipient cells and their internalization, it will be of interest to determine whether other anti-CD9 antibodies interfere with the EV uptake and nuclear transfer of their cargo proteins, as observed here with CD9 Fab derived from 5H9 Ab. The proper localization of their respective epitope might be crucial to promote these effects and it is conceivable that distinct CD9 Fab (or again other CD9 interacting partners) could potentially synergize their inhibitory effect. Other tetraspanin proteins enriched in EVs such as CD81 should also be evaluated in this respect.

The intercellular transfer of materials by cancer cell-produced EVs played a significant role in the transformation of microenvironment, notably in the bone marrow, to favour metastasis and tumour growth.⁷ Interfering locally with these mechanisms, particularly the internalization of cancer cell-derived EVs by MSCs, one of the main targeted cellular constituents of tumour niche,⁵⁸ could find a cutting-edge clinical application. MSCs have an important role in co-ordinating the tumour microenvironment. Transformed MSCs produced growth factors favouring tumour growth and angiogenesis, inhibited anti-tumour immune responses and shaped the tumour inflammatory environment.⁵⁹⁻⁶¹ Thus, our data with MSCs exposed to CD9 Fab might find new avenues to prevent the bone marrow transformation. In addition to cancers, other diseases involving the intercellular transfer of biomaterials mediated by EVs, such as neurodegenerative diseases (eg, Parkinson's disease, Alzheimer's disease,

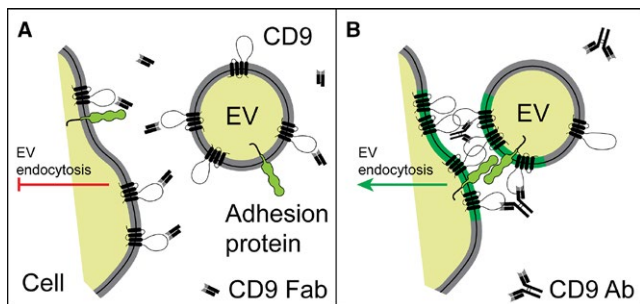


FIGURE 6 Schematic representation showing the negative and positive impact of CD9 Fab and CD9 Ab, respectively, on the endocytosis of CD9-containing extracellular vesicles (EVs). (A, B) CD9 Fab will saturate CD9 proteins present at the surface of cells and EVs, hence interfere with its CD9 function. CD9 Fab can impede the cis/trans-dimerization of CD9, its oligomerization and/or its interaction with other protein partners and block EV endocytosis (red bar). In contrast, divalent CD9 Ab could cross-link CD9 proteins associated with host cells and EVs and consequently stimulate the endocytosis on EVs (green arrow). In the latter case, cis-dimerization/oligomerization of CD9 might organize the components (proteins and lipids) of plasma membrane and/or EV membrane into a specific tetraspanin web (green segment), whose constituents, notably potential adhesion proteins as illustrated would somehow regulate the cell-EV interaction and promote the endocytosis of EVs

amyotrophic lateral sclerosis), could benefit from this new potential therapeutic approach.^{62,63}

Finally, our observations could benefit the areas of regenerative medicine and tissue engineering. Here, the stimulation of EV endocytosis by specific divalent antibodies could favour tissue/organ repair.⁶⁴ Myocardial regeneration might be a good example for such intervention with MSCs as a promising source of donor cell EVs.^{65,66} Such approach could be an interesting alternative to stem cell-based therapy.

ACKNOWLEDGEMENTS

The authors wish to thank Fabio Anzanello for skillful technical assistance, Emmett Findlay and Wolfgang Gilliar for their constant support and Thomas G. Beito of the Mayo Antibody Hybridoma Core for preparation and purification of the anti-CD9 Ab from the 5H9 hybridoma.

CONFLICTS OF INTEREST

United Kingdom patent application number GB1814065.7 and United States provisional patent number 62/724 183 are pending. We have no other potential conflict of interest.

DATA AVAILABILITY

All data that were generated or analysed during this study are included in this published article (and its supplementary information files).

AUTHOR CONTRIBUTIONS

MFS, GR, DC, AL conception and design; MFS, JK, DC, AL development of methodology; MFS, JK, CM acquisition of data; MFS, DC, CV, AL analysis and interpretation of data (eg, statistical analysis, biostatistics, computational analysis); MFS, GR, JK, DC, AL writing, review and/or revision of the manuscript.

ORCID

Denis Corbeil  <https://orcid.org/0000-0003-1181-3659>

Aurelio Lorico  <https://orcid.org/0000-0003-0644-7375>

REFERENCES

- Raposo G, Stoorvogel W. Extracellular vesicles: exosomes, microvesicles, and friends. *J Cell Biol.* 2013;200:373-383.
- van Niel G, D'Angelo G, Raposo G. Shedding light on the cell biology of extracellular vesicles. *Nat Rev Mol Cell Biol.* 2018;19:213-228.
- Valadi H, Ekstrom K, Bossios A, Sjöstrand M, Lee JJ, Lötvalld JO. Exosome-mediated transfer of mRNAs and microRNAs is a novel mechanism of genetic exchange between cells. *Nat Cell Biol.* 2007;9:654-659.
- Kahlert C, Melo SA, Protopopov A, et al. Identification of double-stranded genomic DNA spanning all chromosomes with mutated KRAS and p53 DNA in the serum exosomes of patients with pancreatic cancer. *J Biol Chem.* 2014;289:3869-3875.
- Gyorgy B, Szabo TG, Pasztoi M, et al. Membrane vesicles, current state-of-the-art: emerging role of extracellular vesicles. *Cell Mol Life Sci.* 2011;68:2667-2688.
- Yáñez-Mó M, Siljander PR, Andreu Z. Biological properties of extracellular vesicles and their physiological functions. *J Extracell Vesicles.* 2015;4:27066.
- Peinado H, Alečković M, Lavotshkin S, et al. Melanoma exosomes educate bone marrow progenitor cells toward a pro-metastatic phenotype through MET. *Nat Med.* 2012;18:883-891.
- Hood JL, San RS, Wickline SA. Exosomes released by melanoma cells prepare sentinel lymph nodes for tumor metastasis. *Cancer Res.* 2011;71:3792-3801.
- Huttner HB, Janich P, Köhrmann M, et al. The stem cell marker prominin-1/CD133 on membrane particles in human cerebrospinal fluid offers novel approaches for studying central nervous system disease. *Stem Cells.* 2008;26:698-705.
- Jørgensen M, Baek R, Pedersen S, Søndergaard EK, Kristensen SR, Varming K. Extracellular Vesicle (EV) array: microarray capturing of exosomes and other extracellular vesicles for multiplexed phenotyping. *J Extracell Vesicles.* 2013;2:1.
- Yang Y, Hong Y, Cho E, Kim GB, Kim IS. Extracellular vesicles as a platform for membrane-associated therapeutic protein delivery. *J Extracell Vesicles.* 2018;7:1440131.
- Kowal J, Tkach M, Théry C. Biogenesis and secretion of exosomes. *Curr Opin Cell Biol.* 2014;29C:116-125.
- Marzesco AM, Janich P, Wilsch-Bräuninger M, et al. Release of extracellular membrane particles carrying the stem cell marker prominin-1 (CD133) from neural progenitors and other epithelial cells. *J Cell Sci.* 2005;118:2849-2858.
- Dubreuil V, Marzesco AM, Corbeil D, Huttner WB, Wilsch-Bräuninger M. Midbody and primary cilium of neural progenitors release extracellular membrane particles enriched in the stem cell marker prominin-1. *J Cell Biol.* 2007;176:483-495.
- Tian T, Zhu YL, Zhou YY, et al. Exosome uptake through clathrin-mediated endocytosis and macropinocytosis and mediating miR-21 delivery. *J Biol Chem.* 2014;289:22258-22267.
- Mulcahy LA, Pink RC, Carter DR. Routes and mechanisms of extracellular vesicle uptake. *J Extracell Vesicles.* 2014;3:1.
- Escrevente C, Keller S, Altevogt P, Costa J. Interaction and uptake of exosomes by ovarian cancer cells. *BMC Cancer.* 2011;11:108.
- Javeed N, Sagar G, Dutta SK, et al. Pancreatic cancer-derived exosomes cause paraneoplastic beta-cell dysfunction. *Clin Cancer Res.* 2015;21:1722-1733.
- Svensson KJ, Christianson HC, Wittrup A, et al. Exosome uptake depends on ERK1/2-heat shock protein 27 signaling and lipid Raft-mediated endocytosis negatively regulated by caveolin-1. *J Biol Chem.* 2013;288:17713-17724.
- Kanada M, Bachmann MH, Hardy JW, et al. Differential fates of biomolecules delivered to target cells via extracellular vesicles. *Proc Natl Acad Sci U S A.* 2015;112:E1433-E1442.
- Rappa G, Mercapide J, Anzanello F, et al. Wnt interaction and extracellular release of prominin-1/CD133 in human malignant melanoma cells. *Exp Cell Res.* 2013a;319:810-819.
- Rappa G, Mercapide J, Anzanello F, Pope RM, Lorico A. Biochemical and biological characterization of exosomes containing prominin-1/CD133. *Mol Cancer.* 2013b;12:62.
- Rappa G, Santos MF, Green TM, et al. Nuclear transport of cancer extracellular vesicle-derived biomaterials through nuclear envelope invagination-associated late endosomes. *Oncotarget.* 2017;8:14443-14461.

24. Rappa G, Green TM, Lorico A. The nuclear pool of tetraspanin CD9 contributes to mitotic processes in human breast carcinoma. *Mol Cancer Res.* 2014;12:1840-1850.
25. Nunukova A, Neradil J, Skoda J, et al. Atypical nuclear localization of CD133 plasma membrane glycoprotein in rhabdomyosarcoma cell lines. *Int J Mol Med.* 2015;36:65-72.
26. Dovrat S, Caspi M, Zilberberg A, et al. 14-3-3 and beta-catenin are secreted on extracellular vesicles to activate the oncogenic Wnt pathway. *Mol Oncol.* 2014;8:894-911.
27. Waldenstrom A, Genneback N, Hellman U, Ronquist G. Cardiomyocyte microvesicles contain DNA/RNA and convey biological messages to target cells. *PLoS ONE.* 2012;7:e34653.
28. Cai J, Han Y, Ren H, et al. Extracellular vesicle-mediated transfer of donor genomic DNA to recipient cells is a novel mechanism for genetic influence between cells. *J Mol Cell Biol.* 2013;5:227-238.
29. Santos MF, Rappa G, Karbanová J, Kurth T, Corbeil D, Lorico A. VAMP-associated protein-A and oxysterol-binding protein-related protein 3 promote the entry of late endosomes into the nucleoplasmic reticulum. *J Biol Chem.* 2018;293:13834-13848.
30. Hemler ME. Tetraspanin proteins mediate cellular penetration, invasion, and fusion events and define a novel type of membrane microdomain. *Ann Rev Cell Dev Biol.* 2003;19:397-422.
31. Le Naour F, Rubinstein E, Jasmin C, Prenant M, Boucheix C. Severely reduced female fertility in CD9-deficient mice. *Science.* 2000;287:319-321.
32. Chen MS, Tung KS, Coonrod SA, et al. Role of the integrin-associated protein CD9 in binding between sperm ADAM 2 and the egg integrin alpha6beta1: implications for murine fertilization. *Proc Natl Acad Sci USA.* 1999;96:11830-11835.
33. Tachibana I, Hemler ME. Role of transmembrane 4 superfamily (TM4SF) proteins CD9 and CD81 in muscle cell fusion and myotube maintenance. *J Cell Biol.* 1999;146:893-904.
34. Schmid E, Zurbriggen A, Gassen U, Rima B, ter Meulen V, Schneider-Schaulies J. Antibodies to CD9, a tetraspan transmembrane protein, inhibit canine distemper virus-induced cell-cell fusion but not virus-cell fusion. *J Virol.* 2000;74:7554-7561.
35. Gordon-Alonso M, Yanez-Mo M, Barreiro O, et al. Tetraspanins CD9 and CD81 modulate HIV-1-induced membrane fusion. *J Immunol.* 2006;177:5129-5137.
36. Zöller M. Tetraspanins: push and pull in suppressing and promoting metastasis. *Nat Rev Cancer.* 2009;9:40-55.
37. Longo N, Yáñez-Mó M, Mittelbrunn M, et al. Regulatory role of tetraspanin CD9 in tumor-endothelial cell interaction during transendothelial invasion of melanoma cells. *Blood.* 2001;98:3717-3726.
38. Kobayashi H, Hosono O, Iwata S, et al. The tetraspanin CD9 is preferentially expressed on the human CD4(+)CD45RA+ naive T cell population and is involved in T cell activation. *Clin Exp Immunol.* 2004;137:101-108.
39. Di Fede G, Bronte G, Rizzo S, et al. Monoclonal antibodies and antibody fragments: state of the art and future perspectives in the treatment of non-haematological tumors. *Expert Opin Biol Ther.* 2011;11:1433-1445.
40. Oude Munnink TH, Henstra MJ, Segerink LI, Movig KL, Brummelhuis-Visser P. Therapeutic drug monitoring of monoclonal antibodies in inflammatory and malignant disease: translating TNF-alpha experience to oncology. *Clin Pharmacol Ther.* 2016;99:419-431.
41. Fodstad O, Kjønneksen I, Aamdal S, Nesland JM, Boyd MR, Pihl A. Extrapulmonary, tissue-specific metastasis formation in nude mice injected with FEMX-I human melanoma cells. *Cancer Res.* 1988;48:4382-4388.
42. Rappa G, Fodstad O, Lorico A. The stem cell-associated antigen CD133 (Prominin-1) is a molecular therapeutic target for metastatic melanoma. *Stem Cells.* 2008;26:3008-3017.
43. Kozłowski JM, Fidler IJ, Campbell D, Xu ZL, Kaighn ME, Hart IR. Metastatic behavior of human tumor cell lines grown in the nude mouse. *Cancer Res.* 1984;44:3522-3529.
44. Welch DR, Bisi JE, Miller BE, et al. Characterization of a highly invasive and spontaneously metastatic human malignant melanoma cell line. *Int J Cancer.* 1991;47:227-237.
45. Xi Y, Riker A, Shevde-Samant L, et al. Global comparative gene expression analysis of melanoma patient samples, derived cell lines and corresponding tumor xenografts. *Cancer Genomics Proteomics.* 2008;5:1-35.
46. Larson BL, Ylostalo J, Prockop DJ. Human multipotent stromal cells undergo sharp transition from division to development in culture. *Stem Cells.* 2008;26:193-201.
47. Freund D, Fonseca AV, Janich P, Bornhäuser M, Corbeil D. Differential expression of biofunctional GM1 and GM3 gangliosides within the plastic-adherent multipotent mesenchymal stromal cell population. *Cytotherapy.* 2010;12:131-142.
48. Corbeil D, Röper K, Hannah MJ, Hellwig A, Huttner WB. Selective localization of the polytopic membrane protein prominin in microvilli of epithelial cells - a combination of apical sorting and retention in plasma membrane protrusions. *J Cell Sci.* 1999;112:1023-1033.
49. Schneider CA, Rasband WS, Eliceiri KW. NIH Image to ImageJ: 25 years of image analysis. *Nat Methods.* 2012;9:671-675.
50. Caballero JN, Frenette G, Belleannée C, Sullivan R. CD9-positive microvesicles mediate the transfer of molecules to bovine spermatozoa during epididymal maturation. *PLoS ONE.* 2013;8:e65364.
51. Jégou A, Ziyat A, Barraud-Lange V, et al. CD9 tetraspanin generates fusion competent sites on the egg membrane for mammalian fertilization. *Proc Natl Acad Sci USA.* 2011;108:10946-10951.
52. Hoshino A, Costa-Silva B, Shen TL, et al. Tumour exosome integrins determine organotropic metastasis. *Nature.* 2015;527:329-335.
53. Kawakami Y, Kawakami K, Stealant WF, et al. Tetraspanin CD9 is a "proteolipid", and its interaction with alpha 3 integrin in microdomain is promoted by GM3 ganglioside, leading to inhibition of laminin-5-dependent cell motility. *J Biol Chem.* 2002;277:34349-34358.
54. Ziyat A, Rubinstein E, Monier-Gavelle F, et al. CD9 controls the formation of clusters that contain tetraspanins and the integrin alpha 6 beta 1, which are involved in human and mouse gamete fusion. *J Cell Sci.* 2006;119:416-424.
55. Rocha-Perugini V, Martinez Del Hoyo G, González-Granado JM, et al. CD9 regulates major histocompatibility complex class II trafficking in monocyte-derived dendritic cells. *Mol Cell Biol.* 2017;37. <https://doi.org/10.1128/MCB.00202-17>.
56. Reyes R, Cardeñes B, Machado-Pineda Y, Cabañas C. Tetraspanin CD9: a key regulator of cell adhesion in the immune system. *Front Immunol.* 2018;9:863.
57. Kovalenko OV, Yang X, Kolesnikova TV, Hemler ME. Evidence for specific tetraspanin homodimers: inhibition of palmitoylation makes cysteine residues available for cross-linking. *Biochem J.* 2004;377:407-417.
58. Lin LY, Du LM, Cao K, et al. Tumour cell-derived exosomes endow mesenchymal stromal cells with tumour-promotion capabilities. *Oncogene.* 2016;35:6038-6042.
59. Huang Y, Yu P, Li W, et al. p53 regulates mesenchymal stem cell-mediated tumor suppression in a tumor microenvironment through immune modulation. *Oncogene.* 2014;33:3830-3838.
60. Kidd S, Spaeth E, Dembinski JL, et al. Direct evidence of mesenchymal stem cell tropism for tumor and wounding microenvironments using in vivo bioluminescent imaging. *Stem Cells.* 2009;27:2614-2623.
61. Wang Y, Chen X, Cao W, Shi Y. Plasticity of mesenchymal stem cells in immunomodulation: pathological and therapeutic implications. *Nat Immunol.* 2014;15:1009-1016.

62. Howitt J, Hill AF. Exosomes in the pathology of neurodegenerative diseases. *J Biol Chem*. 2016;291:26589-26597.
63. Soria FN, Pampliega O, Bourdenx M, Meissner WG, Bezard E, Dehay B. Exosomes, an unmasked culprit in neurodegenerative diseases. *Front Neurosci*. 2017;11:26.
64. Basu J, Ludlow JW. Exosomes for repair, regeneration and rejuvenation. *Expert Opin Biol Ther*. 2016;16:489-506.
65. Lai RC, Chen TS, Lim SK. Mesenchymal stem cell exosome: a novel stem cell-based therapy for cardiovascular disease. *Regen Med*. 2011;6:481-492.
66. Maring JA, Beez CM, Falk V, Seifert M, Stamm C. Myocardial Regeneration via Progenitor Cell-Derived Exosomes. *Stem Cells Int*. 2017;2017:7849851.

SUPPORTING INFORMATION

Additional supporting information may be found online in the Supporting Information section at the end of the article.

How to cite this article: Santos MF, Rappa G, Karbanová J, et al. Anti-human CD9 antibody Fab fragment impairs the internalization of extracellular vesicles and the nuclear transfer of their cargo proteins. *J Cell Mol Med*. 2019;00:1-14. <https://doi.org/10.1111/jcmm.14334>

ORIGINAL RESEARCH

CD26 expression is attenuated by TGF- β and SDF-1 autocrine signaling on stromal myofibroblasts in human breast cancers

Yoshihiro Mezawa¹  | Yataro Daigo^{2,3} | Atsushi Takano^{2,3} | Yohei Miyagi⁴ | Tomoyuki Yokose⁵ | Toshinari Yamashita⁶ | Chikao Morimoto⁷ | Okio Hino¹ | Akira Orimo¹ 

¹Department of Molecular Pathogenesis, Graduate School of Medicine, Juntendo University, Tokyo, Japan

²Center for Antibody and Vaccine Therapy, Institute of Medical Science, Research Hospital, The University of Tokyo, Tokyo, Japan

³Department of Medical Oncology and Cancer Center, Shiga University of Medical Science, Otsu, Japan

⁴Molecular Pathology and Genetics Division, Kanagawa Cancer Center Research Institute, Yokohama, Japan

⁵Department of Pathology, Kanagawa Cancer Center, Yokohama, Japan

⁶Department of Breast and Endocrine Surgery, Kanagawa Cancer Center, Yokohama, Japan

⁷Department of Therapy Development and Innovation for Immune Disorders and Cancers, Juntendo University, Tokyo, Japan

Correspondence

Akira Orimo, Department of Molecular Pathogenesis, Graduate School of Medicine, Juntendo University, 2-1-1, Hongo, Bunkyo-ku, Tokyo, 113-8421, Japan.
Email: aorimo@juntendo.ac.jp

Funding information

Ministry of Education, Culture, Sports, Science and Technology, Japan, Grant/Award Number: 24300332, 25640069, 15K14385 and JP 16H06277

Abstract

Human breast carcinoma-associated fibroblasts (CAFs) increasingly acquire both transforming growth factor- β (TGF- β) and stromal cell-derived factor-1 (SDF-1) signaling in an autocrine fashion during tumor progression. Such signaling mediates activated myofibroblastic and tumor-promoting properties in these fibroblasts. CD26/dipeptidyl peptidase-4 is a serine protease that cleaves various chemokines including SDF-1. Stromal CD26 expression is reportedly undetectable in human skin squamous cell carcinomas. However, whether stromal CD26 expression is also downregulated in human breast cancers and which stromal cells potentially lack CD26 expression remain elusive. To answer these questions, sections prepared from 239 human breast carcinomas were stained with antibodies against CD26 and α -smooth muscle actin (α -SMA), a marker for activated myofibroblasts. We found that tumor-associated stroma involving α -SMA-positive myofibroblasts stained negative or negligible for CD26 in 118 out of 193 (61.1%) tumors, whereas noncancerous stromal regions of the breast showed considerable staining for CD26. This decreased stromal CD26 staining in tumors also tends to be associated with poor outcomes for breast cancer patients. Moreover, we demonstrated that CD26 staining is attenuated on stromal myofibroblasts in human breast cancers. Consistently, CD26 expression is significantly downregulated in cultured CAF myofibroblasts extracted from human breast carcinomas as compared to control human mammary fibroblasts. Inhibition of TGF- β or SDF-1 signaling in CAFs by shRNA clearly upregulated the CD26 expression. Taken together, these findings indicate that CD26 expression is attenuated by TGF- β - and SDF-1-autocrine signaling on stromal myofibroblasts in human mammary carcinomas, and that decreased stromal CD26 expression has potential as a prognostic marker.

KEYWORDS

breast cancer, dipeptidyl peptidase 4, myofibroblasts, stromal cell-derived factor 1, TGF-beta

1 | INTRODUCTION

Desmoplastic stroma rich in α -smooth muscle actin (α -SMA)-positive myofibroblasts, a hallmark of activated fibroblasts, is frequently observed in various human carcinomas including those of the breast, prostate, pancreas, lung, and colon.¹⁻³ In contrast, such myofibroblasts are rarely identified within nontumor stromal regions. Large numbers of myofibroblasts and α -SMA-negative fibroblasts often comprise carcinoma-associated fibroblasts (CAFs) in the tumor-associated stroma.

CAFs rich in myofibroblasts produce multiple growth factors, cytokines, chemokines, and exosomes which influence a wide variety of tumor hallmarks.⁴⁻⁷ We and others have previously described that CAF-secreted transforming growth factor- β (TGF- β) and stromal cell-derived factor-1 (SDF-1) promote the growth of apposed carcinoma cells in a paracrine fashion.⁸⁻¹⁰ These stromal cytokines also allow establishment of cross-communicating TGF- β and SDF-1 autocrine signaling by acting on their cognate receptors, resulting in the induction and maintenance of activated, tumor-promoting properties of CAFs without ongoing interaction with tumor cells during tumor progression.⁸⁻¹⁰

Possible CAF markers including α -SMA, fibroblast activation protein alpha, fibroblast-specific protein-1 (also known as S100A4), tenascin-C, platelet-derived growth factor receptor- α/β , and podoplanin have been identified.^{6,11} Although these CAF markers are useful for predicting the outcomes of some human breast carcinoma cohorts,^{12,13} none fully or exclusively identifies activated tumor-promoting CAFs due to various differences in fibroblast populations, as exemplified by resident fibroblasts and bone-marrow-derived progenitors present in tumors. Therefore, no conventional stromal marker has yet been identified for use in routine prognostic determinations for human carcinomas including those of the breast.

CD26/dipeptidyl peptidase-4 (DPP-4) is expressed by a wide variety of cell types and is involved in T-cell activation, immune regulation, cell adhesion, signal transduction, apoptosis, and so on.¹⁴⁻¹⁶ Both membrane-bound and soluble forms of CD26 have serine protease activity that preferentially cleaves dipeptides from the N-terminal region of peptides and proteins with a proline or alanine residue in the penultimate position.^{14,15} Stromal CD26 expression has been shown to be remarkably attenuated in human skin and oral squamous cell carcinomas (SCCs).^{17,18} However, whether stromal CD26 expression is commonly downregulated in different cancer types remains unclear. Moreover, the stromal cell types potentially lacking CD26 expression, as well as the molecular mechanisms underlying attenuated stromal CD26 expression, has not as yet been elucidated.

In the present study, we demonstrated that CD26 expression is attenuated via TGF- β and SDF-1 autocrine signaling on stromal myofibroblasts in human breast carcinomas. This

downregulated stromal CD26 expression in tumors is associated with poor outcomes for breast cancer patients.

2 | MATERIALS AND METHODS

2.1 | Cell culture

Human mammary fibroblasts were extracted from a healthy breast tissue specimen that had been obtained by reduction mammoplasty prior to primary culture and immortalization with human telomerase reverse transcriptase as described previously.⁹ Human breast exp-CAF2 cells and the corresponding control human mammary fibroblasts were also employed.⁹ These cells were cultured in DMEM high glucose GlutaMAX™ (Gibco) supplemented with 10% fetal bovine serum (FBS) and 1% Pen Strep (100 U/mL penicillin and 100 μ g/mL streptomycin) (Gibco). MCF10DCIS.com (DCIS) cells were purchased from Asterand Bioscience. MDA-MB-231 cells were purchased from American Type Culture Collection. These breast cancer cells were cultured in DMEM/F-12, GlutaMAX™ (Gibco) supplemented with 1% PenStrep (Gibco) with 5% FBS (DCIS cells) or 10% FBS (MDA-MB-231 cells).

2.2 | Immunohistochemistry

The use of formalin-fixed paraffin-embedded (FFPE) tissue specimens of breast cancer in this study was approved by the Juntendo University ethics review board. FFPE invasive breast carcinomas were prepared from breast cancer patients who had received either preoperative chemotherapy or hormone therapy. Three-micrometre thick sections were prepared and deparaffinized. The slides were then treated with 0.3% H₂O₂ in methanol for 20 minutes at room temperature. Antigen retrieval was performed by autoclaving in citrate buffer at pH 6.0 for 20 minutes at 121°C. The slides were incubated with primary antibody at 4°C overnight. Secondary antibody was incubated for 1 hour at room temperature. 3,3'-diaminobenzidine was used as the chromogen followed by hematoxylin counterstaining.

Semiquantification of CD26-positive fibroblasts was performed as follows. Ten different fields on both cancerous and noncancerous regions rich in stroma of the breast were captured per slide using $\times 400$ magnification under a microscope. The stromal cells exhibiting a typical fibroblast-like spindle-shape were regarded as “fibroblast-like cells.” Tumor cells, vascular endothelial cells, white blood cells, and adipocytes were also discriminated morphologically. CD26-positive fibroblast-like cells (%) were calculated as the ratio of the number of CD26-positive fibroblast-like cells relative to that of all fibroblast-like cells in cancerous and noncancerous regions of specimens obtained from 10 breast cancer patients.

2.3 | Tissue microarray

Tissue microarrays were constructed using 239 formalin-fixed primary breast cancer specimens, as reported previously.¹⁹ Paraffin-embedded tissue sections were obtained from specimens that had been surgically resected at Kanagawa Cancer Center. Individual institutional ethics

committees approved this study and the use of all clinical materials. Experiments were performed in accordance with all guidelines and regulations indicated by these committees. The tissue area for sampling was selected based on visual alignment with the corresponding hematoxylin and eosin-stained section on a slide. Several tissue cores (diameter 0.6 mm; height 3–4 mm) taken from a donor tumor block were

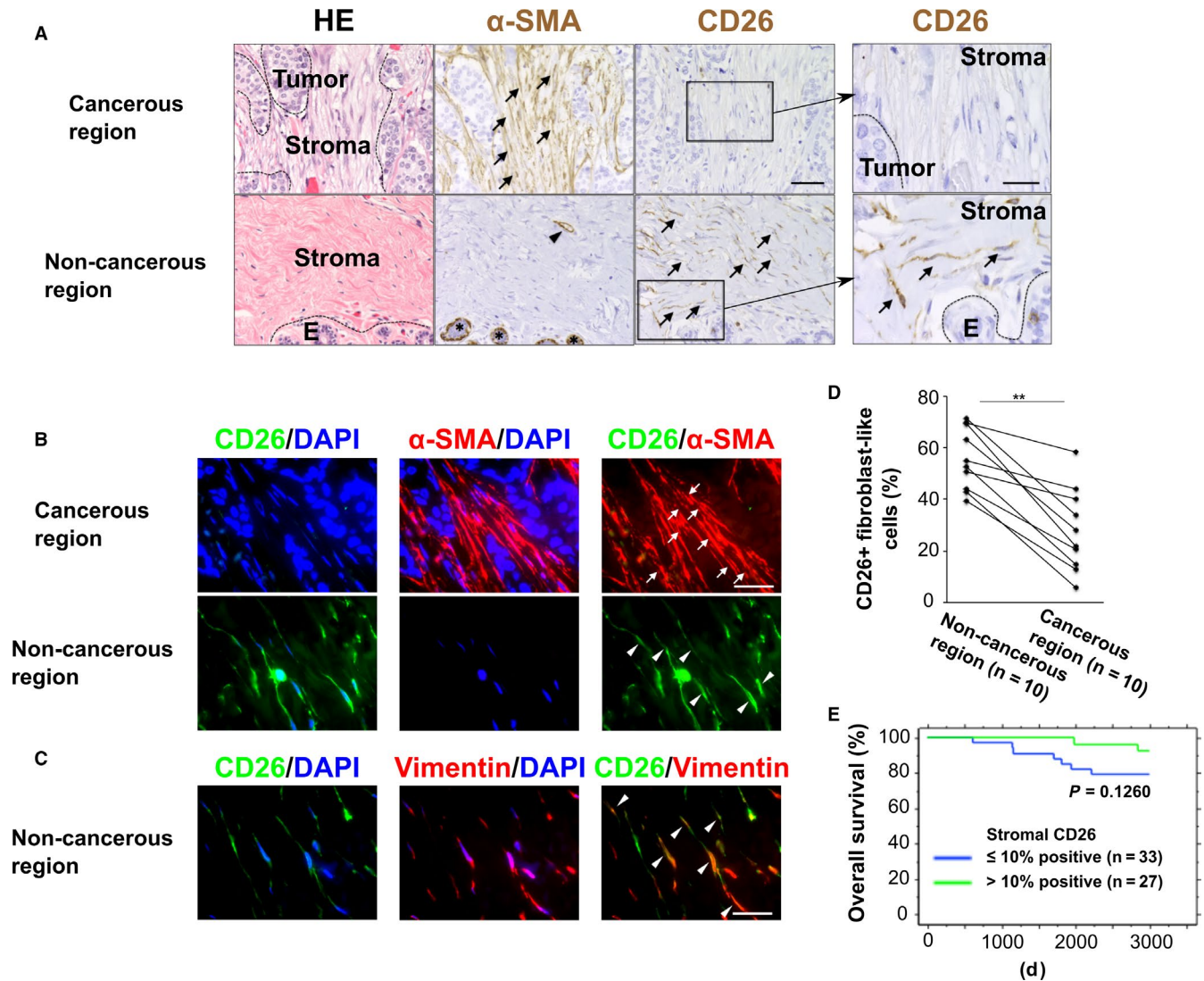


FIGURE 1 Attenuated CD26 staining on stromal myfibroblasts in human breast cancers. **A**, Hematoxylin and eosin (HE) staining and immunohistochemistry of sections prepared from human breast cancer tissue specimens using anti-CD26 or α -smooth muscle actin (α -SMA) antibodies. CD26⁺ fibroblast-like cells in a noncancerous region and α -SMA⁺ myfibroblasts in a cancerous region are indicated by arrows. α -SMA⁺ pericytes associated with a blood vessel (arrowhead) and α -SMA⁺ myoepithelial cells surrounding normal mammary glands (asterisks) are also shown. Scale bar, 50 μ m. Right column, magnified images of CD26 staining. Scale bar, 20 μ m. **B**, Double immunofluorescence of sections prepared from the human breast tissue specimens. CD26⁻ α -SMA⁺ myfibroblasts (arrows) in a cancerous region and CD26⁺ α -SMA⁻ fibroblast-like cells (arrowheads) in a noncancerous region are shown. Scale bar, 30 μ m. **C**, Double immunofluorescence of sections prepared from the noncancerous region of the human breast cancer tissue. CD26⁺ vimentin⁺ fibroblasts are indicated by arrowheads. Scale bar, 30 μ m. **D**, Quantification of CD26-positive fibroblast-like cell populations in tumor-associated stroma of 10 human breast cancer patients. Human breast tissues including noncancerous and cancerous regions were stained with anti-CD26 antibody. ** $P < 0.001$ by paired t -test. **E**, Kaplan-Meier plot indicating overall survival of breast cancer patients. Patients were grouped according to the indicated CD26 staining in tumor-associated stroma rich in myfibroblasts ($>50\%$ positive for α -SMA staining). The P -value was determined based on the Log-rank test. Abbreviation: E, normal human mammary epithelium

placed into a recipient paraffin block using a tissue microarrayer (Beecher Instruments). Resulting microarray blocks were used for immunohistochemical analysis. The sections were stained using anti-CD26 and α -SMA antibody according to the conditions described in the immunohistochemistry section. Immunohistochemical scores for CD26 and α -SMA expressions in stromal fibroblast-like cells were determined by a researcher with no prior knowledge of the clinicopathological results, as follows: negative and negligible (<10% of total area) and moderately and significantly positive (more than 10% of total area) for CD26 staining, and weakly positive (<50% of total area) and strongly positive (more than 50% of total area) for α -SMA staining.

2.4 | Statistical analysis

$P < 0.05$ was considered to indicate a statistically significant difference, as indicated by * in graphs. When the P -value was < 0.001 , it was indicated as **. To investigate the associations of stromal CD26 expression with patient characteristics in stromal α -SMA-positive breast cancer, Fisher's exact test was performed.

3 | RESULTS

3.1 | Attenuated CD26 expression on stromal myofibroblasts in human breast carcinomas

To examine whether stromal CD26 expression is attenuated in human breast carcinomas, paraffin sections were prepared from human breast cancer specimens and stained with anti-CD26 or α -SMA antibody. Few CD26-positive cells were detected in tumor stroma including an abundance

of α -SMA-positive myofibroblasts, while a larger number of CD26-positive fibroblast-like cells were present in a noncancerous region lacking myofibroblasts of the breast far from the outer tumor margin (Figure 1A). A subset of lymphocytes also stained positive for CD26 (Figure S1A), while vascular endothelial cells were negative for CD26 (Figure S1B). Moreover, most breast cancer cells stained negative for CD26 (Figure 1A), consistent with previous reports.^{20,21}

To address whether CD26 expression is attenuated on stromal myofibroblasts in human breast tumors, double immunofluorescence was performed using both anti-CD26 and α -SMA antibodies. CD26 expression was barely detected on α -SMA-positive myofibroblasts in tumor-associated stroma (Figure 1B). In sharp contrast, considerable CD26 expression was observed in α -SMA-negative stromal fibroblasts expressing vimentin, a marker of the mesenchymal cell type in noncancerous regions (Figure 1B,C).

To extend this observation, we performed immunohistochemistry on specimens from 10 patients in total (Table 1). Of note, in all of the examined breast cancer patients, CD26-positive fibroblast-like cell proportions were significantly decreased in the tumor-associated stroma as compared to those in the corresponding noncancerous stroma of the same breast (Figure 1D). Furthermore, we investigated another patient cohort including 239 breast cancers by immunohistochemistry using anti-CD26 and α -SMA antibodies. Stromal myofibroblasts were stained positive for α -SMA in 193 out of 239 (80.8%) tumors. Stromal CD26 staining was also negative or negligible (<10% positive) in 118 out of the 193 (61.1%) tumors including stromal myofibroblasts, and showed no significant correlations with any pathological parameters (Table 2). This decreased stromal CD26 staining tended to be associated with poorer outcomes for breast cancer patients with tumors rich in stromal myofibroblasts than did moderately

TABLE 1 Patients' information

Case	Sex	Age	Histology	Histological grade	ER	PR	HER2	Stage
1	F	40	IDC and DCIS	2	90%	90%	2+	IIB
2	F	47	IDC and DCIS	2	–	–	1+	IA
3	F	75	IDC and DCIS	3	–	–	3+	IIB
4	F	61	IDC and DCIS	2	–	–	1+	IIB
5	F	55	IDC and DCIS	2	>90%	>70%	2+	IA
6	F	44	IDC	2	>90%	>80%	2+	IA
7	F	72	IDC and DCIS	3	–	–	1+	IIA
8	F	53	IDC and DCIS	1	>90%	>90%	2+	IA
9	F	76	IDC and DCIS	3	–	–	1+	IA
10	F	39	IDC and DCIS	2	>90%	>90%	2+	IIB

Note: Information about patients whose breast tumor-derived FFPE tissue was used in this study for immunohistochemistry: diagnosis was performed by pathologists in the Juntendo University Hospital.^{22–24} ER and PR positive cell number (%) and immunoreactivity of HER2 were determined according to ASCO guidelines.^{23,24} Stage was determined according to UICC TNM classification.

Abbreviations: –, negative; DCIS, ductal carcinoma in situ; ER, estrogen receptor; F, female; FFPE, formalin-fixed paraffin-embedded; HER2, human epithelial growth factor receptor type 2; IDC, invasive ductal carcinoma; PR, progesterone receptor.

TABLE 2 Associations of CD26 expression in tumor stroma containing myofibroblasts with clinical parameters of 193 breast cancer patients

Parameters		Total n = 193	Stromal CD26 negative and negligible staining (up to 10%) n = 118	Stromal CD26 moderate and significant staining (more than 10%) n = 75	P-value
Age (years)	~65	148	96	52	0.0576
	66~	45	22	23	
Grading	0	25	15	10	0.7677 (grading 0 and 1 vs 2 and 3)
	1	66	42	24	
	2	53	35	18	
	3	49	26	23	
pT factor	T1	74	44	30	0.762
	T2-3	119	74	45	
pN factor	N0	102	58	44	0.237
	N1-2	91	60	31	
ER	Positive	135	89	46	0.0527
	Negative	58	29	29	
HER2	Positive	28	16	12	0.678
	Negative	165	102	63	

Abbreviations: ER, estrogen receptor; HER2, human epithelial growth factor receptor type 2.

and significantly positive stromal CD26 staining (Figure 1E). Collectively, these data indicate that the attenuated CD26 expression on stromal myofibroblasts in tumors may contribute to poor outcomes in breast cancer patients.

3.2 | Decreased CD26 expression on tumor-promoting human breast CAFs

As CD26 expression was attenuated on stromal myofibroblasts in human breast carcinomas, we investigated whether CD26 expression is also downregulated in primary cultured CAFs extracted from human breast carcinomas, compared to the corresponding control fibroblasts isolated from the adjacent non-cancerous tissues in same patients using public gene expression data.²⁵ A significantly lower level of CD26 mRNA expression was detected in myofibroblastic CAFs that presumably acquired TGF- β and SDF-1 autocrine signaling, as exemplified by increased TGF- β 2 and SDF-1 mRNA expression^{9,26} (Figure 2A).

We also employed exp-CAF2 cells raised from immortalized human mammary fibroblasts that had been incubated with MCF-7-*ras* breast cancer cells in the tumor xenograft and then extracted from the developing tumor for subsequent expansion in culture.²⁷ As mentioned above, the exp-CAF2 cells increasingly acquired myofibroblastic and tumor-promoting traits via establishment of TGF- β and SDF-1 autocrine signaling through interaction with carcinoma cells during tumor progression.⁹ We indeed found CD26 mRNA expression to be downregulated in exp-CAF2 cells, by 74.4% as compared to the control human mammary fibroblasts that were minimally activated, in terms of myofibroblastic and tumor-promoting properties (Figure 2B). Moreover, cell

surface CD26 expression was decreased on exp-CAF2 cells by 64.7%, as demonstrated by flow cytometry (Figure 2C). In addition, CD26 protein expression and DPP-4 activity (CD26 peptidase activity) were decreased in exp-CAF2 cells by 73.0% and 78.2%, respectively (Figure 2D,E). Taken together, these findings indicate that CD26 expression and DPP-4 activity are significantly attenuated on myofibroblastic CAFs with activated TGF- β and SDF-1 autocrine signaling.

3.3 | CD26 expression attenuated by TGF- β -Smad2/3 autocrine signaling on CAFs

We next investigated how CD26 expression is downregulated on CAFs. Given the increasingly activated TGF- β - and SDF-1-autocrine signaling in exp-CAF2 cells during tumor progression,⁹ we reasoned that such signaling might contribute to attenuation of CD26 expression on these cells.

To examine this possibility, exp-CAF2 cells were treated with SB431542, an inhibitor for TGF- β receptor I kinase activity, which is crucial for phosphorylation of the downstream proteins represented by Smad2/3.²⁸ CD26 expression was significantly upregulated at both the mRNA and protein levels on the resulting exp-CAF2 cells relative to the effect of the control dimethyl sulfoxide treatment (Figure 3A-C).

We also sought to determine the roles of the canonical TGF- β -Smad2/3 pathway in the attenuated CD26 expression on CAFs. To this end, we generated two different shRNA constructs against Smad4, which is a central mediator of the Smad2/3 signaling to inhibit Smad4 expression in exp-CAF2 cells. Inhibition of Smad4 expression by shRNA upregulated CD26 mRNA and protein expressions significantly more than

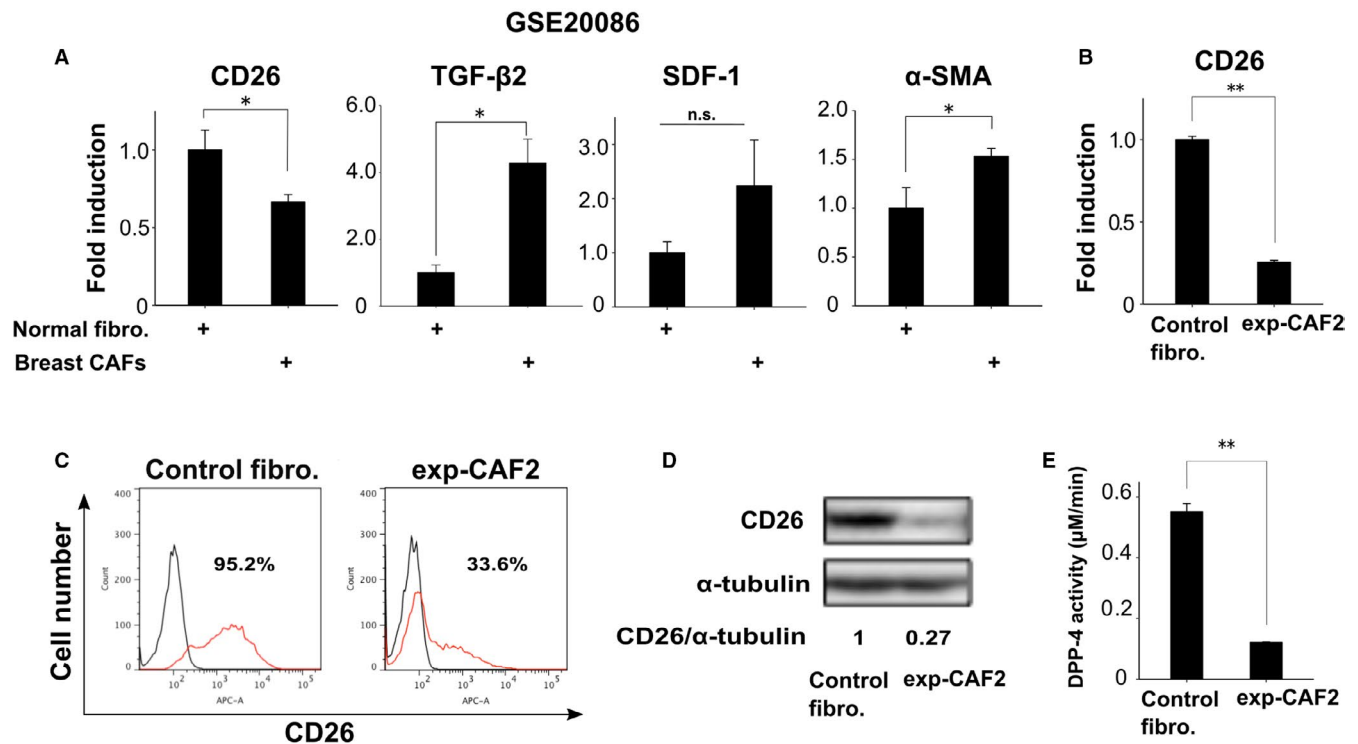


FIGURE 2 Downregulated CD26 expression on human breast carcinoma-associated fibroblasts (CAFs). A, mRNA expressions of the indicated genes in normal human mammary fibroblasts and CAFs ($n = 6$) using public microarray data in GSE20086. B, Real-time PCR of control human mammary fibroblasts and exp-CAF2 cells for CD26 expression. C, Flow cytometry of the indicated cells using anti-CD26 antibody (red line) or the control IgG (black line). The number of CD26-positive cell populations (%) is also indicated. D, Western blotting of the indicated cells using anti-CD26 antibody. The ratio of the signal intensity of CD26 relative to α -tubulin is indicated. E, Dipeptidyl peptidase-4 (DPP-4) activity in whole cell lysates derived from the indicated cells ($n = 3$). ** $P < 0.001$ and * $P < 0.05$ by Student's t -test. Error bars, SE. Abbreviation: n.s., not significant

did the GFP-shRNA (Figure 3D-F). In sharp contrast, the expression level of phosphorylated Smad2 (pSmad2), indicative of the activation of TGF- β signaling,²⁸ was strongly attenuated in exp-CAF2 cells expressing Smad4-shRNA (Figure 3F). These data therefore indicate that the TGF- β -Smad2/3 signaling pathway is required for maintenance of the attenuated CD26 expression on CAFs.

Given the TGF- β -Smad2/3 signaling requirement for the attenuated CD26 expression on CAFs, we also investigated whether this signaling suffices to induce downregulation of CD26 expression. To examine this possibility, human mammary fibroblasts were treated with TGF- β 1. Expression levels of CD26 mRNA and protein were significantly attenuated in these cells (Figure 3G-I). Taken together, these findings demonstrate that activation of TGF- β -Smad2/3 signaling induces and maintains the attenuated CD26 expression on exp-CAF2 cells.

3.4 | SDF-1 signaling and CD26 expression on CAFs

Since SDF-1 signaling is critical for mediating the myofibroblastic tumor-promoting trait in CAFs,⁹ we investigated

whether this signaling regulates CD26 expression on these cells.

To assess this possibility, CD26 expression was measured on exp-CAF2 cells expressing SDF-1-shRNAs, both of which significantly inhibited SDF-1 expression (Figure S2A).⁹ Inhibition of SDF-1 expression upregulated levels of CD26 protein expression on these cells as compared to the effect of GFP-shRNA, as demonstrated by flow cytometry (Figure 4A) and Western blotting (Figure 4B). Furthermore, pSmad2 expression was also attenuated in exp-CAF2 cells expressing each of these SDF-1-shRNAs (Figure 4B). These findings therefore indicate that SDF-1 expression is required for the attenuation of CD26 expression via activation of Smad2/3 signaling on exp-CAF2 cells. This observation is consistent with our previous findings, indicating that SDF-1 signaling mediates TGF- β -Smad2/3 signaling in CAFs.⁹

We next examined whether SDF-1-CXCR4 signaling suffices to attenuate the CD26 expression on mammary fibroblasts. To answer this question, a retroviral construct encoding either human SDF-1 or CXCR4 cDNA was introduced into human mammary fibroblasts (Figure S2B).^{9,10} The levels of CD26 protein expression were similar in parental human mammary fibroblasts and

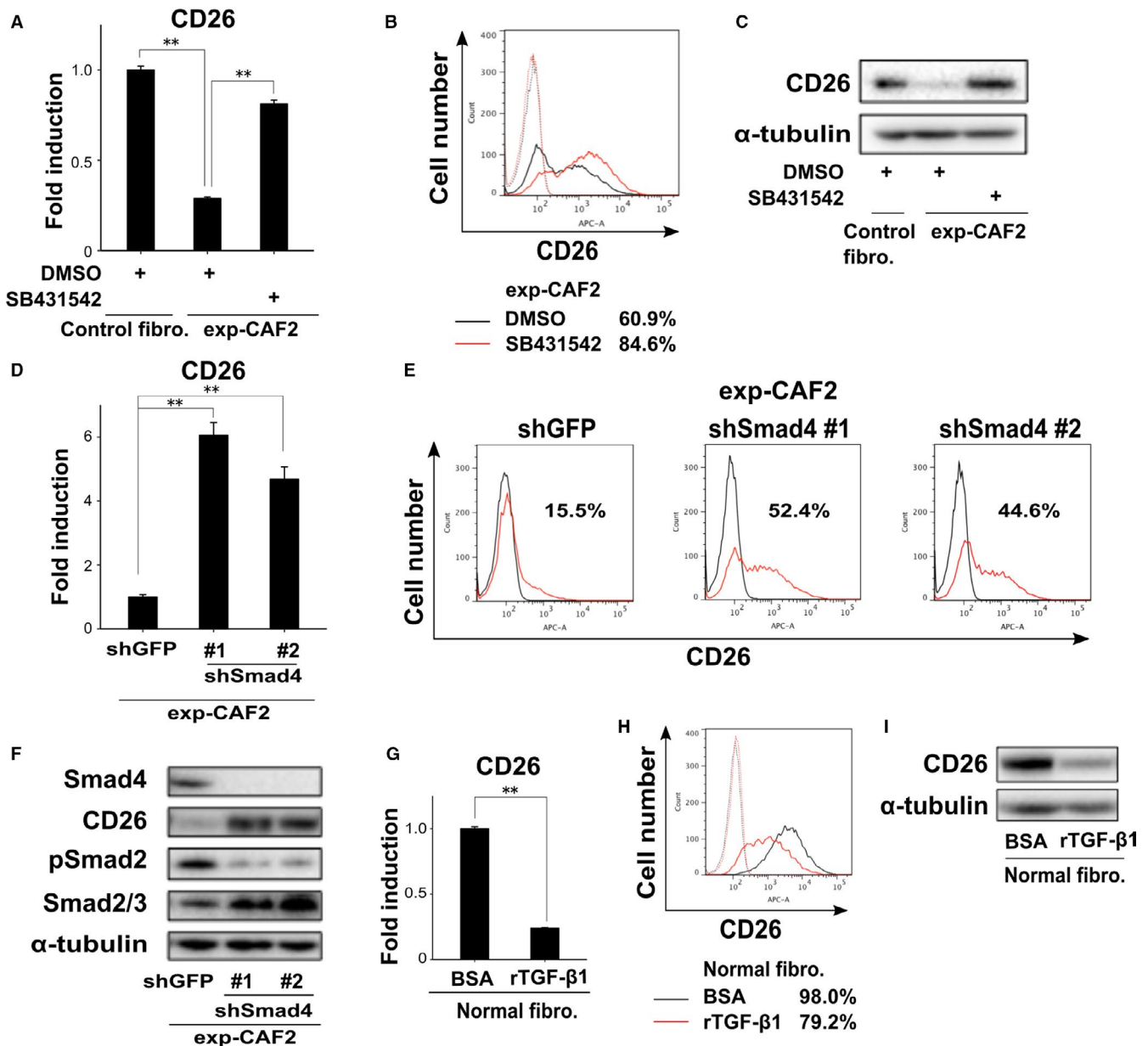


FIGURE 3 Decreased CD26 expression mediated by transforming growth factor- β (TGF- β)-Smad2/3 autocrine signaling on carcinoma-associated fibroblasts (CAFs). A, Real-time PCR of the indicated fibroblasts treated with dimethyl sulfoxide (DMSO) or SB431542 for 24 h to measure CD26 expression. B, Flow cytometry of exp-CAF2 cells treated with DMSO (black line) or SB431542 (red line) for 48 h using anti-CD26 antibody (solid line) or the control IgG (dotted line). The number of CD26-positive cell populations (%) is shown. C, Western blotting of the described cells treated with DMSO or SB431542 for 48 h. D, Real-time PCR of exp-CAF2 cells expressing GFP- and Smad4-shRNA (#1 and #2) for CD26 expression. E, Flow cytometry of indicated cells using anti-CD26 antibody (red line) or the control IgG (black line). The number of CD26-positive cell populations (%) is depicted. F, Western blotting of exp-CAF2 cells expressing GFP- and Smad4-shRNA (#1 and #2). G, Real-time PCR of human mammary fibroblasts treated with bovine serum albumin (BSA) or recombinant TGF- β 1 (10 ng/mL) for 24 h to measure CD26 expression. H, Flow cytometry of human mammary fibroblasts treated with BSA (black line) or TGF- β 1 (10 ng/mL, red line) for 48 h using anti-CD26 antibody (solid line) or the control IgG (dotted line). The number of CD26-positive cell populations (%) is depicted. I, Western blotting of human mammary fibroblasts treated with BSA or recombinant TGF- β 1 (10 ng/mL) for 48 h. $**P < 0.001$ by Student's *t*-test. Error bars, SE

those overexpressing SDF-1 or CXCR4, as demonstrated by flow cytometry (Figure 4C) and Western blotting (Figure 4D). pSmad2 expressions also differed minimally among all of these fibroblasts (Figure 4D). Conversely, CD26 expression was robustly inhibited on human mammary fibroblasts expressing an active TGF- β 1

cDNA⁹ via increased pSmad2 expression (Figures 4D and S2B), confirming earlier data showing attenuated CD26 expression on the TGF- β 1-treated mammary fibroblasts (Figure 3I).

Collectively, these findings indicate that SDF-1 autocrine signaling is required for maintenance of the attenuated CD26

expression on CAFs presumably via Smad2/3 signaling, but is not sufficient for inducing the downregulation of CD26 expression on these cells (Figure 4E). As mentioned above, the activation of TGF- β -Smad2/3 signaling was found to both induce and maintain the downregulated CD26 expression on CAFs (Figure 4E).

3.5 | Roles of decreased DPP-4 activity on CAFs in TGF- β and SDF-1 autocrine signaling

SDF-1 is a major substrate for CD26/DPP-4 peptidase.^{14,29} The resulting failure of transduction of the downstream signaling of CXCR4, an SDF-1 receptor present on the target cells, attenuates hematopoietic stem/progenitor cell homing,³⁰ HIV infection,^{31,32} and cancer cell invasion.³³⁻³⁶ Given these observations, we speculated that the attenuated stromal CD26 expression may influence SDF-1 autocrine signaling and the myofibroblastic state in CAFs. To this end, a retroviral vector encoding the human CD26 cDNA or the corresponding control empty vector was introduced into exp-CAF2 cells or control fibroblasts. CD26 protein expression and DPP-4 activity were markedly increased on exp-CAF2 cells expressing CD26 (exp-CAF2-CD26) as compared to the control vector (exp-CAF2-empty) (Figure 5A,B). However,

TGF- β and SDF-1 autocrine signaling as well as the myofibroblastic trait, as exemplified by TGF- β 1, TGF- β 2, pSmad2, SDF-1, and α -SMA expressions were similar in these cells (Figure 5C,D). These data therefore indicate that the attenuated CD26 expression does not significantly contribute to activation of TGF- β and SDF-1 autocrine signaling or to the myofibroblastic trait in CAFs.

3.6 | Roles of attenuated DPP-4 activity on CAFs in their SDF-1 paracrine signaling toward apposed carcinoma cells

We have previously demonstrated that CAF-produced SDF-1 promotes the growth of nearby breast tumor cells in a paracrine fashion via acting through CXCR4 on these cells.¹⁰ We thus speculated that decreased levels of membrane and soluble CD26 expressions on CAFs may promote paracrine SDF-1 signaling toward nearby carcinoma cells.

To investigate this possibility, the biological activity of stromal SDF-1 was evaluated employing the Boyden chamber cell migration assay using human breast cancer MDA-MB-231 cells and DCIS cells overexpressing CXCR4 (DCIS-CXCR4) (Figure 5E). We observed more

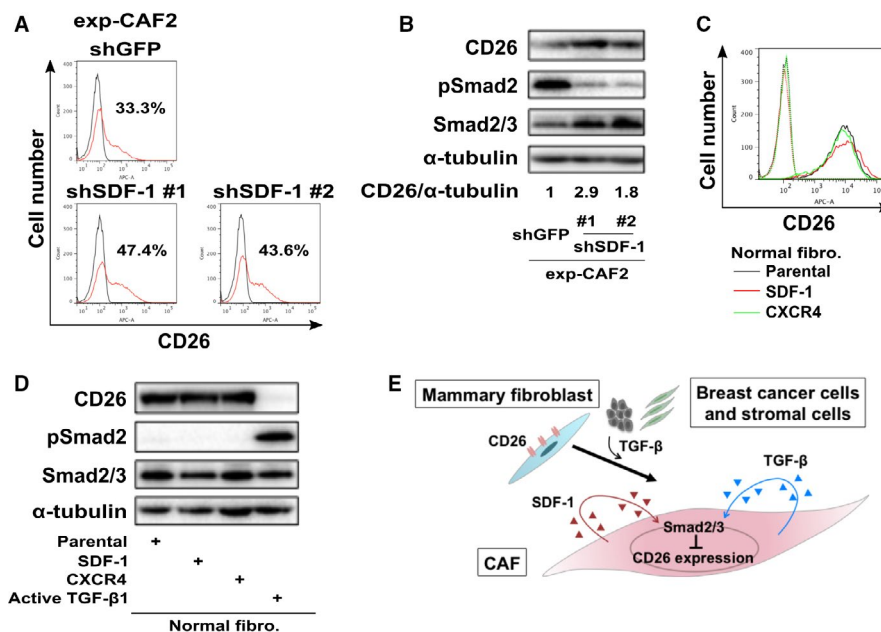


FIGURE 4 Stromal cell-derived factor-1 (SDF-1) autocrine signaling required for the attenuated CD26 expression on exp-carcinoma-associated fibroblasts (CAFs) cells. A, Flow cytometry of indicated cells using anti-CD26 antibody (red line) or the control IgG (black line). The number of CD26-positive cell populations (%) is also depicted. B, Western blotting of exp-CAF2 cells expressing the indicated shRNA. The ratio of the signal intensity of CD26 relative to α -tubulin is indicated. C, Flow cytometry of human normal mammary fibroblasts (parental, black line) expressing SDF-1 (red line) or CXCR4 (green line) cDNA construct using anti-CD26 antibody (solid line) or the control IgG (dotted line). D, Western blotting of human normal mammary fibroblasts expressing the indicated cDNA construct. E, Schematic representation of the attenuated CD26 expression via transforming growth factor- β (TGF- β)-Smad2/3 and SDF-1 autocrine signaling on human breast CAF myofibroblasts. TGF- β released from tumor cells and stromal cells attenuates CD26 expression on human mammary fibroblasts. Acquisition of TGF- β and SDF-1 autocrine signaling pathways then contributes to maintenance of the attenuated CD26 expression on CAFs during tumor progression

robust migration of these cancer cells to be induced by the SDF-1-rich medium conditioned by exp-CAF2-empty relative to control fibroblast-empty (Figure 5F,G). Medium derived from exp-CAF2-CD26 or exp-CAF2-empty cells, when applied to these cancer cells, showed similar tumor cell migration (Figure 5F,G). Furthermore, SDF-1 protein concentrations were similar in media conditioned by these cells (Figure 5H). Moreover, DPP-4 activity was nearly undetectable in media obtained from exp-CAF2-CD26 and control human mammary fibroblasts abundantly

expressing CD26 (Figure 5I), while a markedly higher level of DPP-4 activity was detected in the whole cell lysate extracted from these fibroblasts (Figure 5B). Collectively, these observations indicate that membrane CD26 is barely shed on exp-CAF2-CD26 and human mammary fibroblasts, suggesting that increased membrane CD26 expression by itself may not be enough to inhibit the SDF-1 activity. However, whether attenuated soluble CD26 production promotes paracrine SDF-1 signaling from CAFs could not be resolved by the experiments above.

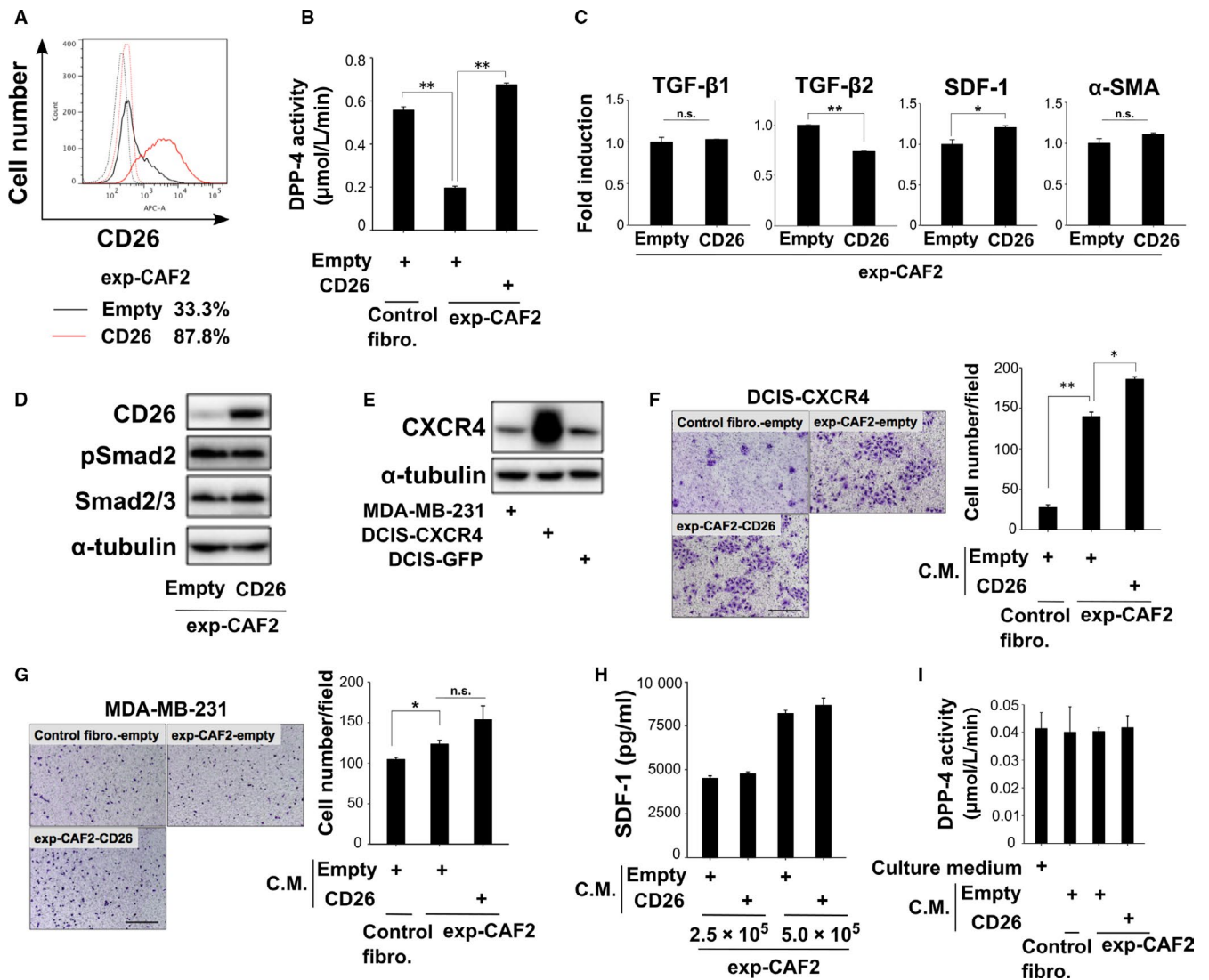


FIGURE 5 Attenuated CD26 expression is not essential for stromal cell-derived factor-1 (SDF-1)-autocrine and -paracrine signaling in carcinoma-associated fibroblasts (CAFs). **A**, Flow cytometry of exp-CAF2-empty (black line) or -CD26 (red line) cells using anti-CD26 antibody (solid line) or the control IgG (dotted line). The number of CD26-positive cell populations (%) is shown. **B**, Dipeptidyl peptidase-4 (DPP-4) activity in the indicated fibroblasts ($n = 3$). **C**, Real-time PCR of indicated cells for transforming growth factor- β 1 (TGF- β 1), TGF- β 2, SDF-1 and α -SMA expressions. **D,E**, Western blotting of the indicated cells. **F,G**, Boyden chamber cell migration assay of DCIS-CXCR4 cells (**F**) or MDA-MB-231 cells (**G**) using conditioned medium (CM) taken from the indicated cells. The cells which had migrated were stained with May-Grünwald Giemsa at 60 h (DCIS-CXCR4, **F**) or at 12 h (MDA-MB231, **G**) after the cell seeding. Scale bar, 300 μ m. The number of tumor cells which migrated per field is shown ($n = 3$). **H**, ELISA of CM taken from the indicated fibroblasts (2.5×10^5 or 5×10^5 cells) for measuring SDF-1. **I**, DPP-4 activity in CM derived from the indicated fibroblasts ($n = 3$). ** $P < 0.001$ and * $P < 0.05$ by Student's t -test. Error bars, SE. Abbreviation: n.s., not significant

4 | DISCUSSION

4.1 | Attenuated CD26 expression in myofibroblastic CAFs is associated with poor outcomes in breast cancer patients

Stromal CD26 expression is known to be barely detectable in different human SCCs.^{17,18} However, whether stromal CD26 expression is also downregulated in human breast carcinomas remains controversial; stromal CD26 expression was reportedly undetectable in a tumor taken from one breast cancer patient,²⁰ while its expression was detected in another human breast carcinoma.²¹ Moreover, particular stromal cell types potentially lacking CD26 expression in tumors and the molecular mechanisms underlying the decreased stromal CD26 expression have not as yet been fully elucidated.

In this study, we showed CD26 staining to be attenuated on myofibroblasts rich in tumor-associated stroma in specimens obtained from breast cancer patients. On the cultured human breast myofibroblastic CAFs, CD26 expression is also significantly attenuated relative to that on control human mammary fibroblasts. TGF- β and SDF-1 autocrine signaling is responsible for the attenuated CD26 expression on these cells via Smad2/3 (Figure 4E). Given the induction of the attenuated CD26 expression on TGF- β -treated human mammary fibroblasts (Figure 3G-I), different sources of TGF- β derived from tumor cells and stromal cells³⁷ in addition to CAFs may contribute to inducing downregulation of CD26 expression on mammary fibroblasts during tumor progression.

Distinct fibroblast populations with inherent functional diversity exist in stroma of human breast³⁸ and skin^{39,40} tissues as well as various human tumors.⁴¹⁻⁴³ CD26 expression has been demonstrated to serve as a marker for stratification of the stromal cell type in human breast and skin tissues.^{38,39,44} CD105/endoglin, a coreceptor for TGF- β family members, is also expressed on a subset of stromal myofibroblasts at the invasive borders of human colon carcinomas.⁴⁵ Moreover, CD26^{low}CD105^{high} fibroblasts with myofibroblast-related characteristics are abundant in the terminal duct lobular unit of the human breast, while interlobular ducts are rich in CD26^{high}CD105^{low} fibroblasts.³⁸ Collectively, these observations indicate the importance of CD26 and CD105 expressions for identifying the particular fibroblast lineages in human mammary tissues including those of breast cancer.

We demonstrated that the attenuated CD26 staining in tumor-associated stroma with an abundance of myofibroblasts is associated with poor outcomes for breast cancer patients, suggesting stromal CD26 staining to be a potentially novel prognostic marker. However, due to the lack of a statistically significant difference, we assume that use of another marker with stromal CD26 staining may improve prognostic power. As CD105 expression in CAFs has been indicated to mediate the activities of these fibroblasts, thereby promoting colon

tumor invasion and metastasis,⁴⁵ whether CD26^{low}CD105^{high} might serve as a valuable prognostic marker must be addressed in future studies.

Increased levels of stromal TGF- β and SDF-1 staining are also reported to be associated with the poor outcomes in breast cancer patients.^{46,47} Although these cytokines are highly produced by CAFs, as indicated earlier, it remains unclear whether CAF-derived TGF- β and SDF-1 in tumors contribute to poor prognoses via downregulated stromal CD26 expression in breast cancer patients.

4.2 | CD26 shedding on stromal fibroblasts

Shedding of membrane CD26 has been widely recognized on various cell types, such as human adipocytes, vascular smooth muscle cells (VSMCs), and peripheral blood mononuclear cells (PBMCs).^{48,49} Several matrix metalloproteinases (MMPs) mediate the membrane CD26 shedding on adipocytes and VSMCs.⁴⁸ Kallikrein-related peptidase 5 (KLK5) also plays roles in the shedding of CD26 on human PBMCs; the CD26 shedding from PBMCs is significantly inhibited by treatment with a KLK5 inhibitor, while treatment with recombinant KLK5 has the opposite effect, dramatically inducing CD26 shedding from CD4⁺ T cells.⁴⁹

On the other hand, DPP-4 activity was barely detectable in media conditioned by human mammary fibroblasts and CAFs expressing a human CD26 cDNA construct. Various proteases, such as MMP2, MMP9, urokinase-type plasminogen activator, and cathepsins potentially regulating membrane CD26 shedding are likely to be detectable in these fibroblasts according to previous reports.⁵⁰⁻⁵³ We thus speculate that these proteases may not be responsible for CD26 shedding on human mammary fibroblasts.

4.3 | Myofibroblastic CAFs and fibrosis-derived myofibroblasts show inverse CD26 expression pattern

Analogies between tumors and wound tissues have been portrayed as “tumors: wounds that do not heal,” based on their similar biological processes, as exemplified by the recruitment of large numbers of myofibroblasts, extracellular matrix deposition, tissue inflammation, and angiogenesis.⁵⁴⁻⁵⁶ These analogous processes are also further supported by gene expression profiles between tumor-associated stroma and tissue regeneration/repair responses.⁵⁷⁻⁵⁹

CD26 expression has been shown to be significantly upregulated on stromal fibroblasts associated with wounds and fibrosis.^{17,60-63} Treatment with a DPP-4 inhibitor also attenuates the activated myofibroblastic states by inhibiting canonical TGF- β -Smad2/3 signaling as well as noncanonical ERK and p38 signaling.^{61,62,64} These findings suggest that CD26 expression is required for maintenance of the activated state

on myfibroblasts present in the damaged tissues via TGF- β signaling during regeneration and repair.

In sharp contrast, we observed significantly attenuated CD26 expression on stromal myfibroblasts in human breast carcinomas. Restoration of CD26 expression also has only a very minor influence on the TGF- β -Smad2/3 pathway in human breast CAFs (Figure 5C,D). Thus, this contrasting CD26 expression pattern and distinct actions modulating TGF- β signaling serve as an exception to the well-recognized analogies between wound-associated fibroblasts and CAFs. To further understand the biology of CAFs, molecular insights into the mechanisms underlying the cell-type specific roles of CD26 expression on these myfibroblasts are needed.

In summary, we obtained the unexpected findings that stromal CD26 expression is significantly attenuated through TGF- β and SDF-1 autocrine signaling on myfibroblastic CAFs in human breast carcinomas. As the attenuated CD26 expression in stromal myfibroblasts correlated with poor outcomes for breast cancer patients, decreased stromal CD26 expression may be useful as a prognostic marker for breast cancer patients.

ACKNOWLEDGMENTS

We thank Naomi Ohtsuji, Wali Nadila, and Katsumi Miyahara for assistance with the immunohistochemistry and HE staining. Masaaki Abe kindly instructed us in the flow cytometry analysis technique. We also thank Kazunori Kajino, Toshiyuki Kobayashi, Ryo Hatano, and Yasuhiko Ito for useful discussions. This work was supported by Grants in-Aid for Scientific Research from the Ministry of Education, Culture, Sports, Science and Technology, Japan (24300332, 25640069 and 15K14385 to A.O. and JP 16H06277 to Y.D.).

CONFLICT OF INTEREST

The authors have no potential conflict of interest to declare.

ORCID

Yoshihiro Mezawa  <https://orcid.org/0000-0002-2095-3867>

Akira Orimo  <https://orcid.org/0000-0001-5330-7282>

REFERENCES

- Desmouliere A, Guyot C, Gabbiani G. The stroma reaction myofibroblast: a key player in the control of tumor cell behavior. *Int J Dev Biol*. 2004;48:509-517.
- Cunha GR, Hayward SW, Wang YZ, Ricke WA. Role of the stromal microenvironment in carcinogenesis of the prostate. *Int J Cancer*. 2003;107:1-10.
- Mueller MM, Fusenig NE. Friends or foes—bipolar effects of the tumour stroma in cancer. *Nat Rev Cancer*. 2004;4:839-849.
- Kalluri R. The biology and function of fibroblasts in cancer. *Nat Rev Cancer*. 2016;16:582-598.
- Mezawa Y, Orimo A. The roles of tumor- and metastasis-promoting carcinoma-associated fibroblasts in human carcinomas. *Cell Tissue Res*. 2016;365:675-689.
- Gascard P, Tlsty TD. Carcinoma-associated fibroblasts: orchestrating the composition of malignancy. *Genes Dev*. 2016;30:1002-1019.
- Ohlund D, Elyada E, Tuveson D. Fibroblast heterogeneity in the cancer wound. *J Exp Med*. 2014;211:1503-1523.
- Calon A, Lonardo E, Berenguer-Llergo A, et al. Stromal gene expression defines poor-prognosis subtypes in colorectal cancer. *Nat Genet*. 2015;47:320-329.
- Kojima Y, Acar A, Eaton EN, et al. Autocrine TGF-beta and stromal cell-derived factor-1 (SDF-1) signaling drives the evolution of tumor-promoting mammary stromal myfibroblasts. *Proc Natl Acad Sci U S A*. 2010;107:20009-20014.
- Orimo A, Gupta PB, Sgroi DC, et al. Stromal fibroblasts present in invasive human breast carcinomas promote tumor growth and angiogenesis through elevated SDF-1/CXCL12 secretion. *Cell*. 2005;121:335-348.
- Polanska UM, Orimo A. Carcinoma-associated fibroblasts: non-neoplastic tumour-promoting mesenchymal cells. *J Cell Physiol*. 2013;228:1651-1657.
- Paulsson J, Micke P. Prognostic relevance of cancer-associated fibroblasts in human cancer. *Semin Cancer Biol*. 2014;25:61-68.
- Hu G, Xu F, Zhong K, Wang S, Huang L, Chen W. Activated tumor-infiltrating fibroblasts predict worse prognosis in breast cancer patients. *J Cancer*. 2018;9:3736-3742.
- Boonacker E, Van Noorden CJ. The multifunctional or moonlighting protein CD26/DPPIV. *Eur J Cell Biol*. 2003;82:53-73.
- Klemann C, Wagner L, Stephan M, von Horsten S. Cut to the chase: a review of CD26/dipeptidyl peptidase-4's (DPP4) entanglement in the immune system. *Clin Exp Immunol*. 2016;185:1-21.
- Ohnuma K, Dang NH, Morimoto C. Revisiting an old acquaintance: CD26 and its molecular mechanisms in T cell function. *Trends Immunol*. 2008;29:295-301.
- Arwert EN, Mentink RA, Driskell RR, et al. Upregulation of CD26 expression in epithelial cells and stromal cells during wound-induced skin tumour formation. *Oncogene*. 2012;31:992-1000.
- Kacar A, Arikok AT, Kokenek Unal TD, Onder E, Hucumenoglu S, Alper M. Stromal expression of CD34, alpha-smooth muscle actin and CD26/DPPIV in squamous cell carcinoma of the skin: a comparative immunohistochemical study. *Pathol Oncol Res*. 2012;18:25-31.
- Daigo Y, Nakamura Y. From cancer genomics to thoracic oncology: discovery of new biomarkers and therapeutic targets for lung and esophageal carcinoma. *Gen Thorac Cardiovasc Surg*. 2008;56:43-53.
- Atherton AJ, Monaghan P, Warburton MJ, Robertson D, Kenny AJ, Gusterson BA. Dipeptidyl peptidase IV expression identifies a functional sub-population of breast fibroblasts. *Int J Cancer*. 1992;50:15-19.
- Scanlan MJ, Raj BK, Calvo B, et al. Molecular cloning of fibroblast activation protein alpha, a member of the serine protease family selectively expressed in stromal fibroblasts of epithelial cancers. *Proc Natl Acad Sci U S A*. 1994;91:5657-5661.

22. Tsuda H, Akiyama F, Kurosumi M, Sakamoto G, Watanabe T. Establishment of histological criteria for high-risk node-negative breast carcinoma for a multiinstitutional randomized clinical trial of adjuvant therapy. Japan National Surgical Adjuvant Study of Breast Cancer (NSAS-BC) Pathology Section. *Jpn J Clin Oncol*. 1998;28:486-491.
23. Wolff AC, Hammond M, Schwartz JN, et al. American Society of Clinical Oncology/College of American Pathologists guideline recommendations for human epidermal growth factor receptor 2 testing in breast cancer. *J Clin Oncol*. 2007;25:118-145.
24. Hammond M, Hayes DF, Dowsett M, et al. American Society of Clinical Oncology/College Of American Pathologists guideline recommendations for immunohistochemical testing of estrogen and progesterone receptors in breast cancer. *J Clin Oncol*. 2010;28:2784-2795.
25. Bauer M, Su G, Casper C, He R, Rehrauer W, Friedl A. Heterogeneity of gene expression in stromal fibroblasts of human breast carcinomas and normal breast. *Oncogene*. 2010;29:1732-1740.
26. Scherz-Shouval R, Santagata S, Mendillo M, et al. The reprogramming of tumor stroma by HSF1 is a potent enabler of malignancy. *Cell*. 2014;158:564-578.
27. Polanska UM, Acar A, Orimo A. Experimental generation of carcinoma-associated fibroblasts (CAFs) from human mammary fibroblasts. *J Vis Exp*. 2011;e3201.
28. Derynck R, Miyazono K. *The Biology of the TGF-beta Family*. Cold Spring Harbor, NY: Cold Spring Harbor Laboratory Press; 2017.
29. Lambeir A-M, Proost P, Durinx C, et al. Kinetic investigation of chemokine truncation by CD26/dipeptidyl peptidase IV reveals a striking selectivity within the chemokine family. *J Biol Chem*. 2001;276:29839-29845.
30. Christopherson KW 2nd, Hangoc G, Mantel CR, Broxmeyer HE. Modulation of hematopoietic stem cell homing and engraftment by CD26. *Science*. 2004;305:1000-1003.
31. Ohtsuki T, Hosono O, Kobayashi H, et al. Negative regulation of the anti-human immunodeficiency virus and chemotactic activity of human stromal cell-derived factor 1alpha by CD26/dipeptidyl peptidase IV. *FEBS Lett*. 1998;431:236-240.
32. Shioda T, Kato H, Ohnishi Y, et al. Anti-HIV-1 and chemotactic activities of human stromal cell-derived factor 1alpha (SDF-1alpha) and SDF-1beta are abolished by CD26/dipeptidyl peptidase IV-mediated cleavage. *Proc Natl Acad Sci U S A*. 1998;95:6331-6336.
33. Sun Y-X, Pedersen EA, Shiozawa Y, et al. CD26/dipeptidyl peptidase IV regulates prostate cancer metastasis by degrading SDF-1/CXCL12. *Clin Exp Metastasis*. 2008;25:765-776.
34. Mizokami Y, Kajiyama H, Shibata K, Ino K, Kikkawa F, Mizutani S. Stromal cell-derived factor-1alpha-induced cell proliferation and its possible regulation by CD26/dipeptidyl peptidase IV in endometrial adenocarcinoma. *Int J Cancer*. 2004;110:652-659.
35. Cutler MJ, Lowthers EL, Richard CL, Hajducek DM, Spagnuolo PA, Blay J. Chemotherapeutic agents attenuate CXCL12-mediated migration of colon cancer cells by selecting for CXCR4-negative cells and increasing peptidase CD26. *BMC Cancer*. 2015;15:882.
36. Kajiyama H, Shibata K, Ino K, Nawa A, Mizutani S, Kikkawa F. Possible involvement of SDF-1alpha/CXCR4-DPPIV axis in TGF-beta1-induced enhancement of migratory potential in human peritoneal mesothelial cells. *Cell Tissue Res*. 2007;330:221-229.
37. Walker RA, Dearing SJ. Transforming growth factor beta 1 in ductal carcinoma in situ and invasive carcinomas of the breast. *Eur J Cancer*. 1992;28:641-644.
38. Morsing M, Klitgaard MC, Jafari A, et al. Evidence of two distinct functionally specialized fibroblast lineages in breast stroma. *Breast Cancer Res*. 2016;18:108.
39. Driskell RR, Lichtenberger BM, Hoste E, et al. Distinct fibroblast lineages determine dermal architecture in skin development and repair. *Nature*. 2013;504:277-281.
40. Rinn JL, Bondre C, Gladstone HB, Brown PO, Chang HY. Anatomic demarcation by positional variation in fibroblast gene expression programs. *PLoS Genet*. 2006;2:e119.
41. Costa A, Kieffer Y, Scholer-Dahirel A, et al. Fibroblast Heterogeneity and Immunosuppressive environment in human breast cancer. *Cancer Cell*. 2018;33:463-479.
42. Ohlund D, Handly-Santana A, Biffi G, et al. Distinct populations of inflammatory fibroblasts and myofibroblasts in pancreatic cancer. *J Exp Med*. 2017;214:579-596.
43. Sugimoto H, Mundel TM, Kieran MW, Kalluri R. Identification of fibroblast heterogeneity in the tumor microenvironment. *Cancer Biol Ther*. 2006;5:1640-1646.
44. Atherton AJ, O'Hare MJ, Buluwela L, et al. Ecto-enzyme regulation by phenotypically distinct fibroblast sub-populations isolated from the human mammary gland. *J Cell Sci*. 1994;107(Pt 10):2931-2939.
45. Paauwe M, Schoonderwoerd M, Helderman RF, et al. Endoglin expression on cancer-associated fibroblasts regulates invasion and stimulates colorectal cancer metastasis. *Clin Cancer Res*. 2018;24:6331-6344.
46. Richardsen E, Uglehus RD, Johnsen SH, Busund LT. Immunohistochemical expression of epithelial and stromal immunomodulatory signalling molecules is a prognostic indicator in breast cancer. *BMC Res Notes*. 2012;5:110.
47. Ahirwar DK, Nasser MW, Ouseph MM, et al. Fibroblast-derived CXCL12 promotes breast cancer metastasis by facilitating tumor cell intravasation. *Oncogene*. 2018;37:4428-4442.
48. Rohrborn D, Eckel J, Sell H. Shedding of dipeptidyl peptidase 4 is mediated by metalloproteases and up-regulated by hypoxia in human adipocytes and smooth muscle cells. *FEBS Lett*. 2014;588:3870-3877.
49. Nargis T, Kumar K, Ghosh AR, et al. KLK5 induces shedding of DPP4 from circulatory Th17 cells in type 2 diabetes. *Mol Metab*. 2017;6:1529-1539.
50. Chabottaux V, Noel A. Breast cancer progression: insights into multifaceted matrix metalloproteinases. *Clin Exp Metastasis*. 2007;24:647-656.
51. Kleer CG, Bloushtain-Qimron N, Chen Y-H, et al. Epithelial and stromal cathepsin K and CXCL14 expression in breast tumor progression. *Clin Cancer Res*. 2008;14:5357-5367.
52. Stuelten CH, DaCosta BS, Arany PR, Karpova TS, Stetler-Stevenson WG, Roberts AB. Breast cancer cells induce stromal fibroblasts to express MMP-9 via secretion of TNF-alpha and TGF-beta. *J Cell Sci*. 2005;118:2143-2153.
53. Siewerts AM, Klijn JG, Henzen-Logmand SC, et al. Urokinase-type-plasminogen-activator (uPA) production by human breast (myo) fibroblasts in vitro: influence of transforming growth factor-beta(1) (TGF beta(1)) compared with factor(s) released by human epithelial-carcinoma cells. *Int J Cancer*. 1998;76:829-835.

54. Foster DS, Jones RE, Ransom RC, Longaker MT, Norton JA. The evolving relationship of wound healing and tumor stroma. *JCI Insight*. 2018;3:pii: 99911.
55. Schafer M, Werner S. Cancer as an overhealing wound: an old hypothesis revisited. *Nat Rev Mol Cell Biol*. 2008;9:628-638.
56. Dvorak HF. Tumors: wounds that do not heal. Similarities between tumor stroma generation and wound healing. *N Engl J Med*. 1986;315:1650-1659.
57. Chang HY, Sneddon JB, Alizadeh AA, et al. Gene expression signature of fibroblast serum response predicts human cancer progression: similarities between tumors and wounds. *PLoS Biol*. 2004;2:E7.
58. Pedersen TX, Leethanakul C, Patel V, et al. Laser capture microdissection-based in vivo genomic profiling of wound keratinocytes identifies similarities and differences to squamous cell carcinoma. *Oncogene*. 2003;22:3964-3976.
59. Riss J, Khanna C, Koo S, et al. Cancers as wounds that do not heal: differences and similarities between renal regeneration/repair and renal cell carcinoma. *Cancer Res*. 2006;66:7216-7224.
60. Min HS, Kim JE, Lee MH, et al. Dipeptidyl peptidase IV inhibitor protects against renal interstitial fibrosis in a mouse model of ureteral obstruction. *Lab Invest*. 2014;94:598-607.
61. Hong SK, Choo EH, Ihm SH, Chang K, Seung KB. Dipeptidyl peptidase 4 inhibitor attenuates obesity-induced myocardial fibrosis by inhibiting transforming growth factor-beta1 and Smad2/3 pathways in high-fat diet-induced obesity rat model. *Metabolism*. 2017;76:42-55.
62. Kaji K, Yoshiji H, Ikenaka Y, et al. Dipeptidyl peptidase-4 inhibitor attenuates hepatic fibrosis via suppression of activated hepatic stellate cell in rats. *J Gastroenterol*. 2014;49:481-491.
63. Shi S, Srivastava SP, Kanasaki M, et al. Interactions of DPP-4 and integrin beta1 influences endothelial-to-mesenchymal transition. *Kidney Int*. 2015;88:479-489.
64. Thielitz A, Vetter RW, Schultze B, et al. Inhibitors of dipeptidyl peptidase IV-like activity mediate antifibrotic effects in normal and keloid-derived skin fibroblasts. *J Invest Dermatol*. 2008;128:855-866.

SUPPORTING INFORMATION

Additional supporting information may be found online in the Supporting Information section at the end of the article.

How to cite this article: Mezawa Y, Daigo Y, Takano A, et al. CD26 expression is attenuated by TGF- β and SDF-1 autocrine signaling on stromal myofibroblasts in human breast cancers. *Cancer Med*. 2019;00:1–13. <https://doi.org/10.1002/cam4.2249>

RESEARCH ARTICLE

Development of novel monoclonal antibodies with specific binding affinity for denatured human CD26 in formalin-fixed paraffin-embedded and decalcified specimens

Ryo Hatano¹, Taketo Yamada^{2,3}, Hiroko Madokoro³, Haruna Otsuka¹, Eriko Komiya¹, Takumi Itoh¹, Yuka Narita¹, Satoshi Iwata¹, Hiroto Yamazaki¹, Shuji Matsuoka⁴, Nam H. Dang⁵, Kei Ohnuma¹, Chikao Morimoto^{1*}

1 Department of Therapy Development and Innovation for Immune Disorders and Cancers, Graduate School of Medicine, Juntendo University, Hongo, Bunkyo-ku, Tokyo, Japan, **2** Department of Pathology, Saitama Medical University, Moroyama-machi, Iruma-gun, Saitama, Japan, **3** Department of Pathology, Keio University School of Medicine, Shinjuku-ku, Tokyo, Japan, **4** Department of Immunological Diagnosis, Juntendo University Graduate School of Medicine, Hongo, Bunkyo-ku, Tokyo, Japan, **5** Division of Hematology/Oncology, University of Florida, Gainesville, FL, United States of America

* Current address: Institute for Environmental and Gender Specific Medicine, Juntendo University Graduate School of Medicine, Tomioka, Urayasu, Chiba, Japan.

* morimoto@ims.u-tokyo.ac.jp



OPEN ACCESS

Citation: Hatano R, Yamada T, Madokoro H, Otsuka H, Komiya E, Itoh T, et al. (2019) Development of novel monoclonal antibodies with specific binding affinity for denatured human CD26 in formalin-fixed paraffin-embedded and decalcified specimens. *PLoS ONE* 14(6): e0218330. <https://doi.org/10.1371/journal.pone.0218330>

Editor: Arun Rishi, Wayne State University, UNITED STATES

Received: March 8, 2019

Accepted: May 30, 2019

Published: June 13, 2019

Copyright: © 2019 Hatano et al. This is an open access article distributed under the terms of the [Creative Commons Attribution License](https://creativecommons.org/licenses/by/4.0/), which permits unrestricted use, distribution, and reproduction in any medium, provided the original author and source are credited.

Data Availability Statement: All relevant data are within the manuscript and its Supporting Information files.

Funding: This work was supported by a grant of the Ministry of Health, Labour, and Welfare, Japan (Grant Number 150401-01 (C.M.) and 180101-01 (C.M.)), and JSPS KAKENHI Grant Numbers JP16H05345 (C.M.), JP16H04714 (T.Y.), JP18H02782 (K.O.), and JP17K10008 (R.H.). The funders had no role in study design, data collection

Abstract

A 110-kDa type II transmembrane glycoprotein with dipeptidyl peptidase IV (DPPIV) activity in its extracellular region, CD26 has a multitude of biological functions and plays an important role in the regulation of inflammatory responses and tumor biology. Our work has focused on CD26 as a novel therapeutic target for various tumors and immune disorders, and we have recently developed a humanized anti-CD26 monoclonal antibody (mAb), YS110, which has promising safety profile and clinical activity in patients with malignant pleural mesothelioma. The development of an anti-human CD26 mAb that can clearly and reliably detect the denatured CD26 molecule in formalin-fixed paraffin-embedded (FFPE) tissues in the clinical setting is therefore of the utmost importance. To develop novel anti-CD26 mAbs capable of binding to denatured CD26, we immunized mice with urea-treated CD26 protein. Hybridoma supernatants were screened for specific reactivity with human CD26 by immunostaining through the use of a set of FFPE human CD26-positive or negative tumor cell lines. This screening method enables us to develop novel anti-human CD26 mAbs suitable for immunohistochemical staining of CD26 in FFPE non-tumor and tumor tissue sections with reliable clarity and intensity. Specifically, these mAbs display strong binding affinity to denatured human CD26 rather than undenatured human CD26, and are capable of detecting denatured human CD26 in decalcified specimens. These novel anti-CD26 mAbs are potentially useful for the analysis of CD26 expression in cancer patients with bony metastasis, and may help decide the appropriateness of YS110 therapy for future cancer patients.

and analysis, decision to publish, or preparation of the manuscript.

Competing interests: Chikao Morimoto is an inventor of the humanized anti-CD26 mAb YS110 (US Patent #7402698). Y's AC Co., Ltd. (Tokyo, Japan) owns this patent, and Taketo Yamada, Nam H. Dang, Kei Ohnuma and Chikao Morimoto are founding members and shareholders of this company. Kissei Pharmaceutical Co., Ltd. (Tokyo, Japan) is the industry sponsor of a phase I/II clinical trial of YS110 for malignant pleural mesothelioma which is currently being conducted in Japan. Nichirei Biosciences, Inc. (Tokyo Japan) is involved in the collaborative development of the companion diagnostic kit utilizing the anti-human CD26 mAb 19-32. Ryo Hatano, Taketo Yamada, Kei Ohnuma and Chikao Morimoto are inventors of the novel anti-human CD26 mAbs U16-3 and U38-8, and are now applying for a patent regarding their invention (Anti-human CD26 monoclonal antibody. Application 2018-03-16 JP2018049308). This does not alter our adherence to PLOS ONE policies on sharing data and materials. Other authors declare no competing financial interests associated with this manuscript, and all authors have approved the manuscript for submission.

Abbreviations: AAs, amino acids; Ab, antibody; CRC, colorectal cancer; DPPIV, dipeptidyl peptidase IV; ELISA, enzyme-linked immunosorbent assay; FFPE, formalin-fixed paraffin-embedded; FIH, first-in-human; GIST, gastrointestinal stromal tumor; HRP, horseradish peroxidase; mAb, monoclonal antibody; MPM, malignant pleural mesothelioma; pAb, polyclonal antibody; RCC, renal carcinoma; sCD26, soluble human CD26; shRNA, short hairpin RNA..

Introduction

CD26 is a homodimeric type II transmembrane glycoprotein with a molecular mass of 220–240 kDa [1, 2]. Human CD26 is composed of 766 amino acids (AAs), including a short cytoplasmic domain of 6 amino acid residues at the N-terminal end (AA 1–6), a transmembrane region of 22 amino acids (AA 7–28), and an extracellular domain, the predominant part of CD26 (AA 29–766) [3, 4]. This C-terminal extracellular domain exhibits dipeptidyl peptidase IV (DPPIV) activity. DPPIV belongs to the serine protease family, able to cleave dipeptides from polypeptides with N-terminal penultimate proline or alanine, and regulates biological activities of a number of mediators such as cytokines, chemokines, neuropeptides and incretin hormones [5]. Although CD26 is expressed on various cell types, including epithelial cells (kidney proximal tubules, bile duct, prostate and intestine), endothelial cells as well as T lymphocytes [3, 4, 6], its function is dependent on cell types and the microenvironment, which influences the multiple biological roles of CD26.

CD26 is expressed on both human CD4⁺ T cells and CD8⁺ T cells in a triphasic fashion, and is associated with T cell signal transduction processes as a costimulatory molecule [7, 8]. In addition to its function as an immunoregulatory molecule, CD26 is expressed on a number of human neoplasms, including malignant pleural mesothelioma (MPM), renal carcinoma (RCC), colorectal cancer (CRC), hepatocellular carcinoma, lung cancer, prostate cancer, gastrointestinal stromal tumor (GIST), thyroid carcinoma, and different subtypes of T-cell malignancies [9]. Although CD26/DPPIV function in cancer biology is not yet fully characterized, CD26 serves as a prognostic marker in multiple tumors such as CRC, GIST, thyroid carcinoma, urothelial carcinoma and prostate cancer [10–14]. Moreover, in several human malignancies including MPM, CRC and chronic myeloid leukemia, CD26/DPPIV expression is reported to be a marker of cancer stem cells [15–18]. Besides our work over the past three decades characterizing its role in the immune system, our group has also had a long-standing interest in the role of CD26 in cancer biology. We have previously demonstrated that anti-CD26 monoclonal antibody (mAb) treatment resulted in both *in vitro* and *in vivo* inhibition of tumor cell growth, migration and invasion, and enhanced survival of mouse xenograft models inoculated with T-cell lymphoma, RCC or MPM via multiple mechanisms of action [19–23]. These findings have led to our focus on CD26 as a novel therapeutic target for various tumors, and the development of YS110, a humanized mAb with high affinity to the CD26 antigen. Results from the first-in-human (FIH) phase I clinical trial of this mAb for CD26-expressing solid tumors, particularly refractory MPM, were recently published [24]. Our FIH study demonstrated that YS110 therapy exhibited a favorable safety profile and resulted in encouraging disease stabilization in a number of patients with advanced/refractory MPM and RCC. A subsequent phase II clinical trial of YS110 for MPM is currently in progress in Japan [25].

Along with the development of novel targeted therapies that can be administered at an optimal dose and schedule to maximize efficacy with tolerable toxicities is the acute need for the concurrent development of accurate companion diagnostic agents to select the appropriate patient population for treatment. It is therefore imperative to develop a detection method for CD26 expression in formalin-fixed paraffin-embedded (FFPE) clinical tumor samples that allows for the selection of potentially eligible patients in the clinical setting for humanized anti-CD26 mAb therapy. Despite our extensive testing of the many anti-CD26 mAbs previously developed in our laboratory [26] and the 23 commercially available anti-CD26 mAbs, none of them can clearly detect the denatured CD26 molecule in FFPE tissues. On the other hand, we have tested 5 commercially available anti-CD26 polyclonal antibodies (pAbs), and among them, a pAb purchased from R&D Systems showed that these reagents exhibited the most reliable staining pattern and intensity [24, 27, 28]. However, the potential lot-to-lot

variability in staining pattern and intensity and the general lack of product uniformity represent shortcomings for the use of pAbs in the clinical setting. These inconsistencies and the difficulty in maintaining a stable supply hence make pAbs not the ideal reagents for diagnostic testing of patient tumor samples. For these reasons, we recently attempted to develop novel anti-human CD26 mAbs by immunizing mice with urea-treated CD26 protein, and succeeded in developing a mAb, clone 19–32, capable of detecting denatured CD26 in FFPE tissue sections with reliable intensity [29]. However, in the process of developing the companion diagnostic kit utilizing our 19–32 mAb for clinical usage, the critical issue involving non-specific immunostaining of control slides has unexpectedly arisen. 19–32 mAb stained not only CD26-positive tumor cell line specimens, but also those from CD26-negative tumor cell lines as well, strongly suggesting that it is inappropriate for the detection of denatured CD26 expression in FFPE clinical tumor samples.

In the present study, to address this critical issue, we have improved the screening methods and succeeded in developing novel anti-human CD26 mAbs with strong binding affinity to denatured human CD26 in FFPE non-tumor and tumor tissue sections, and which do not stain CD26-negative specimens, suggesting that these novel mAbs are potentially useful for the analysis of CD26 expression in cancer patients, and may help decide the appropriateness of YS110 therapy for future cancer patients.

Materials and methods

Animals

Female BALB/c mice were purchased from CLEA Japan (Tokyo, Japan) and female CB17/lcr-*Prkdc^{scid}*/CrlCrlj mice (SCID mice) were purchased from Charles River Laboratories Japan, Inc. (Yokohama, Japan). Mice were housed in a specific pathogen-free facility in micro-isolator cages with ad libitum access to autoclaved water and sterile standard food, and were maintained at $24 \pm 2^\circ\text{C}$ under a 12-hour light-dark cycle (lights on 8 am to 8 pm). All mice were used at 6–8 weeks of age. To minimize suffering and distress, subcutaneous injection in the flank of mice was performed under isoflurane anesthesia through an isoflurane vaporizer set to deliver 2–3% isoflurane.

Cell lines and cultures

A human MPM cell line MSTO-211H (MSTO parent), a human lung cancer cell line A549 and a human T-cell leukemia line Jurkat (Jurkat parent) were obtained from the American Type Culture Collection (Rockville, MD). MSTO parent cells were stably transfected with a full-length human CD26 (MSTO-CD26) using the Lipofectamine2000 reagent (Invitrogen, Carlsbad, CA), and selected with G418 (Sigma-Aldrich, St Louis, MO) [23]. The human MPM cell line JMN was a kind gift from Dr. Brenda Gerwin (Laboratory of Human Carcinogenesis, National Institutes of Health, Bethesda, MD). JMN cells were transduced with the short hairpin RNA (shRNA)-expressing lentivirus (MISSION; Sigma-Aldrich), and the stable cell lines (JMN CD26-shRNA, JMN ctrl-shRNA) were generated by selection with puromycin [16]. Jurkat parent cells were stably transfected with a full-length human CD26 by electroporation (Jurkat-CD26), and generated by selection with G418 [2]. All cell lines were grown in RPMI1640 medium supplemented with 10% FBS at 37°C in a humidified 5% CO_2 incubator.

Antibodies

To characterize the newly developed mouse anti-human CD26 mAbs, murine anti-human CD26 mAbs (clone 1F7, 5F8 or 19–32) which were previously developed in our laboratory

were used for comparison [7, 29, 30]. To compare the staining pattern and intensity of human CD26 on FFPE tissue or cell block, we used a purified goat anti-human CD26 pAb (AF1180) purchased from R&D Systems (Minneapolis, MN) as a control.

Preparation of immunogen

Soluble human CD26 (sCD26) was produced according to the method described previously [29, 31]. Purified sCD26 was denatured in 8 M urea buffer supplemented with 20 mM HEPES and 50 mM dithiothreitol (DTT) by gentle rotation for 8 hours at RT.

Development of hybridomas and monoclonal anti-human CD26 antibodies

The methods for the development of hybridoma were detailed previously [29]. Hybridoma supernatants were first screened for murine IgG production by enzyme-linked immunosorbent assay (ELISA) utilizing Mouse IgG total Ready-SET-Go! ELISA set (eBioscience, San Diego, CA). The supernatants containing high levels of murine IgG (more than 2 $\mu\text{g}/\text{ml}$) were next screened for immunostaining of FFPE cell block and tissue sections. The hybridomas were cloned by limiting dilution. Monoclonal antibodies were purified from the supernatants using Protein A IgG Purification Kit (Pierce, Rockford, IL).

Immunostaining of cell block or tissue specimens

The cultured cell lines were fixed in 10% neutral buffered formalin for 48 hours at RT, and subsequently embedded in paraffin. MSTO parent, MSTO-CD26 or JMN cells (1×10^6 , each) were implanted subcutaneously (s.c.) in the flank of SCID mice. Tumor volumes were measured along three orthogonal areas (a, b and c) by digital vernier calipers (Mitutoyo Corporation, Kanagawa, Japan), and calculated as tumor volume = $abc/2$ (mm^3). Tumor volumes were monitored twice a week, and after 8 weeks of implantation (when the tumor volume reached around 500 mm^3), mice were sacrificed by cervical dislocation and the tumors in the flank were excised and fixed in 10% neutral buffered formalin at RT, and subsequently embedded in paraffin. In this experiment, tumor size was not sufficiently large to impact survival, overall weight and locomotor activity of mice. FFPE tissue specimens of human MPM and normal liver, kidney and prostate were used for positive controls. For the analysis of normal human bone and bone marrow tissue, or bone with metastatic cancer, formalin-fixed samples were decalcified in 10% formic acid at RT or 10% EDTA in Tris buffer, and subsequently embedded in paraffin. FFPE cell block or tissue specimens were cut into 4–6 μm sections and deparaffinized. For histology, sections were stained with hematoxylin and eosin. The methods for immunohistochemistry were detailed previously [29]. To confirm the binding specificity of mAbs to human CD26, 100 μl of anti-human CD26 mAb solution (10 $\mu\text{g}/\text{ml}$ in PBS) was gently rotated with 1 mg/ml of sCD26 at 4°C overnight, and after centrifugation, the supernatant was used instead of the primary anti-human CD26 antibody (Ab).

Western blotting

The cultured cell lines were collected and lysed in RIPA buffer supplemented with 2% protease inhibitor cocktail (Sigma-Aldrich) for 1 hour at 4°C. Following addition of Laemmli 4x SDS sample buffer and DTT, whole cell lysates were boiled for 5 min at 95°C. Each sample was electrophoretically separated on 4–20% Mini-PROTEAN TGX precast gels (Bio-Rad, Hercules, CA) with Tris/glycine buffer, and transferred to PVDF membrane. After blocking with 5% skim milk in TBS for 45 min at RT, membranes were incubated with purified mouse anti-human CD26 mAb (19–32: 5 $\mu\text{g}/\text{ml}$, U16-3: 0.2 $\mu\text{g}/\text{ml}$, U38-8: 0.5 $\mu\text{g}/\text{ml}$) or goat anti-human

CD26 pAb (1 µg/ml) in 5% skim milk-TBS at 4°C overnight. The membranes were washed with TBS containing 0.1% Tween-20 (TBS-T) and incubated with horseradish peroxidase (HRP)-conjugated sheep anti-mouse IgG Ab (GE Healthcare, Buckinghamshire, UK) or HRP-conjugated donkey anti-goat IgG Ab (Santa Cruz Biotechnology, Santa Cruz, CA) in 5% skim milk-TBS for 1 hour at RT. Proteins were detected with enhanced chemiluminescence using the Western Lightning Plus-ECL (Perkin Elmer, Waltham, MA). The images were taken using Luminescent Image Analyzer LAS-4000 (GE Healthcare) and data were analyzed with Image Reader LAS-4000 and Multi Gauge software (GE Healthcare). For reprobing, the same membranes were treated with stripping solution. After blocking with 5% skim milk in TBS, the membranes were reblotted with mouse anti-β-actin mAb (clone AC-15, Sigma-Aldrich) in 5% skim milk-TBS for 1 hour at RT, and subsequently incubated with HRP-conjugated sheep anti-mouse IgG Ab in 5% skim milk-TBS for 1 hour at RT. Protein detection was performed as described above.

Flow cytometry

The methods for flow cytometry were detailed previously [29]. In brief, The cultured cell lines were incubated with 10 µg/ml of purified mouse anti-human CD26 mAb (19–32, U16-3 or U38-8) or goat anti-human CD26 pAb or isotype controls for 25 min at 4°C, and subsequently stained with PE-conjugated goat anti-mouse Ig pAb (BD Biosciences, San Jose, CA) or PE-conjugated donkey anti-goat IgG Ab (Santa Cruz Biotechnology) for 25 min at 4°C. PE-labeled mouse anti-human CD26 mAb (clone M-A261, BD Biosciences) was utilized as a positive control. PE-labeled or unlabeled mouse IgG_{1,κ} isotype control (clone MOPC-21, BD Biosciences) and normal goat polyclonal IgG (AB-108-C, R&D Systems) were utilized as negative controls.

ELISA

For the preparation of denatured sCD26 used for ELISA, purified sCD26 protein was boiled for 10 min at 95°C in PBS. The 96-well immunoplates (NUNC, Roskilde, Denmark) were coated with native (undenatured) sCD26 or denatured sCD26 in carbonate bicarbonate buffer (12.5, 25, 50, 100, 200 ng/well, respectively) or buffer alone as a negative control at 4°C overnight. Each well of the plate was blocked with 2% BlockAce (DS Pharma Biomedical, Osaka, Japan) in deionized distilled water for 1 hour at RT, and then incubated with 2 µg/ml of purified mouse anti-human CD26 mAb (5F8, 1F7, 19–32, U16-3 or U38-8) or goat anti-human CD26 pAb in 1% BlockAce solution for 1 hour at RT, and subsequently incubated with HRP-conjugated goat anti-mouse Ig pAb (BD Biosciences) or HRP-conjugated donkey anti-goat IgG Ab (Santa Cruz Biotechnology) in 1% BlockAce solution for 1 hour at RT. Colorimetric methods and data analysis were detailed previously [29].

Ethics approval and consent to participate

Animal experiments were conducted following protocols approved by the Animal Care and Use Committee at Juntendo University (Authorization Numbers: 250170 and 290131). For the use of human materials, experimental procedures and study protocols were approved by the Saitama Medical University ethical review board (Authorization Number: 794), the Keio University School of Medicine ethical review board (Authorization Number: 2012–0100) and the Juntendo University School of Medicine ethical review board (Authorization Number: 2014029), and the purpose of the study was explained to all patients and their written informed consent was obtained. The use of human samples from autopsy cases was generously permitted by the written informed consent obtained from the next of kin. All studies on human subjects were carried out according to the principles set out in the Declaration of Helsinki.

Results

Development of novel anti-CD26 mAbs

Following the development of a mouse anti-human CD26 mAb, clone 19–32, capable of detecting denatured CD26 in FFPE tissue sections [29], we attempted to establish the companion diagnostic kit utilizing this mAb. The control slides containing samples from a set of FFPE cell lines expressing CD26 or CD26-negative cell lines are included in the kit as positive or negative controls for immunostaining, respectively. For this purpose, we selected the human CD26-negative lung cancer cell line A549 and 3 pairs of human CD26-positive or negative tumor cell lines (MSTO, JMN and Jurkat cells) which have been previously characterized by our group [2, 16, 23]. To confirm mRNA and cell surface protein expression of human CD26 in these cell lines, we conducted real-time RT-PCR and flow cytometry analyses. MSTO parent, A549 and Jurkat parent were endogenous human CD26-deficient cell lines, and neither mRNA nor cell surface protein expression was detected in these cells, while both MSTO-CD26 and Jurkat-CD26 which were stably transfected with a full-length human CD26 expressed CD26 at both mRNA and protein levels (S1A and S1B Fig). On the other hand, stable shRNA knockdown of CD26 in JMN, an endogenous human CD26-positive cell line, markedly reduced the expression at both mRNA and protein levels as compared with JMN ctrl-shRNA cells (S1A and S1B Fig). We next prepared the FFPE cell block of these tumor cell lines (the results of H&E staining of each tumor cell line were shown in Fig 1A-i), and examined immunostaining with 19–32 mAb. However, although FFPE tissue specimens of normal liver, kidney, prostate, and malignant mesothelioma stained with 19–32 mAb exhibited reliable staining pattern and intensity [29], specimens from both CD26-positive MSTO-CD26 and JMN ctrl-shRNA cells as well as CD26-negative MSTO parent, JMN CD26-shRNA and A549 cells were all unexpectedly stained with 19–32 mAb (Fig 1A-ii). Meanwhile, cell block specimens stained with anti-CD26 pAb purchased from R&D Systems (control pAb) exhibited a clear staining pattern of CD26, (Fig 1A-iii), revealing 19–32 mAb to be inappropriate for the detection of denatured CD26 expression in FFPE clinical tumor samples.

Given these observations, we again attempted to develop novel anti-human CD26 mAbs that are useful for the analysis of tumor CD26 expression in the clinical setting. To achieve this objective, we improved the hybridoma screening methods that are summarized in Table 1.

The host mice, preparation of immunogen, and the immunization method used for our current study were exactly the same as in our previous study [29]. In our previous study, the hybridoma supernatants were screened for selective reactivity with human CD26. As a result of the screening, 31 clones that secreted anti-human CD26 mAbs were evaluated by both flow cytometry and ELISA. After testing the hybridoma supernatants from the 31 clones for immunostaining of CD26 in FFPE tissue sections, we finally obtained 19–32 mAb [29]. On the other hand, in the present study, hybridoma cells were first screened for murine IgG production by ELISA, since it is possible that mAbs suitable for immunostaining of denatured human tumor CD26 in FFPE cell block and tissue specimens would not react well to native (undenatured) CD26 or urea-treated CD26 protein, as analyzed by flow cytometry or ELISA.

Immunostaining with novel anti-CD26 mAbs

The positive supernatants containing high levels of murine IgG were next screened for immunostaining of CD26 in FFPE cell block of various human CD26-positive or negative tumor cell lines as described above. After testing the hybridoma supernatants from a total of 429 clones for immunostaining of FFPE cell block, we finally obtained 5 clones capable of staining CD26 in CD26-positive tumor cell lines without any non-specific staining in CD26-negative tumor

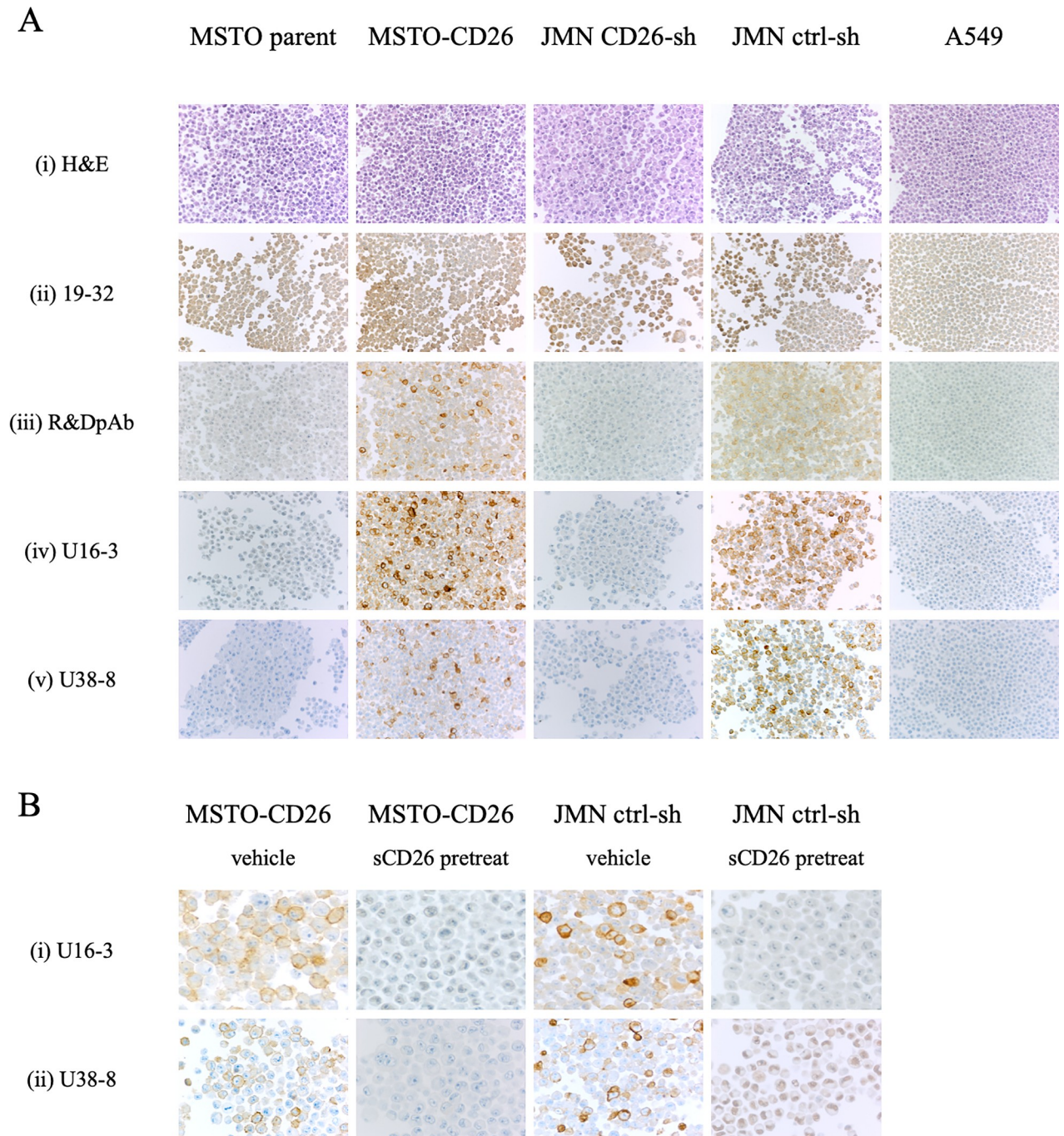


Fig 1. Representative results of immunostaining of FFPE cell block with novel anti-CD26 mAbs. **A.** The cell block sections of MSTO parent, MSTO-CD26, JMN CD26-shRNA, JMN ctrl-shRNA or A549 cells were stained with hematoxylin and eosin (H&E) (i), or purified mouse anti-human CD26 mAb (19-32 (ii), U16-3 (iv), U38-8 (v)), or purified goat anti-human CD26 pAb (R&D Systems (iii)). Original magnification, 10x. **B.** The cell block sections of MSTO-CD26 or JMN ctrl-shRNA cells were stained with purified novel mouse anti-human CD26 mAbs (U16-3 (i) or U38-8 (ii)) in the presence of excessive amounts of soluble human CD26 protein (sCD26) or vehicle. Original magnification, 40x. All specimens were counterstained with hematoxylin.

<https://doi.org/10.1371/journal.pone.0218330.g001>

cell lines. Among them, two representative clones (clone U16-3 or U38-8) clearly distinguished CD26-positive cells from CD26-negative cells by immunostaining. As shown in Fig 1A,

Table 1. A method for development of novel anti-human CD26 monoclonal antibodies.

	Host	Immunogen	1st screening	2nd screening	3rd screening
The previous method (19–32 mAb)	BALB/c mice	8M urea-treated recombinant sCD26 ^a (protein)	Flow cytometry Jurkat-CD26 (CD26 ⁺) Jurkat parent (CD26 ⁻)	ELISA Native sCD26 ^a Urea-treated sCD26 ^a	Immunostaining [Tissue] Liver Kidney Prostate Mesothelioma
The present method (U16-3 mAb, U38-8 mAb)	BALB/c mice	8M urea-treated recombinant sCD26 ^a (protein)	ELISA Mouse total IgG	Immunostaining [Cell line] MSTO parent (CD26 ⁻) MSTO-CD26 (CD26 ⁺) JMN CD26-sh ^b (CD26 ⁻) JMN ctrl-sh ^b (CD26 ⁺) A549 (CD26 ⁻)	Immunostaining [Tissue] Liver Kidney Prostate Mesothelioma

^a sCD26: soluble human CD26 (the extracellular domain of CD26)

^b sh: short hairpin RNA

<https://doi.org/10.1371/journal.pone.0218330.t001>

MSTO-CD26 and JMN ctrl-shRNA cells stained with the purified U16-3 mAb or U38-8 mAb exhibited reliable staining intensity comparable to the control pAb, while MSTO parent, JMN CD26-shRNA and A549 cells stained with these mAbs showed extremely low background signals as compared with the control pAb (panels iii, iv, v). In addition, to determine the optimal Ab concentration for immunostaining, we evaluated the Abs in concentrations ranging from 0.1 µg/ml to 10 µg/ml of U16-3 mAb, U38-8 mAb or control pAb. As a result of this evaluation, staining of FFPE cell block with 0.2–0.5 µg/ml of U16-3 mAb or 0.5–1 µg/ml of U38-8 mAb resulted in similar staining intensity as compared with those stained with 1–2 µg/ml of control pAb (Fig 1A-iii, 1A-iv and 1A-v), strongly suggesting that the newly developed mAbs have a higher binding affinity for denatured human CD26 in FFPE sections than that of control pAb. To further confirm the binding specificity of these novel mAbs to human CD26, the FFPE cell block of MSTO-CD26 and JMN ctrl-shRNA cells was treated with U16-3 mAb or U38-8 mAb preincubated with excessive amounts of native (undenatured) sCD26 or vehicle. As shown in Fig 1B, the binding of these mAbs was completely inhibited by sCD26 (panels i, ii).

Moreover, we examined immunohistochemical staining of *in vivo* tumor samples with U16-3 mAb or U38-8 mAb. For this purpose, MSTO parent, MSTO-CD26 or JMN cells were implanted s.c. in the flank of SCID mice, and the tumors in the flank were excised from those mice. Histology of mesothelioma formed by MSTO parent, MSTO-CD26 or JMN cells was shown in H&E staining of each tumor sample (Fig 2A-i). Staining of tumors derived from MSTO-CD26 and JMN cells with U16-3 mAb or U38-8 mAb showed more bright staining intensity than control pAb, while no apparent staining was observed in MSTO parent-derived tumors stained with these two mAbs (Fig 2A-iii, 2A-iv and 2A-v). Meanwhile, not only tumors derived from MSTO-CD26 and JMN cells but also tumors derived from MSTO parent cells were all stained with 19–32 mAb (Fig 2A-ii), which was similar with the results of cell block shown in Fig 1A-ii.

Finally, we examined immunohistochemical staining of CD26 in FFPE tissue specimens of normal liver, kidney, prostate, and MPM with U16-3 mAb or U38-8 mAb. The staining pattern of CD26 in these tissues was detailed previously [29]. As shown in Fig 2B, the surface membrane of bile canaliculi, the brush border of renal proximal tubular epithelial cells and prostate epithelial cells were specifically stained with extremely low background (panels i, ii). The specific staining of CD26 in epithelioid type of MPM was also observed with the use of U16-3 mAb or U38-8 mAb. Of note, although both cell surface and cytoplasm of MPM cells

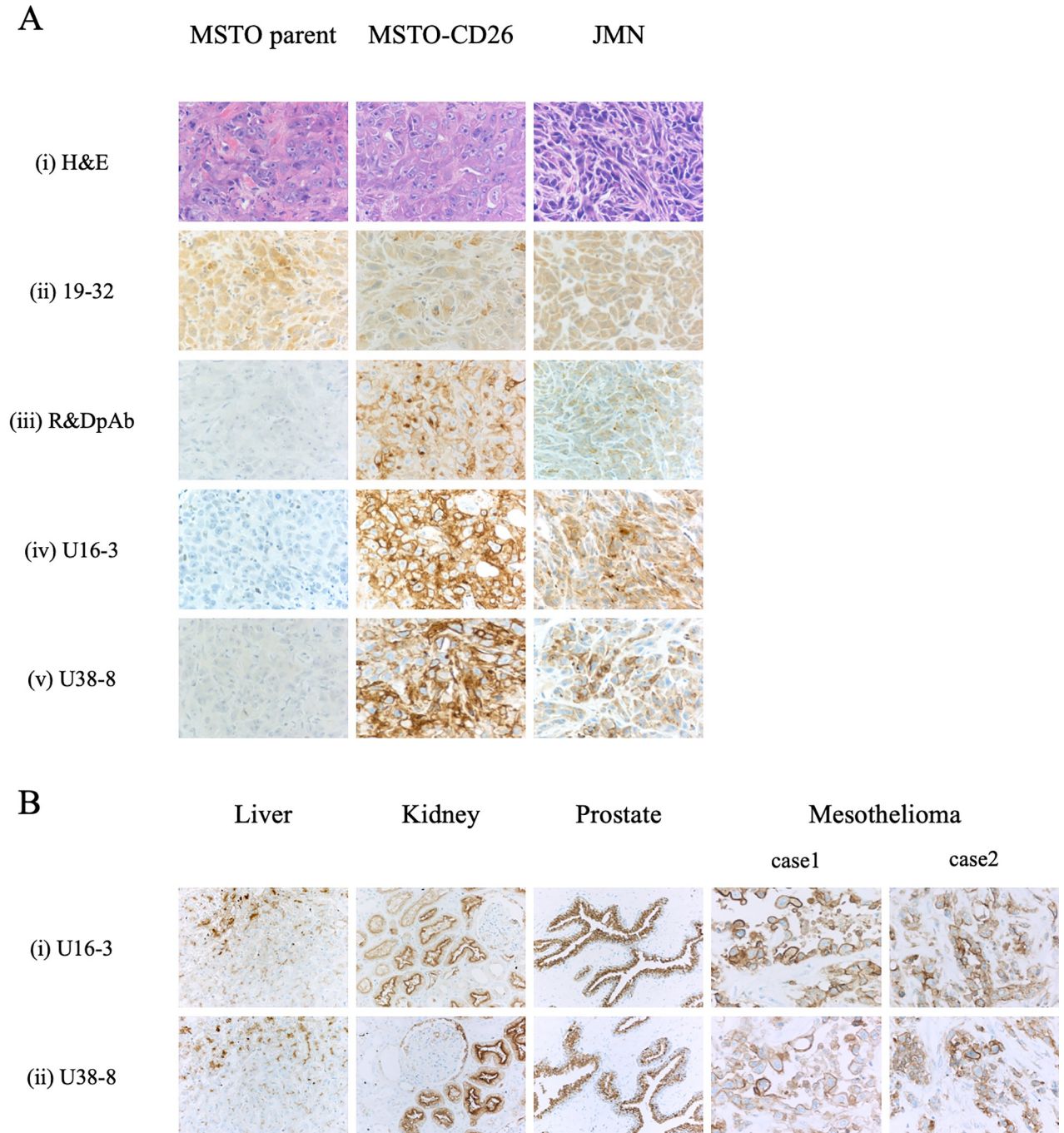


Fig 2. Representative results of immunostaining of FFPE tissue specimens with novel anti-CD26 mAbs. A. MSTO parent, MSTO-CD26 or JMN cells were implanted subcutaneously (s.c.) in the flank of SCID mice. The *in vivo* tumor samples were stained with hematoxylin and eosin (H&E) (i), or purified mouse anti-human CD26 mAb (19-32 (ii), U16-3 (iv), U38-8 (v)), or purified goat anti-human CD26 pAb (R&D Systems (iii)). Original magnification, 20x. B. The tissue specimens of liver, kidney, prostate or two cases of malignant mesothelioma were stained with purified novel mouse anti-human CD26 mAbs (U16-3 (i) or U38-8 (ii)). Original magnification, 4x. All specimens were counterstained with hematoxylin.

<https://doi.org/10.1371/journal.pone.0218330.g002>

were stained with U16-3 mAb or U38-8 mAb, cell surface membrane was stained more intensely than cytoplasm. This staining pattern of CD26 in MPM cells was similar with the staining results of control pAb [29].

Taken together, these data indicate that U16-3 mAb and U38-8 mAb were capable of detecting denatured human CD26 in FFPE non-tumor and tumor tissue sections and tumor cell blocks with reliable staining pattern comparable to the control pAb. Importantly, with respect to signal-to-noise ratio, the newly developed mAbs were superior to the commercial anti-CD26 pAb in immunostaining of FFPE samples.

Characteristics of novel anti-CD26 mAbs

To further analyze the binding specificity and affinity of novel anti-CD26 mAbs for denatured or undenatured human CD26, we next conducted Western blot analysis utilizing the same human CD26-positive or negative tumor cell lines described above. We used the same enhanced chemiluminescence reagent, and the images were taken at the same exposure time to compare the detection sensitivity of anti-CD26 Abs. As shown in Fig 3, when each sample was immunoblotted with U38-8 mAb, clear bands were detected in the whole cell lysate of MSTO-CD26, JMN ctrl-shRNA and Jurkat-CD26 in molecular mass regions around 110 kDa, while these bands were not observed in the lysate of MSTO parent, JMN CD26-shRNA, A549 or Jurkat parent (panel iii). Importantly, no other non-specific bands were ever observed in all of the samples. The band intensity of Jurkat-CD26 was the most prominent, whereas the band intensity of JMN ctrl-shRNA was considerably weaker compared with those of Jurkat-CD26 and MSTO-CD26. These results correlated with the mRNA and cell surface protein expression levels of human CD26 in these cell lines, as shown in S1 Fig. In addition, U16-3 mAb or the control pAb detected CD26 expression in Jurkat-CD26 and MSTO-CD26, while the CD26 band was only slightly detected in whole cell lysate of JMN ctrl-shRNA (Fig 3-ii and 3-iv). Meanwhile, when each sample was immunoblotted with 19-32 mAb, the clear band was only observed in Jurkat-CD26 (Fig 3-i). When images were obtained at longer exposure times, several non-specific bands in molecular mass regions other than 110 kDa were observed in each sample when immunoblotted with 19-32 mAb. As was the case with immunostaining assay, we evaluated the Abs in concentrations ranging from 0.1 µg/ml to 10 µg/ml of anti-CD26 Abs

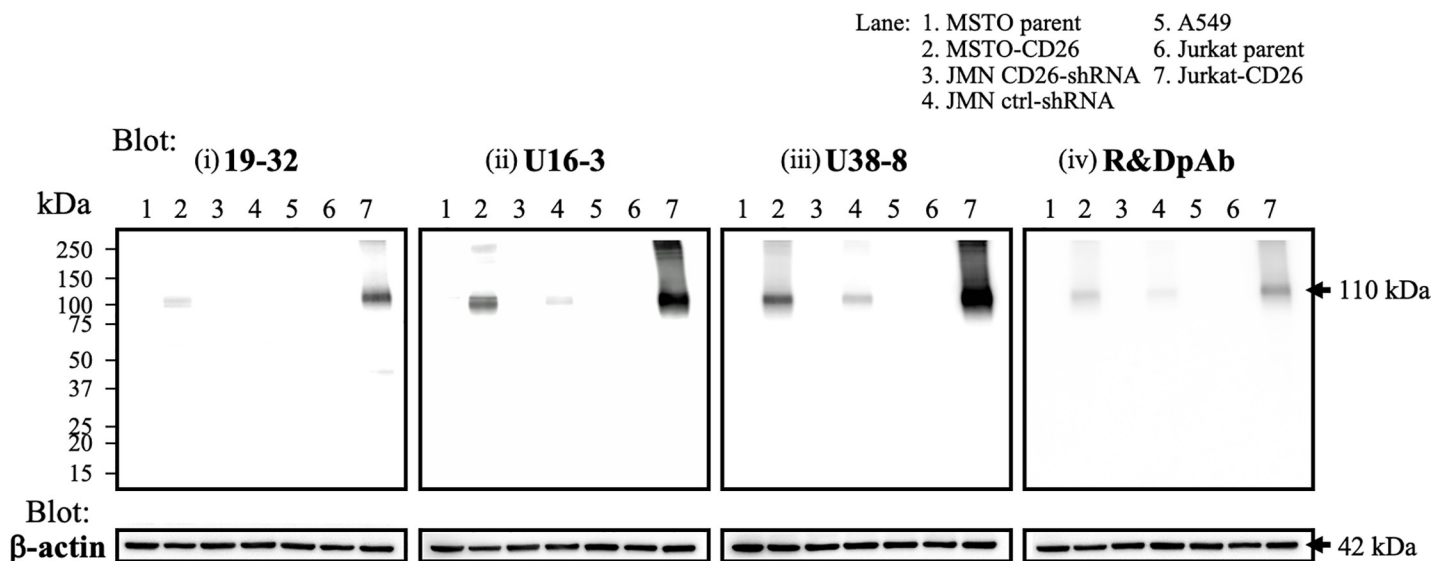


Fig 3. Western blotting analysis with novel anti-CD26 mAbs. Whole cell lysates of MSTO parent, MSTO-CD26, JMN CD26-shRNA, JMN ctrl-shRNA, A549, Jurkat parent or Jurkat-CD26 cells were separated by SDS-PAGE (each, 20 µg), and CD26 was detected by immunoblotting with purified mouse anti-human CD26 mAb (19-32 (i), U16-3 (ii), U38-8 (iii)), or purified goat anti-human CD26 pAb (R&D Systems (iv)). The same blots were stripped and reprobed with antibodies specific for β-actin as a loading control. Data shown are representative of three independent experiments, and similar results were obtained in each experiment.

<https://doi.org/10.1371/journal.pone.0218330.g003>

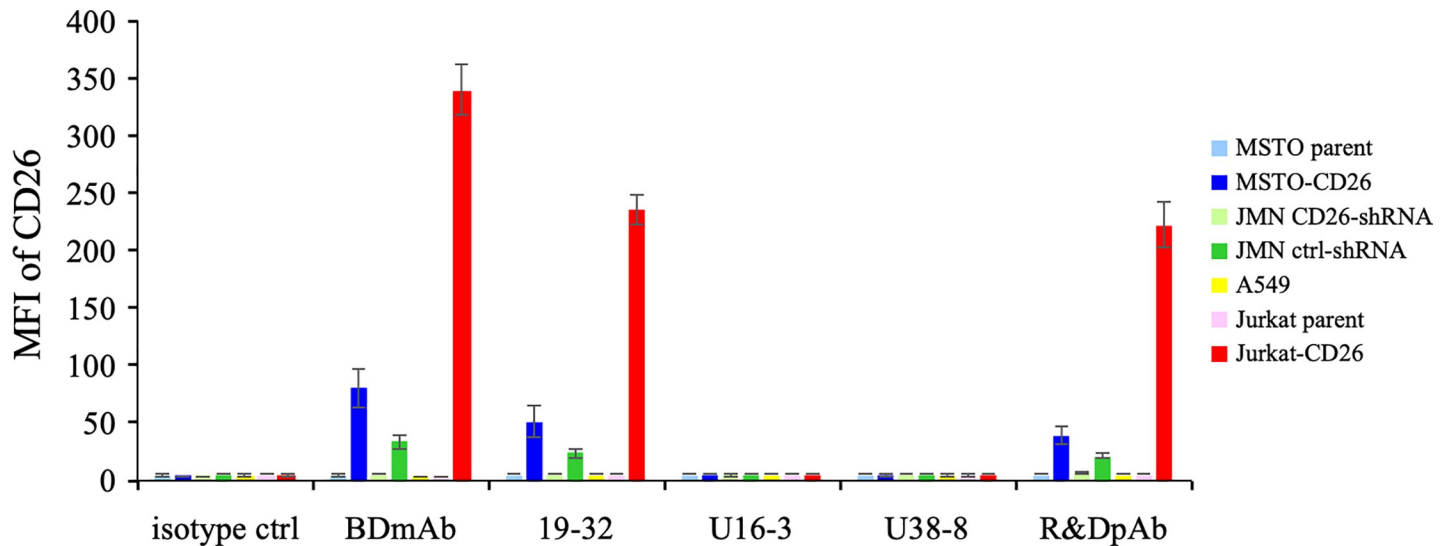


Fig 4. Flow cytometry analysis with novel anti-CD26 mAbs. MSTO parent, MSTO-CD26, JMN CD26-shRNA, JMN ctrl-shRNA, A549, Jurkat parent or Jurkat-CD26 cells were incubated with unlabeled isotype control or purified mouse anti-human CD26 mAb (19-32, U16-3 or U38-8) or purified goat anti-human CD26 pAb (R&D Systems), and subsequently stained with PE-labeled goat anti-mouse Ig pAb or PE-labeled donkey anti-goat IgG Ab, and analyzed by flow cytometry. PE-labeled commercial mouse anti-human CD26 mAb (BD Biosciences, clone M-A261) was utilized as a positive control. Representative data of three independent experiments are shown as mean \pm S.D. of the mean fluorescence intensity (MFI) from triplicate samples, and similar results were obtained in each experiment.

<https://doi.org/10.1371/journal.pone.0218330.g004>

to determine the optimal Ab concentration for Western blotting. This evaluation demonstrated that immunoblotting with 0.2 μ g/ml of U16-3 mAb or 0.5 μ g/ml of U38-8 mAb resulted in greater band intensity than that obtained following immunoblotting with 1 μ g/ml of control pAb or 5 μ g/ml of 19-32 mAb (Fig 3). These results indicate that the newly developed mAbs exhibited significantly greater binding specificity and affinity for denatured human CD26 protein in boiled Western blot samples as compared with those of control pAb or 19-32 mAb.

We next conducted flow cytometry analysis to analyze the binding affinity of novel anti-CD26 mAbs for native (undenatured) human CD26 protein. Human CD26-positive or negative tumor cell lines were incubated with a sufficient amount (10 μ g/ml) of unlabeled mouse anti-human CD26 mAb (19-32, U16-3 or U38-8) or control pAb or isotype controls, and subsequently stained with PE-labeled anti-mouse Ig pAb or PE-labeled anti-goat IgG Ab. PE-labeled commercial anti-CD26 mAb purchased from BD Biosciences or isotype control was utilized as a positive or negative control. As shown in Fig 4 (representative histograms are shown in S2 Fig), anti-CD26 mAb purchased from BD Biosciences, 19-32 mAb or control pAb could stain MSTO-CD26, JMN ctrl-shRNA or Jurkat-CD26 while MSTO parent, JMN CD26-shRNA, A549 or Jurkat parent showed no staining with these anti-CD26 Abs. In contrast, both U16-3 mAb and U38-8 mAb did not stain any of the tumor cell lines, similar to the results obtained with isotype controls (Fig 4). We also evaluated staining with directly fluorochrome-labeled U16-3 mAb or U38-8 mAb, and again these two mAbs did not stain any of the tumor cell lines. These data demonstrate that these novel anti-CD26 mAbs cannot bind to native (undenatured) human CD26 protein on the cell surface.

To further confirm the binding affinity of the novel anti-CD26 mAbs for denatured or undenatured human CD26, we next conducted ELISA assay. To prepare denatured sCD26, purified sCD26 protein was boiled for 10 min at 95°C. The 96-well immunoplates were coated with native (undenatured) sCD26 or denatured sCD26, and the reactivity of anti-CD26 Abs to these proteins was analyzed. Mouse anti-human CD26 mAbs 5F8 and 1F7, which were

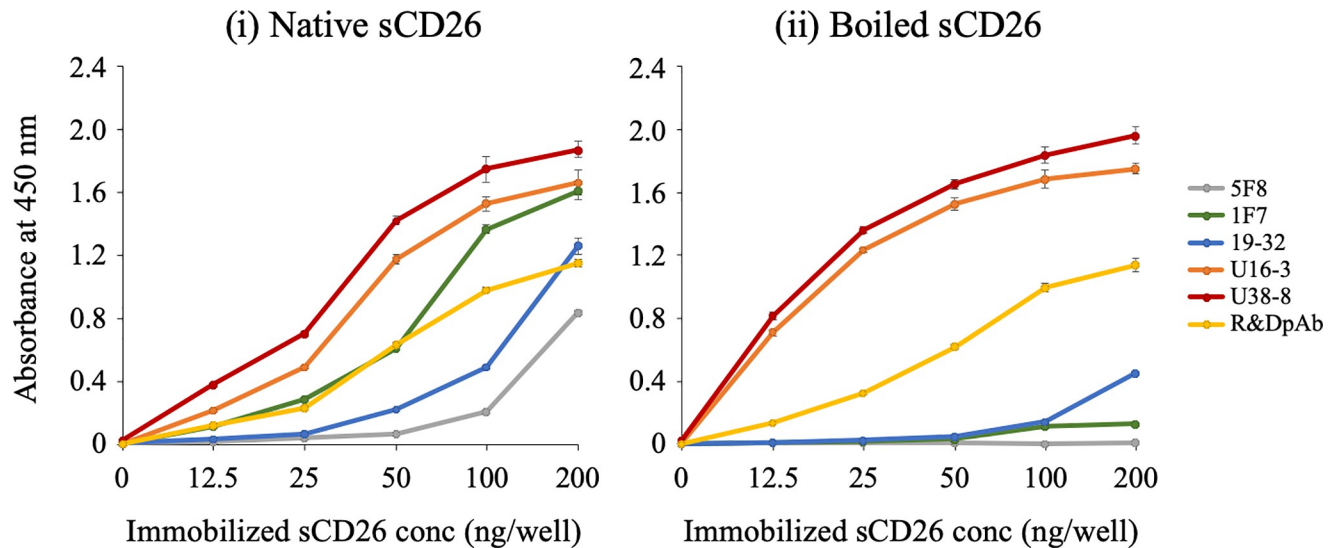


Fig 5. ELISA analysis with novel anti-CD26 mAbs. Immobilized native (undenatured) soluble human CD26 protein (sCD26) (i) or boiled (denatured) sCD26 (ii) was incubated with purified mouse anti-human CD26 mAb (5F8, 1F7, 19-32, U16-3 or U38-8) or purified goat anti-human CD26 pAb (R&D Systems). The absorbance at 450 nm/570 nm was measured. Representative data of three independent experiments are shown as mean \pm S.D. of triplicate samples, and similar results were obtained in each experiment.

<https://doi.org/10.1371/journal.pone.0218330.g005>

previously developed by our group as described in *Materials and methods*, were used as controls. Both 5F8 mAb and 1F7 mAb exhibited strong binding affinity to native (undenatured) human CD26 as confirmed by flow cytometry and ELISA, whereas these mAbs did not recognize denatured human CD26 in the FFPE tissue specimens (representative results are shown in S3 Fig). As shown in Fig 5, all the anti-CD26 Abs tested reacted well to the native sCD26, and the absolute value of absorbance was increased in an antigen dose-dependent manner (panel i). On the other hand, when sCD26 was denatured, the absorbance of 5F8 mAb, 1F7 mAb and 19-32 mAb was markedly reduced, while the absorbance of control pAb was maintained (Fig 5-ii). However, intriguingly, the absolute value of absorbance to the denatured sCD26 incubated with U16-3 mAb or U38-8 mAb appeared to be higher than the absorbance to the native sCD26 incubated with U16-3 mAb or U38-8 mAb, and the observed difference was particularly prominent at the low antigen doses (Fig 5). Moreover, the absolute value of absorbance to the denatured sCD26 incubated with U16-3 mAb or U38-8 mAb was much higher than that of control pAb. We next evaluated the potential suitability of U16-3 mAb or U38-8 mAb for sandwich ELISA. For this purpose, we selected 5 mouse anti-human CD26 mAbs (19-32, 1F7, 5F8, 16D4B or 9C11) and a humanized anti-CD26 mAb (YS110) which were all previously developed in our laboratory. We have previously shown that these mAbs recognized distinct CD26 regions [26, 29]. All of these mAbs were labeled with biotin or HRP, and we tested all possible combinations of U16-3 mAb and other mAb, or U38-8 mAb and other mAb. However, the absolute value of absorbance was nearly at blank level for all of the combinations, suggesting that both U16-3 mAb and U38-8 mAb are not suitable for sandwich ELISA, and that these two mAbs hardly recognize native sCD26 in the liquid phase.

Taken together, our results obtained from immunostaining, Western blotting, flow cytometry and ELISA assays demonstrate that the newly developed mAbs exhibit significant binding specificity and affinity for denatured human CD26 protein in FFPE cell block and tissue specimens or boiled Western blot samples and recombinant sCD26 protein, as compared with those of control pAb or 19-32 mAb.

Advances in future CD26-related research

Since our data reveal that the newly developed anti-CD26 mAbs can specifically stain denatured human CD26 in FFPE tumor cells with reliable clarity and intensity, we then conducted immunohistochemical staining of FFPE CD26-expressing tumor tissues of hepatocellular carcinoma, renal cell carcinoma, prostate adenocarcinoma, colon adenocarcinoma, and lung adenocarcinoma with U16-3 mAb or U38-8 mAb. As shown in Fig 6A, each tumor tissue stained with U16-3 mAb or U38-8 mAb (panels i and ii) exhibited stronger and broader staining patterns as compared with staining with control pAb [29]. Results from the immunostaining studies indicate that CD26 can be detected both on the cell surface as well as in the cytoplasm of these carcinoma tissues.

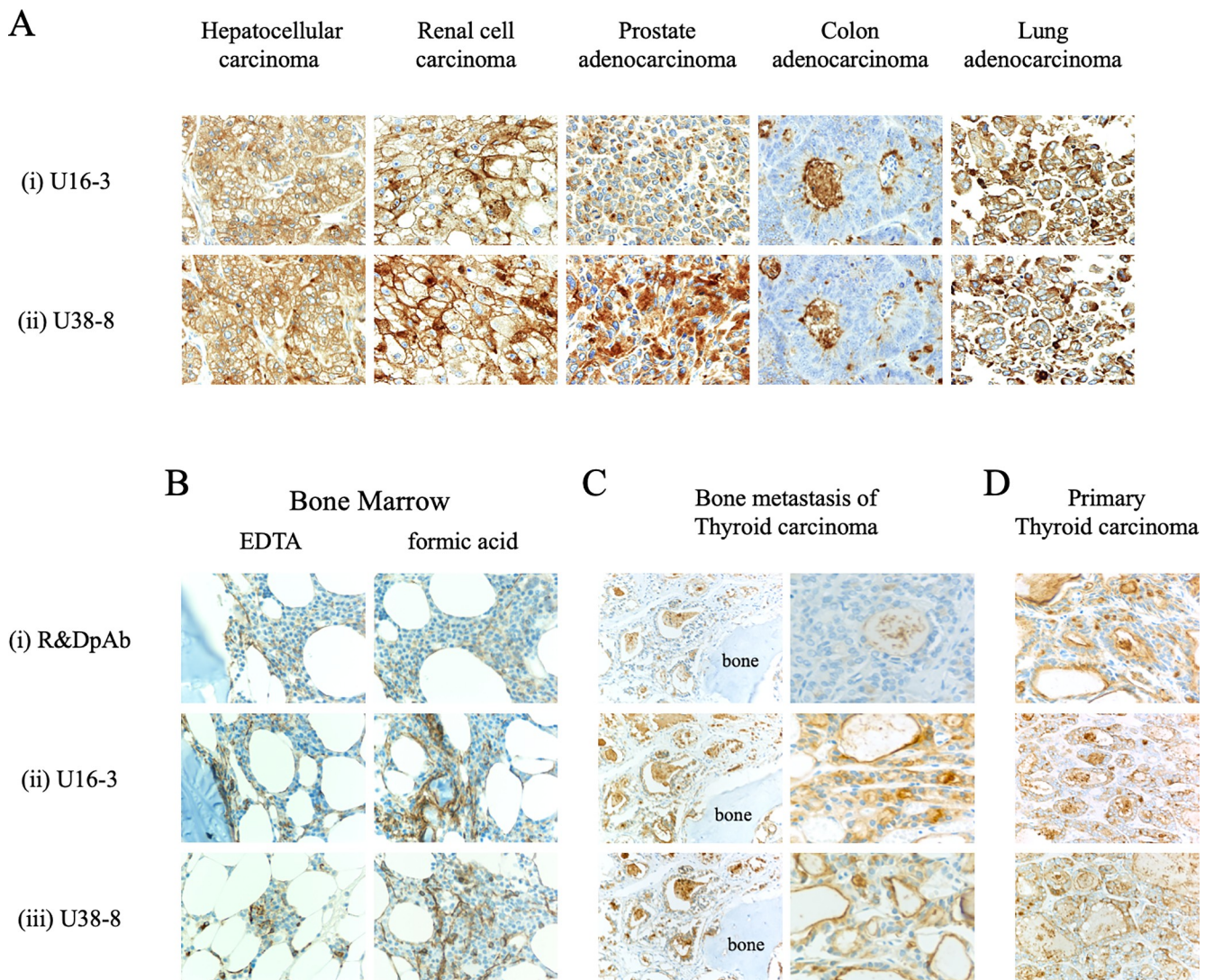


Fig 6. Novel anti-CD26 mAbs exhibit a reliable staining pattern and intensity for various tumors and decalcified specimens. **A.** The tissue specimens of hepatocellular carcinoma, renal cell carcinoma, prostate adenocarcinoma, colon adenocarcinoma or lung adenocarcinoma were stained with purified novel mouse anti-human CD26 mAbs (U16-3 (i) or U38-8 (ii)). Original magnification, 40x. **B, C, D.** The EDTA-decalcified (left panels) or formic acid-decalcified (right panels) tissue specimens of normal human bone and bone marrow (B), formic acid-decalcified tissue specimens of metastatic thyroid carcinoma in the bone (C), or the tissue specimens of primary thyroid carcinoma without decalcification (D) were stained with purified goat anti-human CD26 pAb (R&D Systems (i)) or purified novel mouse anti-human CD26 mAbs (U16-3 (ii) or U38-8 (iii)). Original magnification, 10x (B, left panels of C, D) or 40x (right panels of C). All specimens were counterstained with hematoxylin.

<https://doi.org/10.1371/journal.pone.0218330.g006>

Staining of decalcified specimens with reliable clarity and intensity is well-known to be challenging since proteins are further denatured and/or degenerated in the process of decalcification. Since our results demonstrate that the novel anti-CD26 mAbs have a higher binding affinity for denatured human CD26 protein than that of commercial anti-CD26 pAb (Figs 1, 2, 3 and 5), we proceeded to conduct immunohistochemical staining of decalcified specimens with U16-3 mAb or U38-8 mAb. As shown in Fig 6B, both EDTA-decalcified and formic acid-decalcified normal human bone and bone marrow tissue specimens stained with U16-3 mAb or U38-8 mAb exhibited a bright staining pattern of CD26, with even the distinct vasculature of marrow being specifically stained with reliable intensity, while control pAb could not stain decalcified bone tissue with reliable clarity and intensity (panels i, ii, iii). Moreover, we stained decalcified specimens of metastatic thyroid carcinoma in the bone. CD26 expression was clearly visible on the cell surface and in the cytoplasm of carcinoma cells when stained with U16-3 mAb or U38-8 mAb following decalcification (Fig 6C-ii and 6C-iii). On the other hand, staining of decalcified specimens with control pAb was only faintly observed in colloid space whereas bright staining was observed in the specimens of primary thyroid carcinoma without decalcification (Fig 6C-i and 6D-i). Taken together, these data strongly suggest that the newly developed anti-CD26 mAbs are potentially useful as companion diagnostic agents to analyze tumor CD26 expression in the clinical setting, while advancing future CD26-related research.

Discussion

Although it is difficult to develop anti-human CD26 mAbs that can clearly detect denatured CD26 in FFPE tissues, the anti-CD26 pAb purchased from R&D Systems is able to stain CD26 with reliable clarity and intensity. However, since treatment with targeted therapeutic agents is dependent on detection of the appropriate target antigens on clinical samples, uniformity of the diagnostic reagents is critical, suggesting that mAbs are desirable for diagnostic uses in the clinical setting. In the present study, we have improved the screening methods and succeeded in developing novel anti-human CD26 mAbs that can potentially be used as diagnostic reagents clinically.

CD26 is highly expressed on the surface of MPM cells, especially tumors of the epithelioid and biphasic types, but not on benign mesothelial tissues [21, 28]. We have previously evaluated the prognostic significance of CD26 membrane expression on MPM cells and other clinicopathological factors in those patients, and concluded that the CD26 molecule is a reliable biomarker for predicting potential therapeutic outcome of MPM patients following chemotherapy [28]. Our previous study showed that CD26 is associated with high proliferative activity and invasiveness of MPM cells [22, 23, 28]. Although the exact role of CD26/DPPIV in other cancers remains to be elucidated, CD26 serves as a prognostic marker in multiple tumors. Significantly higher CD26 expression has been shown to be correlated with poorly differentiated CRC, late tumor node metastasis stage, and development of metastasis [10]. In addition, a high CD26 expression level is a predictor of poor outcome after resection of CRC. The disease-free survival of patients with CD26-positive GIST of the stomach is worse than that of patients with CD26-negative GIST [11]. CD26, secretogranin V (SCG5) and carbonic anhydrase XII (CA12) are a three-gene signature that can distinguish malignant thyroid cancers, and is useful for preoperative diagnosis of thyroid cancer [12]. The mRNA level of CD26 is significantly upregulated in advanced-stage urothelial carcinoma and the upregulation of CD26 is most significantly associated with clinical aggressiveness [13]. CD26 expression level in prostate cancer tissues is higher than that of normal prostatic tissues, and is enhanced with prostate cancer stage advancement [14]. These observations strongly suggest that immunohistochemical staining of CD26 in FFPE tumor tissues is important for diagnosis and prognosis

of multiple tumors. Also, more detailed analysis regarding the localization and quantification of CD26 expression may provide additional benefit in the clinical setting.

Specific binding with its target molecule is a well-known characteristic of antibody. However, in Western blot assay, several non-specific bands may often be observed in each sample when immunoblotted with commercial Abs. Similarly, a FFPE negative control sample is often non-specifically stained with the Abs. Under denaturing conditions, the conformation of proteins is changed, and conformational amino acid sequences that do not exist in the physiological condition are generated. If the generated amino acid sequences are similar to the epitope of the Abs, these Abs react with several proteins in the denaturing conditions. Different denaturing conditions such as FFPE treatment, urea treatment and boiling may result in different conformational amino acid sequences. Our previous 19–32 mAb was first screened for selective reactivity with native (undenatured) human CD26 by flow cytometry and ELISA, and we confirmed that 19–32 mAb did not stain Jurkat parent cells by flow cytometry and did not react with blocking protein by ELISA (Fig 4, S2 Fig, Fig 5-i). In addition, we have conducted immunohistochemical staining of nearly one hundred FFPE MPM tissue specimens with 19–32 mAb, and found that not all of the MPM samples were stained with 19–32 mAb. However, on the other hand, FFPE cell block specimens of CD26-negative tumor cell lines were all unexpectedly stained with 19–32 mAb (Fig 1A-ii), suggesting that 19–32 mAb binds with human CD26 as well as denatured antigen(s) commonly expressed in tumor cell lines. Selection of screening methods is crucially important for the development of novel mAb designed to serve specific purpose. In the present study, hybridomas producing high levels of murine IgG were all screened for immunostaining of FFPE cell blocks. From a total of 429 clones, we obtained only 5 clones capable of distinguishing CD26-positive cells from CD26-negative cells by immunostaining. These screening methods utilizing a set of various human CD26-positive or negative tumor cell lines are useful for selecting mAbs that specifically recognize denatured CD26 with a high signal-to-noise ratio.

Meanwhile, results from flow cytometry showed that both U16-3 mAb and U38-8 mAb did not bind to native (undenatured) human CD26 on the cell surface (Fig 4, S2 Fig). Moreover, although both U16-3 mAb and U38-8 mAb exhibited strong binding affinity to the immobilized native sCD26 protein (Fig 5-i), these two mAbs barely recognized native sCD26 protein in the liquid phase as confirmed by sandwich ELISA. In contrast, the antibody-absorption test showed that staining of MSTO-CD26 and JMN ctrl-shRNA cells with U16-3 mAb or U38-8 mAb was completely inhibited by native sCD26 protein (Fig 1B). In that experiment, 6.67 pmol of U16-3 mAb or U38-8 mAb was preincubated with 909 pmol of native sCD26 protein. More than one hundred times larger amount of antigen was needed for the antibody-absorption test, suggesting that these two mAbs did not react well with native sCD26 protein. Although the precise difference in the conformation of CD26 protein on the cell surface and that of sCD26 protein in the liquid phase is not elucidated, our data strongly suggest that these novel anti-CD26 mAbs do not have strong binding affinity to native human CD26. We have previously shown that the epitopes of human CD26 defined by anti-CD26 mAbs were roughly categorized by 5 separate groups utilizing human CD26 deletion mutant- or human-rat CD26 swap mutant-transfected cells [26]. Cross-blocking studies such as flow cytometry or sandwich ELISA using several anti-CD26 mAbs, the binding regions of which were already characterized, enabled us to speculate on the epitope defined by 19–32 mAb [29]. However, both U16-3 mAb and U38-8 mAb cannot be used for flow cytometry and sandwich ELISA. Moreover, it is quite difficult to prepare denatured CD26 protein that can exactly replicate the conformation of CD26 in FFPE section or in decalcified tissue section. These limitations have limited our ability to analyze the precise epitopes defined by the novel anti-CD26 mAbs. However, accumulating evidences regarding the conformational change of denatured proteins are found in

the protein database, and we have already obtained data regarding the amino acid sequence of the variable region in both heavy chain and light chain of U16-3 mAb and U38-8 mAb, utilizing the 5'-RACE PCR method. We are currently examining *in silico* predictions of the three-dimensional structure of an antigen-antibody complex utilizing such program as Rosetta [32].

The mAbs capable of staining target molecules with reliable clarity and intensity in decalcified specimens are valuable. We have recently reported that CD26 is expressed on normal human osteoclasts, with its expression being enhanced following activation [33]. CD26 expression is increased in the process of osteoclast differentiation, and may be involved in p38 MAPK signaling. Interestingly, the humanized anti-CD26 mAb (YS110) inhibits early osteoclast precursor differentiation into osteoclasts [33]. Since our present data indicate that both U16-3 mAb and U38-8 mAb can clearly stain CD26 in the bone or on tumor cells in calcified tissues (Fig 6B and 6C), these mAbs are expected to contribute to future CD26-related research involving normal tissues and tumor/inflammatory lesions accompanied by calcification. Furthermore, these mAbs are potentially useful for the analysis of CD26 expression in cancer patients with bony metastasis, and may help decide the appropriateness of YS110 therapy for future cancer patients.

Supporting information

S1 Fig. mRNA and cell surface protein expression of CD26 in the human tumor cell lines used in this study.

A. Total RNA was extracted from the indicated cell lines by the use of Rneasy Mini Kit according to the manufacturer's instructions (QIAGEN, Valencia, CA), and cDNA was produced by using PrimeScript II 1st strand cDNA Synthesis Kit (TaKaRa Bio, Shiga, Japan) with oligo dT primer. Quantification of mRNA was performed using the 7500 Real-Time PCR System and SYBR Select Master Mix (Applied Biosystems, Foster City, CA). The obtained data were analyzed with 7500 System SDS Software (Applied Biosystems), being normalized to hypoxanthine phosphoribosyltransferase 1 (HPRT1) expression. The PCR was performed using the following primers: CD26 forward primer, 5' -GTACACAGAACGTTACA TGGGTCTC-3'; reverse primer, 5' -TCAGCTCTGCTCATGACTGTTG-3'; HPRT1 forward primer, 5' -CAGTC AACAGGGGACATAAAAG-3'; reverse primer, 5' -CCTGACCAAGGAAAGCAAAG-3'. Data are shown as mean \pm S.D. of triplicate samples.

B. The indicated cells were incubated with PE-labeled isotype control (BD Biosciences, clone MOPC-21 (i)) or PE-labeled commercial mouse anti-human CD26 mAb (BD Biosciences, clone M-A261 (ii)), and cell surface expression of CD26 was analyzed by flow cytometry. Two-dimensional dot plot (horizontal axis: CD26, longitudinal axis: non-staining) gated for viable cells is shown. A representative plot of three independent experiments is shown, and similar results were obtained with each experiment.

Among cell lines used in this study, mRNA and cell surface protein expression of CD26 in Jurkat-CD26 is the most prominent, and the expression levels of MSTO-CD26 are higher than those of JMN ctrl-shRNA cells, whereas CD26 is hardly expressed even at mRNA level in MSTO parent, JMN CD26-shRNA, A549 and Jurkat parent.

(PDF)

S2 Fig. Representative results of flow cytometry with novel anti-CD26 mAbs. MSTO parent, MSTO-CD26, JMN CD26-shRNA, JMN ctrl-shRNA, A549, Jurkat parent or Jurkat-CD26 cells were incubated with unlabeled isotype control or purified mouse anti-human CD26 mAb (19-32 (ii), U16-3 (iii) or U38-8 (iv)) or purified goat anti-human CD26 pAb (R&D Systems (v)), and subsequently stained with PE-labeled goat anti-mouse Ig pAb or PE-labeled donkey anti-goat IgG Ab, and analyzed by flow cytometry. PE-labeled commercial mouse anti-human CD26 mAb (BD Biosciences, clone M-A261 (i)) was utilized as a positive control. Data are

shown as histogram of CD26 intensity (red lines), and the gray area in each histogram shows data of the isotype control. A representative histogram of three independent experiments is shown, and similar results were obtained in each experiment.

PE-labeled anti-CD26 mAb purchased from BD Biosciences, 19–32 mAb or anti-CD26 pAb purchased from R&D Systems could stain MSTO-CD26, JMN ctrl-shRNA or Jurkat-CD26 while MSTO parent, JMN CD26-shRNA, A549 or Jurkat parent did not demonstrate staining with these anti-CD26 Abs. In contrast, both U16-3 mAb and U38-8 mAb did not stain any of the tumor cell lines (similar to results seen with isotype controls).

(PDF)

S3 Fig. Immunohistochemical staining with anti-CD26 mAbs incapable of detecting denatured human CD26. The tissue specimens of liver, kidney, prostate or two cases of malignant mesothelioma were stained with purified mouse anti-human CD26 mAbs (1F7 (i) or 5F8 (ii)), which were previously developed in our laboratory. Original magnification, 4x. All specimens were counterstained with hematoxylin.

No apparent staining of CD26 was observed in the formalin-fixed paraffin-embedded tissue specimens stained with 1F7 mAb or 5F8 mAb.

(PDF)

Author Contributions

Conceptualization: Ryo Hatano, Taketo Yamada, Chikao Morimoto.

Funding acquisition: Ryo Hatano, Taketo Yamada, Kei Ohnuma, Chikao Morimoto.

Investigation: Ryo Hatano, Taketo Yamada, Hiroko Madokoro, Haruna Otsuka, Eriko Komiya, Takumi Itoh, Yuka Narita.

Supervision: Taketo Yamada, Kei Ohnuma, Chikao Morimoto.

Validation: Shuji Matsuoka.

Visualization: Ryo Hatano, Taketo Yamada.

Writing – original draft: Ryo Hatano.

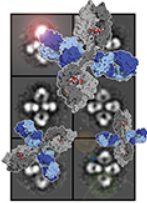
Writing – review & editing: Taketo Yamada, Satoshi Iwata, Hiroto Yamazaki, Nam H. Dang, Kei Ohnuma, Chikao Morimoto.

References

1. Fox DA, Hussey RE, Fitzgerald KA, Acuto O, Poole C, Palley L, et al. Ta1, a novel 105 KD human T cell activation antigen defined by a monoclonal antibody. *J Immunol.* 1984; 133(3):1250–6. PMID: [6205075](#)
2. Tanaka T, Camerini D, Seed B, Torimoto Y, Dang NH, Kameoka J, et al. Cloning and functional expression of the T cell activation antigen CD26. *J Immunol.* 1992; 149(2):481–6. PMID: [1352530](#)
3. Morimoto C, Schlossman SF. The structure and function of CD26 in the T-cell immune response. *Immunol Rev.* 1998; 161:55–70. PMID: [9553764](#)
4. Ohnuma K, Dang NH, Morimoto C. Revisiting an old acquaintance: CD26 and its molecular mechanisms in T cell function. *Trends Immunol.* 2008; 29(6):295–301. <https://doi.org/10.1016/j.it.2008.02.010> PMID: [18456553](#)
5. Ohnuma K, Takahashi N, Yamochi T, Hosono O, Dang NH, Morimoto C. Role of CD26/dipeptidyl peptidase IV in human T cell activation and function. *Front Biosci.* 2008; 13:2299–310. PMID: [17981712](#)
6. De Meester I, Korom S, Van Damme J, Scharpe S. CD26, let it cut or cut it down. *Immunol Today.* 1999; 20(8):367–75. PMID: [10431157](#)
7. Morimoto C, Torimoto Y, Levinson G, Rudd CE, Schrieber M, Dang NH, et al. 1F7, a novel cell surface molecule, involved in helper function of CD4 cells. *J Immunol.* 1989; 143(11):3430–9. PMID: [2479677](#)

8. Hatano R, Ohnuma K, Yamamoto J, Dang NH, Morimoto C. CD26-mediated co-stimulation in human CD8(+) T cells provokes effector function via pro-inflammatory cytokine production. *Immunology*. 2013; 138(2):165–72. <https://doi.org/10.1111/imm.12028> PMID: 23113658
9. Havre PA, Abe M, Urasaki Y, Ohnuma K, Morimoto C, Dang NH. The role of CD26/dipeptidyl peptidase IV in cancer. *Front Biosci*. 2008; 13:1634–45. PMID: 17981655
10. Lam CS, Cheung AH, Wong SK, Wan TM, Ng L, Chow AK, et al. Prognostic significance of CD26 in patients with colorectal cancer. *PLoS One*. 2014; 9(5):e98582. <https://doi.org/10.1371/journal.pone.0098582> PMID: 24870408
11. Yamaguchi U, Nakayama R, Honda K, Ichikawa H, Hasegawa T, Shitashige M, et al. Distinct gene expression-defined classes of gastrointestinal stromal tumor. *J Clin Oncol*. 2008; 26(25):4100–8. <https://doi.org/10.1200/JCO.2007.14.2331> PMID: 18757323
12. Zheng B, Liu J, Gu J, Lu Y, Zhang W, Li M, et al. A three-gene panel that distinguishes benign from malignant thyroid nodules. *Int J Cancer*. 2015; 136(7):1646–54. <https://doi.org/10.1002/ijc.29172> PMID: 25175491
13. Liang PI, Yeh BW, Li WM, Chan TC, Chang IW, Huang CN, et al. DPP4/CD26 overexpression in urothelial carcinoma confers an independent prognostic impact and correlates with intrinsic biological aggressiveness. *Oncotarget*. 2017; 8(2):2995–3008. <https://doi.org/10.18632/oncotarget.13820> PMID: 27936466
14. Lu Z, Qi L, Bo XJ, Liu GD, Wang JM, Li G. Expression of CD26 and CXCR4 in prostate carcinoma and its relationship with clinical parameters. *J Res Med Sci*. 2013; 18(8):647–52. PMID: 24379839
15. Ghani FI, Yamazaki H, Iwata S, Okamoto T, Aoe K, Okabe K, et al. Identification of cancer stem cell markers in human malignant mesothelioma cells. *Biochem Biophys Res Commun*. 2011; 404(2):735–42. <https://doi.org/10.1016/j.bbrc.2010.12.054> PMID: 21163253
16. Yamazaki H, Naito M, Ghani FI, Dang NH, Iwata S, Morimoto C. Characterization of cancer stem cell properties of CD24 and CD26-positive human malignant mesothelioma cells. *Biochem Biophys Res Commun*. 2012; 419(3):529–36. <https://doi.org/10.1016/j.bbrc.2012.02.054> PMID: 22369943
17. Pang R, Law WL, Chu AC, Poon JT, Lam CS, Chow AK, et al. A subpopulation of CD26+ cancer stem cells with metastatic capacity in human colorectal cancer. *Cell Stem Cell*. 2010; 6(6):603–15. <https://doi.org/10.1016/j.stem.2010.04.001> PMID: 20569697
18. Herrmann H, Sadovnik I, Cerny-Reiterer S, Rulicke T, Stefanzi G, Willmann M, et al. Dipeptidylpeptidase IV (CD26) defines leukemic stem cells (LSC) in chronic myeloid leukemia. *Blood*. 2014; 123(25):3951–62. <https://doi.org/10.1182/blood-2013-10-536078> PMID: 24778155
19. Ho L, Aytac U, Stephens LC, Ohnuma K, Mills GB, McKee KS, et al. In vitro and in vivo antitumor effect of the anti-CD26 monoclonal antibody 1F7 on human CD30+ anaplastic large cell T-cell lymphoma Karpas 299. *Clin Cancer Res*. 2001; 7(7):2031–40. PMID: 11448921
20. Inamoto T, Yamochi T, Ohnuma K, Iwata S, Kina S, Inamoto S, et al. Anti-CD26 monoclonal antibody-mediated G1-S arrest of human renal clear cell carcinoma Caki-2 is associated with retinoblastoma substrate dephosphorylation, cyclin-dependent kinase 2 reduction, p27(kip1) enhancement, and disruption of binding to the extracellular matrix. *Clin Cancer Res*. 2006; 12(11 Pt 1):3470–7.
21. Inamoto T, Yamada T, Ohnuma K, Kina S, Takahashi N, Yamochi T, et al. Humanized anti-CD26 monoclonal antibody as a treatment for malignant mesothelioma tumors. *Clin Cancer Res*. 2007; 13(14):4191–200. <https://doi.org/10.1158/1078-0432.CCR-07-0110> PMID: 17634548
22. Okamoto T, Iwata S, Yamazaki H, Hatano R, Komiya E, Dang NH, et al. CD9 negatively regulates CD26 expression and inhibits CD26-mediated enhancement of invasive potential of malignant mesothelioma cells. *PLoS One*. 2014; 9(1):e86671. <https://doi.org/10.1371/journal.pone.0086671> PMID: 24466195
23. Yamamoto J, Ohnuma K, Hatano R, Okamoto T, Komiya E, Yamazaki H, et al. Regulation of somatostatin receptor 4-mediated cytostatic effects by CD26 in malignant pleural mesothelioma. *Br J Cancer*. 2014; 110(9):2232–45. <https://doi.org/10.1038/bjc.2014.151> PMID: 24743707
24. Angevin E, Isambert N, Trillet-Lenoir V, You B, Alexandre J, Zalcman G, et al. First-in-human phase 1 of YS110, a monoclonal antibody directed against CD26 in advanced CD26-expressing cancers. *Br J Cancer*. 2017; 116(9):1126–34. <https://doi.org/10.1038/bjc.2017.62> PMID: 28291776
25. ClinicalTrials.gov. 2017. Clinical Study of YS110 in Patients With Malignant Pleural Mesothelioma. <https://www.clinicaltrials.gov/ct2/show/NCT03177668?term=YS110&cond=Mesotheliomas+Pleural&rank=1>
26. Dong RP, Tachibana K, Hegen M, Scharpe S, Cho D, Schlossman SF, et al. Correlation of the epitopes defined by anti-CD26 mAbs and CD26 function. *Mol Immunol*. 1998; 35(1):13–21. PMID: 9683260
27. Yamada K, Hayashi M, Madokoro H, Nishida H, Du W, Ohnuma K, et al. Nuclear localization of CD26 induced by a humanized monoclonal antibody inhibits tumor cell growth by modulating of POLR2A

- transcription. *PLoS One*. 2013; 8(4):e62304. <https://doi.org/10.1371/journal.pone.0062304> PMID: [23638030](https://pubmed.ncbi.nlm.nih.gov/23638030/)
28. Aoe K, Amatya VJ, Fujimoto N, Ohnuma K, Hosono O, Hiraki A, et al. CD26 overexpression is associated with prolonged survival and enhanced chemosensitivity in malignant pleural mesothelioma. *Clin Cancer Res*. 2012; 18(5):1447–56. <https://doi.org/10.1158/1078-0432.CCR-11-1990> PMID: [22261805](https://pubmed.ncbi.nlm.nih.gov/22261805/)
 29. Hatano R, Yamada T, Matsuoka S, Iwata S, Yamazaki H, Komiya E, et al. Establishment of monoclonal anti-human CD26 antibodies suitable for immunostaining of formalin-fixed tissue. *Diagn Pathol*. 2014; 9:30. <https://doi.org/10.1186/1746-1596-9-30> PMID: [24502396](https://pubmed.ncbi.nlm.nih.gov/24502396/)
 30. Torimoto Y, Dang NH, Tanaka T, Prado C, Schlossman SF, Morimoto C. Biochemical characterization of CD26 (dipeptidyl peptidase IV): functional comparison of distinct epitopes recognized by various anti-CD26 monoclonal antibodies. *Mol Immunol*. 1992; 29(2):183–92. PMID: [1371820](https://pubmed.ncbi.nlm.nih.gov/1371820/)
 31. Tanaka T, Duke-Cohan JS, Kameoka J, Yaron A, Lee I, Schlossman SF, et al. Enhancement of antigen-induced T-cell proliferation by soluble CD26/dipeptidyl peptidase IV. *Proc Natl Acad Sci U S A*. 1994; 91(8):3082–6. <https://doi.org/10.1073/pnas.91.8.3082> PMID: [7909158](https://pubmed.ncbi.nlm.nih.gov/7909158/)
 32. Weitzner BD, Jeliaskov JR, Lyskov S, Marze N, Kuroda D, Frick R, et al. Modeling and docking of antibody structures with Rosetta. *Nat Protoc*. 2017; 12(2):401–16. <https://doi.org/10.1038/nprot.2016.180> PMID: [28125104](https://pubmed.ncbi.nlm.nih.gov/28125104/)
 33. Nishida H, Suzuki H, Madokoro H, Hayashi M, Morimoto C, Sakamoto M, et al. Blockade of CD26 signaling inhibits human osteoclast development. *J Bone Miner Res*. 2014; 29(11):2439–55. <https://doi.org/10.1002/jbmr.2277> PMID: [24821427](https://pubmed.ncbi.nlm.nih.gov/24821427/)



Characterization of novel anti-IL-26 neutralizing monoclonal antibodies for the treatment of inflammatory diseases including psoriasis

Ryo Hatano, Takumi Itoh, Haruna Otsuka, Sayo Okamoto, Eriko Komiya, Satoshi Iwata, Thomas M. Aune, Nam H. Dang, Kyoko Kuwahara-Arai, Kei Ohnuma & Chikao Morimoto

To cite this article: Ryo Hatano, Takumi Itoh, Haruna Otsuka, Sayo Okamoto, Eriko Komiya, Satoshi Iwata, Thomas M. Aune, Nam H. Dang, Kyoko Kuwahara-Arai, Kei Ohnuma & Chikao Morimoto (2019) Characterization of novel anti-IL-26 neutralizing monoclonal antibodies for the treatment of inflammatory diseases including psoriasis, *mAbs*, 11:8, 1428-1442, DOI: [10.1080/19420862.2019.1654305](https://doi.org/10.1080/19420862.2019.1654305)

To link to this article: <https://doi.org/10.1080/19420862.2019.1654305>

 View supplementary material [↗](#)

 Accepted author version posted online: 09 Aug 2019.
Published online: 18 Aug 2019.

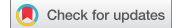
 Submit your article to this journal [↗](#)

 Article views: 174

 View related articles [↗](#)

 View Crossmark data [↗](#)

REPORT



Characterization of novel anti-IL-26 neutralizing monoclonal antibodies for the treatment of inflammatory diseases including psoriasis

Ryo Hatano^a, Takumi Itoh ^a, Haruna Otsuka ^a, Sayo Okamoto ^a, Eriko Komiya^{a,b}, Satoshi Iwata ^a, Thomas M. Aune ^c, Nam H. Dang^d, Kyoko Kuwahara-Arai^e, Kei Ohnuma^a, and Chikao Morimoto ^a

^aDepartment of Therapy Development and Innovation for Immune Disorders and Cancers, Graduate School of Medicine, Juntendo University, Tokyo, Japan; ^bInstitute for Environmental and Gender Specific Medicine, Juntendo University Graduate School of Medicine, Urayasu, Japan; ^cDepartment of Medicine, Vanderbilt University School of Medicine, Vanderbilt University Medical Center, Nashville, TN, USA; ^dDivision of Hematology/Oncology, University of Florida, Gainesville, FL, USA; ^eDepartment of Microbiology, Juntendo University School of Medicine, Tokyo, Japan

ABSTRACT

Interleukin (IL)-26, known as a Th17 cytokine, acts on various cell types and has multiple biological functions. Although its precise role still remains to be elucidated, IL-26 is suggested to be associated with the pathology of diverse chronic inflammatory diseases such as psoriasis, inflammatory bowel diseases and rheumatoid arthritis. To develop novel neutralizing anti-human IL-26 monoclonal antibodies (mAbs) for therapeutic use in the clinical setting, we immunized mice with human IL-26 protein. Hybridomas producing anti-IL-26 mAbs were screened for various *in vitro* functional assays, STAT3 phosphorylation and antibiotic assays. Although the IL-20RA/IL-10RB heterodimer is generally believed to be the IL-26 receptor, our data strongly suggest that both IL-20RA-dependent and -independent pathways are involved in IL-26-mediated stimulation. We also investigated the potential therapeutic effect of anti-IL-26 mAbs in the imiquimod-induced psoriasis-like murine model using human IL-26 transgenic mice. These screening methods enabled us to develop novel neutralizing anti-human IL-26 mAbs. Importantly, administration of IL-26-neutralizing mAb did not have an effect on the antimicrobial activity of IL-26. Taken together, our data strongly suggest that our newly developed anti-human IL-26 mAb is a potential therapeutic agent for the treatment of diverse chronic inflammatory diseases including psoriasis.

ARTICLE HISTORY

Received 14 June 2019
Revised 25 July 2019
Accepted 6 August 2019

KEYWORDS

Interleukin-26; monoclonal antibody; neutralization; chronic inflammatory diseases; psoriasis

Introduction

Originally discovered in *herpesvirus saimiri*-transformed T cells,¹ human interleukin (IL)-26 is a 171-amino acid protein that belongs to the IL-10 family of cytokines, a family that includes IL-10, IL-19, IL-20, IL-22 and IL-24.^{2,3} Human IL-26 protein is encoded by the *IL26* gene located on chromosome 12q15 between the genes for interferon (IFN)- γ and IL-22, and is conserved in several vertebrate species but not found in mice and rats.⁴ Production of IL-26 was first reported from memory CD4⁺ T cells and natural killer (NK) cells,⁵ and IL-26 is now known as a Th17 cytokine.⁶ Recently, production of IL-26 by various cell types, such as synoviocytes from rheumatoid arthritis patients, alveolar macrophages and bronchial epithelial cells, has been reported.^{7–9} It is generally believed that the IL-20RA/IL-10RB heterodimer is the IL-26 receptor. Binding of IL-26 to IL-20RA/IL-10RB results in functional activation via STAT3 phosphorylation.¹⁰ While IL-10RB is ubiquitously expressed in various cells, expression of IL-20RA, the key IL-26 receptor subunit that mediates IL-26 signaling, is observed in epithelial cell types such as keratinocytes, intestinal and lung epithelial cells, strongly suggesting that IL-26 likely plays important roles in cutaneous and mucosal immunity.

Studies on the effect of IL-26 on IL-20RA-expressing cells have shown that IL-26 regulates production of IL-8 from keratinocytes, and enhances the production of IL-10, IL-8, and tumor necrosis factor (TNF) and the surface expression of CD54 (ICAM-1) on intestinal epithelial cells.^{10,11} Although the expression of IL-20RA is not observed in human peripheral blood T cells, B cells, NK cells and monocytes,⁵ IL-26 effects on human monocytes and NK cells have also been reported recently. IL-26 acts on human monocytes and NK cells to induce the production of inflammatory cytokines and to enhance cell surface TRAIL expression.^{7,12} Moreover, we have recently shown that IL-26 directly acts on vascular endothelial cells to promote proliferation and tube formation at a similar level as vascular endothelial growth factor (VEGF) regardless of the deficiency of IL-20RA expression in vascular endothelial cells.¹³ These findings strongly implicate the existence of a distinct IL-26 receptor other than the IL-20RA/IL-10RB heterodimer. In addition to its immunological effects, IL-26 exerts antimicrobial activity and contributes to host defense against both extracellular and intracellular bacteria.^{14,15} However, the antimicrobial activity of IL-26 seems to be inefficient in hidradenitis suppurativa patients, a chronic inflammatory skin disorder accompanied by severe and recurrent skin infections, suggesting

CONTACT Chikao Morimoto  morimoto@ims.u-tokyo.ac.jp  Department of Therapy Development and Innovation for Immune Disorders and Cancers, Graduate School of Medicine, Juntendo University, 2-1-1, Hongo, Bunkyo-ku, Tokyo 113-8421, Japan

This article has been republished with minor changes. These changes do not impact the academic content of the article.

 Supplemental data for this article can be accessed on the [publisher's website](#).

that cutaneous antimicrobial incompetence in hidradenitis suppurativa may be related to IL-26.¹⁶

Due to the deficiency of the gene encoding IL-26 in mice, the precise functions and identification of target cells of IL-26 in inflammatory disorders remain to be elucidated. Meanwhile, recent studies have demonstrated that IL-26 is locally expressed at inflammatory sites, and its expression level is increased in serum, sputum, synovial fluid, bronchoalveolar lavage fluid and cerebrospinal fluid of patients with diverse chronic inflammatory diseases such as psoriasis, inflammatory bowel diseases, rheumatoid arthritis, spondyloarthritis, multiple sclerosis, pediatric asthma, Behcet's disease, allergic contact dermatitis and chronic obstructive pulmonary disease.^{6,7,11,17–23} Our group has used human IL-26 bacterial artificial chromosome (BAC) transgenic (hIL-26Tg) mice^{24,25} or human T cell-transplanted immunodeficient mice to elucidate the role of IL-26 in inflammatory disorders. We recently showed that IL-26 activates both human and murine fibroblasts, leading to increased collagen production, and that human IL-26-producing CD4 T cells are deeply involved in the pathophysiology of pulmonary chronic graft-versus-host disease (GVHD).^{26,27} More recently, we found that vascularization and immune cell infiltration were dramatically enhanced in hIL-26Tg mice in the imiquimod (IMQ), a potent agonist of Toll-like receptor (TLR) 7 and TLR8, -induced psoriasis-like murine model.¹³ These findings strongly suggest that IL-26 may represent a novel promising therapeutic target for refractory chronic inflammatory diseases, for which currently available drugs cannot yet achieve the desired therapeutic outcome.

Although several anti-human IL-26 monoclonal antibodies (mAbs) are commercially available, these mAbs are designated as research reagents for Western blotting, flow cytometry or enzyme-linked immunosorbent assay (ELISA), not for neutralization. We and other groups showed that polyclonal antibodies (pAb) purchased from R&D Systems completely blocked IL-26 stimulation *in vitro* while also having *in vivo* functions.^{10,12,26} However, pAbs are not the ideal reagents for therapeutic use in the clinical setting. Selection of the appropriate screening methods is crucially important for the development of novel mAbs designed to serve specific purposes. In contrast with the mAbs that are only suitable for flow cytometry or ELISA, anti-human IL-26 mAbs useful for neutralization can recognize specific regions of IL-26 that are essential for binding with its receptor. Although the number of uncharacterized receptors involved in IL-26-mediated activation is not yet known, the binding regions of IL-26 to these receptors would be different from the IL-26 binding domain for IL-20RA/IL-10RB, and the inhibitory effect of anti-IL-26 neutralizing mAbs on the binding of IL-26 to its receptors would be different, depending on the kind of receptor.

For these reasons, to accurately evaluate the neutralizing capacity of mAbs in this study, our chosen screening methods included both *in vitro* functional assays utilizing various cell types and *in vivo* evaluation of the potential therapeutic effect, resulting in the successful development of novel neutralizing anti-human IL-26 mAbs. Our data strongly suggest that the newly developed anti-human IL-26 mAbs may represent a novel promising therapeutic strategy for the treatment of diverse chronic inflammatory diseases including psoriasis and chronic GVHD.

Results

Development of novel neutralizing anti-human IL-26 mAbs

To develop novel anti-human IL-26 neutralizing mAbs for therapeutic use, we immunized mice with recombinant human IL-26 protein. After the fusion of splenocytes of immunized mice and P3U1 myeloma cells, the culture supernatant was first screened by ELISA for selective reactivity with human IL-26. In the first screening, 40 ng of recombinant human IL-26 was coated per well. To exclude the possibility of non-specific binding to the blocking proteins, we prepared the wells coated with carbonate bicarbonate buffer alone (without recombinant human IL-26), subsequently blocked with blocking proteins and incubated with hybridoma supernatants. From our examination of various blocking proteins such as bovine serum albumin, fetal bovine serum (FBS) and milk proteins, BlockAce containing milk proteins was the best blocking buffer to reduce the background absorbance. If the absorbance to human IL-26 was higher than 0.5, the clone was judged to be sufficiently reactive to human IL-26. As a result of the first screening, more than 80 clones were selected for the next screening.

Binding with the IL-20RA/IL-10RB heterodimer resulting in functional activation via STAT3 phosphorylation is a well-known characteristic of IL-26. Therefore, to screen for anti-human IL-26 mAbs suitable for neutralization of IL-26, *in vitro* functional assays utilizing IL-20RA-expressing cells were conducted for the next round of screening. We examined mRNA and cell surface protein expression of IL-20RA and IL-10RB in several cell lines by real-time RT-PCR and flow cytometry, respectively. As reported previously,^{5,10,11,28} mRNA expression of IL-20RA was detected in the human keratinocyte cell line HaCaT, human colon cancer cell lines COLO205, LoVo, HT-29 and human gastric cancer cell line MKN45 (Figure S1(a)). Among them, the expression of IL-20RA in COLO205 was the most prominent at both mRNA and cell surface protein levels. In contrast, neither mRNA nor cell surface protein expression was detected in human umbilical vein endothelial cells (HUVEC) (Figure S1). The expression of IL-10RB was detected at both mRNA and cell surface protein levels in all the cells. Although multiple biological effects of IL-26 on various cell types have been reported, we focused on ICAM-1 expression on COLO205 following IL-26 stimulation. COLO205 was then stimulated with IL-26 in the presence of the culture supernatant from more than 80 clones, and cell surface ICAM-1 expression on COLO205 was analyzed by flow cytometry. The clones that had the potential to inhibit ICAM-1 expression on IL-26-stimulated COLO205 were screened, and the neutralizing capacity of each clone was reexamined following purification of mAbs from culture supernatants. As a result of the second screening utilizing COLO205, we obtained 4 clones with the potential to neutralize human IL-26.

The reactivity of the representative 4 clones to human IL-26 was confirmed by ELISA. As shown in Figure 1(a), all the novel anti-IL-26 mAbs reacted well to the immobilized IL-26, and the absolute value of absorbance increased in an antigen dose-dependent manner. Among them, the absolute value of absorbance to IL-26 incubated with 20–3 mAb or 69–10 mAb was

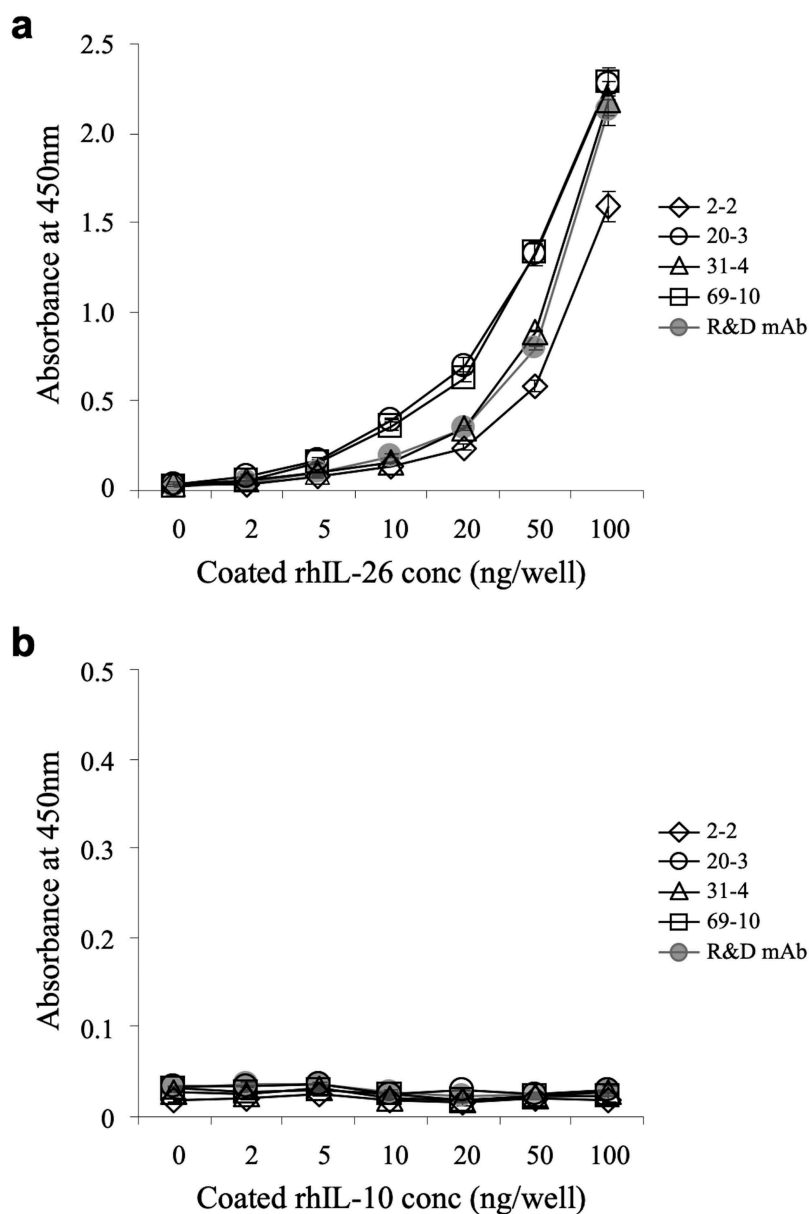


Figure 1. Representative results of ELISA analysis with novel anti-IL-26 mAbs.

Immobilized recombinant human IL-26 (rhIL-26) (a) or IL-10 (rhIL-10) (b) was incubated with purified novel mouse anti-human IL-26 mAb (2-2, 20-3, 31-4 or 69-10) or commercial mouse anti-human IL-26 mAb (R&D Systems). The absorbance at 450 nm/570 nm was measured. Representative data of three independent experiments are shown as mean \pm S.D. of triplicate samples, and similar results were obtained in each experiment.

particularly higher than the absorbance to IL-26 incubated with the commercially available anti-IL-26 mAb (Figure 1(a)). Since human IL-26 has been categorized into the IL-10 family, with approximately 25% homology and 47% similarity to human IL-10,²⁹ the reactivity of the novel anti-IL-26 mAbs to immobilized human IL-10 was analyzed. No non-specific binding to human IL-10 was observed in the 4 mAbs and commercially available anti-IL-26 mAb (Figure 1(b)).

The inhibitory effect of the novel anti-IL-26 mAbs on cell surface ICAM-1 expression on IL-26-stimulated COLO205 cells

Although we could not obtain mAb that completely suppressed ICAM-1 expression on IL-26-stimulated COLO205, the addition of 2-2 mAb, 20-3 mAb, 31-4 mAb or 69-10 mAb partially

inhibited ICAM-1 expression on IL-26-stimulated COLO205 (Figure 2(a)). Of note, while addition of the commercially available anti-IL-26 pAb completely inhibited ICAM-1 expression on IL-26-stimulated COLO205 to a level similar to unstimulated COLO205, addition of the commercially available anti-IL-20RA pAb only partially inhibited ICAM-1 expression on IL-26-stimulated COLO205 to a level similar to 69-10 mAb (Figure 2(a)). Addition of the commercially available anti-IL-10RB pAb hardly affected ICAM-1 expression on IL-26-stimulated COLO205 (Figure 2(a)).

We also examined the inhibitory effect of a combination of novel anti-IL-26 mAbs on ICAM-1 expression. As shown in Figure 2(b), a combination of 69-10 mAb and 2-2 mAb additively inhibited ICAM-1 expression on IL-26-stimulated COLO205 compared with 69-10 mAb alone. Moreover, addition of 20-3

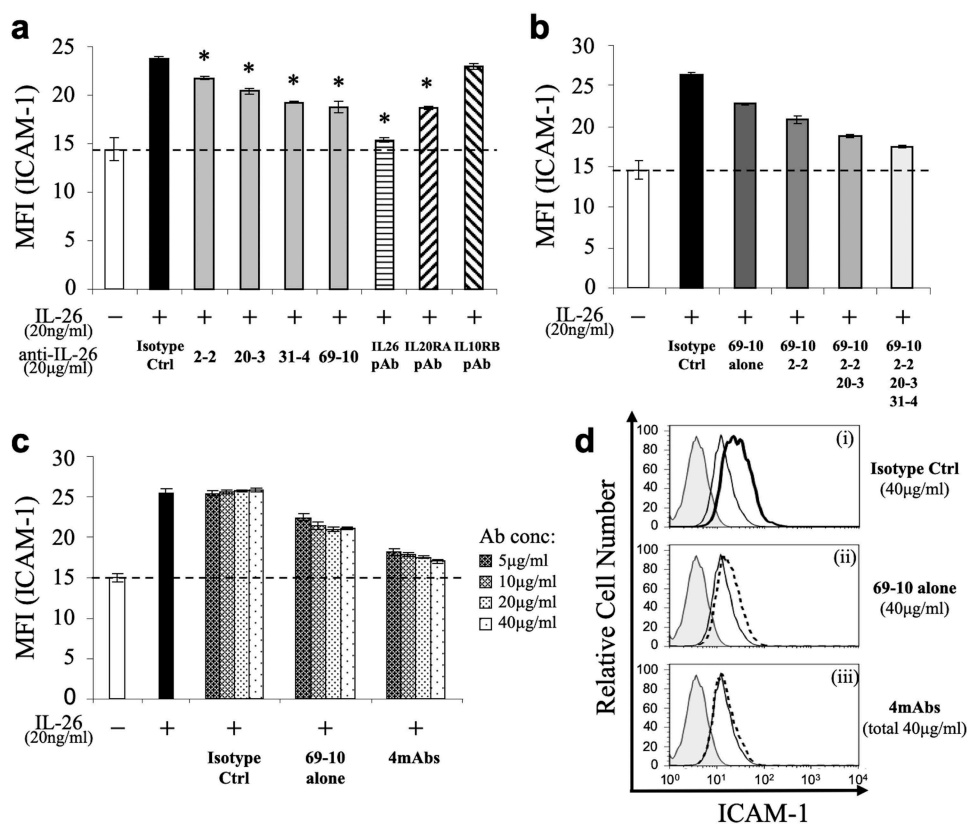


Figure 2. Addition of novel anti-IL-26 mAbs inhibits cell surface ICAM-1 expression on IL-26-stimulated COLO205 cells.

COLO205 cells were stimulated with recombinant human IL-26 (20 ng/ml) for 24 hr. Cell surface ICAM-1 gated for viable cells was detected by flow cytometry. (a) Prior to the onset of stimulation, the indicated Ab or isotype control Ab (isotype ctrl) was added to the culture wells to give a final concentration of 20 µg/ml each. (b) Prior to the onset of stimulation, isotype control mAb (5 µg/ml), 69–10 mAb alone (5 µg/ml) or the combination of 69–10 mAb and 2–2 mAb, 20–3 mAb, 31–4 mAb (5 µg/ml, respectively) was added to the culture wells. (c) Prior to the onset of stimulation, the indicated concentrations of isotype control mAb, 69–10 mAb alone or the combination of 4 mAbs were added to the culture wells. (a–c) The dashed line is the standard value of unstimulated cells (vehicle). Representative data of five independent experiments are shown as mean \pm S.D. of mean fluorescence intensity (MFI) from triplicate samples, comparing values in each Ab to those in isotype control ($* p < 0.01$), and similar results were obtained in each experiment. (d) Data are shown as histogram of ICAM-1, and are representative of five independent experiments. The thin black lines in each histogram show the data of ICAM-1 expression on unstimulated cells. The bold black line (i) and the dotted lines (ii, iii) in each histogram show the data of ICAM-1 expression on IL-26-stimulated cells in the presence of the indicated Abs (40 µg/ml each). The gray areas in each histogram show the data of the PE-labeled isotype control.

mAb and 31–4 mAb further suppressed ICAM-1 expression on IL-26-stimulated COLO205. (Figure 2(b)). As shown in Figure 2(c) (representative histograms are shown in Figure 2(d)), ICAM-1 expression on IL-26-stimulated COLO205 was inhibited in an antibody dose-dependent manner, and the combination of 4 mAbs almost completely inhibited ICAM-1 expression on IL-26-stimulated COLO205 to a level nearly identical to the commercially available anti-IL-26 pAb.

The inhibitory effect of the novel anti-IL-26 mAbs on STAT3 phosphorylation in IL-26-stimulated COLO205 cells

We next analyzed the inhibitory effect of the novel anti-IL-26 mAbs on STAT3 phosphorylation in IL-26-stimulated COLO205. We first examined the phosphorylation level of STAT3 in COLO205 following IL-26 stimulation by Western blotting, with recombinant human IL-22 and IL-6 used as positive controls. As shown in Figure 3(a), stimulation with IL-26 resulted in the prominent phosphorylation of STAT3 in COLO205 with a peak around 10 min. The peak intensity of STAT3 phosphorylation in COLO205 following IL-26 stimulation was stronger than IL-6 stimulation, a well-known inducer of STAT3 phosphorylation, although the intensity was further amplified following IL-22

stimulation for 10 min (Figure 3(a)). We then examined the effect of anti-IL-26 mAbs on STAT3 phosphorylation in COLO205 following IL-26 stimulation for 10 min. Similar to the results obtained with the ICAM-1 expression assays, addition of 2–2 mAb, 20–3 mAb, 31–4 mAb or 69–10 mAb partially inhibited STAT3 phosphorylation in IL-26-stimulated COLO205, while the commercially available anti-IL-26 pAb completely blocked STAT3 phosphorylation to a level seen in unstimulated COLO205 (Figure 3(b)). The combination of 4 mAbs resulted in a deeper level of inhibition compared with anti-IL-26 mAb alone, one which was similar to that observed with the commercially available anti-IL-20RA pAb (Figure 3(b)). Considering that the combination of 4 mAbs markedly suppressed ICAM-1 expression on IL-26-stimulated COLO205 as compared with anti-IL-20RA pAb (as shown in Figure 2(a,c)), our data strongly suggest that IL-20RA and STAT3-independent pathways are involved in ICAM-1 expression on COLO205 following IL-26 stimulation.

The inhibitory effect of the novel anti-IL-26 mAbs on FGF7 and VEGF expression in IL-26-stimulated HaCat cells

Since keratinocytes expressing IL-20RA are thought to be one of the primary targets of IL-26, we examined the inhibitory effect of

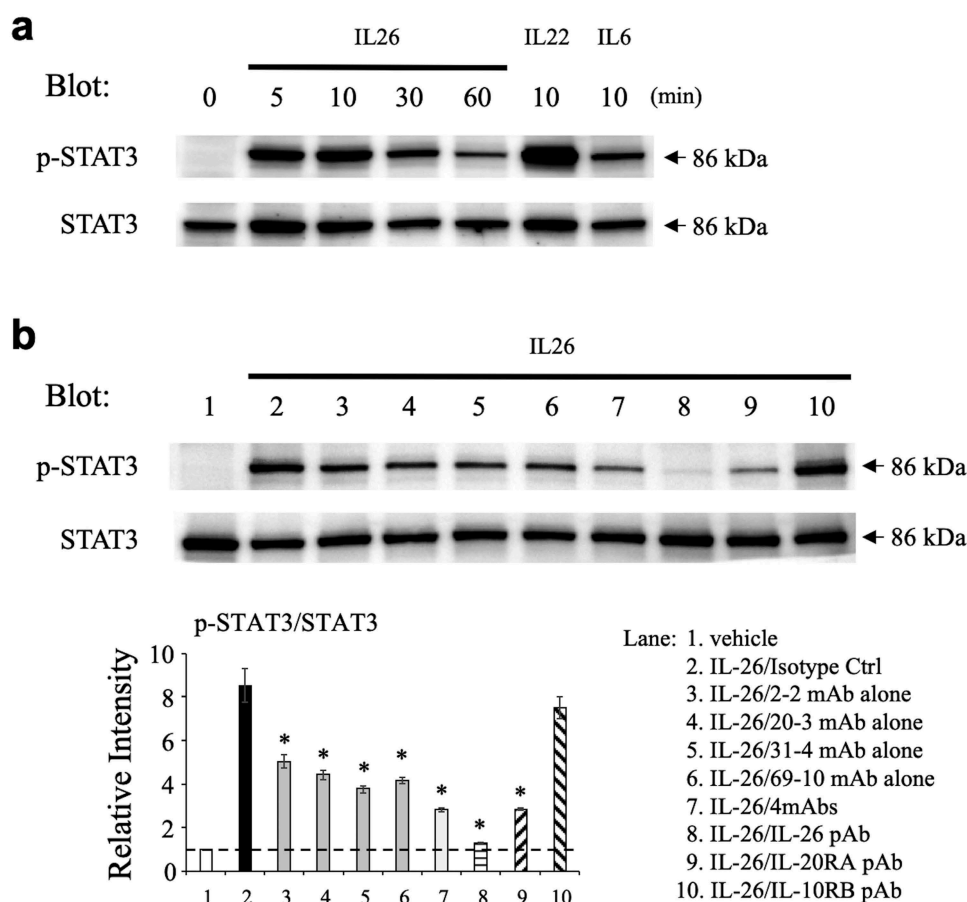


Figure 3. Addition of novel anti-IL-26 mAbs inhibits phosphorylation of STAT3 in IL-26-stimulated COLO205 cells.

(a) COLO205 cells were stimulated with recombinant human IL-26 (20 ng/ml) for the indicated times, or stimulated with recombinant human IL-6 (20 ng/ml) or IL-22 (20 ng/ml) for 10 min. (b) COLO205 cells were stimulated with recombinant human IL-26 (20 ng/ml) for 10 min in the presence of the indicated Ab or isotype control Ab (isotype ctrl) (20 μ g/ml, respectively). (a, b) Whole cell lysates were separated by SDS-PAGE (each, 25 μ g), and phospho(p)-STAT3 was detected by immunoblotting. The same blots were stripped and reprobbed with antibodies specific for pan STAT3. Data shown are representative of three independent experiments with similar results. Band intensity of p-STAT3 was normalized to pan STAT3, and relative intensity compared with unstimulated cells was indicated in the bottom graph (b). The dashed line is the standard value of unstimulated cells (vehicle). Data are shown as mean \pm S.E. of relative intensity from three independent experiments, comparing values in each Ab to those in isotype control (* $p < 0.01$).

the novel anti-IL-26 mAbs on keratinocytes activation following IL-26 stimulation. We have recently shown that IL-26 upregulates the expression of fibroblast growth factor (FGF)-1 and FGF2 in primary human keratinocytes.¹³ Considering the uniformity of the assay, the human keratinocyte cell line HaCaT was used in this study. Although we examined mRNA expression levels of FGF1 and FGF2 in HaCaT following IL-26 stimulation, significant increase was not observed as compared with unstimulated HaCaT (data not shown). On the other hand, IL-26 enhanced mRNA expression levels of FGF7 and VEGF in HaCaT (Figure 4(a,b)). We then examined the effect of anti-IL-26 mAbs on FGF7 and VEGF expression in HaCaT following IL-26 stimulation. As shown in Figure 4(a), addition of 2-2 mAb, 20-3 mAb, 31-4 mAb or 69-10 mAb inhibited FGF7 expression in IL-26-stimulated HaCaT. Of note, the inhibitory effect of each mAb, particularly 31-4 mAb and 69-10 mAb, on FGF7 expression in HaCaT was much more prominent compared with ICAM-1 expression or STAT3 phosphorylation in IL-26-stimulated COLO205 (as shown in Figures 2 and 3). Addition of 31-4 mAb or 69-10 mAb almost completely inhibited FGF7 expression in IL-26-stimulated HaCaT to a level seen in unstimulated HaCaT, whereas the commercially available

anti-IL-20RA pAb only slightly inhibited FGF7 expression in IL-26-stimulated HaCaT (Figure 4(a)). Similar results were also obtained regarding VEGF expression in IL-26-stimulated HaCaT (Figure 4(b)).

The inhibitory effect of the novel anti-IL-26 mAbs on proliferation and tube formation of IL-26-stimulated HUVEC

Given the fact that IL-20RA may be differentially involved in IL-26-mediated stimulation depending on cell types, we next examined the inhibitory effect of the novel anti-IL-26 mAbs on vascular endothelial cells activation following IL-26 stimulation. We recently found that IL-26 directly acts on HUVEC to promote proliferation and tube formation at a level similar to VEGF regardless of the lack of IL-20RA expression.¹³ We therefore examined the effect of the anti-IL-26 mAbs on proliferation and tube formation of HUVEC following IL-26 stimulation. As shown in Figure 5(a,b), addition of 2-2 mAb, 20-3 mAb, 31-4 mAb or 69-10 mAb inhibited both proliferation and tube formation of IL-26-stimulated HUVEC. Similar to the results obtained with IL-26-stimulated HaCaT shown in Figure 4, addition of the anti-IL-26

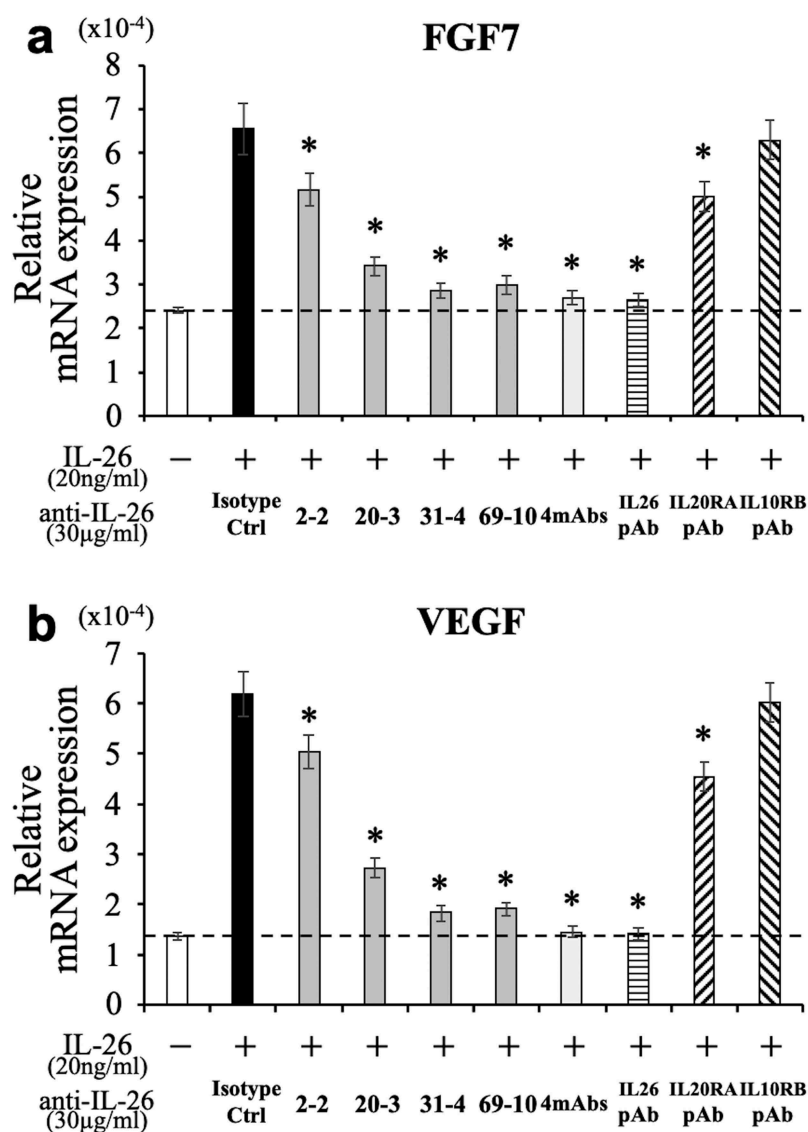


Figure 4. Addition of novel anti-IL-26 mAbs inhibits the expression of FGF7 and VEGF in IL-26-stimulated HaCaT cells.

HaCaT cells were stimulated with recombinant human IL-26 (20 ng/ml) for 6 hr. Prior to the onset of stimulation, the indicated Ab or isotype control Ab (isotype ctrl) was added to the culture wells to give a final concentration of 30 μg/ml each. mRNA expression of FGF7 (a) and VEGF (b) was quantified by real-time RT-PCR. Each expression was normalized to hypoxanthine phosphoribosyltransferase 1 (HPRT1). The dashed line is the standard value of unstimulated cells (vehicle). Representative data of three independent experiments are shown as mean ± S.D. of triplicate samples, comparing values in each Ab to those in isotype control (* $p < 0.01$), and similar results were obtained in each experiment.

mAb, particularly 31-4 mAb and 69-10 mAb, strongly inhibited proliferation and tube formation of IL-26-stimulated HUVEC to a level nearly identical to that seen in unstimulated HUVEC. In contrast, the commercially available anti-IL-20RA pAb and anti-IL-10RB pAb hardly affected proliferation and tube formation of IL-26-stimulated HUVEC (Figure 5(a,b)). Taken together, our data indicate that both IL-20RA-dependent and -independent pathways are involved in IL-26-mediated stimulation, and strongly suggest the existence of distinct receptor(s) other than the IL-20RA/IL-10RB heterodimer.

Lack of effect on the antimicrobial activity of IL-26 by the novel anti-IL-26 mAbs

IL-26 has been reported to have a multitude of biological functions. Due to its cationic amphipathic feature, similar to that seen with

antimicrobial peptides, IL-26 exerts its killing effect on extracellular bacteria via membrane-pore formation and appears to have an important role in host defense.¹⁴ Therefore, the development of novel anti-IL-26 mAb-targeted therapy for chronic inflammatory diseases should also include investigation into its effect on IL-26-mediated antimicrobial activity. Binding assays revealed that both lipopolysaccharide (LPS) from gram-negative bacteria (*Escherichia coli* O111:B4) and lipoteichoic acid (LTA) from gram-positive bacteria (*Staphylococcus aureus*) strongly bound to recombinant human IL-26 in a dose-dependent manner as compared with recombinant human IL-10 and IL-22 (other IL-10 family cytokines) (Figure 6(a)).

We next examined the antimicrobial capacity of IL-26 through the use of *Escherichia coli* (ATCC 8739), and *Staphylococcus aureus* (ATCC 29213) as representative gram-negative and gram-positive bacteria, respectively. Representative antimicrobial peptides LL-37 and human β-defensin 3 (hBD3)

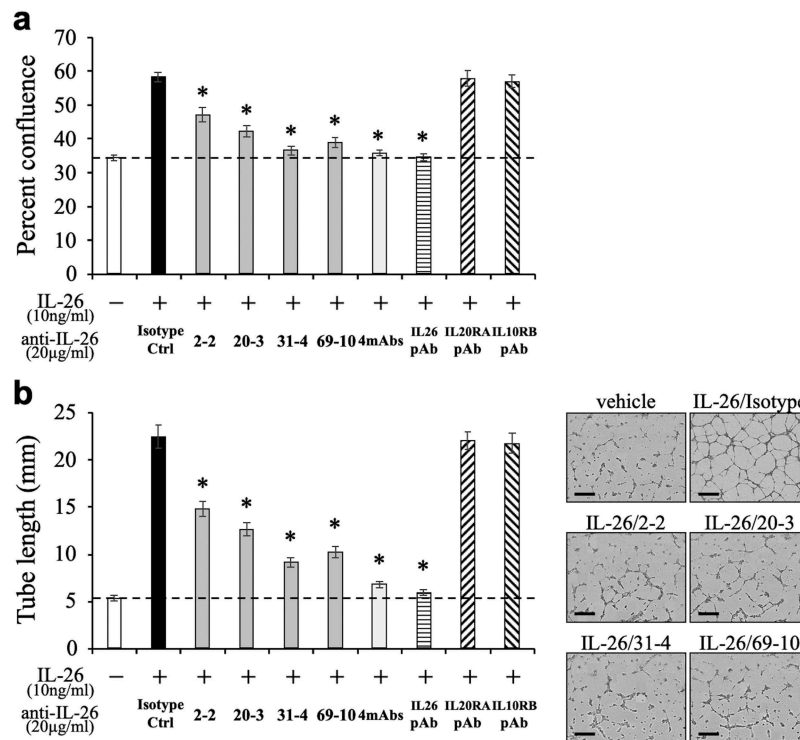


Figure 5. Addition of novel anti-IL-26 mAbs inhibits proliferation and tube formation of IL-26-stimulated HUVEC.

HUVEC were stimulated with recombinant human IL-26 (10 ng/ml) for 48 hr (a) or 9 hr (b). Prior to the onset of stimulation, the indicated Ab or isotype control Ab (isotype ctrl) was added to the culture wells to give a final concentration of 20 µg/ml each. (a) Proliferation was assessed by cell confluence. (b) Tube formation was assessed by cell sprouts formation. Representative images are shown in the right panels. Scale bar, 300 µm. Quantification of tube length is demonstrated in the graph in the left panel. (a, b) The dashed line is the standard value of unstimulated cells (vehicle). Representative data of three independent experiments are shown as mean ± S.D. of triplicate samples, comparing values in each Ab to those in isotype control (* $p < 0.01$), and similar results were obtained in each experiment.

were used for comparison. Growth kinetics analysis showed that 10 µM human IL-26 substantially inhibited and delayed the growth of *Escherichia coli*, although this antimicrobial activity was not as prominent as that seen with hBD3 and LL-37 in our assay system (Figure 6(b)). hBD3 exhibited the strongest antimicrobial capacity, with 10 µM hBD3 being able to completely eradicate both *Escherichia coli* and *Staphylococcus aureus*, while 10 µM human IL-26 or LL-37 only slightly delayed the growth of *Staphylococcus aureus*, and no inhibition was observed with 5 µM human IL-26 or LL-37 (Figure 6(c)).

Since the growth of *Escherichia coli* incubated with vehicle reached saturation level from 6 to 8 hrs of incubation, the difference in the number of bacteria incubated with vehicle and 10 µM human IL-26 was most prominently observed after 6 hrs of culture. We thus investigated the effect of anti-IL-26 mAbs on antimicrobial activity of IL-26 under the experimental conditions described in the Materials and methods section. Considering the clinically effective dose range of therapeutic antibody in the blood, we examined the effect of anti-IL-26 Ab up to 150 µg/ml, equivalent to 1 µM. As shown in Figure 6(d), addition of 2-2 mAb, 20-3 mAb, 31-4 mAb or 69-10 mAb hardly affected the antimicrobial activity of IL-26. Even the commercially available anti-IL-26 pAb showed little effect on the antimicrobial activity of IL-26, strongly suggesting that 1 µM of antibody is insufficient to neutralize 10 µM human IL-26. Taken together, these results strongly suggest that at least at physiological doses, the novel anti-human IL-26 mAb does not inhibit the antimicrobial activity of IL-26.

Anti-IL-26 mAb administration suppresses skin inflammation by inhibiting angiogenesis and infiltration of inflammatory cells in psoriatic lesions of IMQ-treated hIL-26Tg mice

Since the IL-26 gene is absent in rodents,⁴ we recently examined the role of IL-26 in angiogenesis and skin inflammation utilizing hIL-26Tg mice.¹³ In this study, we conducted *in vivo* experiments to determine the potential therapeutic effect of the newly developed anti-IL-26 mAbs. Importantly, although the IL-26 gene is absent in mice, the IL-20RA and IL-10RB subunits that are part of the receptor complex of the other IL-10 cytokine family members are also expressed in mice.¹⁰ In addition, our recent report showed that human IL-26 functions in both human and murine fibroblasts and vascular endothelial cells.^{13,26} For the *in vivo* studies, Δconserved noncoding sequence (CNS)-77 Tg mice (control BAC Tg mice with deleting human IL-26 transcription) were used as controls. The therapeutic effect of anti-IL-26 mAbs was assessed in the low dose (20 mg) IMQ-induced psoriasis model, since scaling and thickness of the back skin were prominent even in the human IL-26 transcription-lacking ΔCNS-77 Tg mice treated with high dose (more than 40 mg) IMQ.¹³ We previously confirmed that the expression of human IL-26 was increased at both mRNA and protein levels in the skin lesions of hIL-26Tg mice following daily application of IMQ cream, while no expression of human IL-26 was detected in the skin of ΔCNS-77 Tg mice.¹³

As shown in Figure 7(a,b), the back skin of hIL-26Tg mice injected with isotype control mAb appeared markedly affected

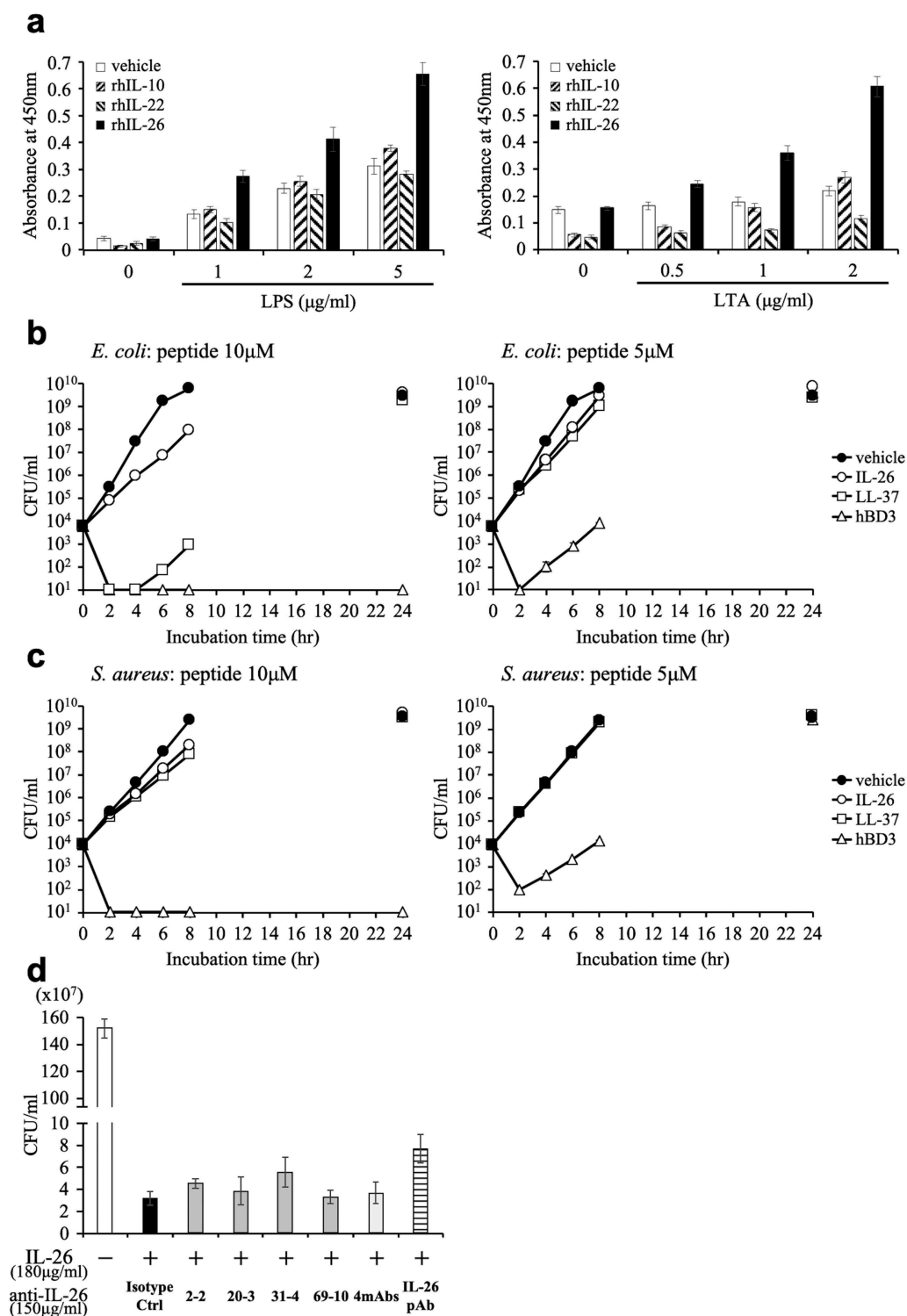


Figure 6. Addition of novel anti-IL-26 mAbs hardly affects the antimicrobial activity of IL-26.

(a) Immobilized recombinant human IL-10 (rhIL-10), IL-22 (rhIL-22), IL-26 (rhIL-26) or vehicle (PBS) alone was incubated with the indicated concentrations of purified LPS (left panel) or LTA (right panel). The absorbance at 450 nm/570 nm was measured. Representative data of three independent experiments are shown as mean \pm S.D. of triplicate samples, and similar results were obtained in each experiment. (b, c) Growth kinetics of *Escherichia coli* (b) and *Staphylococcus aureus* (c) cultured with 10 μM (left panels) or 5 μM (right panels) rhIL-26, LL-37 or human β -defensin 3 (hBD3). (d) *Escherichia coli* was cultured with 10 μM rhIL-26 for 6 hr. Prior to the onset of culture, the indicated Ab or isotype control Ab (isotype ctrl) was added to the culture wells to give a final concentration of 150 $\mu\text{g/ml}$ each. (b-d) Serial dilutions of bacterial cultures were plated onto agar plates, and the number of colonies was counted. Representative data of three independent experiments are shown as mean \pm S.D. of triplicate samples, and similar results were obtained in each experiment.

as compared with $\Delta\text{CNS-77}$ Tg mice, and the scores of erythema, scaling and thickness in isotype control-injected hIL-26Tg mice were all higher than those of $\Delta\text{CNS-77}$ Tg

mice. In contrast, the clinical symptoms of erythema, scaling and thickening of the skin lesion were all remarkably suppressed in the hIL-26Tg mice treated with 69-10 mAb or the

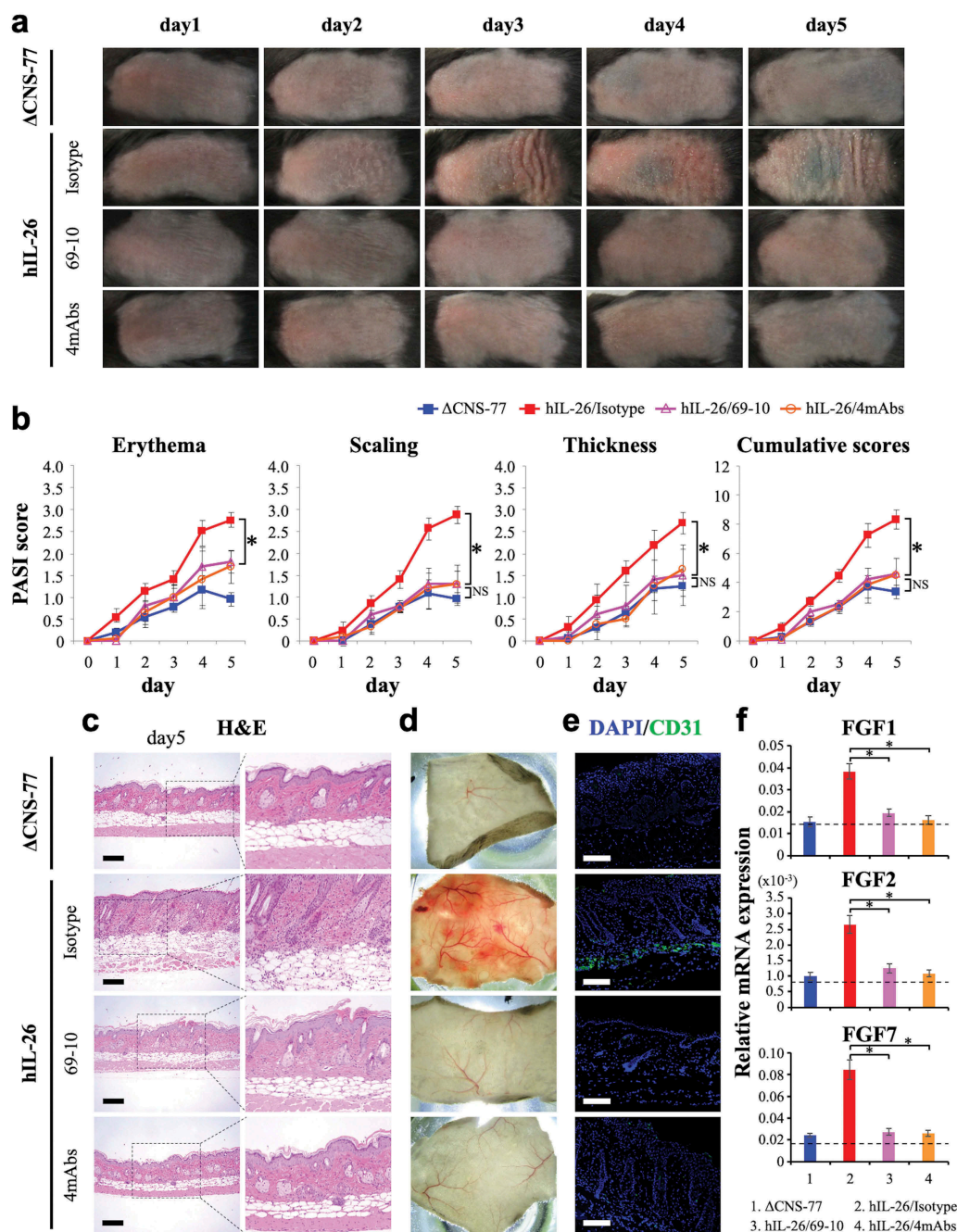


Figure 7. Anti-IL-26 mAb treatment suppresses IMQ-induced skin inflammation via inhibition of angiogenesis and infiltration of inflammatory cells.

Data are shown from IMQ (20 mg)-treated back skin in Δ CNS-77 Tg mice, hIL-26Tg mice treated with anti-IL-26 mAb (69–10 mAb alone or the combination of 4 mAbs) or isotype control mAb. (a) Phenotypical representation of each group. Representative images are shown ($n = 6$ mice for each group at each time point). (b) Time course of PASI scores (erythema, scaling and thickness were scored daily on a scale from 0 to 4, respectively) in each group ($n = 6$ mice for each group at each time point). Data are shown as mean \pm S.D. of each group, comparing values in hIL-26Tg mice treated with anti-IL-26 mAb to those in hIL-26Tg mice injected with isotype control mAb or those in Δ CNS-77 Tg mice ($* p < 0.01$). NS denotes 'not significant'. Data represent the combined results of two independent experiments. (c) H&E staining of skin lesions from each group on day-5. Higher magnification images show inflammatory cell infiltration. Original magnification $\times 100$. Scale bar, 200 μ m. (d) Subcutaneous vascular formation of each group on day-5. (e) Immunofluorescence staining of skin lesions from each group on day-5 using anti-CD31 pAb. Positive cells were shown in green. All sections were stained with DAPI to mark the nuclei (blue). Original magnification $\times 100$. Scale bar, 200 μ m. (c-e) Representative images are shown with similar results (for each, $n = 6$ mice). (f) mRNA expression levels of FGF1, FGF2 and FGF7 in skin lesions from each group on day-3 ($n = 6$ mice for each group). Each expression was normalized to hypoxanthine phosphoribosyltransferase (HPRT). The dashed line is the mean value of non-treated mice. Data are shown as mean \pm S.D. of each group, comparing values in hIL-26Tg mice treated with anti-IL-26 mAb to those in hIL-26Tg mice injected with isotype control mAb ($* p < 0.01$).

combination of 4 mAbs, as compared with the hIL-26Tg mice injected with isotype control mAb, with Psoriasis Area and Severity Index (PASI) score of the hIL-26Tg mice treated with anti-IL-26 mAb being at almost the same level as the Δ CNS-77 Tg mice (Figure 7(a,b)). We also examined the potential

therapeutic effect of 31–4 mAb, and similar results with those obtained with 69–10 mAb were observed (data not shown).

Histologic studies of the skin showed the development of psoriasis-like skin inflammation characterized by acanthosis, parakeratosis, papillomatosis, infiltration of inflammatory cells

and altered dermal vascularity,³⁰ in the hIL-26Tg mice injected with isotype control mAb, while anti-IL-26 mAb-treated mice had similar appearance as Δ CNS-77 Tg mice (Figure 7(c)). Excessive blood vessel formation and vascular invasion were observed in subcutaneous tissues of isotype control-injected hIL-26Tg mice compared to Δ CNS-77 Tg mice, whereas blood vessel formation was significantly suppressed in the subcutaneous tissue of anti-IL-26 mAb-treated hIL-26Tg mice (Figure 7(d)). To further examine the vascular invasion, we conducted immunofluorescence staining for CD31 in the back skin sections of each mouse. As shown in Figure 7(e), levels of CD31-positive cells in the lower dermis were clearly decreased in the hIL-26Tg mice treated with anti-IL-26 mAb as compared with isotype control-injected mice. Moreover, expression levels of FGF1, FGF2 and FGF7, key angiogenic factors in this model,¹³ were all increased in the skin of isotype control-injected hIL-26Tg mice, and they were remarkably suppressed in the subcutaneous tissue of anti-IL-26 mAb-treated hIL-26Tg mice, resulting in expression levels similar to those seen in Δ CNS-77 Tg mice (Figure 7(f)).

We also examined the kinetics of mRNA expression of the major effector cytokines involved in psoriasis pathogenesis. The mRNA expression levels of IL-1 β and IL-6 were significantly increased in the skin lesions from hIL-26Tg mice as compared with Δ CNS-77 Tg mice, while there was no marked difference in the expression levels of TNF, IL-17A, IL-23 p19 and IL-12 p40 between hIL-26Tg mice and control mice (Figure S2(a)). Similar with the results of FGF1, FGF2 and FGF7, expression levels of IL-1 β and IL-6 were prominently suppressed in the subcutaneous tissue of anti-IL-26 mAb-treated hIL-26Tg mice to levels nearly identical to those seen in Δ CNS-77 Tg mice (Figure S2(b)). Taken together, our results strongly suggest that administration of novel neutralizing anti-IL-26 mAb (31–4 mAb and 69–10 mAb) provides a novel therapeutic approach for psoriasis by regulating angiogenesis and skin inflammation.

Discussion

Although its precise function in inflammatory disorders is not fully understood, IL-26 is thought to play a role in the pathology of diverse chronic inflammatory diseases such as psoriasis, inflammatory bowel diseases, rheumatoid arthritis and chronic GVHD. In this study, we used precise screening methods that incorporated both IL-20RA-expressing and -deficient cells, as well as assays examining potential *in vivo* therapeutic effects, to develop novel neutralizing anti-human IL-26 mAbs that may be of future use as therapeutic agents for the treatment of diverse chronic inflammatory diseases.

Selection of the appropriate screening methods is crucially important for the development of novel mAb designed to serve specific purposes. Although multiple biological effects of IL-26 on various cell types have been reported, we focused on ICAM-1 expression on COLO205 following IL-26 stimulation. The key points of this assay were its reproducibility and simplicity. Cell surface expression of ICAM-1 on COLO205 was enhanced following IL-26 stimulation at similar levels in all of the independent experiments. Moreover, when COLO205 was stimulated with IL-26 in triplicates or more, the standard deviation of the mean ICAM-1 expression in

each group was extremely small, which is critical for the evaluation of the neutralizing capacity of each mAb. Furthermore, COLO205 can be collected without trypsin treatment and the expression level of ICAM-1 can be easily and promptly analyzed shortly after acquisition of data, which is crucially important for evaluating the neutralizing capacity of a multitude of candidate clones. From these reasons, we chose this screening method as the first *in vitro* functional assay.

IL-20RA/IL-10RB heterodimer is generally believed to be the IL-26 receptor. Previous work has demonstrated that IL-26 binding to IL-20RA/IL-10RB results in functional activation via STAT3 phosphorylation.¹⁰ However, although commercially available anti-IL-20RA pAb and the combination of 4 novel anti-IL-26 mAbs strongly suppressed STAT3 phosphorylation in IL-26-stimulated COLO205 at similar levels (Figure 3(b)), anti-IL-20RA pAb only partially inhibited ICAM-1 expression on IL-26-stimulated COLO205, a much less inhibitory effect than that seen with the combination of 4 mAbs (Figure 2(a,c)). In addition, anti-IL-20RA pAb exhibited only a slight or no inhibitory effect on IL-26-stimulated HaCaT or HUVEC, respectively (Figures 4 and 5). These results strongly suggest that both IL-20RA-mediated signals and the hitherto uncharacterized receptor(s)-mediated signals are involved in IL-26-mediated stimulation, and that the relative involvement of each receptor in IL-26-mediated stimulation would depend on cell types due to differences in expression levels and binding affinities of those receptors. Our data indicate that blockade of IL-20RA with anti-IL-20RA antibody is insufficient to inhibit IL-26-mediated stimulation. Moreover, IL-20RA not only forms IL-20RA/IL-10RB heterodimer, but also is able to form IL-20RA/IL-20RB heterodimer, a receptor for IL-19, IL-20 and IL-24,²⁷ suggesting that blockade of IL-20RA may interfere with these signaling pathways. These findings indicate that IL-20RA may not be an appropriate target for novel IL-26-directed therapeutic approaches, and neutralization of IL-26 itself may be more effective than blockade of IL-20RA. To better understand the precise biological functions of IL-26 and the exact mechanisms of action of anti-IL-26 mAb, it is essential to identify the uncharacterized second receptor of human IL-26, and we are currently examining this important topic.

IL-26 is an unusual cationic and amphipathic cytokine, with the predominance of cationic residues on one side and hydrophobic amino acids on the opposite side.¹⁴ These characteristics closely resemble the structure of antimicrobial peptides. In fact, Meller *et al.*¹⁴ first reported that IL-26 disrupted bacterial membranes via pore forming and exhibited direct bacterial killing effects, similar to other antimicrobial peptides such as LL-37 and human β -defensin. Their group showed that recombinant human IL-26 markedly inhibited the growth of several gram-negative bacterial strains, including *Pseudomonas aeruginosa* (ATCC 27853, PA14), *Escherichia coli* (O1:K1:H7, O18:K1:H7, O111:B4, O111:K58:H2) and *Klebsiella pneumoniae* (O1:K2), as well as gram-positive *Staphylococcus aureus* (ATCC 6538), while no inhibition was observed with *Enterococcus faecalis* or *Candida albicans*.¹⁴ Our data showed that although 10 μ M human IL-26 certainly inhibited and delayed the growth of *Escherichia coli* (ATCC 8739), the number of bacteria gradually increased and finally

reached the same saturation level as seen with bacteria cultured with vehicle only (Figure 6(b)). The difference in the antimicrobial activity of IL-26 between the previous report¹⁴ and this study may be due to the difference in the bacterial strains. In addition, there is also a critical difference in the bacterial culture conditions. Meller *et al.*¹⁴ examined the antimicrobial activity of IL-26 in relatively unconventional culture conditions. Bacteria were incubated for 24 hr at 37°C under low-ionic-strength conditions (water only containing 10 mM NaCl without any nutrients), and then IL-26 or other antimicrobial peptides were added to these cultures. Under that culture condition, growth of bacteria other than *Pseudomonas aeruginosa* even cultured with vehicle only was slightly decreased during the culture period.¹⁴ In this study, bacteria was cultured in Mueller-Hinton broth, the nutrient-rich international standard culture medium to evaluate antimicrobial activity of agents, and rapid bacterial growth was observed during the period of assay (Figure 6(b,c)). An important point is that 5–10 μ M (considering that the molecular weight of human IL-26 is 19.8 kDa, 5–10 μ M is therefore equivalent to 100–200 μ g/ml), which is an extremely high concentration, of IL-26 is needed to exert antimicrobial activity. For *in vitro* neutralization assay, to sufficiently block 1–50 ng/ml of cytokines, much higher levels (5–50 μ g/ml) of antibodies are usually used. While the relative local concentrations of human IL-26 in such tissues as skin, intestine or lung are unknown, considering the serum dose range of therapeutic antibody in the clinical setting, it is reasonable to project from our findings that administered anti-human IL-26 mAb may hardly affect the antimicrobial activity of IL-26, as shown in Figure 6(d).

IL-17 is a proinflammatory cytokine that plays a key role in the pathology of various autoimmune diseases including psoriasis,^{30–32} inducing hyperproliferation of keratinocytes and stimulating production of psoriasis-associated molecules such as CCL20, CXCL8, matrix metalloproteinase 3, and angiogenic factors such as VEGF, which lead to the chronic skin inflammation of psoriasis.^{33,34} MAbs directly targeting IL-17, such as secukinumab (Cosentyx®), have shown very promising results in the treatment for psoriasis.^{35,36} However, IL-17 plays a pivotal role in host defense by enhancing the production of antimicrobial peptides from keratinocytes and mucosal epithelial cells, and recruiting neutrophils to inflammation/infection sites.³⁷ As expected, cases of adverse effects of IL-17-targeting therapy for psoriasis involving neutropenia and fungal infection, especially *Candida* infection, have been reported.^{38,39} Our study showed that anti-IL-26 mAb markedly suppressed the pathognomonic symptoms of angiogenesis and infiltration of inflammatory cells in IMQ-induced psoriatic skin of hIL-26Tg mice (Figure 7). Invasion of blood vessels in the dermis, which is one of the histological hallmarks of psoriatic skin lesions, induces the deterioration of psoriatic skin lesions.⁴⁰ In addition, mRNA expression levels of IL-1 β and IL-6, key cytokines for inducing and enhancing Th17 response, were significantly increased in the skin lesions from hIL-26Tg mice as compared with Δ CNS-77 Tg mice (Figure S2(a)). Scala *et al.*¹⁶ have recently shown similar results through different experimental approaches. We analyzed the expression levels of cytokines in the skin lesions of hIL-26 BAC Tg mice, whereas Scala *et al.* used skin lesions obtained from hidradenitis suppurativa patients. Addition of

commercial anti-human IL-26 pAb to an *ex vivo* culture of human skin samples significantly decreased the expression levels of IL-1 β and IL-6 in the skin, while IL-23 and IL-17A were not affected. Although we have not identified the main source of IL-1 β and IL-6 in the skin lesion of IMQ-treated hIL-26Tg mice, monocytes and fibroblasts may be possible candidates from recent findings.^{7,17,41}

In contrast to IL-1 β and IL-6, there was no significant difference in the expression levels of IL-17A and TNF between hIL-26Tg mice and control mice, at least in the total skin samples (Figure S2(a)). To analyze the precise effect of IL-26 on the T cell phenotype in inflammatory diseases, detailed analyses of T cell subsets at the inflammatory sites and gene expression profiles following purification of T cells would be essential for future studies. Moreover, multiple functions of human IL-26 have been reported. Due to clustered cationic charges, IL-26 can bind extracellular DNA/RNA released from bacteria or dying cells to form complexes that are highly protected from degradation by extracellular DNase/RNase and promote DNA/RNA immunogenicity. These IL-26-DNA complexes trigger IFN- α production from plasmacytoid dendritic cells via activation of TLR9, and enhance the expression of IL-1 β , IL-6 and IFN- β in monocytes and CXCL8 in neutrophils in a STING- and inflammasome-dependent manner.^{14,41} In addition, IL-26 enhances the chemotactic response of neutrophils toward bacterial stimuli and IL-8.⁸ Moreover, IL-26 is associated with monocyte and NK cell activation.^{7,12} Since IL-26 is broadly associated with innate immune activation, the effects of neutralizing anti-IL-26 mAb on these functions of IL-26 need to be investigated in future studies.

In conclusion, our current work indicates that IL-20RA is differentially involved in IL-26-mediated stimulation depending on cell types, and anti-IL-20RA blocking antibody is insufficient to inhibit IL-26-mediated stimulation. Our screening methods enabled us to develop 4 novel neutralizing anti-human IL-26 mAbs. Among them, both 31–4 mAb and 69–10 mAb clearly suppressed the excessive angiogenesis and inflammation in the skin lesions in a IMQ-induced psoriasis-like murine model. Our data strongly suggest that IL-26-targeted therapy may be an effective novel therapeutic approach for diverse chronic inflammatory diseases, including psoriasis and chronic GVHD.

Materials and methods

Cell culture

The human colon cancer cell line COLO205 was purchased from RIKEN Bioresource Center (Ibaraki, Japan) and grown in RPMI 1640 medium supplemented with 10% FBS. The human keratinocyte cell line HaCaT was a kind gift from Dr. Nobuhiro Nakano (Juntendo University, Tokyo, Japan) and grown in DMEM medium supplemented with 10% FBS. HUVEC were purchased from LONZA (Walkersville, MD) and grown in EGM-2 medium (LONZA). Cells were cultured at 37°C in a humidified 5% CO₂ incubator.

Antibodies and reagents

To characterize the novel mouse anti-human IL-26 mAbs, purified mouse anti-human IL-26 mAb (clone 510414), goat anti-human

IL-26 pAb (AF1375), goat anti-human IL-20RA pAb (AF1176), or goat anti-human IL-10RB pAb (AF874) purchased from R&D Systems (Minneapolis, MN) were used for comparison. Mouse IgG_{1,κ} isotype control mAb (clone MG1-45) purchased from BioLegend (San Diego, CA) or goat IgG isotype control pAb (AB-108-C) purchased from R&D Systems was used as a negative control. For Western blot analysis, rabbit anti-human phospho-STAT3 (Tyr705) pAb (AF4607) was purchased from R&D Systems. Rabbit anti-human/mouse/rat/monkey STAT3 mAb (clone 79D7) was purchased from Cell Signaling Technology (Danvers, MA). Horseradish peroxidase (HRP)-conjugated donkey anti-rabbit IgG was purchased from GE Healthcare (Buckinghamshire, UK). For immunofluorescence staining of mouse skin sections, rabbit anti-mouse CD31 pAb (ab28364) was purchased from Abcam (Cambridge, U.K.). Alexa Fluor 488-conjugated donkey anti-rabbit IgG pAb (A21206) was purchased from Thermo Fisher Scientific (Waltham, MA). Recombinant human IL-26 monomer and dimer were purchased from R&D Systems. Recombinant human IL-6, IL-10 and IL-22 were purchased from BioLegend. For binding assay, ultra-pure LPS from *Escherichia coli* O111:B4 and purified LTA from *Staphylococcus aureus* were purchased from InvivoGen (San Diego, CA). Mouse anti-*E. coli* and LPS mAb (clone 1C6) purchased from Chondrex, Inc. (Redmond, WA) and mouse anti-native LTA mAb (clone 55) purchased from Novus Biologicals (Centennial, CO) were biotinylated utilizing Biotin Labeling Kit-NH₂ (Dojindo Laboratories, Kumamoto, Japan). For analyzing antimicrobial activity of IL-26, LL-37 fragment (18–37 amino acids) purchased from KareBay Biochem, Inc. (Monmouth Junction, NJ) and hBD3 purchased from the Peptide Institute, Inc. (Osaka, Japan) were used for comparison.

Mice

Female BALB/c mice were purchased from CLEA Japan (Tokyo, Japan). C57BL/6 mice carrying a 190-kb BAC transgene with human *IFNG* and *IL26* gene (hIL-26Tg) and a BAC Tg-deleting CNS positioned at 77 kb upstream of the *IFNG* transcription start site, an enhancer element required for IL-26 mRNA expression (Δ CNS-77 Tg) were developed in Thomas Aune's laboratory.^{24,25} The hIL-26Tg mice exhibited production of human IL-26 by CD4 T cells under Th1- or Th17-polarizing conditions, whereas expression of human IL-26 was completely abrogated in Δ CNS-77 Tg mice carrying human *IFNG* transgene with deleting *IL26* transcription.²⁵ All mice used in this study were housed in a specific pathogen-free facility in micro-isolator cages, and used at 8–12 weeks of age.

Development of hybridomas and monoclonal anti-human IL-26 antibodies

Forty μ g of recombinant human IL-26 monomer per 50 μ l of phosphate-buffered saline (PBS) was emulsified with 50 μ l of adjuvant, TiterMax Gold (TiterMax USA, Norcross, GA). A 6-wk-old female BALB/c mouse was immunized via subcutaneous administration with 100 μ l of the emulsion five times every two weeks and finally intravenously injected with half volume of the emulsion. Three days after the final

immunization, the spleen was removed and 1×10^8 spleen cells were fused with 1×10^8 P3U1 myeloma cells by using polyethylene glycol 4000 (Merck, Darmstadt, Germany) and were cultured in serum-free GIT medium (Wako Pure Chemicals, Osaka, Japan), 5% BriClone (NICB, Dublin, Ireland) and HAT (Invitrogen, Carlsbad, CA) in 96-well flat-bottom plates (Costar, Corning Incorporated, Corning, NY). Hybridoma supernatants were first screened for selective reactivity with human IL-26 by ELISA. The supernatants containing mAbs that were reactive to human IL-26 were next screened for neutralization assay. The hybridomas were cloned by limiting dilution. MAbs were purified from the supernatants using Protein A IgG Purification Kit (Pierce, Rockford, IL).

ELISA

The 96-well immunoplates (NUNC, Roskilde, Denmark) were coated with recombinant human IL-26 or IL-10 in carbonate bicarbonate buffer (2, 5, 10, 20, 50, 100 ng/well) or buffer alone as a negative control at 4°C overnight. Each well of the plate was blocked with 2% BlockAce (DS Pharma Biomedical, Osaka, Japan) in deionized distilled water for 1 hr at room temperature (RT), and then incubated with 10 μ g/ml of purified novel mouse anti-human IL-26 mAb (2–2, 20–3, 31–4 or 69–10) or commercial mouse anti-human IL-26 mAb in RPMI 1640 medium for 1 hr at RT, and subsequently incubated with HRP-conjugated goat anti-mouse Ig pAb (BD Biosciences) in 1% BlockAce solution for 1 hr at RT. Tetramethylbenzidine (TMB) Peroxidase Substrate (KPL, Gaithersburg, MD) was finally added to each well and the reaction was stopped by 2 N H₂SO₄. The absorbance at 450 nm/570 nm was measured in a Microplate Reader (Bio-Rad, Hercules, CA) and data were analyzed with Microplate Manager 6 software (Bio-Rad).

Flow cytometry

COLO205 cells (5×10^4) were stimulated with recombinant human IL-26 (20 ng/ml) in the presence or absence of neutralizing or blocking antibody in 120 μ l of RPMI 1640 medium in 96-well flat-bottom plates for 24 hr at 37°C. After stimulation, cells were collected and washed in PBS containing 1% FBS and 0.1% sodium azide (FCM buffer), and stained with phycoerythrin (PE)-labeled mouse anti-human ICAM-1 mAb (clone 15.2, Bay Bioscience, Kobe, Japan) or PE-labeled mouse IgG_{1,κ} isotype control (clone MOPC-21, BioLegend) for 25 min at 4°C. Acquisition was performed using FACSCalibur (BD Biosciences) and data were analyzed with FlowJo software (Tree Star, Ashland, OR).

Western blotting

To analyze phosphorylation of STAT3, COLO205 cells (1×10^6) were stimulated with recombinant human IL-26 (20 ng/ml), IL-6 (20 ng/ml) or IL-22 (20 ng/ml) in 1.5 ml of RPMI 1640 medium in 12-well plates (Corning) for 5, 10, 30 or 60 min at 37°C. After stimulation, cells were collected and lysed in RIPA buffer supplemented with 2% protease inhibitor cocktail (Sigma-Aldrich, St. Louis, MO) and 1x PhosSTOP (Roche Diagnostics, Tokyo,

Japan), being resolved by SDS-PAGE in reducing condition (25 µg/Lane) and immunoblotted using anti-phosphorylated STAT3 antibody. The methods for Western blotting were detailed previously.⁴² For reprobing, the membranes were submerged in a stripping buffer. After a stripping procedure, the membranes were reprobed with anti-pan STAT3 antibody. The images were taken using luminescent image analyzer LAS 4000 (GE Healthcare, Pittsburgh, PA), and data were analyzed with image reader LAS 4000 and Multi Gauge software (GE Healthcare).

Quantitative real-time RT-PCR

HaCaT cells (3 × 10⁵) were incubated overnight at 37°C in DMEM medium in 24-well plates (Corning). The next day, cells were stimulated with recombinant human IL-26 (20 ng/ml) in the presence or absence of neutralizing antibody in 750 µl of DMEM medium for 6 hr at 37°C. After stimulation, cells were lysed and total RNA was extracted by the use of RNeasy Mini kit according to the manufacturer's instructions (Qiagen, Valencia, CA). The methods for cDNA synthesis and quantitative real-time RT-PCR were detailed previously.⁴³ Sequences of primers used in quantitative real-time RT-PCR analysis are shown in Table S1.

Proliferation assay for HUVEC

HUVEC (5 × 10³) were incubated overnight at 37°C in EGM-2 medium containing 2% FBS and half volume of adjunctive growth factors in 96-well flat-bottom plates. The next day, cells were stimulated with recombinant human IL-26 (10 ng/ml) in the presence or absence of neutralizing antibody in EGM-2 medium containing 2% FBS and no growth factors for 48 hr at 37°C. Cell growth was measured as cell confluence using IncuCyte ZOOM (Essen Bioscience, Ann Arbor, MI).

Tube formation assay

HUVEC (1 × 10⁶) were incubated overnight at 37°C in EGM-2 medium containing 2% FBS and no growth factors in 100-mm dish. The next day, cells (1.5 × 10⁴) were seeded on 50 µl of Cultex Basement Membrane Extract (R&D Systems) in 96-well flat-bottom plates. Seeded cells were stimulated with recombinant human IL-26 (10 ng/ml) in the presence or absence of neutralizing antibody for 9 hr at 37°C. Cell growth was observed as cell sprouts formation using IncuCyte ZOOM. Tube form length was measured using the MetaMorph image analysis system (Molecular Device, Sunnyvale, CA).

Binding assay

The 96-well immunoplates were coated with 2 µg/ml of recombinant human IL-10, IL-22 or IL-26 in PBS or PBS alone as a negative control at 4°C overnight. Each well of the plate was blocked with 2% BlockAce in deionized distilled water for 1 hr at RT, and then incubated with ultra-pure LPS (1, 2, 5 µg/ml) or purified LTA (0.5, 1, 2 µg/ml) in PBS for 2 hr at RT, and next incubated with 1 µg/ml of biotinylated anti-LPS mAb or 0.2 µg/ml of biotinylated anti-LTA mAb in PBS for 1 hr at RT, and subsequently incubated with

Streptavidin-HRP (BD Biosciences) in PBS for 1 hr at RT. Colorimetric methods and data analysis were described in the ELISA section.

CFU assay

Escherichia coli (ATCC 8739), and *Staphylococcus aureus* (ATCC 29213) were cultured overnight at 37°C in trypticase soy broth (BD Biosciences) in 14-ml polystyrene round-bottom tube (Corning) to achieve mid-logarithmic phase growth. Bacterial concentrations were measured by spectrophotometry at 600 nm and diluted in Mueller-Hinton broth (BD Biosciences) to a final concentration of 1–2 × 10⁴ CFU/ml. Fifty µl of the diluted bacterial suspension was cultured in 96-well round-bottom plates (Corning), and then 50 µl of recombinant human IL-26, LL-37 or hBD3 diluted in Mueller-Hinton broth was added to these cultures. After 2, 4, 6, 8 or 24 hrs of incubation at 37°C, serial dilutions of bacterial cultures were plated onto lysogeny broth (LB) agar plates. The number of colonies formed after overnight incubation was counted by two independent investigators.

IMQ-induced psoriasis model

Mice received a daily topical dose of 20 mg 5% IMQ cream (Beselna Cream; Mochida Pharmaceutical, Tokyo, Japan) on their shaved back for 5 consecutive days. For mAb treatment, IL-26 mAb (31–4 mAb alone, 69–10 mAb alone or combination of 4 mAbs) or mouse IgG₁ isotype control was diluted in sterile PBS at 1 mg/ml and 200 µl (200 µg) was injected intraperitoneally on day 0 and day 3. The severity of inflammation of the back skin was measured by an objective scoring system based on the clinical PASI. Erythema, scaling, and thickness were scored independently on a score from 0 to 4: 0, none; 1, slight; 2, moderate; 3, marked; 4, very marked. The cumulative score (erythema plus scaling plus thickness) served as a measure of the severity of inflammation (score 0–12).⁴⁴ H&E staining and immunofluorescence staining of skin lesions, and RNA isolation from skin lesions were conducted as described previously.¹³

Statistics

Data were analyzed by two-tailed Student *t* test for two-group comparison or by one-way ANOVA test with Tukey's for multiple comparison testing. The assay was performed in triplicates, and data are presented as mean ± S.D. of triplicate samples of the representative experiment, or mean ± S.E. of triplicate samples of independent experiments. Significance was analyzed using GraphPad Prism 6 (GraphPad Software, San Diego, CA) and values of *p* < 0.01 were considered significant and are indicated in the corresponding figures and figure legends.

Study approval

Animal experiments were conducted following protocols approved by the Animal Care and Use Committees at Juntendo University (Tokyo, Japan).

Abbreviations

BAC	bacterial artificial chromosome
CNS	conserved noncoding sequence
ELISA	enzyme-linked immunosorbent assay
FBS	fetal bovine serum
FGF	fibroblast growth factor
GVHD	graft-versus-host disease
hIL-26Tg	human IL-26 transgenic
HRP	horseradish peroxidase
IFN	interferon
IL	interleukin
IMQ	imiquimod
hBD3	human β -defensin 3
HUVEC	human umbilical vein endothelial cells
LPS	lipopolysaccharide
LTA	lipoteichoic acid
mAb	monoclonal antibody
NK	natural killer
pAb	polyclonal antibodies
PBS	phosphate-buffered saline
RT	room temperature
TLR	Toll-like receptor
TNF	tumor necrosis factor
VEGF	vascular endothelial growth factor

Acknowledgments

The authors thank members of Atopy (Allergy) Research Center (Juntendo University Graduate School of Medicine, Japan), members of the Laboratory of Morphology and Image Analysis, Research Support Center (Juntendo University Graduate School of Medicine, Japan), and members of the Laboratory of Cell Biology, Research Support Center (Juntendo University Graduate School of Medicine, Japan) for technical assistance and for the use of the experimental apparatus.

Disclosure statement

Ryo Hatano, Takumi Itoh, Kei Ohnuma and Chikao Morimoto are inventors of the novel anti-human IL-26 mAbs 2-2, 20-3, 31-4 and 69-10, and are now applying for a patent regarding their invention (Anti-human IL-26 antibody. Application 2017-12-01 JP2017231439). Other authors declare no competing financial interests associated with this manuscript.

Funding

This study was supported in part by a grant of the Ministry of Health, Labor, and Welfare, Japan (Grant Number 180101-01 (C.M.)), JSPS KAKENHI Grant Numbers JP16H05345 (C.M.), JP18H02782 (K.O.), JP17K10008 (R.H.), JP18H06169 (T.I.). This work was also supported by a research grant from the Japanese Society of Hematology (R.H.), and a research grant from the Japan Research Institute of Industrial Science (K.O.).

ORCID

Takumi Itoh  <http://orcid.org/0000-0002-6535-1042>
 Haruna Otsuka  <http://orcid.org/0000-0001-9346-2658>
 Sayo Okamoto  <http://orcid.org/0000-0002-1831-6770>
 Satoshi Iwata  <http://orcid.org/0000-0002-9160-4461>
 Thomas M. Aune  <http://orcid.org/0000-0002-4968-4306>
 Chikao Morimoto  <http://orcid.org/0000-0002-3140-3596>

References

1. Knappe A, Hor S, Wittmann S, Fickenscher H. Induction of a novel cellular homolog of interleukin-10, AK155, by transformation of T lymphocytes with herpesvirus saimiri. *J Virol.* 2000;74:3881–87. doi:10.1128/jvi.74.8.3881-3887.2000.
2. Kotenko SV. The family of IL-10-related cytokines and their receptors: related, but to what extent? *Cytokine Growth Factor Rev.* 2002;13:223–40.
3. Donnelly RP, Sheikh F, Dickensheets H, Savan R, Young HA, Walter MR. Interleukin-26: an IL-10-related cytokine produced by Th17 cells. *Cytokine Growth Factor Rev.* 2010;21:393–401. doi:10.1016/j.cytogfr.2010.09.001.
4. Schoenborn JR, Dorschner MO, Sekimata M, Santer DM, Shnyreva M, Fitzpatrick DR, Stamatoyannopoulos JA, Wilson CB. Comprehensive epigenetic profiling identifies multiple distal regulatory elements directing transcription of the gene encoding interferon-gamma. *Nat Immunol.* 2007;8:732–42. doi:10.1038/ni1474.
5. Wolk K, Kunz S, Asadullah K, Sabat R. Cutting edge: immune cells as sources and targets of the IL-10 family members? *J Immunol.* 2002;168:5397–402. doi:10.4049/jimmunol.168.11.5397.
6. Wilson NJ, Boniface K, Chan JR, McKenzie BS, Blumenschein WM, Mattson JD, Basham B, Smith K, Chen T, Morel F, et al. Development, cytokine profile and function of human interleukin 17-producing helper T cells. *Nat Immunol.* 2007;8:950–57. doi:10.1038/ni1497.
7. Corvaisier M, Delneste Y, Jeanvoine H, Preisser L, Blanchard S, Garo E, Hoppe E, Barre B, Audran M, Bouvard B, et al. IL-26 is overexpressed in rheumatoid arthritis and induces proinflammatory cytokine production and Th17 cell generation. *PLoS Biol.* 2012;10:e1001395. doi:10.1371/journal.pbio.1001395.
8. Che KF, Tengvall S, Levanen B, Silverpil E, Smith ME, Awad M, Vikstrom M, Palmberg L, Qvarfordt I, Skold M, et al. Interleukin-26 in antibacterial host defense of human lungs. Effects on neutrophil mobilization. *Am J Respir Crit Care Med.* 2014;190:1022–31. doi:10.1164/rccm.201404-0689OC.
9. Che KF, Kaarteenaho R, Lappi-Blanco E, Levanen B, Sun J, Wheelock A, Palmberg L, Skold CM, Linden A. Interleukin-26 production in human primary bronchial epithelial cells in response to viral stimulation: modulation by Th17 cytokines. *Mol Med.* 2017;23. doi:10.2119/molmed.2016.00064.
10. Hor S, Pirzer H, Dumoutier L, Bauer F, Wittmann S, Sticht H, Renaud JC, de Waal Malefyt R, Fickenscher H. The T-cell lymphokine interleukin-26 targets epithelial cells through the interleukin-20 receptor 1 and interleukin-10 receptor 2 chains. *J Biol Chem.* 2004;279:33343–51. doi:10.1074/jbc.M405000200.
11. Dambacher J, Beigel F, Zitzmann K, De Toni EN, Goke B, Diepolder HM, Auernhammer CJ, Brand S. The role of the novel Th17 cytokine IL-26 in intestinal inflammation. *Gut.* 2009;58:1207–17. doi:10.1136/gut.2007.130112.
12. Miot C, Beaumont E, Duluc D, Le Guillou-Guillemette H, Preisser L, Garo E, Blanchard S, Hubert Fouchard I, Creminon C, Lamourette P, et al. IL-26 is overexpressed in chronically HCV-infected patients and enhances TRAIL-mediated cytotoxicity and interferon production by human NK cells. *Gut.* 2015;64:1466–75. doi:10.1136/gutjnl-2013-306604.
13. Itoh T, Hatano R, Komiya E, Otsuka H, Narita Y, Aune TM, Dang NH, Matsuoka S, Naito H, Tominaga M, et al. Biological effects of IL-26 on T cell-mediated skin inflammation, including psoriasis. *J Invest Dermatol.* 2019;139:878–89. doi:10.1016/j.jid.2018.09.037.
14. Meller S, Di Domizio J, Voo KS, Friedrich HC, Chamilos G, Ganguly D, Conrad C, Gregorio J, Le Roy D, Roger T, et al. T(H)17 cells promote microbial killing and innate immune sensing of DNA via interleukin 26. *Nat Immunol.* 2015;16:970–79. doi:10.1038/ni.3211.
15. Dang AT, Teles RM, Weiss DI, Parvatiyar K, Sarno EN, Ochoa MT, Cheng G, Gilliet M, Bloom BR, Modlin RL. IL-26 contributes to host defense against intracellular bacteria. *J Clin Invest.* 2019;130:1926–39. doi:10.1172/JCI99550.
16. Scala E, Di Caprio R, Cacciapuoti S, Caiazza G, Fusco A, Tortorella E, Fabbrocini G, Balato A. A new T helper 17 cytokine in hidradenitis suppurativa: antimicrobial and proinflammatory role of interleukin-26. *Br J Dermatol.* 2019. doi:10.1111/bjd.17854.
17. Fujii M, Nishida A, Imaeda H, Ohno M, Nishino K, Sakai S, Inatomi O, Bamba S, Kawahara M, Shimizu T, et al. Expression

- of Interleukin-26 is upregulated in inflammatory bowel disease. *World J Gastroenterol.* 2017;23:5519–29. doi:10.3748/wjg.v23.i30.5519.
18. Heftdal LD, Andersen T, Jaehger D, Woetmann A, Ostgard R, Kenngott EE, Syrbe U, Sieper J, Hvid M, Deleuran B, et al. Synovial cell production of IL-26 induces bone mineralization in spondyloarthritis. *J Mol Med (Berl).* 2017;95:779–87. doi:10.1007/s00109-017-1528-2.
 19. Esendagli G, Kurne AT, Sayat G, Kilic AK, Guc D, Karabudak R. Evaluation of Th17-related cytokines and receptors in multiple sclerosis patients under interferon beta-1 therapy. *J Neuroimmunol.* 2013;255:81–84. doi:10.1016/j.jneuroim.2012.10.009.
 20. Konradsen JR, Nordlund B, Levanen B, Hedlin G, Linden A. The cytokine interleukin-26 as a biomarker in pediatric asthma. *Respir Res.* 2016;17:32. doi:10.1186/s12931-016-0351-6.
 21. Kaabachi W, Bouali E, Berraies A, Dhifallah IB, Hamdi B, Hamzaoui K, Hamzaoui A. Interleukin-26 is overexpressed in Behcet's disease and enhances Th17 related -cytokines. *Immunol Lett.* 2017;190:177–84. doi:10.1016/j.imlet.2017.08.008.
 22. Caiazzo G, Di Caprio R, Lembo S, Raimondo A, Scala E, Patruno C, Balato A. IL-26 in allergic contact dermatitis: resource in a state of readiness. *Exp Dermatol.* 2018;27:681–84. doi:10.1111/exd.13521.
 23. Savchenko L, Mykytiuk M, Cinato M, Tronchere H, Kunduzova O, Kaidashev I. IL-26 in the induced sputum is associated with the level of systemic inflammation, lung functions and body weight in COPD patients. *Int J Chron Obstruct Pulmon Dis.* 2018;13:2569–75. doi:10.2147/COPD.S164833.
 24. Collins PL, Chang S, Henderson M, Soutto M, Davis GM, McLoed AG, Townsend MJ, Glimcher LH, Mortlock DP, Aune TM. Distal regions of the human IFNG locus direct cell type-specific expression. *J Immunol.* 2010;185:1492–501. doi:10.4049/jimmunol.1000124.
 25. Collins PL, Henderson MA, Aune TM. Lineage-specific adjacent IFNG and IL26 genes share a common distal enhancer element. *Genes Immun.* 2012;13:481–88. doi:10.1038/gene.2012.22.
 26. Ohnuma K, Hatano R, Aune TM, Otsuka H, Iwata S, Dang NH, Yamada T, Morimoto C. Regulation of pulmonary graft-versus-host disease by IL-26+CD26+CD4 T lymphocytes. *J Immunol.* 2015;194:3697–712. doi:10.4049/jimmunol.1402785.
 27. Ohnuma K, Hatano R, Itoh T, Iwao N, Dang NH, Morimoto C. Role of IL-26+CD26+CD4 T cells in pulmonary chronic graft-versus-host disease and treatment with caveolin-1-Ig Fc conjugate. *Crit Rev Immunol.* 2016;36:239–67. doi:10.1615/CritRevImmunol.2016018772.
 28. You W, Tang Q, Zhang C, Wu J, Gu C, Wu Z, Li X. IL-26 promotes the proliferation and survival of human gastric cancer cells by regulating the balance of STAT1 and STAT3 activation. *PloS One.* 2013;8:e63588. doi:10.1371/journal.pone.0063588.
 29. Stephen-Victor E, Fickenscher H, Bayry J. IL-26: an emerging proinflammatory member of the IL-10 cytokine family with multifaceted actions in antiviral, antimicrobial, and autoimmune responses. *PLoS Pathog.* 2016;12:e1005624. doi:10.1371/journal.ppat.1005624.
 30. Boehncke WH, Schon MP. Psoriasis. *Lancet.* 2015;386:983–94. doi:10.1016/S0140-6736(14)61909-7.
 31. Lowes MA, Bowcock AM, Krueger JG. Pathogenesis and therapy of psoriasis. *Nature.* 2007;445:866–73. doi:10.1038/nature05663.
 32. Golden JB, McCormick TS, Ward NL. IL-17 in psoriasis: implications for therapy and cardiovascular co-morbidities. *Cytokine.* 2013;62:195–201. doi:10.1016/j.cyto.2013.03.013.
 33. Suzuki T, Hirakawa S, Shimauchi T, Ito T, Sakabe J, Detmar M, Tokura Y. VEGF-A promotes IL-17A-producing gammadelta T cell accumulation in mouse skin and serves as a chemotactic factor for plasmacytoid dendritic cells. *J Dermatol Sci.* 2014;74:116–24. doi:10.1016/j.jdermsci.2013.12.013.
 34. Honorati MC, Neri S, Cattini L, Facchini A. Interleukin-17, a regulator of angiogenic factor release by synovial fibroblasts. *Osteoarthritis Cartilage.* 2006;14:345–52. doi:10.1016/j.joca.2005.10.004.
 35. Reszke R, Szepletowski JC. Secukinumab in the treatment of psoriasis: an update. *Immunotherapy.* 2017;9:229–38. doi:10.2217/imt-2016-0128.
 36. Ariza ME, Williams MV, Wong HK. Targeting IL-17 in psoriasis: from cutaneous immunobiology to clinical application. *Clin Immunol.* 2013;146:131–39. doi:10.1016/j.clim.2012.12.004.
 37. Interleukin VM. 17 is a chief orchestrator of immunity. *Nat Immunol.* 2017;18:612–21. doi:10.1038/ni.3742.
 38. Gordon KB, Blauvelt A, Papp KA, Langley RG, Luger T, Ohtsuki M, Reich K, Amato D, Ball SG, Braun DK, et al. Phase 3 trials of ixekizumab in moderate-to-severe plaque psoriasis. *N Engl J Med.* 2016;375:345–56. doi:10.1056/NEJMoa1512711.
 39. Esfahani K, Miller WH Jr. Reversal of autoimmune toxicity and loss of tumor response by interleukin-17 blockade. *N Engl J Med.* 2017;376:1989–91. doi:10.1056/NEJMc1703047.
 40. Heidenreich R, Rocken M, Ghoreschi K. Angiogenesis drives psoriasis pathogenesis. *Int J Exp Pathol.* 2009;90:232–48. doi:10.1111/j.1365-2613.2009.00669.x.
 41. Poli C, Augusto JF, Dauve J, Adam C, Preisser L, Larochette V, Pignon P, Savina A, Blanchard S, Subra JF, et al. IL-26 confers proinflammatory properties to extracellular DNA. *J Immunol.* 2017;198:3650–61. doi:10.4049/jimmunol.1600594.
 42. Hatano R, Yamada T, Madokoro H, Otsuka H, Komiya E, Itoh T, Narita Y, Iwata S, Yamazaki H, Matsuoka S, et al. Development of novel monoclonal antibodies with specific binding affinity for denatured human CD26 in formalin-fixed paraffin-embedded and decalcified specimens. *PloS One.* 2019;14:e0218330. doi:10.1371/journal.pone.0218330.
 43. Hatano R, Ohnuma K, Otsuka H, Komiya E, Taki I, Iwata S, Dang NH, Okumura K, Morimoto C. CD26-mediated induction of EGR2 and IL-10 as potential regulatory mechanism for CD26 costimulatory pathway. *J Immunol.* 2015;194:960–72. doi:10.4049/jimmunol.1402143.
 44. Alrefai H, Muhammad K, Rudolf R, Pham DA, Klein-Hessling S, Patra AK, Avots A, Bukur V, Sahin U, Tenzer S, et al. NFATc1 supports imiquimod-induced skin inflammation by suppressing IL-10 synthesis in B cells. *Nat Commun.* 2016;7:11724. doi:10.1038/ncomms11724.

Article

Novel Antibody-Drug Conjugate with Anti-CD26 Humanized Monoclonal Antibody and Transcription Factor IIH (TFIIH) Inhibitor, Triptolide, Inhibits Tumor Growth via Impairing mRNA Synthesis

Mutsumi Hayashi ^{1,2}, Hiroko Madokoro ¹, Koji Yamada ^{1,3}, Hiroko Nishida ¹,
Chikao Morimoto ⁴, Michiie Sakamoto ¹, Hiroshi Yanagawa ^{5,6} and Taketo Yamada ^{1,7,*}

¹ Department of Pathology, Keio University School of Medicine, 35 Shinanomachi, Shinjuku-ku, Tokyo 160-8582, Japan

² Department of Pediatrics, Keio University School of Medicine, 35 Shinanomachi, Shinjuku-ku, Tokyo 160-8582, Japan

³ Department of Biochemistry, The Jikei University School of Medicine, 3-25-8 Nishi-Shimbashi, Minato-ku, Tokyo 105-8461, Japan

⁴ Department of Therapy Development and Innovation for Immune Disorders and Cancers, Juntendo University Graduate School of Medicine, 2-1-1 Hongo, Bunkyo-ku, Tokyo 113-8421, Japan

⁵ Department of Fundamental Science and Technology, Keio University School of Science and Technology, 3-14-1 Hiyoshi, Kouhoku-ku, Yokohama City 233-8522, Kanagawa, Japan

⁶ IDAC Theranostics Inc., 1-1-48 Suehirocho, Tsurumi-ku, Yokohama City 230-0045, Kanagawa, Japan

⁷ Department of Pathology, Saitama Medical University, 38 Morohongo, Moroyama-machi, Saitama 350-0495, Japan

* Correspondence: taketo@saitama-med.ac.jp; Tel.: +81-49-276-1162

Received: 17 July 2019; Accepted: 5 August 2019; Published: 8 August 2019



Abstract: Here, we report a novel antibody drug conjugate (ADC) with the humanized anti-CD26 monoclonal antibody YS110 and triptolide (TR-1). YS110 has an inhibitory activity against the CD26-positive tumor growth via the immunological and direct pathway, such as intra-nuclear transportation of CD26 and YS110, and suppressed transcription of RNA polymerase II (Pol II) subunit POLR2A. The ADC conjugated with YS110 and an antitumor compound triptolide (TR-1), which is an inhibitor for TFIIH, one of the general transcription factors for Pol II was developed. YS110 and triptolide were crosslinked by the heterobifunctional linker succinimidyl 4-(N-maleimidomethyl)cyclohexane-1-carboxylate (SMCC) and designated Y-TR1. Antitumor efficacy of Y-TR1 against malignant mesothelioma and leukemia cell lines were assessed by the in vitro cell viability assay and in vivo assay using xenografted mouse models. Y-TR1 showed significant cytotoxicity against CD26-positive cell lines but not CD26-negative counterparts in a dose-dependent manner via suppression of mRNA synthesis by impairment of the Pol II activity. The tumors in xenografted mice administered Y-TR1 was smaller than that of the unconjugated YS110 treated mice without severe toxicity. In conclusion, the novel compound Y-TR1 showed antitumor properties against CD26-positive cancer cell lines both in vitro and in vivo without toxicity. The Y-TR1 is a unique antitumor ADC and functions against Pol II.

Keywords: antibody drug conjugate; targeted therapy; CD26; triptolide; RNA polymerase II; malignant mesothelioma

1. Introduction

CD26 is a type II glycoprotein that has intrinsic dipeptidyl peptidase IV (DPP-IV) activity [1] and is implicated in broad and various physiological processes, including metabolism of glucose, activation of T lymphocytes, and cell adhesion [2,3]. CD26 has also been known as a cell surface marker associated with varied malignancies and as a part of cancer stem cells in mesothelioma and colon carcinoma [4–6]. Recent studies suggest that the expression of CD26 is functioned in tumor growth, tumor invasion, and metastasis [3,7,8].

We have already generated anti-CD26 monoclonal antibodies (mAbs) that have certain inhibitory effects against the growth of tumor cells and xenografted tumors [9,10]. This humanized anti-CD26 mAb YS110, that binds to the cell membrane-proximal glycosylated region starting at the 20-amino acid flexible stalk region of human CD26, has showed anti-tumor effects in malignant mesothelioma (MM) models [4]. Recently, the first-in-human phase 1/2 study of anti-CD26 mAbs in advanced cases with CD26-expressing mesothelioma and renal cell carcinoma has been done in France. As a result, anti-CD26 mAbs are well tolerated up to 6 mg/kg Q1W, which has been defined as RP2D, with encouraging prolonged disease stabilizations observed in a number of patients with advanced/refractory mesothelioma [11].

YS110 with a human IgG1 backbone recruits immune effector cells to human tumors, including natural killer (NK) cells, which express Fc receptors at the cell membrane, in antibody-dependent cellular cytotoxicity (ADCC). This Fc domain-based mechanism is observed with other therapeutic mAbs (e.g., trastuzumab and rituximab) commonly. These mAbs, approved for cancer therapy, also show direct inhibition of tumor growth. It has been reported that treatment with trastuzumab, a humanized anti-ErbB2 mAb, inhibits the cell growth of carcinoma cells by impairing a signaling pathway.

The nuclear localization of CD26 has been reported in cultured malignant mesothelioma and T cell leukemia lines and in human thyroid carcinomas [12]. The previous studies have shown that murine anti-CD26 mAb 1F7, which recognizes the identical epitope to YS110 and has anti-tumor effects against T cell lymphomas, induces internalization of CD26 and subsequently promotes its nuclear accumulation [12]. We have previously showed that the nuclear localization of CD26 is functionally involved in the anti-tumor process following the YS110 treatment and that the nuclear translocation of CD26 and YS110 contributes to growth inhibition of malignant mesothelioma cells after the YS110 treatment [13]. It was shown that the nuclear CD26 interacted with a specific genome target flanking the gene for the RNA polymerase II (Pol II) subunit POLR2A, which is indispensable for the transcription of almost genes, using chromatin immunoprecipitation (ChIP) cloning. This interaction between the flanking region of the POLR2A gene and CD26 led to the suppressed transcription of POLR2A mRNA. Furthermore, the impairing nuclear translocation of CD26 and YS110 prevented both the nuclear translocation of these two proteins and the YS110-induced transcriptional repression of the POLR2A gene [13]. These results reveal a novel function of CD26 as a transcriptional modulator in the nucleus and provide insight into the development of anti-cancer therapy through alteration of the nuclear translocation of cell-surface proteins.

Herein, we designed a novel compound against CD26-positive cancers, which is constituted with YS110 and triptolide derivative TR-1 (Figure 1), an inhibitor for one of the general transcription factors for Pol II, TFIIH, and designated Y-TR1 [14]. It may be a reasonable strategy that the YS110 treatment specifically induces internalization of both CD26 and Y-TR1 into the nucleus from the cell surface in cancer cells but not in normal CD26-positive cells, such as the endothelium or lymphocytes, and then, YS110 suppresses the POLR2A transcription, and TR-1 inhibits TFIIH and POLII, which leads to additive or synergistic anti-tumor effects [15,16]. In this paper, it was revealed that Y-TR1 inhibits both cell growth of CD26-positive cancer cells and in vivo tumor growth in a xenograft model with CD26-positive tumor cells without toxicity.

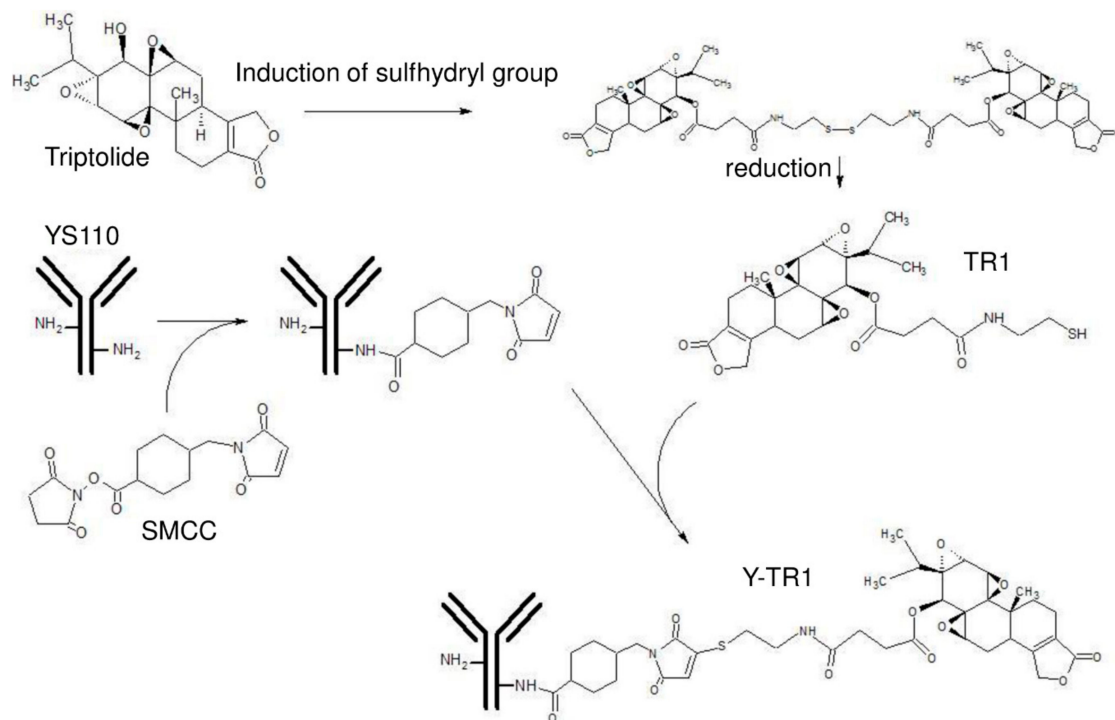


Figure 1. Structural formula of triptolide and conjugation protocol of Y-TR1 (SMCC). Triptolide was modified by a sulfhydryl (SH) group and was provided as an S-S dimer for chemical stability. The SH group-induced triptolide was designated TR1. The S-S bond was reduced to the SH monomer by the tris(2-carboxyethyl) phosphine (TCEP) reducing gel just before reaction. The humanized anti-CD26 monoclonal antibody YS110 was modified by the heterobifunctional linker SMCC. SMCC-modified YS110 and TR1 monomers were mixed and allowed to react overnight and purified. See Methods for details.

2. Results

2.1. Cytotoxicity of Triptolide and TR-1 against MM and Leukemia Cell Lines

As shown in Figure 2A–E, triptolide showed dose-dependent cytotoxic effects against the MM cell lines MSTO-wt, MSTO-clone12, JMN, and leukemia cell lines Jurkat, Jurkat CD26(+) after 48 h of treatment in WST-1 assays. The IC₅₀ values of triptolide against these cell lines calculated from WST-1 assays are shown in Table 1.

Cytotoxicity and IC₅₀ of triptolide derivative TR-1, designed for conjugation to the linkers, were tested in the same way and are shown in Figure 2F,G and Table 1. TR-1 was reduced by the immobilized tris(2-carboxyethyl) phosphine (TCEP) reducing gel (Thermo Scientific Inc., Waltham, MA, USA) from the S-S dimer before the assay.

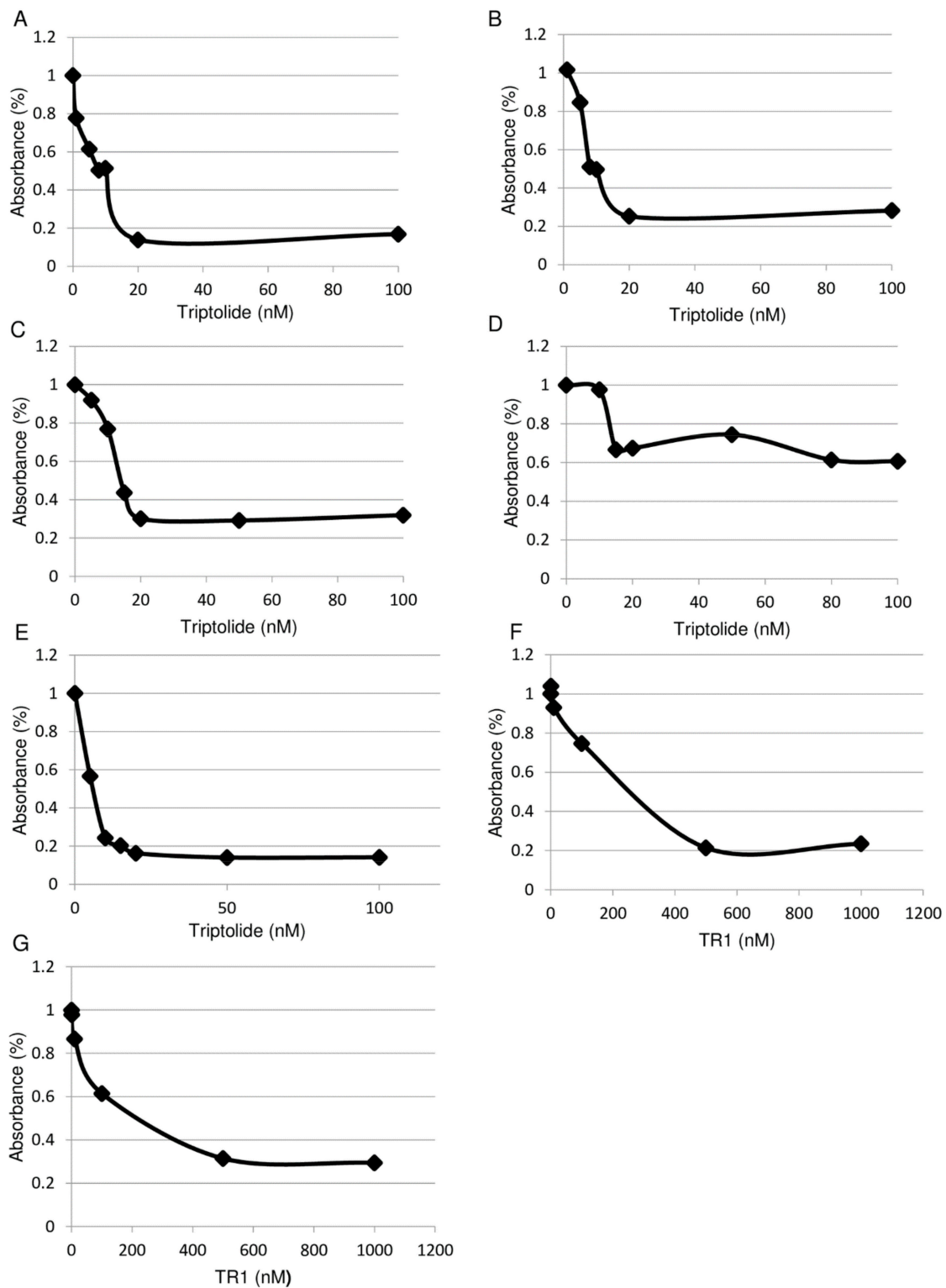


Figure 2. In vitro cytotoxic effect of Triptolide and TR1 against MM cells and leukemia cells. Horizontal axis shows the concentration of the compounds in nM. Vertical axis shows the percent of control of the absorbance value in the WST-1 assay. The representative results of at least three independent experiments are shown. (A) Triptolide against MSTO wt; (B) triptolide against MSTO clone12; (C) triptolide against JMN; (D) triptolide against Jurkat (-); (E) triptolide against Jurkat CD26(+); (F) TR-1 against MSTO wt; (G) TR-1 against MSTO clone12.

Table 1. IC50 of Triptolide, TR1 and Y-TR1 against MM and leukemia cell lines.

Cell Line	Origin	CD26	IC50 of Triptolide (nM)	IC50 of TR1 (nM)	IC50 of Y-TR1 (µg/mL)
MSTO wt	Mesothelioma	(-)	10	250	35
MSTO clone12	Mesothelioma	(+)	10	250	15
JMN	Mesothelioma	(+)	15	ND	30
Jurkat (-)	Leukemia	(-)	>100	ND	>100
Jurkat CD26(+)	Leukemia	(+)	6	ND	30

2.2. Conjugation of YS110 and TR-1, the Drug Antibody Ratio of Y-TR, and the Binding Activity of Y-TR1 to CD26-Positive Cell Line

Conjugation of YS110 and TR-1 using heterobifunctional linkers (succinimidyl 3-(2-pyridyldithio)propionate (SPDP), N-γ-maleimidobutyryl-oxysuccinimide ester (GMBS), succinimidyl 4-(N-maleimidomethyl)cyclohexane-1-carboxylate (SMCC)) was performed following the procedures shown in Materials and Methods (Figure 1). The concentration of the final products measured by the BCA protein assay reagent kit (Thermo Scientific Inc.) was approximately 1 mg/mL. The remaining unconjugated TR1-SH in the product measured by the DTNB assay was almost undetectable.

The intact masses of unconjugated YS110 and Y-TR1 (SMCC) measured by the MALDI-TOF mass analysis were 147,012.7 and 151,815.6, respectively (Figure 3A,B). The estimated molecular weight of a group of TR1 and SMCC conjugated with the antibody is 739.6. According to this molecular weight, the mean number of the TR1-SMCC groups conjugated with one molecule of YS110 is calculated by the calculation of $(151,815.6 - 147,012.7) / 739.6$, and the result is 6.489. This means 6.489 TR-1 molecules, on average, are conjugated with one molecule of YS110.

The binding activity of Y-TR1 to the CD26-positive MM cell line MSTO clone12 was shown by the flow cytometry analysis (Figure 3C).